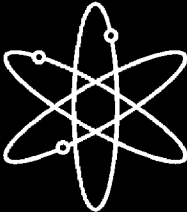


Barrier Integrity Research Program



Final Report



Argonne National Laboratory



**U.S. Nuclear Regulatory Commission
Office of Nuclear Regulatory Research
Washington, DC 20555-0001**



Barrier Integrity Research Program

Final Report

Manuscript Completed: November 2004

Date Published: December 2004

Prepared by

D.S. Kupperman¹, S.H. Sheen¹, W.J. Shack¹, and D.R. Diercks¹

and

P. Krishnaswamy², D. Rudland², and G.M. Wilkowski²

¹ Argonne National Laboratory
Argonne, IL 60439

² Engineering Mechanics Corporation of Columbus
Columbus, OH 43221

M. Srinivasan, NRC Project Manager

Prepared for
Division of Engineering Technology
Office of Nuclear Regulatory Research
U.S. Nuclear Regulatory Commission
Washington, DC 20555-0001
Job Code Y6869



Barrier Integrity Research Program: Final Report

D. S. Kupperman, S. H. Sheen, W. J. Shack, and D. R. Diercks

and

P. Krishnaswamy, D. Rudland, and G. M. Wilkowski

Abstract

In response to the vessel head event at the Davis-Besse reactor, the NRC formed a Lessons Learned Task Force (LLTF). Four action plans were formulated to respond to the recommendations of the LLTF. The action plans involve barrier integrity, stress corrosion cracking (SCC), operating experience, and inspection and program management. One part of the action plan on barrier integrity is an assessment to identify potential safety benefits from changes in requirements pertaining to leakage in the reactor coolant system (RCS). In this report, experiments and models were reviewed to identify correlations between crack size, crack-tip-opening displacement (CTOD), and leak rate in the RCS. Sensitivity studies using SQUIRT (Seepage Quantification of Upsets In Reactor Tubes) were carried out to correlate crack parameters, such as crack size and CTOD, with leak rate for various types of crack configurations in RCS components. A database that identifies the leak source, leak rate, and resulting actions from RCS leaks discovered in U.S. light water reactors was developed. For each leak event, the database provides information on what equipment detected the leakage, how it was determined that the leakage was through the pressure boundary, and what caused the leakage. The sensitivity, reliability, response time and accuracy of each type of leakage detection system were evaluated. Acoustic emission crack monitoring systems for the detection of crack initiation and growth before a leak occurs were also considered. New approaches to the detection of a leak in the reactor head region by monitoring boric-acid aerosols were also considered. Infrared spectroscopy could be used for this purpose. The focus of the report is on the available technologies.

Contents

Abstract	iii
Figures	vii
Tables	xi
Executive Summary.....	xiii
Foreword	xvi
Acknowledgments	xvii
Acronyms and Abbreviations	xix
1. Introduction	1
2. Determination of RCS Components Susceptible to Stress Corrosion Cracking.....	2
3. Review of RCS Leakage Experiments and Leak-Rate Models	4
Leak Rate Models.....	4
Sensitivity Studies	7
Importance of Crack Morphology Parameters and Effect of COD	7
Variation in Leak Rate due to Statistical Variation of Crack Morphology Parameters	9
Relative Leakage Crack Lengths due to Different Crack Morphology Parameters ..	10
Leaks in CRDM Nozzle	12
Determination of Leak Rates Expected from Typical SCC in RCS Components	14
Review of Leak Rates from Non-SCC Type of Cracking and Other Variables.....	17
4. Leakage Operating Experience	24
Basis for RCS Leakage Monitoring Requirements	25
Consequences of Lowering Leak Rate Limits.....	31
Correlation between Crack Size and Leak Rate.....	32
5. Leak Monitoring Systems.....	36
Acoustic Emission Leak Monitoring.....	42
Monitoring with Humidity Sensors	43
Airborne Particulate Radiation Monitor	45
Improved Radioactive Gas Monitors.....	46
Visual Observation of Leaks.....	47
Detection of Boric Acid from Leaks	47
6. Crack Growth Monitoring Systems	49
7. Conclusions	51
8. References	53

Appendix A	56
Failure Scenarios for Reactor Coolant Systems.....	56
Appendix B	65
Review of NRC-Sponsored ANL Study of Acoustic Leak Detection.....	65
Appendix C. Computational Fluid Dynamics (CFD) Analysis of 2-Dimensional Duct Flow with Turns.	68
Appendix D. Sensitivity Analysis Results for Leak Rate versus Crack Length	94
Appendix E. ASME Codes on Continuous Acoustic Emission (Article 13).....	111

Figures

1.	Comparison of two-phase flow leak rate tests used to validate the initial SQUIRT model.	5
2.	Comparison of PICEP- and SQUIRT-predicted leak rates with experimentally measured leak rates from Japanese leak-rate experiments.	6
3.	Comparison of SQUIRT-predicted leak rates versus experimentally measured leak rates for Ontario-Hydro experiments.	6
4.	Local and global surface roughness and number of turns.	8
5.	Crack morphology variables versus normalized COD.	8
6.	Fluid flow velocity field inside crack: (a) $\delta/\mu_G = 0.5$, (b) $\delta/\mu_G = 1.0$, (c) $\delta/\mu_G = 3.0$, and (d) $\delta/\mu_G = 5.0$. Flow conditions: P = 2250 psi (15.5 MPa), T = 550°F (288°C), pipe thickness = 25.4 mm. Single-phase all liquid water flow, and no local surface roughness.	9
7.	Histogram of leak rate at 50% Service Level A for case BWR-1 in NUREG/CR-6004. ...	11
8.	Length of leaking corrosion cracks along with the length of air-fatigue cracks for actual LBB submittal cases.	12
9.	Schematic showing long direction of dendritic grains in the buttered regions and main butt weld fill beads.	13
10.	PWSCC growth across the long direction of the dendritic grains.	13
11.	Percent of critical crack length versus diameter for BWR cases at 50% Service Level A stresses.	23
12.	Percent of critical crack length versus diameter for PWR cases at 50% Service Level A stresses.	23
13.	An example of a database entry for a leak. Each field can be expanded for additional information by clicking on the box containing the initial information.	25
14.	Number of occurrences (percentage) that a location was mentioned in a leak event report. For example, almost 20% of the time the leak involved a weld. About 8% of the leak events reviewed involved CRDMs, usually detected through visual detection of boric acid crystals. Cracks were involved with leaks about 40% of the time with a wide range of leak rates [< 0.00063 to 6.3 kg/s ; 0.01 to >100 gpm].	29
15a.	The relative frequency of SCCs and fatigue cracks reported in the database for PWRs and BWRs. Many SCC involved a CRDM or pressurizer. The SCCs are tight and thus result in lower leak rates compared to fatigue cracks for a given crack length. For cracks with leak rates > 0.0063 kg/s (0.1 gpm) (excluding steam generators) fatigue cracks were noted to have about 50% more occurrences than SCCs.	30
15b.	Number of leakage events reported per year in database. A decrease in number of leakage events from 1985 is evident.	31
16.	The PWR-to-BWR ratio of leak events involving valves, seals, fatigue cracks, SCCs, and welds. The ratio of PWRs to BWRs in the U.S. is 2 and is represented in the figure by the horizontal line.	34
17.	Distribution of leak rates by magnitude recorded in the database beginning with 1970. The number of leaks in a given leak rate range is indicated.	34
18.	Through-wall crack length vs. leak rate for variety of leaks in database. Most of the leaks were cracks in welds.	35
19.	Trends in U.S. fuel failure rates (2004 results are incomplete).	36
20.	Comparison of leak detection methods reported in the leak event reports. Small leaks were detected visually. Test refers to hydrostatic pressure test. Vol refers to high makeup rate to volume control tank.	40

21.	Time to recognize action is required after leak detected with sump monitor.	41
22.	Time to recognize action is required after leak detected with radiation monitor.....	42
23.	Schematic representation of the ALUS system [27]......	44
24.	Schematic representation of the FLUS humidity sensor system. The sensitivity for the FLUS system is reported to be 0.0003 kg/s (0.004 gpm) [22].	45
25.	Schematic of AE sensor developed by PNNL for continuous monitoring of nuclear reactor components [18].	50
B1.	Predicted signal-to-noise ratios vs. distance along a 254-mm Schedule 80 pipe for three leak rates and three levels of estimated acoustic background noise.	66
B2.	Leak rate vs. acoustic signal amplitude in the 300–400 kHz bandwidth for SCC, fatigue crack, valve, and flange leaks.....	67
C1.	Sketch of a 2D duct with turns.	68
C2.	Rough pipe friction correlation and experiment data. Curve 1 for laminar flow; curve 2 for turbulent flow; curve 3 is the plot for the universal law of friction. K_S is equivalent to the local roughness μ_L , and R to δ , the duct opening.	70
C3.	Pressure contours for $Re=10,000$ and $50,000$ for COD-to-global-roughness ratio = 0.1, 0.5, 1, 5, and 10. For each case there are two pictures showing results for $Re=10,000$ and $50,000$, respectively.	74
C4.	Velocity fields for flows of $Re=10,000$ and $50,000$ with COD-to-global-roughness ratio = 0.1, 0.5, 1, 5, and 10.	77
C5.	Turbulence intensity contours for flows of $Re=10,000$ and $50,000$ with COD-to-global-roughness ratio = 0.1, 0.5, 1, 5, and 10.....	80
C6.	Detailed velocity profiles for a tight duct at $Re=50,000$. Fully developed velocity profiles are observed before and after the turn.	80
C7.	Friction coefficient vs. Reynolds number for different δ/μ_g values.....	81
C8.	Friction coefficient as a function of the ratio of COD to global roughness.	82
C9.	Friction coefficient as a function of ratio of COD to global roughness for different local roughnesses.....	83
C10.	Comparison of calculated flow flux vs. measured data.	87
C11.	Comparison of calculated flow flux and the measurements.	88
C12.	Comparison of calculated leak rate and the measurements	89
C13.	Measured versus predicted leak rate for COD = 0.02 mm.....	90
C14.	Measured versus predicted leak rate for COD = 0.04 mm.....	91
C15.	Measured versus predicted leak rate for COD = 0.074 mm.....	91
C16.	Measured versus predicted leak rate for COD = 0.108 mm.....	92
C17.	Measured versus predicted leak rate for COD = 0.2 mm.....	92
D1a.	Predicted leak rate versus crack length for large-diameter PWR piping.	96
D1b.	Predicted leak rate versus crack length for large-diameter PWR piping (log-log scale showing power law correlation).	97
D2.	Predicted leak rate versus crack length for intermediate-diameter PWR piping.	98
D3.	Predicted leak rate versus crack length for small-diameter PWR piping.	99
D4.	Predicted leak rate versus crack length for large-diameter BWR piping.....	100
D5.	Predicted leak rate versus crack length for intermediate-diameter BWR piping.....	101
D6.	Predicted leak rate versus crack length for small-diameter BWR piping.	102
D7.	Effect of surface crack depth on critical crack length as a function of diameter (PWR SS piping).	103
D8.	Effect of surface crack depth on critical crack length as a function of diameter (PWR CS piping).	104

D9. Effect of surface crack depth on critical crack length as a function of diameter (BWR SS piping).	105
D10. Effect of surface crack depth on critical crack length as a function of diameter (BWR CS piping).	106
D11. Effect of residual stresses on critical crack length as a function of diameter (PWR SS piping).	107
D12. Effect of residual stresses on critical crack length as a function of diameter (PWR CS piping).	108
D13. Effect of residual stresses on critical crack length as a function of diameter (BWR SS piping).	109
D14. Effect of residual stresses on critical crack length as a function of diameter (BWR CS piping).	110

Tables

1.	Typical RCS piping used for sensitivity studies.....	3
2.	Estimated mean and standard deviation of crack morphology parameters.....	10
3.	Matrix of variables for leak rate calculations using windows SQUIRT 1.1.....	15
4.	PWR stainless steel piping cases with PWSCC degradation mechanism.....	16
5.	BWR stainless steel piping cases with PWSCC degradation mechanism.....	17
6.	PWR carbon steel piping cases with corrosion fatigue degradation mechanism.....	18
7.	BWR carbon steel piping cases with corrosion fatigue degradation mechanism.....	19
8.	Sensitivity runs for BWR and PWR cases – leak rate versus percent of critical crack lengths.....	21
9.	Leakage requirements for PWRs not in the standard technical specifications.....	28
10.	Variability of throughwall crack lengths for a given leak rate in SS (PS cases) and carbon steel (PC cases) piping in PWR RCSs.....	33
11.	Effectiveness of leak monitoring systems.....	36
12.	Average reported median leak rate range for sump pump, radiation monitors, and other leak detection methods.....	40
13.	Reported leak rates for valves, pumps and CRDM.....	40
14.	Reported leak rates for cracks and valves and pump seals.....	41
15.	Estimated leakage sensitivity for the ALUS acoustic monitoring system as a function of background noise level.....	44
A-1.	BWR LOCA–Sensitive Piping Systems.....	57
A-2.	PWR LOCA–Sensitive Piping Systems.....	58
A-3.	BWR Reference Case Conditions.....	59
A-4.	PWR Reference Case Conditions.....	60
A-5.	Pressurizer Failure Scenarios.....	61
A-6.	Reactor Pressure Vessel (RPV) Failure Scenarios.....	62
A-7.	Valve Failure Scenarios.....	63
A-8.	Pump Failure Scenarios.....	64

Executive Summary

In response to the vessel head event at the Davis-Besse reactor, the NRC formed a Lessons Learned Task Force (LLTF). The LLTF conducted an independent evaluation of the NRC's regulatory processes related to ensuring reactor vessel head integrity in order to identify and recommend areas of improvement applicable to the NRC and the industry. Four action plans were formulated to respond to the recommendations. The plans involve barrier integrity, stress corrosion cracking (SCC), operating experience, and inspection and program management.

This report is intended to provide a technical basis for determining the technical feasibility of implementing recommendation LLTF: 3.2.1(1) – *Improve the requirements pertaining to leakage detection to ensure that RCS [reactor coolant system] unidentified leakage can be discriminated from RCPB (reactor coolant pressure boundary) leakage and provide reasonable assurance that plants are not operated at power with RCPB leakage.* It does not include safety or cost analyses. The structural calculations provide insights into the degree of defense in depth provided by leak detection systems. This provides a technical basis for assessing the potential benefit of improved leak detection and thus addresses LLTF: 3.1.5(1) – *Determine whether PWR (pressurized water reactor) plants should install on-line enhanced leakage detection systems on critical plant components, which would be capable of detecting leakage rates significantly less than 0.063 kg (1 gpm).*

A database that identifies the leak source, leak rate, and resulting actions from RCS leaks in U.S. LWRs was developed. For each leak event, the database describes the (a) Licensee Event Record (LER) number if an LER is the source of information, (b) location of leak, (c) leak rate [actual leak rate if known; however, for many cases the actual leak rates are small (<0.0006 kg/s; 0.01 gpm) and not known precisely, although some qualitative information (“slowly dripping”, etc.) are available], (d) operation of reactor when leak was detected, (e) how the leak was detected, (f) the basis for the decision that a leak has occurred, (g) time required to recognize there was a unidentified leak, (h) action that was taken, (i) relevant nondestructive and destructive evaluation reports, (j) cause of leak, (k) leakage requirements, (l) crack type and size if crack was cause of leak, and (m) any environmental impact. The database also includes information on the leak detection systems, including (a) method of detection, (b) vendor for system, (c) sensitivity, (d) reliability, (e) response time, (f) accuracy, (g) estimated false alarm rate, (h) area of coverage, (i) maintenance required, (j) training required for its implementation, (k) calibration procedures, (l) site validation procedure, (m) experience under field conditions, and (n) source of information.

The analysis of leak events show that (a) many leaks reported are very small (<0.0006 kg/s; 0.01 gpm) are detected visually, and are reported as drips, weeping, seepage, “very small” boric acid deposits, etc., (b) large leaks have been detected primarily through inventory balance, change in pressure, rise in sump level, or radiation alarms, (c) almost 20% of the leaks in the database involved a weld with about 8% of the leak events reviewed involving the control rod drive mechanism (CRDM), usually detected through visual detection of boric acid crystals, and (d) cracks were involved with leaks about 40% of the time with a wide range of leak rates (<0.0006 kg/s to >6.3 kg/s; <0.01 gpm to >100 gpm).

The capabilities of each type of leakage detection system currently considered acceptable in Regulatory Guide (RG) 1.45 were evaluated to determine their sensitivity, reliability,

response time, and accuracy. Although not currently included in RG 1.45, an acoustic emission crack monitoring system capable of detecting crack initiation and growth before a leak occurs was also evaluated. In addition, technology that can monitor or detect other (noncracking) degradation modes such as boric acid corrosion or erosion/corrosion was studied.

These evaluations show that leak detection technology is available that can be used to provide greater detection sensitivity and more accurate determination of leakage locations. Even some of the existing systems have sufficient sensitivity to detect unidentified leakage of 0.032 kg/s (0.5 gpm) or even less.

Experiments and models for RCS leak rate were reviewed to identify correlations between crack size, crack-tip-opening displacement (CTOD), and leak rate. Sensitivity studies using SQUIRT (Seepage Quantification of Upsets In Reactor Tubes) were carried out to correlate crack parameters such as crack size and CTOD and leak rate for various types of crack configurations in RCS components.

Results from validation of the SQUIRT code are presented. For leak rates greater than 0.02 kg/s (0.32 gpm) most of the deviations between the data and the SQUIRT predictions are bounded by a factor of 2. Leak rates from tighter cracks are predicted less accurately. For leak rates less than 0.02 kg/s (0.32 gpm), the differences between the data and the SQUIRT predictions are bounded by factors of +10 and -5. Factors describing the roughness and tortuosity of the crack are part of the input to SQUIRT. For very tight cracks, these parameters are dependent on the crack opening displacement (COD), but the relations between these factors and the crack opening displacement are not precisely known.

The results obtained for crack lengths at various leak-rate values were compared to the critical crack length for which the specified value of the bending moment represents the maximum load to obtain a "margin of safety" against additional crack growth. Calculations giving the percent of critical crack length versus diameter for boiling water reactor (BWR) cases at 50% Service Level A stresses and leak rates versus percent of critical crack lengths were carried out for this study. Such calculations give an estimate of the margins of safety for typical piping joints under normal operating loads.

For most piping systems, the model calculations show that the current technical specification limits on unidentified leakage provide a significant margin against gross structural failure. However, a bounding analysis of the leakage from a CRDM annulus for circumferential cracks above the J-weld shows that the typical 0.063-kg/s (1 gpm) leakage specification would not be exceeded even for cracks large enough for incipient CRDM tube failure.

Although the current requirements provide margin against gross structural failure in most cases, a 0.063 kg/s (1 gpm) leak could correspond to a crack of length from 26 to 460 mm (1.0 to 18.1 in.) for stainless steel piping and 51 to 310 mm (2.0-12.2 in.) for carbon steel piping, depending on pipe diameter and the loading during normal operation. Because the throughwall crack length corresponding to a given leak rate, Q , varies as $\approx Q^{0.24}$, decreasing the threshold leak rate by a factor of 2, decreases the possible crack lengths by only about 20%.

Localized leak detection systems such as acoustic emission and humidity monitors as well as video systems would be required to obtain significant additional margin for those portions of the RPCB for which global leakage monitoring may give very little assurance against a significant loss-of-coolant accident (LOCA) and to provide a high degree of assurance that leak rates are low enough to minimize high corrosion rates due to boric acid corrosion. Such localized leak systems would also help discriminate between RCS and RCPB leaks.

Significant improvements in leak detection capability will require new systems which are sensitive and accurate, and which provide the location of leaks and thus help to minimize unnecessary shutdowns. Newer, commercially available systems (with vendor reported sensitivity) include acoustic emission (AE) monitoring [ALUS; 0.0002 to 0.016 kg/s (0.003 to 0.25 gpm)], humidity sensors [FLUS; 0.0003 to 0.032 kg/s (0.005 to 0.5 gpm)], and air particulate detectors [ARMS; <0.006 kg/s (0.1 gpm)]. Instrumentation of the pressure vessel head with an acoustic emission (AE) system has a demonstrated capability to detect leaks as small as 0.0003 kg/s (0.005 gpm). While additional technologies for leak detection, such as the detection of boric acid leaks by using infrared (IR) spectroscopy to detect boric acid vapor in the vessel head (VH) region, may be possible, existing technologies, especially AE, already offer demonstrated capability and great flexibility. There is little need for additional research on fundamentally different approaches to leak detection technology at this time.

In addition to early detection of leaks, AE sensors can be used on components of special interest to detect crack initiation and growth during plant operation. This use is already incorporated in the ASME Pressure Vessel Code Section XI as a substitute for ultrasonic monitoring of known non-throughwall cracks. AE systems have been installed in operating reactors and have been shown to tolerate reactor environments, including significant radiation fields. Broader demonstration of AE capability and implementation of AE monitoring of crack growth during plant operation could have significant advantages over current inspection and monitoring approaches. Cracks in targeted areas could be detected prior to leakage. On-line monitoring of cracks could replace periodic ultrasonic technique (UT) inspections, which could result in significant cost savings. Cracks could be detected at locations not normally inspected, or in materials where UT inspection has not been appropriately demonstrated (i.e., cast stainless steels). With greater assurance that no cracks of significant size exist, current leak-before-break requirements could be relaxed.

If RG 1.45 is revised, then inclusion of acoustic emission monitoring as an acceptable method for leak detection should be considered. Because of the reductions in coolant activity levels, the value of monitoring gaseous radioactivity is greatly diminished. Elimination of gaseous radioactivity monitoring should be considered in any revision of RG 1.45, as it can no longer be considered an adequate substitute for particulate monitoring.

Acknowledgments

The authors gratefully acknowledge the contributions, suggestions, and guidance of Cayetano Santos, Makuteswara Srinivasan (program manager), and Dr. Joseph Muscara (Senior Technical Advisor). The authors also acknowledge the contributions of Jonathan Meagher. This work was sponsored by the Office of Nuclear Regulatory Research, U. S. Nuclear Regulatory Commission, under Job Code Y6869.

Acronyms and Abbreviations

ADAMS	(U.S. NRC) Agency-wide documents access and management system
AE	Acoustic emission
AEM	Acoustic emission monitoring
ALUS	Acoustic leak detection system
ANL	Argonne National Laboratory
ARMS	Airborne Particulate Radioactivity Monitoring
ASME	American Society of Mechanical Engineers (Boiler & Pressure Vessel Code)
BWR	Boiling water reactor
CFM	Computational fluid mechanics
COD	Crack opening displacement
CRDM	Control rod drive mechanism
CTOD	Crack-tip-opening displacement
DOP	Diethyl phthalate
DPZP	Dimensionless plastic zone parameter
EdF	Electricité de France
EPRI	Electric Power Research Institute
FLÜS	Humidity-leakage monitoring system
GDC	General Design Criteria
gpm	Gallons per minute
IGSCC	Intergranular stress corrosion cracking
IR	Infrared
ISA	Instrument Society of America
LB	Licensing basis
LBB	Leak before break
LER	Licensee event report
LLTF	Lessons Learned Task Force
LOCA	Loss of coolant accident
LWR	Light water reactor
NRC	U.S. Nuclear Regulatory Commission
NRCPIPE	Code for predicting crack-opening displacement for circumferential cracks
PICEP	Pipe Crack Evaluation Program
PNNL	Pacific Northwest National Laboratory
PWR	Pressurized water reactor
PWSCC	Primary water stress corrosion cracking
PZT	Piezoelectric transducer
RCPB	Reactor coolant pressure boundary
RCS	Reactor coolant system
RG	Regulatory guide
RPV	Reactor pressure vessel
RVH	Reactor vessel head
SCC	Stress corrosion cracking; stress corrosion cracks
SKI	Swedish Nuclear Power Inspectorate (Statens Kärnkraftinspektion)
SQUIRT	Seepage Quantification of Upsets In Reactor Tubes
SS	Stainless Steel
T/H	Thermal/hydraulic
UT	Ultrasonic (technique) inspection

VHP
VICNIS

Vessel head penetration
Vessel Integrity Control using Nitrogen-13 Sensor

1. Introduction

In light water reactors, the integrity of the reactor coolant pressure boundary (RCPB) is important to safety because it forms one of the three defense-in-depth barriers to the release of radioactivity. General Design Criteria (GDC) 14, 30, and 32 of Appendix A to 10 CFR Part 50 specify the following requirements for the RCPB:

GDC 14 states in part that; “the reactor coolant pressure boundary shall be designed, fabricated, erected, and tested so as to have an extremely low probability of abnormal leakage.”

GDC 30 states in part that; “means shall be provided for detecting and, to the extent practical, identifying the location of the source of reactor coolant leakage.”

GDC 32 states in part that; “components which are part of the reactor coolant pressure boundary shall be designed to permit periodic inspection and testing of important areas and features to assess their structural and leak-tight integrity.”

One of the primary challenges to the integrity of the RCPB is stress corrosion cracking (SCC). Primary water stress corrosion cracking (PWSCC) of Alloy 600 nozzles was first observed in pressurizer instrument nozzles in a number of U.S. reactors in 1986. In 1991, similar cracking was found in vessel head penetration (VHP) nozzles at a French plant (Bugey). At the time, it was thought that circumferential cracking of Alloy 600 nozzles was unlikely. However, in 2001, inspections at the Oconee Nuclear Station revealed significant circumferential cracks in VHP nozzles. As a result of the Oconee event and some subsequent findings at other reactors, the NRC issued Bulletin 2001-01 requesting information to verify that licensees were in compliance with existing regulations with respect to the integrity of the RCPB.

In March 2002, while inspections were underway in response to Bulletin 2001-01, three control rod drive mechanism (CRDM) nozzles with indication of through-wall axial cracking that resulted in RCPB leakage were identified at the Davis-Besse Nuclear Power Station. During the nozzle repair activities, the licensee removed boric acid deposits from the reactor vessel head (RVH), conducted a visual examination of the area, and identified a cavity (178 mm by 102-127 mm)] at the widest part that extended down to the stainless steel cladding on the downhill side of nozzle 3. The extent of the damage indicated that it had occurred over an extended period, and that the licensee’s programs to inspect the reactor pressure vessel (RPV) head and to identify and correct boric acid leakage were ineffective.

In response to the Davis-Besse event, the NRC formed a Lessons Learned Task Force (LLTF). The LLTF conducted an independent evaluation of the NRC’s regulatory processes related to ensuring RVH integrity in order to identify and recommend areas of improvement applicable to the NRC and the industry. Four action plans were formulated to respond to the recommendations. The action plans involve barrier integrity, stress corrosion cracking, operating experience, and inspection and program management. One part of the action plan on barrier integrity is an assessment of potential safety benefits of changes in requirements pertaining to leakage in the reactor coolant system (RCS).

Leakage limits alone cannot be relied upon to ensure the RCPB integrity. Detectable leakage could indicate the pressure boundary has already been breached, although the pressure boundary may still be able to perform its intended safety functions. In addition, the leakage expected from stress corrosion cracks in susceptible RCPB components may result in leak rates too small to be detected (in some cases, no leakage would occur under normal operating conditions).

To prevent a breach (through-wall flow) of the RCPB, we currently rely on periodic inspection of RCPB components. An additional approach would be to monitor continuously the RCPB (or critical locations or components) by methods capable of detecting material degradation before leakage occurs. The two approaches could be implemented in combination to provide greater assurance of barrier integrity.

From a practical standpoint, the RCPB cannot be made completely leak-tight because some leakage will occur through pump and valve seals, etc. However, as part of a defense-in-depth philosophy for ensuring the integrity of the RCPB, improved leakage requirements (e.g., establishment of action requirements based on increases in unidentified leak rates, and more accurate identification, measurement, and collection of leakage from known sources to minimize interference with the detection of leakage from unknown sources) could better identify RCPB breaches. This knowledge would allow reactor operators to take action to prevent additional degradation of the pressure boundary. Such improvements could be achieved through additional requirements on the use of existing leak detection systems [e.g., reductions in the global leakage limits to 0.032 kg/s (0.5 gpm)]. However, existing systems may not be adequate to provide assurance that leakage is low enough to avoid boric-acid induced corrosion of carbon and low alloy steel components.

A distinction should be made between the objectives of this effort to study leakage events and the capabilities of leakage monitoring systems and the objectives of leak-before-break (LBB) evaluations for piping systems. The LBB evaluation is used in U.S. nuclear power plants to allow the removal or noninstallation of pipe-whip-restraints and jet impingement shields designed to mitigate the effects of postulated pipe ruptures. Before new requirements can be implemented, the basis for all existing leakage requirements needs to be reevaluated. The current study entails a survey of plant experiences with RCS leakage, an evaluation of plant leakage detection system capabilities, a determination of the abilities of state-of-the-art leak detection systems, and an evaluation of critical leak rates. The capabilities of various systems that can continuously monitor or inspect the integrity of fluid pressure boundaries have been evaluated, as has been the feasibility of using correlations between leak rate and crack sizes to establish leakage limits. The majority of this effort has involved reviews of operating experience and earlier research studies. Areas where additional analytical or experimental efforts are needed have been identified.

2. Determination of RCS Components Susceptible to Stress Corrosion Cracking

As part of the NRC's Elicitation Program on the re-definition of large-break loss-of-coolant accidents (LB-LOCA), a comprehensive table of failure scenarios of RCS components was developed. A compilation of these tables is provided in Appendix A and was used as the basis for selecting components for further sensitivity analysis.

For the purpose of the sensitivity calculations, the RCS components selected were classified into large-, intermediate-, and small-diameter carbon and stainless steel piping typically used in BWRs or PWRs. Table 1 shows the type of piping system represented by the various pipe sizes and materials chosen for the sensitivity analyses.

Table 1. Typical RCS piping used for sensitivity studies (SS = stainless steel, CS = carbon steel, IGSSC = intergranular stress corrosion cracking).

Case No.	Piping System	Material	Material Spec	Outer Diameter mm	Wall Thickness mm	Weld Metal	Cracking Mechanism
BWR-1	Side Riser	SS	TP304	711	36	SS Flux	IGSCC
BWR-2	Main Steam	CS	A516Gr70	711	36	CS Flux	Corr Fatigue
BWR-3	Recirc Branch Line	SS	TP304	324	17	SS Flux	IGSCC
BWR-4	Feedwater	CS	A106B	324	17	CS Flux	Corr Fatigue
BWR-5	Bypass Line	SS	TP304	114	8.6	SS Flux	IGSCC
BWR-6	Reactor Water Clean-up	CS	A106B	114	8.6	CS Flux	Corr Fatigue
PWR-1	Main Coolant	SS	CF8M	813	76	SS Flux	Thermal Fatigue
PWR-2	Main Coolant	CS	A516Gr70	813	76	CS Flux	Corr Fatigue
PWR-3	Surge Line	SS	CF8M	356	914	SS Flux	Thermal Fatigue
PWR-4	Feedwater	CS	A106B	356	914	CS Flux	Corr Fatigue
PWR-5	Spray Line	SS	TP304	114	13	SS Flux	IGSCC
PWR-6	SG Blowdown Line	CS	A106B	114	13	CS Flux	Corr Fatigue

3. Review of RCS Leakage Experiments and Leak-Rate Models

Essentially three major sets of leak-rate experiments are available for comparison with predictive models. The initial sets of data used to validate the SQUIRT code [1], includes the Sozzi and Sutherland (1975) data, the Collier (1975) data on tight slits, the Yano (1987) data, the Amos and Shrock (1983) data, and the Collier (1984) IGSCC cracked pipe data. The tight slit and IGSCC cracked pipe data of Collier et al. were developed for the Electric Power Research Institute (EPRI) [2]. More recent sets of data were developed in Japan by Hitachi [3] and in Canada by Ontario-Hydro [4]. All of these tests involved two-phase flow of subcooled water through cracks or tight slits to simulate cracks with different roughnesses and crack openings. All the available data have been used to benchmark leak-rate model predictions.

Figure 1 shows results from the original validation of the SQUIRT code. The most pertinent data are from the Collier IGSCC cracked-pipe tests done at Battelle for EPRI, the other data are for slits or capillaries. Above 0.02 kg/s (0.32 gpm) there is less scatter in the data, i.e., most of the data are within a factor of 2 of the predicted values. Below 0.02 kg/s (0.32 gpm) the scatter of the data is larger, and the data can differ from the predicted values by factors of +10 and -5. The IGSCC cracks with larger openings (Cases H and I in Fig. 1) fell within the scatter of the rest of the data, but as expected, the prediction of the leak rates from tighter cracks [crack opening displacement (COD) < 0.1 mm] are less accurate.

The Japanese experiments [3] were conducted primarily using plate test specimens with well-defined COD, crack length, and surface roughness values. Tests were also done with water or steam in pipes with fatigue cracks. These data are compared with the SQUIRT and PICEP (Pipe Crack Evaluation Program) codes in Fig. 2. These are the only data for the flow of saturated steam, which is important for the validation of leak-detection models for steam lines. SQUIRT and PICEP appeared to give reasonable predictions for leak rates of about 0.02-0.05 kg/s (0.3 to 0.8 gpm). At leak rates above ≈ 0.13 kg/s (2 gpm), the analyses underpredict the experimental leak rates for a given crack and crack-opening displacement. PICEP was a little more conservative than SQUIRT at the lowest leak rates. Under-prediction of the leak rate is conservative for LBB analyses.

The Ontario-Hydro experiments [4] employed circumferential crack geometries that were precise, smooth-surfaced, straight-sided, and artificial. Some single-phase leak rate tests at low temperatures were performed. The experimental results are compared with the SQUIRT predictions in Fig. 3. Most of the test results were predicted well, within a factor of $\pm 20\%$, with more scatter below a leak rate of 0.15 kg/s (2.3 gpm).

Leak Rate Models

The most frequently used software packages for predicting leak rates in RCS piping components in the US are the PICEP and SQUIRT codes. Both use the same Henry-Fauske model for flow-through tubes to describe two-phase flow through the crack. The PICEP [5] software code was developed for EPRI by Collier at Battelle. PICEP can be used to compute two-phase flow rates through cracks in LWR piping systems given the material properties of the piping, thermo-hydraulic conditions under load, crack geometry, crack type, and orientation.

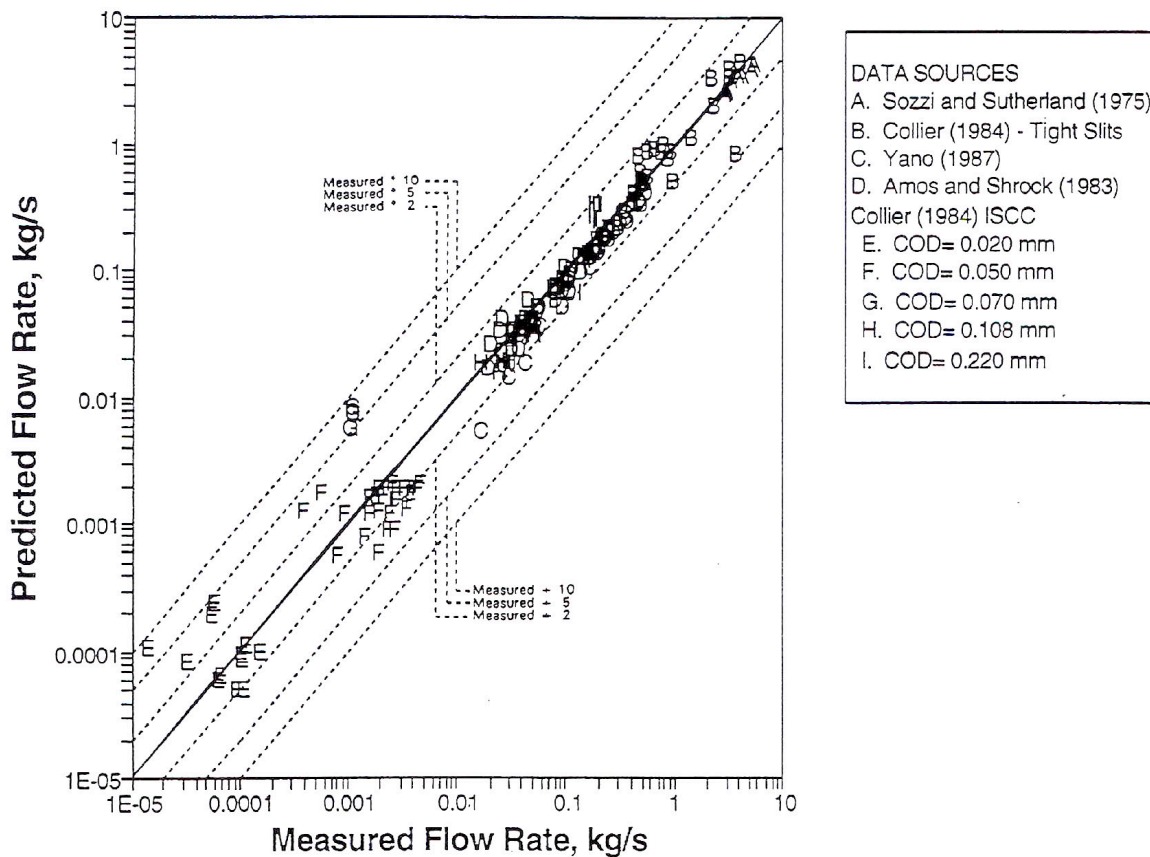


Figure 1. Comparison of two-phase flow leak rate tests used to validate the initial SQUIRT model.

The second software code for predicting leak rates, SQUIRT Version 2.2, was developed by Battelle for the USNRC [1]. This software package included improvements in the basic thermohydraulic model used in the earlier versions of the code and in the fracture mechanics analysis portion of the code, which was derived from the NRC PIPE code for predicting crack-opening displacement for circumferential cracks in piping [6].

As part of the ongoing LB-LOCA program for the NRC, additional improvements have been made in SQUIRT. These included the following [7]:

- Upgrading of SQUIRT to operate in an MS Windows environment,
- Elimination of duplicate modules within SQUIRT, such as SQUIRT1 and SQUIRT3,
- Incorporation of corrections for the effect of weld residual stresses on leak rate,
- Setting of default parameters for PWSCC crack morphologies,
- Incorporation of the NUREG/CR-6004 Crack Morphology Correction Module [8], and
- New Thermal/Hydraulic (T/H) Modules for all liquid and all steam cases.

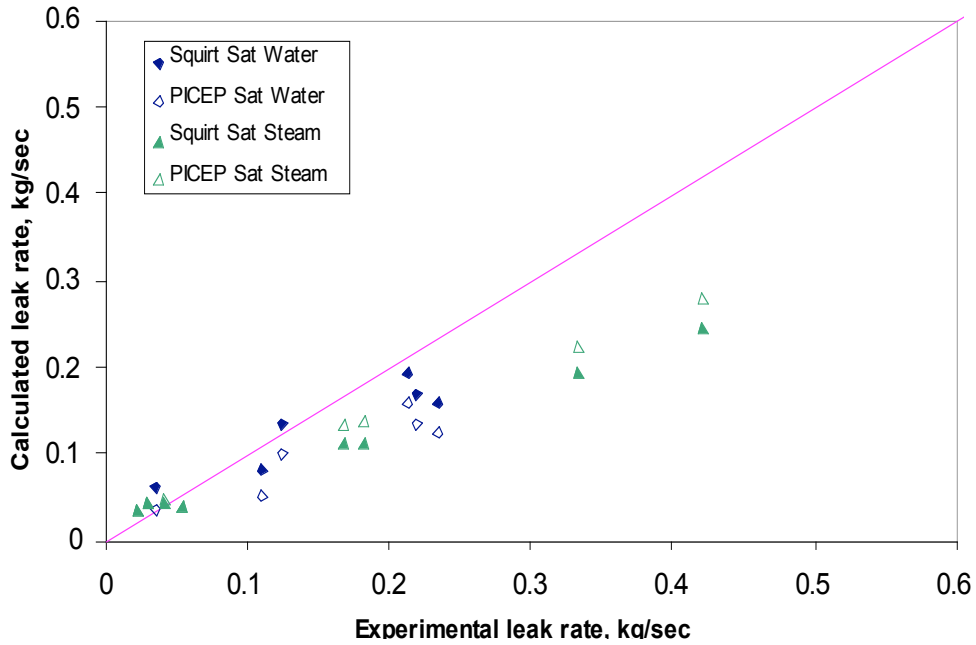


Figure 2. Comparison of PICEP- and SQUIRT-predicted leak rates with experimentally measured leak rates from Japanese leak-rate experiments [3].

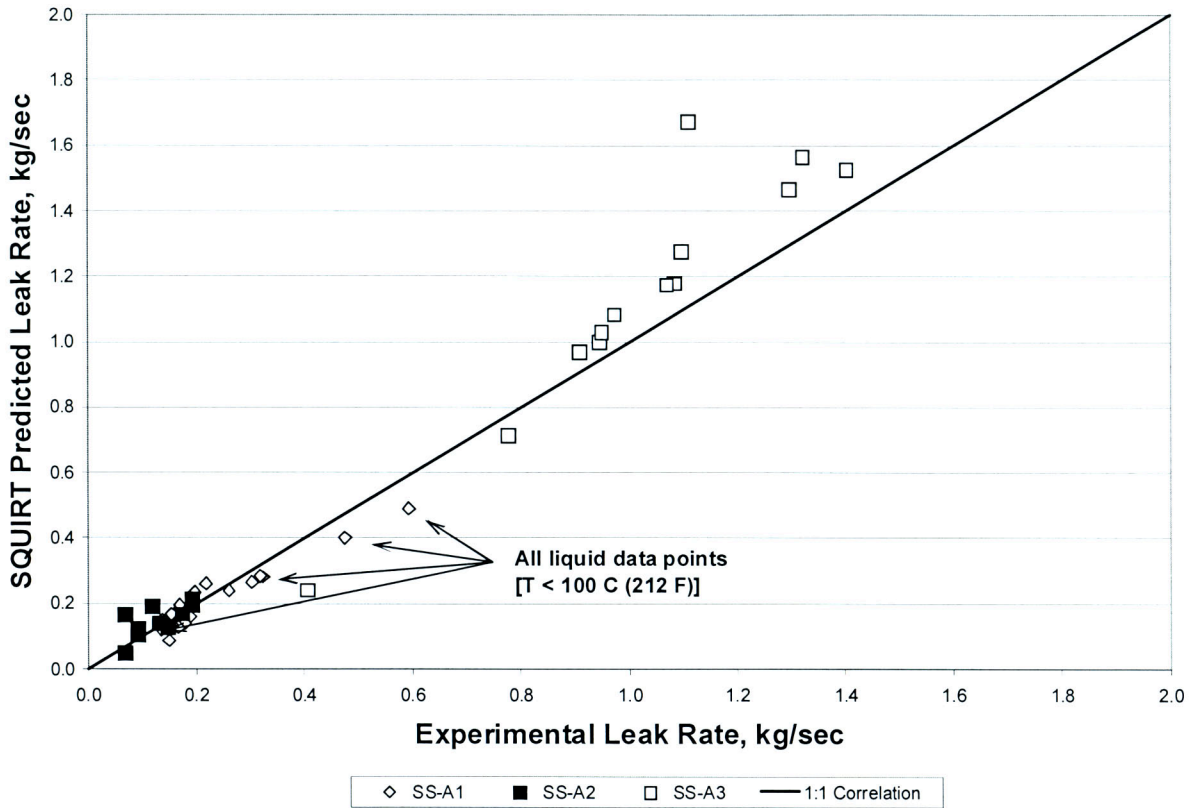


Figure 3. Comparison of SQUIRT-predicted leak rates versus experimentally measured leak rates for Ontario-Hydro experiments [4].

Additional comparisons were also made between SQUIRT predictions and existing experimental data on leak rates. Figures 2 and 3 show comparisons for the new version of SQUIRT.

Sensitivity Studies

Importance of Crack Morphology Parameters and Effect of COD

Recent NRC studies have shown that the selection of the crack morphology parameters describing the crack flow path has a significant impact on predicted leak rates. The crack morphology parameters are the surface roughness, the number of turns the crack takes, and the ratio of the actual flow path length to the thickness of the pipe. Based on a study of numerous cracks removed from service, it was determined that the proper values for these parameters were dependent on the crack-opening displacement [8]. For a very tight IGSCC the appropriate roughness is that along the grain boundary, and as the crack goes from one grain to the next there could be a turn. In such a case the roughness is low, but the number of turns is high, and the actual length of the flow path is much greater than the thickness of the pipe. On the other hand, if the crack opening is very large compared to the grain size, then the appropriate roughness would be that corresponding to about half of the grain size, there would be very few turns, and the length of the flow path would be close to the thickness of the pipe.

Figure 4 illustrates the two situations. When the COD is comparable to the grain size, the local surface roughness is that along the grain boundary for an IGSCC, and the number of turns is large. For the case when the COD is large compared to the grain size, the roughness is on the order of the mean grain size, and the number of turns is much smaller.

Before the publication of NUREG/CR-6004 [8], the crack-morphology parameters were considered to be independent of COD. In NUREG/CR-6004, it was recognized that the appropriate roughness should be large (global) or small (local) depending on whether the COD is large or small. In this report, the dependence of surface roughness, μ , and other crack morphology parameters on COD was assumed to be piecewise linear. The roughness, μ , is given by Equation 1.* The dependence of μ , the number of turns, and flow path to the thickness ratio on COD is shown in Fig. 5. The key scale parameter is the ratio of the crack-opening displacement (δ) to the global surface roughness (μ), which is comparable to the grain size. As given in Equation 1 and shown in Fig. 5, if the COD is larger than the global roughness, then the global roughness should be used. If the COD is much smaller than the global roughness, then the local roughness should be used. The use of COD-dependant relationships like that in Equation 1 is needed to get reasonable results from the leak-rate models for very tight cracks. Figure 3 shows that predictions using the COD-dependant relationships are in agreement with experimental data even for leak rates <0.013 kg/s (0.2 gpm).

The piecewise linear models shown in Fig. 5 were developed by Dr. G. Wilkowski and Dr. D. Paul and are based on engineering judgment. Predictions from these models agree with the

* Equations similar to Equation 1 exist for the number of turns and actual flow path to pipe thickness ratio. These are illustrated in Figure 5.

limited data available for tight geometries. The models are thought to be conservative for LBB analyses, i.e., they will underpredict the leakage through tight cracks.

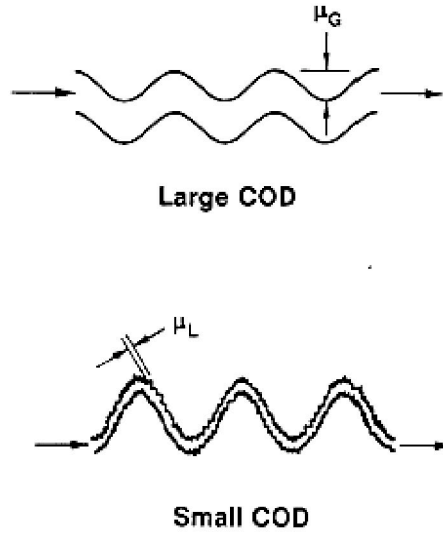


Figure 4. Local and global surface roughness and number of turns.

$$\mu = \begin{cases} \mu_L, & 0.0 < \frac{\delta}{\mu_G} < 0.1 \\ \mu_L + \frac{\mu_G - \mu_L}{9.9} \left[\frac{\delta}{\mu_G} - 0.1 \right], & 0.1 < \frac{\delta}{\mu_G} < 10 \\ \mu_G, & \frac{\delta}{\mu_G} > 10 \end{cases} \quad (1)$$

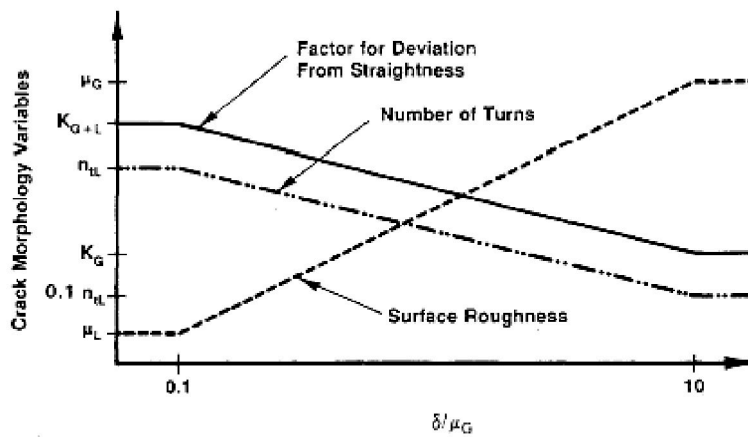


Figure 5. Crack morphology variables versus normalized COD.

However, the transition values of δ/μ_G could be better defined either by experiments or computational fluid dynamics (CFD) analysis. Some initial CFD analyses were undertaken to see if this could be done. Figure 6 shows some initial CFD results. The leak rate from the CFD models can be normalized and compared to the results of approximate equations like Equation 1.

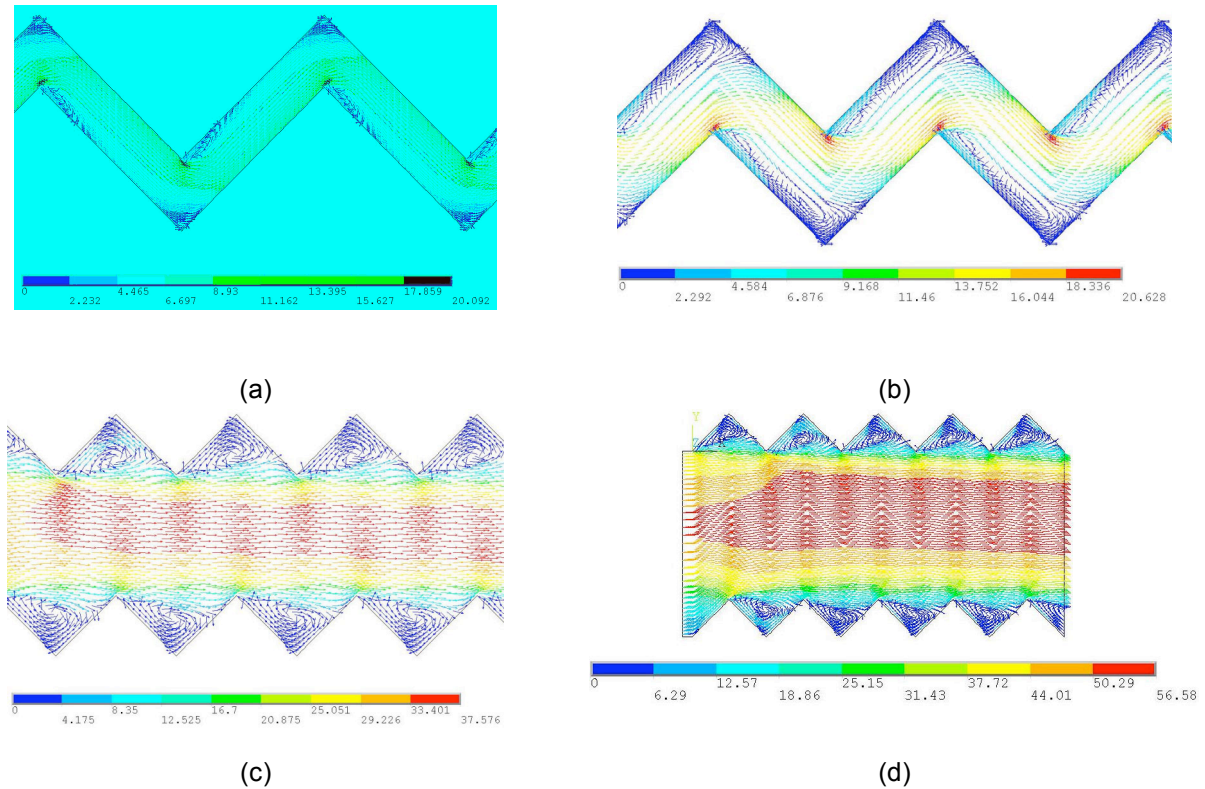


Figure 6. Fluid flow velocity field inside crack: (a) $\delta/\mu_G = 0.5$, (b) $\delta/\mu_G = 1.0$, (c) $\delta/\mu_G = 3.0$, and (d) $\delta/\mu_G = 5.0$. Flow conditions: $P = 2250$ psi (15.5 MPa), $T = 550^\circ\text{F}$ (288°C), pipe thickness = 1 in. (25.4 mm). Single-phase all liquid water flow, and no local surface roughness.

From the results for the large crack opening, it appears that a better normalizing parameter might be $\mu_G/(\delta-\mu_G)$ rather than μ_G/δ . The development of the CFD model and a 2-D analysis for an improved basis for modeling crack morphology parameters are described in Appendix C.

Variation in Leak Rate due to Statistical Variation of Crack Morphology Parameters

In order to understand what information a leak rate provides about the cracks that may be present in the RCPB, it is important to understand how the crack morphology parameters can affect the leak rate through a crack of a given size. In NUREG/CR-6004 [8], statistical distributions for the roughness (local and global), number of turns (local and global), and actual flow path to thickness ratios (local and global) were determined from studies of service-removed cracks. Such distributions were developed for several types of cracks, but the effort

focused on IGSCC in BWR piping and corrosion fatigue cracks. More recently, distributions for the morphology appropriate for PWSCC in Alloy 600 and 82/182 welds were developed[9]. If the crack grows through the main part of the Alloy 82/182 weld, then the crack morphology parameters in Table 2 are applicable. Cracks in the weld butter regions can grow perpendicular to the weld, and in the only service crack case available, the crack had a much higher global roughness and actual flow path to thickness ratio than indicated by the crack morphology parameters in Table 2.

Table 2. Estimated Mean and standard deviation of crack morphology parameters.

Crack Morphology Variable	Corrosion Fatigue		IGSCC		PWSCC – Alloy 600 Base		PWSCC – Weld ^a	
	Mean	Standard Dev.	Mean	Standard Dev.	Mean	Standard Dev.	Mean	Standard Dev.
$\mu_L, \mu\text{m}$	8.814	2.972	4.70	3.937	10.62	9.870	16.86	13.57
$\mu_G, \mu\text{m}$	40.51	17.65	80.0	39.01	92.67	65.26	113.9	90.97
n_L, mm^{-1}	6.730	8.070	28.2	18.90	8.043	2.043	5.940	4.540
K_G	1.017	0.0163	1.07	0.100	1.060	0.095	1.009	0.011
K_{G+L}	1.060	0.0300	1.33	0.170	1.327	0.249	1.243	0.079

^aCrack growth parallel to long direction of dendritic grains, i.e., not in buttered region of pipe girth weld.

Figure 7 shows the variability in leak rate that can be observed when the crack length is held constant and the crack morphology parameters are independently varied based on the statistical distributions in Table 2. The ratio between the mean value and the 2-percent upper fractile is typically a factor of ~2. For the relatively large leak rate shown in Fig. 7, the variability in leak rates due to the variability in the crack morphology parameters is consistent with the scatter in the observed and predicted results shown in Fig. 1. The variability in the leakage rate due to variation in the morphology parameters is not sufficient to account for the scatter in the data at lower leak rates. For small cracks additional factors such as the effect of the difference between actual crack shape and the rectangular crack assumed in the model may have a significant effect.

Relative Leakage Crack Lengths due to Different Crack Morphology Parameters

In a study for the NRC on the effects of PWSCC cracks on LBB analyses [9], a comparison was made between the crack size used in actual LBB submittals (which assumed air-fatigue cracks with no turns so the crack length was quite short for the given leak rate) and the crack sizes that would be determined for PWSCC using the parameters in Table 2. Figure 8 compares the lengths of corrosion cracks with the lengths of air-fatigue cracks with the same leak rate. The results show that for a given leak rate, corrosion fatigue cracks would have to be 1.43 times longer than air-fatigue cracks, IGSCC cracks would have to be 1.89 times longer than air-fatigue cracks, and PWSCC cracks (growing parallel to the dendritic grains) would have to be 1.69 times longer than air-fatigue cracks. Hence, PWSCC cracks growing parallel to

the dendritic grains are bounded by IGSCC cracks. This is the direction that a PWSCC crack would grow in the main part of the weldment of a bimetallic weld, as shown in Fig. 9.

As noted previously, cracks in the butter region can grow perpendicular to the long dendritic grains in the weld. The only service-crack case of this type of cracking that has been

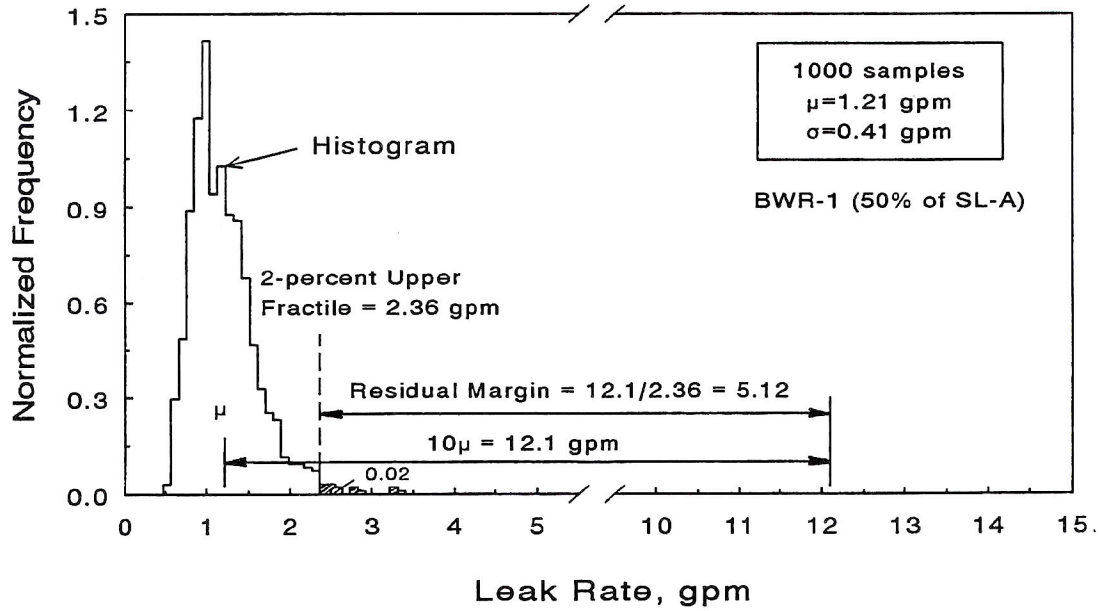


Figure 7. Histogram of leak rate at 50% Service Level A for case BWR-1 in NUREG/CR-6004 (IGSCC crack case).

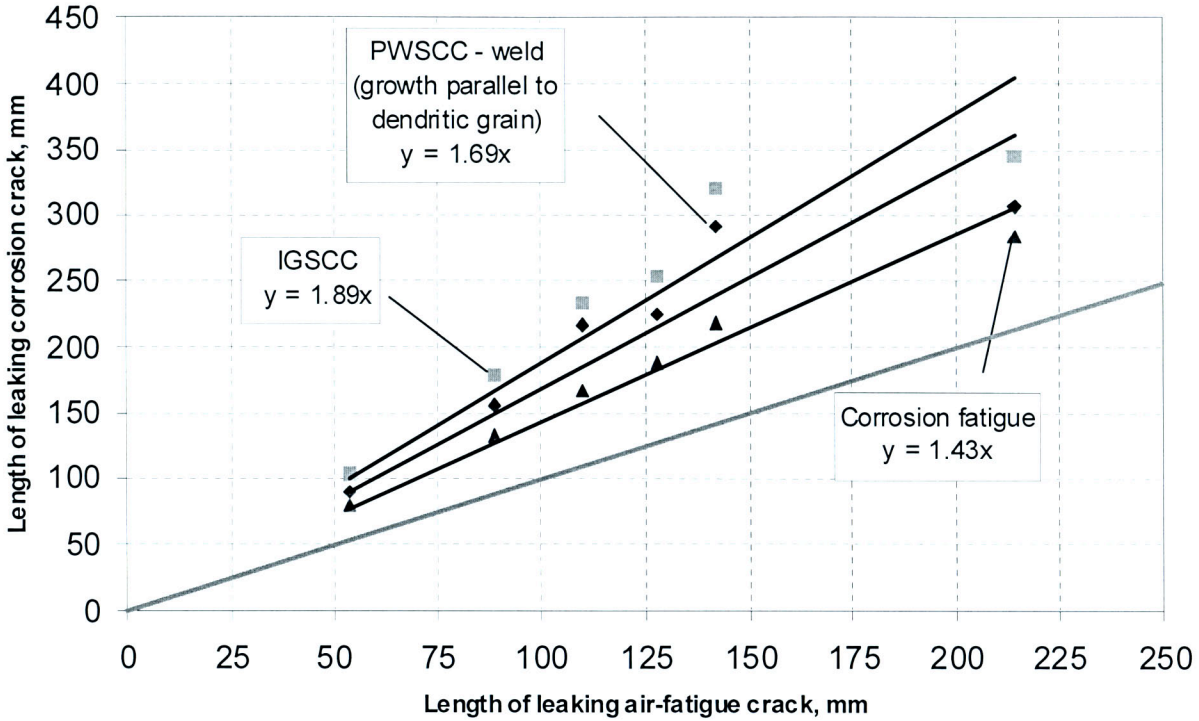


Figure 8. Length of leaking corrosion cracks along with the length of air-fatigue cracks for actual LBB submittal cases.

analyzed is shown in Fig. 10. The flow path length is tortuous. The length of the PWSCC crack is 2.2 times greater than that of the air-fatigue crack, which is much worse than the IGSCC crack. (However, the crack growth rate in this direction is probably slower than when the crack is growing parallel to the dendritic grains.)

In the analyses discussed in Section 4, the COD-dependent crack-morphology relationships illustrated in Fig. 5 are used with the default values in the SQUIRT code, i.e., the mean values in Table 2. The PWSCC values used were those for cracks growing in the main part of the weldment, not in the butter region. For the same leak rate, leaking PWSCC cracks in the butter region would be approximately 30% longer ($2.2/1.69 - 1$) than the PWSCC cracks growing parallel to the weld.

Leaks in CRDM Nozzle

In Ref. 10, leakage from a CRDM annulus was calculated for circumferential cracks above the J-weld. This calculation requires a leakage analysis that accounts for the pressure drops through both the circumferential crack and the annular region to the outside of the RPV head. The solution for the flow through the crack could not be obtained using the SQUIRT and PICEP leak-rate codes, because the leakage through the crack did not result in critical flow at the exit plane of the circumferential crack going into the annular region. The requirement of a critical flow velocity at the exit plane is a basic assumption of the Henry-Fauske analysis. A bounding value for the leak rate was obtained by assuming that the pressure drop in the crack could be ignored, and only the pressure drop through the annular region need be considered. Known values for the average shrink fit and detailed 3D finite-element analyses of the CRDM nozzle

deformations were used to determine the annular gap at the operating temperature. For these gap dimensions and typical surface roughness values for the ground tube and the reamed hole in the RPV head, the leak rate was below 0.063 kg/s (1 gpm). Since this was a bounding analysis that should overestimate the leak rate, the typical 0.063 kg/s (1 gpm) leakage specification would not appear to be exceeded even for cracks large enough to result in a limit-load failure of the CRDM tube.

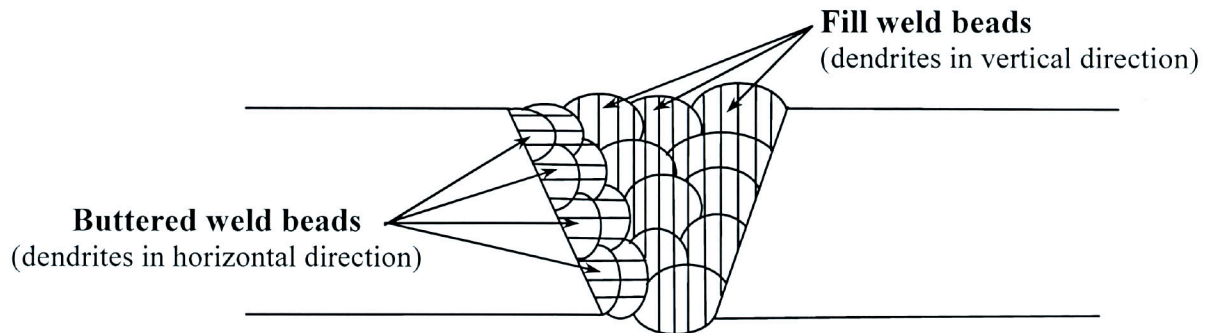


Figure 9. Schematic showing long direction of dendritic grains in the buttered regions and main butt weld fill beads.

New acoustic, radiation, and humidity systems for leak detection can have leak rate sensitivities on the order of 0.0003 kg/s (0.005 gpm). However, based on the volumes of boric acid that have been associated with most CRDM nozzle leaks, through-wall cracks up to 165° in extent can have much lower leak rates than this. Thus, it is not clear whether even such systems would provide substantial defense-in-depth against CRDM nozzle failure.

Crack growth and shortest path leakage direction

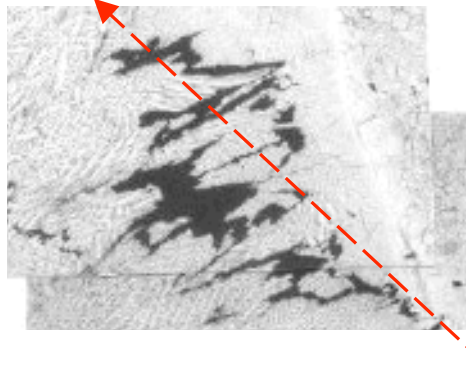


Figure 10. PWSCC growth across the long direction of the dendritic grains.

Determination of Leak Rates Expected from Typical SCC in RCS Components

Table 3 lists the various material, geometrical, and thermohydraulic parameters for BWR and PWR components that control leak rates and the range of values considered for these parameters in leak-rate computations. Tables 4 and 5 show the crack geometries that were investigated for BWR and PWR stainless steel piping with circumferential through-wall cracks (IGSCC for BWR and PWSCC for PWR). In all cases, the COD-dependent crack-morphology option in SQUIRT was used. As noted previously, using the COD-dependent parameters option gives better agreement with available data for low leak rates. In these calculations, the rotation of the crack faces due to residual stresses, which creates a diverging flow channel, was ignored, because prior studies showed this was not a large effect.

In Tables 4 and 5, a leak rate (such as 0.006, 0.063, 0.63 or 6.3 kg/s; 0.1, 1, 10 or 100 gpm) was specified for each run, and the total circumferential through-wall crack length was obtained as an output from SQUIRT. For some of these cases involving large leak rates [usually 6.3 kg/s (100 gpm) and in some cases 0.63 kg/s (10 gpm), problems occurred with numerical convergence for the algorithm within SQUIRT. For each pipe size the crack lengths were determined for three loading conditions corresponding to 25%, 50%, and 100% of normal operating stress at Service Level A (per ASME Section III). These should span the range of expected operating stresses, with the 50% Service Level A values representing the “typical” value.

The results obtained for crack lengths at various leak-rate values are compared to the critical crack length for which the specified value of the bending moment represents maximum load. These values were computed using NRCPIPE Version 3.0 and the dimensionless-plastic-zone-parameter (DPZP) analysis [11]. This computer code [6] was developed at Battelle for the NRC to predict moment-rotation behavior of circumferential through-wall-cracked piping under combined pressure-and-bending loads. The value of this critical crack length is also shown in Tables 4 and 5. The ratio of the crack length for the given leak rate to the critical crack length for the specified moment represents a “margin of safety” against additional crack growth. Note, however, that only Service Level A loads are considered in these calculations. The margins could be substantially smaller for accident or earthquake loads.

Table 3. Matrix of variables for leak rate calculations using windows SQUIRT 1.1.

Material Type	Variable Range for BWR's		Variable Range for PWR's	
	Stainless Steel (TP304)	Carbon Steel (A516 Grade 70)	Stainless Steel (TP304)	Carbon Steel (A516 Grade 70)
Material (Inconel may be used for some cases)				
Pipe Geometry				
Outer Diameter, in.	4.5, 12.75, 28	4.5, 12.75, 28	4.5, 14, 32	4.5, 14, 32
Wall thickness, in.	0.337, 0.687, 1.41	0.337, 0.687, 1.41	0.53, 1.41, 3.0	0.53, 1.41, 3.0
Mechanical Properties				
Modulus, ksi	26,500	28,000	26,500	28,000
Yield Strength, ksi	22.5	42.8	22.5	42.8
Ultimate Strength, ksi	64.3	70	64.3	70
Sm (per ASME Section III App I), ksi	16.95	19.6	16.95	19.6
Ramberg Osgood Parameter - Sig-O, ksi	22.5	42.8	22.5	42.8
Ramberg Osgood Parameter - Eps-O, ksi	0.000849	0.001528571	0.000849	0.001528571
Ramberg Osgood Parameter - Alpha	8.073	1.89	8.073	1.89
Ramberg Osgood Parameter - Exponent - n	3.78	5.84	3.78	5.84
Toughness - J-R Curve	High J-R Curve (eg. JD-A8)			
Loading				
Pressure, psi	1050	1050	2250	2250
Temperature, F	550	550	600	600
Load Combination	Pressure + Bending	Pressure + Bending	Pressure + Bending	Pressure + Bending
Bending Stress, % of 1.5Sm (Service Level A)	25, 50, 100 and special cases			
Bending Moment value, ksi	ASME Section III - NB-3652			
Weird Residual Stresses Effects	both with and without			
Crack Geometry				
Crack Shape	Elliptical	Elliptical	Elliptical	Elliptical
Type of Cracking Mechanism	IGSCC, and Air Fatigue	Corrosion and Air Fatigue	PWSCC, and Air Fatigue	Corrosion and Air Fatigue
Effect of COD dependence	both with and without			
Complex Crack Effects	include for specific cases			
Through wall Crack length - exterior	OUTPUT FROM SQUIRT	OUTPUT FROM SQUIRT	OUTPUT FROM SQUIRT	OUTPUT FROM SQUIRT
Fluid Flow Parameters				
Leak rate - vol flow rate, gpm	0.1, 1, 10, 100	0.1, 1, 10, 100	0.1, 1, 10, 100	0.1, 1, 10, 100
Fluid State	Subcooled Liquid	Subcooled Liquid	Subcooled Liquid	Subcooled Liquid
Discharge Coefficient	0.6	0.6	0.6	0.6
External Pressure, ksi	14.7	14.7	14.7	14.7
Analysis Type				
Estimation Scheme for Moment-Rotation Calcs	GE-EPRI	GE-EPRI	GE-EPRI	GE-EPRI

Table 4. PWR stainless steel piping cases with PWSCC degradation mechanism.

Case No.	Diameter, m	Wall Thickness, t, mm	Tension Load, kN	Tension Stress, MPa	Stress/ ^o Service Level A - 1.5Sm	Moment, m-kN	Bending Stress, MPa	Leak Rate, kg/s	Throughwall Crack Length, mm	Percent of DPZP Crack Length
PSL-25-1C	0.81	76.2	5313.8	30.1	25%	73.1	2.8	0.0063	314.2	27.6%
PSL-25-2C	0.81	76.2	5313.8	30.1	25%	73.1	2.8	0.063	460.5	40.5%
PSL-25-3C	0.81	76.2	5313.8	30.1	25%	73.1	2.8	0.63	724.4	63.7%
PSL-25-4C	0.81	76.2	5313.8	30.1	25%	73.1	2.8	6.3	969.0	85.2%
PSL-50-1C	0.81	76.2	5313.8	30.1	50%	1376.8	46	0.0063	51.8	6.2%
PSL-50-2C	0.81	76.2	5313.8	30.1	50%	1376.8	46	0.063	135.6	16.2%
PSL-50-3C	0.81	76.2	5313.8	30.1	50%	1376.8	46	0.63	331.0	39.6%
PSL-50-4C	0.81	76.2	5313.8	30.1	50%	1376.8	46	6.3	536.7	64.2%
PSL-100-1C	0.81	76.2	5313.8	30.1	100%	3984.4	134	0.0063	17.8	5.0%
PSL-100-2C	0.81	76.2	5313.8	30.1	100%	3984.4	134	0.063	47.8	13.4%
PSL-100-3C	0.81	76.2	5313.8	30.1	100%	3984.4	134	0.63	107.4	30.2%
PSL-100-4C	0.81	76.2	5313.8	30.1	100%	3984.4	134	6.3	240.0	67.5%
PSM-25-1C	0.36	35.8	982.6	27.3	25%	13.9	5.5	0.0063	158.8	29.2%
PSM-25-2C	0.36	35.8	982.6	27.3	25%	13.9	5.5	0.063	242.6	44.6%
PSM-25-3C	0.36	35.8	982.6	27.3	25%	13.9	5.5	0.63	361.4	66.4%
PSM-25-4C	0.36	35.8	982.6	27.3	25%	13.9	5.5	6.3		0.0%
PSM-50-1C	0.36	35.8	982.6	27.3	50%	128.7	49	0.0063	43.9	10.1%
PSM-50-2C	0.36	35.8	982.6	27.3	50%	128.7	49	0.063	106.7	24.6%
PSM-50-3C	0.36	35.8	982.6	27.3	50%	128.7	49	0.63	225.3	51.9%
PSM-50-4C	0.36	35.8	982.6	27.3	50%	128.7	49	6.3		0.0%
PSM-100-1C	0.36	35.8	982.6	27.3	100%	358.4	137	0.0063	14.2	5.3%
PSM-100-2C	0.36	35.8	982.6	27.3	100%	358.4	137	0.063	37.6	14.1%
PSM-100-3C	0.36	35.8	982.6	27.3	100%	358.4	137	0.63	83.8	31.2%
PSM-100-4C	0.36	35.8	982.6	27.3	100%	358.4	137	6.3		0.0%
PSS-25-1C	0.11	13.5	93.0	21.8	25%	1.05	11	0.0063	75.4	40.7%
PSS-25-2C	0.11	13.5	93.0	21.8	25%	1.05	11	0.063	102.1	55.1%
PSS-25-3C	0.11	13.5	93.0	21.8	25%	1.05	11	0.63	NC	
PSS-25-4C	0.11	13.5	93.0	21.8	25%	1.05	11	6.3	NC	
PSS-50-1C	0.11	13.5	93.0	21.8	50%	5.29	54	0.0063	33.0	21.4%
PSS-50-2C	0.11	13.5	93.0	21.8	50%	5.29	54	0.063	65.0	42.1%
PSS-50-3C	0.11	13.5	93.0	21.8	50%	5.29	54	0.63	NC	
PSS-50-4C	0.11	13.5	93.0	21.8	50%	5.29	54	6.3	NC	
PSS-100-1C	0.11	13.5	93.0	21.8	100%	13.75	142	0.0063	10.7	9.7%
PSS-100-2C	0.11	13.5	93.0	21.8	100%	13.75	142	0.063	26.4	24.1%
PSS-100-3C	0.11	13.5	93.0	21.8	100%	13.75	142	0.63	NC	
PSS-100-4C	0.11	13.5	93.0	21.8	100%	13.75	142	6.3	NC	

NC indicates that no convergence was achieved in the run and the crack length could not be determined.

Table 5. BWR stainless steel piping cases with PWSCC degradation mechanism.

Case No.	Diameter, m	Wall Thickness, t, mm	Tension Load, kN	Tension Stress, MPa	Stress/% Service Level A - 1.5Sm	Moment, m-kN	Bending Stress, MPa	Leak Rate, kg/s	Throughwall Crack Length, mm	Percent of DPZP Crack Length
BSL-25-1C	0.71	35.8	2325.8	30.6	25%	96.4	7.9	0.0063	170.18	16.52%
BSL-25-2C	0.71	35.8	2325.8	30.6	25%	96.4	7.9	0.063	372.61	36.18%
BSL-25-3C	0.71	35.8	2325.8	30.6	25%	96.4	7.9	0.63	593.09	57.58%
BSL-25-4C	0.71	35.8	2325.8	30.6	25%	96.4	7.9	6.3	NC	
BSL-50-1C	0.71	35.8	2325.8	30.6	50%	631.9	51.7	0.0063	71.882	9.45%
BSL-50-2C	0.71	35.8	2325.8	30.6	50%	631.9	51.7	0.063	191.26	25.14%
BSL-50-3C	0.71	35.8	2325.8	30.6	50%	631.9	51.7	0.63	345.44	45.41%
BSL-50-4C	0.71	35.8	2325.8	30.6	50%	631.9	51.7	6.3	NC	
BSL-100-1C	0.71	35.8	2325.8	30.6	100%	1703.2	139.3	0.0063	24.257	7.35%
BSL-100-2C	0.71	35.8	2325.8	30.6	100%	1703.2	139.3	0.063	58.166	17.62%
BSL-100-3C	0.71	35.8	2325.8	30.6	100%	1703.2	139.3	0.63	NC	
BSL-100-4C	0.71	35.8	2325.8	30.6	100%	1703.2	139.3	6.3	NC	
BSM-25-1C	0.32	17.4	474.71	28.3	25%	12.5	10.2	0.0063	119.88	23.53%
BSM-25-2C	0.32	17.4	474.71	28.3	25%	12.5	10.2	0.063	239.77	47.06%
BSM-25-3C	0.32	17.4	474.71	28.3	25%	12.5	10.2	0.63	337.82	66.30%
BSM-25-4C	0.32	17.4	474.71	28.3	25%	12.5	10.2	6.3	NC	
BSM-50-1C	0.32	17.4	474.71	28.3	50%	66.0	54.1	0.0063	58.928	14.48%
BSM-50-2C	0.32	17.4	474.71	28.3	50%	66.0	54.1	0.063	139.95	34.39%
BSM-50-3C	0.32	17.4	474.71	28.3	50%	66.0	54.1	0.63	223.52	54.93%
BSM-50-4C	0.32	17.4	474.71	28.3	50%	66.0	54.1	6.3	NC	
BSM-100-1C	0.32	17.4	474.71	28.3	100%	173.1	141.7	0.0063	19.837	7.99%
BSM-100-2C	0.32	17.4	474.71	28.3	100%	173.1	141.7	0.063	47.345	19.06%
BSM-100-3C	0.32	17.4	474.71	28.3	100%	173.1	141.7	0.63	NC	
BSM-100-4C	0.32	17.4	474.71	28.3	100%	173.1	141.7	6.3	89.662	36.09%
BSS-25-1C	0.11	8.56	53.69	18.9	25%	1.376	19.7	0.0063	70.358	36.84%
BSS-25-2C	0.11	8.56	53.69	18.9	25%	1.376	19.7	0.063	121.66	63.70%
BSS-25-3C	0.11	8.56	53.69	18.9	25%	1.376	19.7	0.63	NC	
BSS-25-4C	0.11	8.56	53.69	18.9	25%	1.376	19.7	6.3	NC	
BSS-50-1C	0.11	8.56	53.69	18.9	50%	4.445	63.5	0.0063	42.926	27.13%
BSS-50-2C	0.11	8.56	53.69	18.9	50%	4.445	63.5	0.063	84.328	53.29%
BSS-50-3C	0.11	8.56	53.69	18.9	50%	4.445	63.5	0.63	NC	
BSS-50-4C	0.11	8.56	53.69	18.9	50%	4.445	63.5	6.3	112.52	71.11%
BSS-100-1C	0.11	8.56	53.69	18.9	100%	10.58	151.1	0.0063	15.367	14.04%
BSS-100-2C	0.11	8.56	53.69	18.9	100%	10.58	151.1	0.063	NC	
BSS-100-3C	0.11	8.56	53.69	18.9	100%	10.58	151.1	0.63	NC	
BSS-100-4C	0.11	8.56	53.69	18.9	100%	10.58	151.1	6.3	64.008	58.47%

NC indicates that no convergence was achieved in the run and the crack length could not be determined.

Review of Leak Rates from Non-SCC Type of Cracking and Other Variables

The only non-SCC type of cracking studied so far has been corrosion fatigue of carbon steel piping in both BWRs and PWRs. A matrix similar to that shown for stainless steel piping (Table 5) was developed for these cases, and SQUIRT runs combined with PIPE were performed. These results are shown in Tables 6 and 7 for PWRs and BWRs, respectively.

Table 6. PWR carbon steel piping cases with corrosion fatigue degradation mechanism.

Case No.	Diameter, m	Wall Thickness, t, mm	Tension Load, kN	Tension Stress, MPa	Stress/% Service Level A - 1.5Sm	Moment, m-kN	Bending Stress, MPa	Leak Rate, kg/s	Throughwall Crack Length, mm	Percent of DPZP Crack Length
PCL-25-1C	0.81	76.2	5313.8	30	25%	276.9	9.7	0.0063	151.6	12.4%
PCL-25-2C	0.81	76.2	5313.8	30	25%	276.9	9.7	0.063	309.6	25.3%
PCL-25-3C	0.81	76.2	5313.8	30	25%	276.9	9.7	0.63	589.3	48.2%
PCL-25-4C	0.81	76.2	5313.8	30	25%	276.9	9.7	6.3	812.3	66.4%
PCL-50-1C	0.81	76.2	5313.8	30	50%	1784.5	60	0.0063	49.3	5.2%
PCL-50-2C	0.81	76.2	5313.8	30	50%	1784.5	60	0.063	133.9	14.2%
PCL-50-3C	0.81	76.2	5313.8	30	50%	1784.5	60	0.63	297.9	31.5%
PCL-50-4C	0.81	76.2	5313.8	30	50%	1784.5	60	6.3	594.4	62.9%
PCL-100-1C	0.81	76.2	5313.8	30	100%	4799.6	161	0.0063	31.2	6.0%
PCL-100-2C	0.81	76.2	5313.8	30	100%	4799.6	161	0.063	85.3	16.5%
PCL-100-3C	0.81	76.2	5313.8	30	100%	4799.6	161	0.63	176.8	34.1%
PCL-100-4C	0.81	76.2	5313.8	30	100%	4799.6	161	6.3	438.2	84.6%
PCM-25-1C	0.36	35.8	982.6	28	25%	31.9	12	0.0063	108.5	18.8%
PCM-25-2C	0.36	35.8	982.6	28	25%	31.9	12	0.063	201.4	34.8%
PCM-25-3C	0.36	35.8	982.6	28	25%	31.9	12	0.63	323.3	55.9%
PCM-25-4C	0.36	35.8	982.6	28	25%	31.9	12	6.3	NC	
PCM-50-1C	0.36	35.8	982.6	28	50%	164.6	63	0.0063	42.9	9.0%
PCM-50-2C	0.36	35.8	982.6	28	50%	164.6	63	0.063	107.7	22.6%
PCM-50-3C	0.36	35.8	982.6	28	50%	164.6	63	0.63	217.9	45.8%
PCM-50-4C	0.36	35.8	982.6	28	50%	164.6	63	6.3	NC	
PCM-100-1C	0.36	35.8	982.6	28	100%	430.1	164	0.0063	26.7	8.2%
PCM-100-2C	0.36	35.8	982.6	28	100%	430.1	164	0.063	71.6	22.0%
PCM-100-3C	0.36	35.8	982.6	28	100%	430.1	164	0.63	158.8	48.8%
PCM-100-4C	0.36	35.8	982.6	28	100%	430.1	164	6.3	NC	
PCS-25-1C	0.11	13.5	93.0	22	25%	1.72	18	0.0063	62.5	32.0%
PCS-25-2C	0.11	13.5	93.0	22	25%	1.72	18	0.063	98.3	50.3%
PCS-25-3C	0.11	13.5	93.0	22	25%	1.72	18	0.63	158.8	81.3%
PCS-25-4C	0.11	13.5	93.0	22	25%	1.72	18	6.3	NC	
PCS-50-1C	0.11	13.5	93.0	22	50%	6.61	68	0.0063	34.0	20.5%
PCS-50-2C	0.11	13.5	93.0	22	50%	6.61	68	0.063	71.6	43.1%
PCS-50-3C	0.11	13.5	93.0	22	50%	6.61	68	0.63	113.5	68.2%
PCS-50-4C	0.11	13.5	93.0	22	50%	6.61	68	6.3	NC	
PCS-100-1C	0.11	13.5	93.0	22	100%	16.39	170	0.0063	21.6	17.3%
PCS-100-2C	0.11	13.5	93.0	22	100%	16.39	170	0.063	50.8	40.7%
PCS-100-3C	0.11	13.5	93.0	22	100%	16.39	170	0.63	83.8	67.1%
PCS-100-4C	0.11	13.5	93.0	22	100%	16.39	170	6.3	NC	

NC indicates that no convergence was achieved in the run and the crack length could not be determined.

Table 7. BWR carbon steel piping cases with corrosion fatigue degradation mechanism.

Case No.	Diameter, m	Wall Thickness, t, mm	Tension Load, kN	Tension Stress, MPa	Stress/% Service Level A - 1.5Sm	Moment, m-kN	Bending Stress, MPa	Leak Rate, kg/s	Throughwall Crack Length, mm	Percent of DPZP Crack Length
BCL-25-1C	0.71	35.8	2326.0	30	25%	180.1	14	0.0063	125.5	11.3%
BCL-25-2C	0.71	35.8	2326.0	30	25%	180.1	14	0.063	273.8	24.6%
BCL-25-3C	0.71	35.8	2326.0	30	25%	180.1	14	0.63	484.6	43.6%
BCL-25-4C	0.71	35.8	2326.0	30	25%	180.1	14	6.3	NC	
BCL-50-1C	0.71	35.8	2326.0	30	50%	799.4	66	0.0063	55.9	6.5%
BCL-50-2C	0.71	35.8	2326.0	30	50%	799.4	66	0.063	150.6	17.5%
BCL-50-3C	0.71	35.8	2326.0	30	50%	799.4	66	0.63	286.0	33.2%
BCL-50-4C	0.71	35.8	2326.0	30	50%	799.4	66	6.3	NC	
BCL-100-1C	0.71	35.8	2326.0	30	100%	2038.0	167	0.0063	36.1	7.6%
BCL-100-2C	0.71	35.8	2326.0	30	100%	2038.0	167	0.063	95.8	20.0%
BCL-100-3C	0.71	35.8	2326.0	30	100%	2038.0	167	0.63	200.7	41.9%
BCL-100-4C	0.71	35.8	2326.0	30	100%	2038.0	167	6.3	NC	
BCM-25-1C	0.32	17.4	474.6	28	25%	20.9	17	0.0063	95.5	17.5%
BCM-25-2C	0.32	17.4	474.6	28	25%	20.9	17	0.063	187.2	34.4%
BCM-25-3C	0.32	17.4	474.6	28	25%	20.9	17	0.63	287.5	52.8%
BCM-25-4C	0.32	17.4	474.6	28	25%	20.9	17	6.3	NC	
BCM-50-1C	0.32	17.4	474.6	28	50%	82.8	68	0.0063	48.0	10.7%
BCM-50-2C	0.32	17.4	474.6	28	50%	82.8	68	0.063	119.6	26.7%
BCM-50-3C	0.32	17.4	474.6	28	50%	82.8	68	0.63	210.8	47.0%
BCM-50-4C	0.32	17.4	474.6	28	50%	82.8	68	6.3	NC	0.0%
BCM-100-1C	0.32	17.4	474.6	28	100%	206.5	169	0.0063	30.7	10.1%
BCM-100-2C	0.32	17.4	474.6	28	100%	206.5	169	0.063	79.8	26.3%
BCM-100-3C	0.32	17.4	474.6	28	100%	206.5	169	0.63	154.2	50.7%
BCM-100-4C	0.32	17.4	474.6	28	100%	206.5	169	6.3	NC	
BCS-25-1C	0.11	8.6	53.8	19	25%	1.85	26	0.0063	60.5	29.9%
BCS-25-2C	0.11	8.6	53.8	19	25%	1.85	26	0.063	102.9	50.9%
BCS-25-3C	0.11	8.6	53.8	19	25%	1.85	26	0.63	NC	
BCS-25-4C	0.11	8.6	53.8	19	25%	1.85	26	6.3	NC	
BCS-50-1C	0.11	8.6	53.8	19	50%	5.40	77	0.0063	39.6	23.1%
BCS-50-2C	0.11	8.6	53.8	19	50%	5.40	77	0.063	84.1	49.1%
BCS-50-3C	0.11	8.6	53.8	19	50%	5.40	77	0.63	NC	
BCS-50-4C	0.11	8.6	53.8	19	50%	5.40	77	6.3	NC	
BCS-100-1C	0.11	8.6	53.8	19	100%	12.50	179	0.0063	26.2	20.6%
BCS-100-2C	0.11	8.6	53.8	19	100%	12.50	179	0.063	58.9	46.4%
BCS-100-3C	0.11	8.6	53.8	19	100%	12.50	179	0.63	NC	
BCS-100-4C	0.11	8.6	53.8	19	100%	12.50	179	6.3	NC	

NC indicates that no convergence was achieved in the run and the crack length could not be determined.

To help illustrate the results from Tables 4 to 7, a summary table (Table 8) was created for the 50% Service Level A cases, which are assumed to represent “normal” loading. The values in Table 8 were then used to create Figs. 11 and 12, which show the ratio of the crack length necessary to produce a given leak rate, the “leakage crack length”, to the critical crack length as a function of pipe diameter for two leak rates. This ratio is a measure of the margin of safety provided by the limit on leakage. The two leak rates are the Tech. Spec. (TS) leak rate for PWRs (0.063 kg/s; 1 gpm) and BWRs (0.32 kg/s; 5 gpm), as well as a lower leak rate of 0.006 kg/s (0.1 gpm) for both types of plants.

As expected, the ratio of the leakage crack length to the critical crack length increases as the diameter decreases, i.e., the margin for LBB gets smaller for smaller pipes. For BWRs, which have a higher TS leak rate than for PWRs, the leakage crack length is from ≈ 40 to ≈ 60 percent of the critical crack length at normal operating loads for pipes from 711 to 102 mm (28 to 4 in), respectively.

For the PWRs, which have a lower TS leak rate, the leakage crack length at normal operating loads is from ~ 15 to ~ 40 percent of the critical crack length for pipes from 813 to 102 mm (32 to 4 in.), respectively.

At the 0.0063-kg/s (0.1 gpm) leak rate, the leakage crack length is about 5 to 20% of the critical crack size at normal operating conditions. The leakage crack sizes are a smaller percent of the critical crack size at a transient load, like N+SSE (normal plus safe shutdown earthquake) loading or startup/shutdown transients for a surge line.

The calculations in Tables 4–8 are for idealized circumferential through-wall cracks. This type of crack gives the smallest size for a given leak rate. In reality, the crack will likely be longer on the inside surface. For some IGSCC cracks that have been observed in the field, part-throughwall cracks on the inner surface extend completely around the pipe in the same circumferential plane as the through-wall portion of the crack. Such cracks have been called compound or complex.

Additional calculations on the relationship between crack length and leak rate are presented in Appendix D. These include the effects of complex cracks as well as residual stresses.

The fracture mechanics solutions discussed thus far focus on the possibility of structural failure by crack growth. Another possibility is that boric acid leakage could cause substantial corrosion such as occurred on the reactor vessel head at Davis-Besse. Dry boric acid results in very low corrosion rates [12,13]. However, with moisture present, concentrated boric acids at temperatures of 90–160°C can produce very high corrosion rates (up to 15 cm/y).

At the extremely low leak rates ($\approx 10^{-7}$ to 10^{-6} kg/s; $\approx 10^{-6}$ to 10^{-5} gpm) such as have been observed in most leaking CRDM nozzles, the leaking flow completely vaporizes to steam immediately downstream from the principal flashing location. This results in a dry condition and no loss of material, although some dry boric acid may accumulate. At the other extreme is a situation where liquid boric acid solution is concentrated through boiling and enhanced by oxygen available directly from the ambient atmosphere.

Local cooling can create conditions for rapid corrosion by allowing aerated, concentrated boric acid solution to form on surfaces. The extent of cooling due to the leak is primarily a function of the leak rate since the rate of heat transfer required to completely vaporize the effluent is directly proportional to the leak rate. In Ref. 14 a simple enthalpy balance was used to estimate the potential loss of heat from the surface of the head as a function of the leak rate

Table 8. Sensitivity runs for BWR and PWR cases – leak rate versus percent of critical crack lengths.

		BWR - Stainless Steel - IGSCC		
Leak rate, gpm (Kg/s)	711	324	114	
	% Critical Crack Length at 25% Service Level A			
0.1 (0.0063)	16.52%	23.53%	36.84%	
1 (0.063)	36.18%	47.06%	63.70%	
5 (0.32) (interpolated)	52.00%	60.50%	NC	
10 (0.63)	57.58%	66.30%	NC	
100 (6.3)	NC	NC	NC	
Critical Crack Length,mm	1030	510	191	
	% Critical Crack Length at 50 % Service Level A			
0.1 (0.0063)	9.45%	14.48%	27.13%	
1 (0.063)	25.14%	34.39%	53.29%	
5 (0.32) (interpolated)	40.00%	49.00%	59.00%	
10 (0.63)	45.41%	54.93%	NC	
100 (6.3)	NC	NC	71.11%	
Critical Crack Length,mm	761	407	158	
	% Critical Crack Length at 100% Service Level A			
0.1 (0.0063)	7.35%	7.99%	14.04%	
1 (0.063)	17.62%	19.06%	NC	
5 (0.32) (interpolated)	25.00%	22.00%	38.50%	
10 (0.63)	NC	NC	NC	
100 (6.3)	NC	36.09%	58.47%	
Critical Crack Length,mm	330	248	109	
BWR - Carbon Steel - Corr Fatigue				
Leak rate, gpm (Kg/s)	711	324	114	
	% Critical Crack Length at 25% Service Level A			
0.1 (0.0063)	11.28%	17.55%	29.94%	
1 (0.063)	24.62%	34.39%	50.94%	
5 (0.32) (interpolated)	38.00%	47.50%	NC	
10 (0.63)	43.58%	52.82%	NC	
100 (6.3)	NC	NC	NC	
Critical Crack Length,mm	1112	544	202	
	% Critical Crack Length at 50 % Service Level A			
0.1 (0.0063)	6.46%	10.71%	23.13%	
1 (0.063)	17.46%	26.69%	49.13%	
5 (0.32) (interpolated)	28.50%	41.00%	NC	
10 (0.63)	33.16%	47.03%	NC	
100 (6.3)	NC	NC	NC	
Critical Crack Length,mm	863	448	1695	
	% Critical Crack Length at 100% Service Level A			
0.1 (0.0063)	7.55%	10.11%	20.62%	
1 (0.063)	19.99%	26.26%	46.40%	
5 (0.32) (interpolated)	35.50%	43.50%	NC	
10 (0.63)	41.89%	50.74%	NC	
100 (6.3)	NC	NC	NC	
Critical Crack Length,mm	479	304	127	
PWR - Carbon Steel - Corr Fatigue				
Leak rate, gpm(Kg/s)	711	324	114	
	% Critical Crack Length at 25% Service Level A			
0.1 (0.0063)	12.40%	18.75%	31.99%	
1 (0.063)	25.32%	34.83%	50.33%	
10 (0.63)	48.18%	55.91%	81.27%	
100 (6.3)	66.42%	NC	NC	
Critical Crack Length,mm	1223	578	195	
	% of Critical Crack Length at 50% Service Level A			
0.1 (0.0063)	5.22%	9.01%	20.46%	
1 (0.063)	14.17%	22.61%	43.05%	
10 (0.63)	31.53%	45.76%	68.24%	
100 (6.3)	62.90%	NC	NC	
Critical Crack Length,mm	945	476	166	
	% Critical Crack Length at 100% Service Level A			
0.1 (0.0063)	6.03%	8.20%	17.34%	
1 (0.063)	16.47%	22.03%	40.65%	
10 (0.63)	34.12%	48.83%	67.07%	
100 (6.3)	84.56%	NC	NC	
Critical Crack Length,mm	518	325	125	
PWR - Stainless Steel - PWSCC				
Leak rate, gpm(Kg/s)	711	324	114	
	% Critical Crack Length at 25% Service Level A			
0.1 (0.0063)	27.62%	29.16%	40.73%	
1 (0.063)	40.48%	44.56%	55.07%	
10 (0.63)	63.69%	66.40%	NC	
100 (6.3)	85.19%	NC	NC	
Critical Crack Length,mm	1137	544	185	
	% of Critical Crack Length at 50% Service Level A			
0.1 (0.0063)	6.20%	10.12%	21.43%	
1 (0.063)	16.24%	24.56%	42.11%	
10 (0.63)	39.60%	51.87%	NC	
100 (6.3)	64.22%	NC	NC	
Critical Crack Length,mm	836	434	154	
	% Critical Crack Length at 100% Service Level A			
0.1 (0.0063)	4.97%	5.34%	9.74%	
1 (0.063)	13.41%	14.07%	24.07%	
10 (0.63)	30.24%	31.23%	NC	
100 (6.3)	67.50%	NC	NC	
Critical Crack Length,mm	356	268	109	

NC indicates that no convergence was achieved in the run and the crack length could not be determined.

and the steam quality or superheat of the escaping steam. It was assumed that the flow exits to atmospheric pressure.

For leaking primary water at 316°C, 45% of the effluent will flash to steam without any heat input. Heat transfer from the head to the effluent will increase the quality to saturated conditions and then superheat the steam back to a temperature of 316°C. The amount of heat required to bring the exit flow to the superheated condition provides an estimate of the heat lost from the head due to the leak, and its effects on the surface temperature can be calculated [14].

For a leak rate of 0.00006 kg/s (0.001 gpm), the vaporization of the effluent will result in a heat loss of roughly 316 kJ/h. The extent of cooling of the head surface due to this heat loss is relatively small, on the order of 6°C. For a leak rate of 0.00063 kg/s (0.01 gpm), the corresponding heat loss is 3160 kJ/h, and the resultant surface cooling is about 55°C, still not enough to create conditions on the surface that would result in high corrosion rates. However, a leak rate of 0.0063 kg/s (0.1 gpm) was calculated to be sufficient to cool the local metal surface to temperatures below the boiling point of water at atmospheric pressure [14]. Because this degree of cooling would conflict with the assumption complete vaporization occurs in the in the annulus region, it cannot actually occur. Instead, the steam quality exiting the annulus would be less than 100%, indicating development of a liquid pool on the head surface [14].

Although the precise values of the leak rate needed to lower metal surface temperatures to the 100–160°C range associated with high boric acid corrosion rates will depend on details of the actual geometries involved, the calculations in Ref. [14] suggest that the critical leak rates needed to produce high corrosion rates, are of the order of 0.00063 to 0.0063 kg/s (0.01 to 0.1 gpm), well below the current TS limit. Such rates are probably also at or below the resolution limit for unidentified leakage of sump flow monitors.

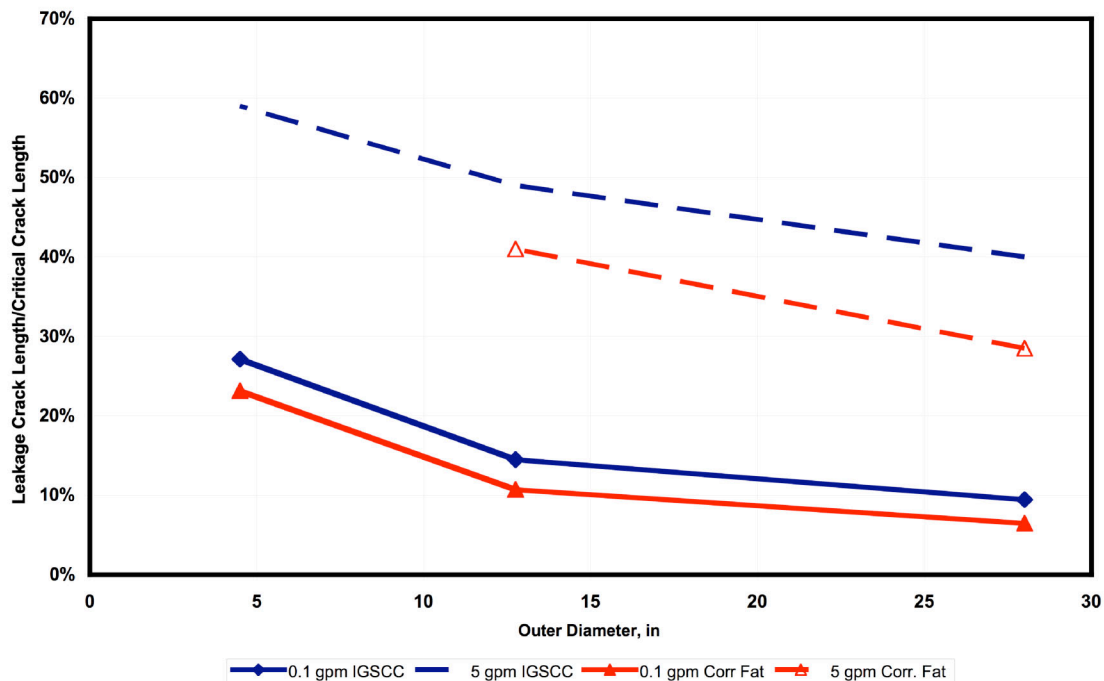


Figure 11. Percent of critical crack length versus diameter for BWR cases at 50% Service Level A stresses.

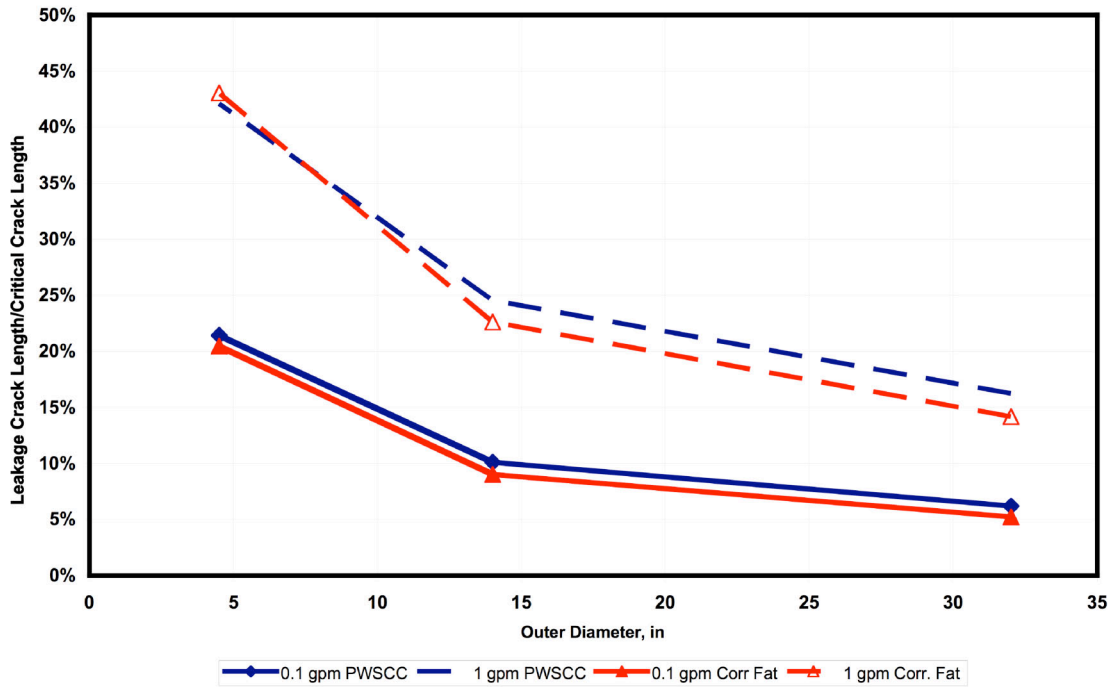


Figure 12. Percent of critical crack length versus diameter for PWR cases at 50% Service Level A stresses.

4. Leakage Operating Experience

A leakage operating experience database has been developed for this research program. The database contains information on LWR leak events and leak detection systems back to 1970. The software chosen for the database is FileMaker Pro 6.

The fields for LWR leak events include (a) LER number if an LER is the source of information, (b) location of leak, (c) leak rate [actual leak rate if known, however, for many cases the actual leak rates are small (<0.0006 kg/s (0.01 gpm)) and not known precisely, although some qualitative information ("slowly dripping", etc.) may be available], (d) operation of reactor when leak was detected, (e) how the leak was detected, (f) the basis for the decision that a leak has occurred, (g) time required to recognize there was an unidentified leak, (h) action that was taken, (i) relevant nondestructive and destructive evaluation reports, (j) cause of leak, (k) leakage requirements, (l) crack type and size if crack was cause of leak, and (m) any environmental impact. The fields for leak detection systems include (a) method of detection, (b) vendor for system, (c) sensitivity, (d) reliability, (e) response time, (f) accuracy, (g) estimated false alarm rate, (h) area of coverage, (i) maintenance required, (j) training required for its implementation, (k) calibration procedures, (l) site validation procedure, (m) experience under field conditions, and (n) source of information. Note that under the field "how the leak was detected," the first method to detect the leak is recorded. However, other leak detection systems that may have responded to the leak and subsequent visual inspections may be discussed in the extended input to one or more fields of the leak event.

Sources used to provide input to the database include Licensee Event Reports and NRC Information Notices through 2004 and NRC reports covering prior work such as the "Assessment of PWR Primary System Leaks," NUREG/CR-6582, published in 1998 [15]; "Assessment of Leak Detection Systems for LWRs," NUREG/CR-4813, 1988 [16]; "Research to Advance the State-of-the-Art of Acoustic Leak Detection," NUREG/CR-5134, 1988 [17]; and "Validation of the Application of Acoustic Emission to Monitor Nuclear Reactor Pressurized Components," NUREG/CR-5645, 1991 [18]. Literature searches were carried out to identify other relevant publications (e.g., articles from *Nuclear Safety*) and databases such as an EPRI report co-sponsored by the Swedish Nuclear Power Inspectorate (SKI) on reactor piping failures, 1998 [19]. The Internet search engines Google and Yahoo were used to locate about 15 leak events not found in other sources.

Internet access to ADAMS (Agencywide Documents Access and Management System) using a desktop computer permitted efficient review of LERs, NRC documents, and plant technical specifications. The database currently contains over 400 events dating from 1970. In addition to RCS leaks, three leaks of interest on the secondary side are included in the database, but not included in the statistics. Also, 13 steam generator leaks of interest are included in the database, but not included in the statistics. An example of a database entry is shown in Fig. 13. Each field can be expanded for additional information by clicking on the box containing the initial information.

A discussion of leak detection requires differentiation of identified and unidentified leakage. Leakage to containment that has been located and quantified and is not from a crack or other flaw in the RCS is classified as "identified." In such cases leakage from an identified component is directed to a collection system where it is measured (e.g., leakage from a pump

seal, valve packing, gland seals, reactor-head pressure seals, equipment gaskets, and pressure relief valves). Leakage that is not identified is defined as “unidentified” leakage. Flow rates from unidentified leakage are to be monitored separately.

Barrier Integrity Program

LWR Leak Events

Event Number	20021007
LER Number	313/2002-003-00
Source of Information	LER 313/2002-003-00 and
Location of Leak	Arkansas Nuclear One 1; leaking crack in CRDM nozzle #56 that
Leak Rate	<0.284 gpm
Reactor Operation	PWR
How Leak Detected	Visual observation of boric acid deposits near a CRDM nozzle
Basis of Decision on Breach	Presence of crack confirmed by UT and PT, and indications were
Time to Recognizing Problem	N/A
Action Taken	CRDM nozzle #56 weld repaired using an improved technique that
NDE Report	UT and PT inspections found indications in nozzle #56 just outside
DE Report	No DE results reported.
Cause of Failure	SCC, Boric acid build-up found on one CRDM nozzle, PWSCC
Leakage Requirements	1 gpm
Crack Type	PWSCC
Crack Size	Not stated
Environmental Impact	None
Reference	# http://scss.ornl.gov/ScssScripts/Results/resLERDetl.cfm?lernmb

Figure 13. An example of a database entry for a leak. Each field can be expanded for additional information by clicking on the box containing the initial information.

Basis for RCS Leakage Monitoring Requirements

The NRC Regulatory Guide (RG) 1.45, issued in 1973, established capabilities for leak detection systems acceptable to staff. It does not define limiting conditions of operation. RG 1.45 does note, however, that technical specifications (TSs) that define the limiting conditions for operation for identified and unidentified leakage and address the availability of the leak detection systems are generally implemented. RG 1.45 proposes that leaks should be monitored to a sensitivity of 0.063 kg/s (1 gpm) or better with at least three detection methods. The leak detection system should be able to detect a 0.063 kg/s (1 gpm) leak in less than 1 hour, and alarms for the leak detection systems should be located in the control room. Sump level and airborne particulate radioactivity monitors are required. The third method could be either a condensate flow monitor or a radiation monitor. This capability has typically been provided through an airborne gaseous radioactivity monitor. Such monitors do not provide leakage rates but have the capability of indicating an increase of 0.063 kg/s (1 gpm) within an

hour. However, because failed fuel is much less likely to occur and primary systems have become less contaminated than was the case when RG 1.45 was issued, the value of monitoring gaseous radioactivity has been greatly diminished. In RG 1.45 monitoring of the bulk humidity, temperature, and pressure in the containment are considered as indirect indications of leakage

The capabilities considered acceptable for leak detection systems were established without a strong technical basis, although the first draft of RG 1.45, based on some analytical studies and some experimental data, stated that cracks leaking at a rate of 0.063 kg/s (1 gpm) would be smaller than critical size by a factor of at least two. The assessment of the capabilities of the different leak detection systems appears to have been based on an analysis of the sensitivities of the sump, particulate, and gaseous detectors as well as condensate flow rate and humidity monitors for PWRs. It appeared that for 1% and 0% failed fuel a particulate monitor could detect a 0.063 kg/s (1 gpm) leak within 1 minute for both failed fuel assumptions, and that the gaseous monitor could detect a 0.063 kg/s (1 gpm) leak in about 2 minutes for 1% failed fuel and 100 minutes for 0% failed fuel. This activity level is very high by today's standards, and hence, actual sensitivities and response times are worse than earlier estimates would be. The sump pump was estimated to be capable of detecting 0.063 kg/s (1 gpm) leaks within an hour. The condensate flow rate monitor could detect 0.063 kg/s (1 gpm) leaks within 10 minutes, and a humidity monitor within 40 minutes (PWR). Air particulate monitors could (at that time) detect 0.0013 kg/s (0.02 gpm) within minutes when background radiation levels were low. Since particulate monitors were equally effective for BWRs and PWRs and they became required monitors. With the sump monitor being effective for detecting 0.063 kg/s (1 gpm) within an hour under all conditions, it was also identified as required. The water inventory method was introduced in 1972.

Seven years after NRC Regulatory Guide 1.45 was published, "Standard for Light Water Reactor Coolant Pressure Boundary Leak Detection," ISA-S67.03-1982 [20], was issued by the Instrument Society of America (ISA). It is a detailed, comprehensive document that could be a supplement or replacement for RG 1.45. The ISA position for the detection of leakage changes is also based on known capabilities at the time, and specifies that a 0.063 kg/s (1 gpm) increase in a PWR leak rate, and a 0.13-kg/s (2 gpm) increase in a BWR leak rate be detected within 1 hour. ISA-S67.03-1982 also provides general equations for measurement sensitivities and response times of sump level and leakage flow monitoring. Equations for sensitivity and response times of radiation, humidity, and temperature monitors are also presented. By 1991, acoustic monitors had already been used in the field to monitor valves (Peach Bottom, Dresden, and V.C. Summer). In Germany a reactor used 18 acoustic sensors to monitor the primary line and pressure vessel. Although no leaks were detected or missed (that were detected by other means), no false alarms occurred over a two-year period. Also at that time, EPRI had reported that for 15 fossil plant boilers, acoustic systems detected 60% of all reported leaks. It was possible at that time, for BWRs, to recommend that radiation monitors be made mandatory for PWRs rather than optional (though high background radiation and false alarm problems diminish the effectiveness of radiation alarms), and that acoustic leak detection be added as an option to meet the requirement that three methods of leak detection be employed.

In 1991 a contractor for the NRC recommended that for PWRs, acoustic leak detection and inventory balance be added as options to meet the NRC position that three methods be employed for leak detection. In addition, monitoring the rate of change of leakage was suggested. No action followed this recommendation.

For a plant, the establishment of leak monitoring systems and protocols for action when an anomaly is recognized is governed by TSs. With respect to leakage, TSs are generally the same from plant to plant with some differences in the details (Table 9). One of the first TS limits was for the Monticello BWR in 1969. An identified limit of 1.6 kg/s (25 gpm) and unidentified limit of 0.32 kg/s (5 gpm), based on inventory makeup, was established. The total allowed limit (identified plus unidentified) appears to be based on the inventory makeup capability and sump capacity rather than RCS integrity. No documentation has been found on the technical basis used to establish these limits in 1969. Typical limits used today for PWRs are 0.063 kg/s (1 gpm) unidentified leakage and 10 gpm (0.63-kg/s) total identified leakage. For BWRs, they are 0.32-kg/s (5 gpm) unidentified and 1.6-kg/s (25 gpm) total identified, with a capability to detect a 0.13-kg/s (2 gpm) increase within 24 h. Subsequent studies of the failure behavior of reactor coolant systems showed that for many piping systems these limits provide significant margin against gross failure of reactor piping to sustained stress loads. The calculations summarized in Table 8 show that margins increase with increasing pipe diameter and increasing loads under normal operation up to the Service Level A limit. The margins are larger for cracks due to corrosion fatigue, than for cracks due to SCC. Detection systems such as the sump typically measure total leakage. To identify a leak with such a system, one must often compare the amount of leakage from all known sources to the total measured leakage. The difference between these two quantities is then the unidentified leakage.

The current PWR standard technical specifications require that for any leak in the RCS pressure boundary that cannot be isolated, if unidentified RCS leakage exceeds 0.063 kg/s (1 gpm) or if identified leakage exceeds 0.63 kg/s (10 gpm) for a PWR, the plant must be placed in hot standby (mode 3) within 6 hours and cold shutdown within the following 30 h. The evaluation related to safety should begin within four hours of detecting the leak. Two leak detection systems based on different principles, one capable of detection radiation, must be functioning when the reactor is operating. However, a radiation monitor can be inoperative for two days if two other leak detection systems are operating.

In some cases, plant TSs provide additional requirements. For example the TSs for Peach Bottom (2000) require that when in mode 1 (full power), if unidentified leakage increases more than 0.13 kg/s (2 gpm) within 24 h, an evaluation of the source must be initiated. Note that the ISA recommendation suggests a response within one hour. Also for Peach Bottom, following the observation of an increase in leakage, four hours is allowed to reduce the leakage rate before the reactor is shut down.

Table 9, from the Barrier Integrity Action Plan, Action Item 1 (ADAMS ML030660105), shows some leakage requirements for PWRs that are not in the standard technical specifications.

Table 9. Leakage requirements for PWRs not in the standard technical specifications.

Plant Name, Vendor, and Year of Operation	Technical Specification Requirements for Plant-Specific Reactor Coolant Pressure Boundary
Fort Calhoun Combustion Engineering 9/26/1973	<p>TS Section 2.0 does not differentiate between RCPB leakage and other RCS leakage</p> <p>If RCS leakage exceeds 0.063 kg/s (1 gpm) and the source is not identified within 12 hours, the unit is placed in hot shutdown. If leakage exceeds 0.063 kg/s (1 gpm) and the source is not identified within 24 hours, the unit is placed in cold shutdown.</p> <p>If leakage exceeds 0.63 kg/s (10 gpm), the unit is placed in hot shutdown within 12 hours. If leakage exceeds 0.63 kg/s (10 gpm) for 24 hours, the unit is placed in cold shutdown.</p>
Kewaunee Westinghouse 6/16/1974	<p>If any coolant leakage exists through nonisolable fault in an RCS component (exterior wall of the reactor vessel, piping valve body, relief valve, pressurizer, steam generator head, or pump seal leakoff), then the reactor shall be shut down; and cool down to the COLD SHUTDOWN condition shall be initiated within 25 hours of detection.</p>
Millstone Unit 2 Combustion Engineering 12/26/1975	<p>With any PRESSURE BOUNDARY LEAKAGE, be in COLD SHUTDOWN within 36 hours.</p>

Review of Licensee Event Reports provides some insight into what action is taken when a leak is indicated. Frequently, the initial response from the control room operator is to initiate a surveillance test of an RCS water inventory balance. In one case, for a leak detected by a sump level alarm after about 3 h, the inventory balance confirmed that the RCS had unidentified leakage greater than 0.063 kg/s (1 gpm), and so the unit was shut down. The leak was determined to be from a pump seal.

In another case, a leak was indicated by a radiation monitor and was accompanied by decreasing pressurizer level. An RCS water inventory balance was performed for 15 minutes with an estimated leakage of 0.6 kg/s (9.5 gpm). Since the leakage could not be located immediately, it was defined as unidentified leakage greater than 0.063 kg/s (1 gpm), and shutdown from full power began. The leak was determined to be from valve packing.

In many cases, plant procedures take action before required by TS, based on trends in unidentified leakage. In one example, unidentified leakage increased over a period of four days from 0.0063 to 0.019 kg/s (0.1 to 0.3 gpm), but was still well below the TS limit of 0.063 kg/s (1 gpm). Nevertheless, the plant was shut down from full power in accordance with procedures to confirm the source of the leak and make repairs. A fitting thought to be the source of the increased leakage was found not to be the source. A crack in the above-head seal weld of the CRDM was determined to be the cause. This example indicates that leaks below

0.063 kg/s (1 gpm) can be detected with current systems in some cases [sump pumps are typically set to alarm at 0.032-0.063 kg/s (0.5–1.0 gpm)].

The database for leak events has been analyzed to determine the relative frequency of involvement of various components, and the incidence of leakage attributable to fatigue or SCC. Figure 14 shows the distribution in the location of leaks for valves, seals, flanges, nozzles, welds, etc. “Seal” implies leaks from pump seals. “Pipe” leaks includes piping, lines, and small tubing but not leaks from steam generator tubes. “Valve” implies leaks from valves (packing or stem) that do not involve a leaking weld or valve body. “Weld” includes “pin-hole” leaks as well as cracks. “Nozzle” covers nozzles not associated with CRDM. “Sleeve” includes pressurizer heater sleeves. Cracks in CRDM nozzles tend to have very small leak rates and have been found primarily from visual detection of boric acid. Leaks from welds represent nearly 20% of the leaks in the database. Valve leaks not involving a weld were another frequent source of leaks (18%). Leaks from piping account for 26% of the leaks. Though not categorized in Fig. 14, leaks from all types of cracks are involved in over 40% of all leak events in the database. In 19% of the PWR leak events boric acid was visually observed at the site of the leak.

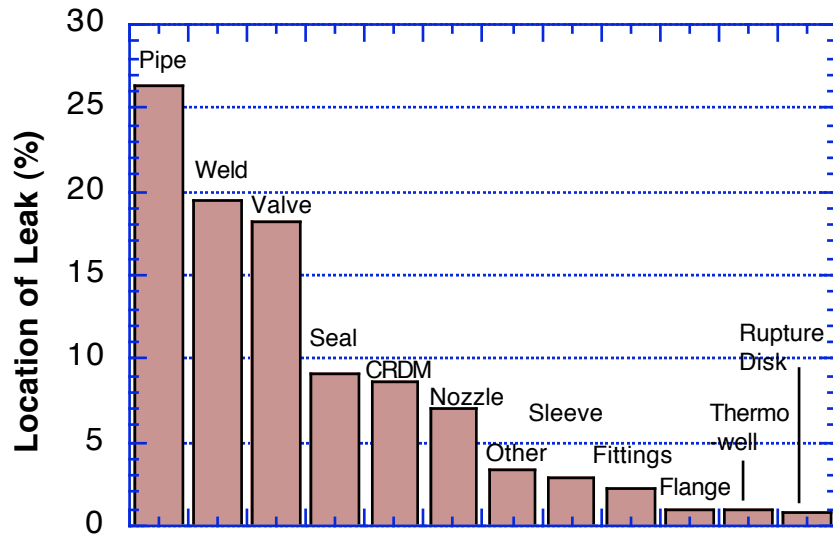


Figure 14. Number of occurrences (percentage) that a location was mentioned in a leak event report. For example, almost 20% of the time the leak involved a weld. About 8% of the leak events reviewed involved CRDMs, usually detected through visual detection of boric acid crystals. Cracks were involved with leaks about 40% of the time with a wide range of leak rates [<0.00063 to 6.3 kg/s ; 0.01 to >100 gpm].

One result regarding welds and seals is similar to that reported in 1988 [16]. The percent of the time leaks in welds and seals were reported (2.1:1) is virtually the same as that reported in 1988 (2.0:1) [16]. Figure 15 shows the relative frequency of cracks when reported as fatigue cracks and SCC for PWRs and BWRs. Stress corrosion cracks were the source of a leak more often than fatigue cracks in PWRs, while fatigue cracks were reported more often in BWRs. When fatigue cracks were the cause of the leak and the description noted more than just “fatigue” as the cause, “high-cycle fatigue” was mentioned much more often than “low-cycle fatigue,” with “thermal-fatigue” noted only occasionally. For cracks with leak rates

>0.0063 kg/s (0.1 gpm) (excluding steam generators) fatigue cracks were noted as the type of crack about 50% more of the time than were SCC. This finding is consistent with the observation that SCCs are tighter and thus result in lower leak rates compared to fatigue cracks for a given crack length.

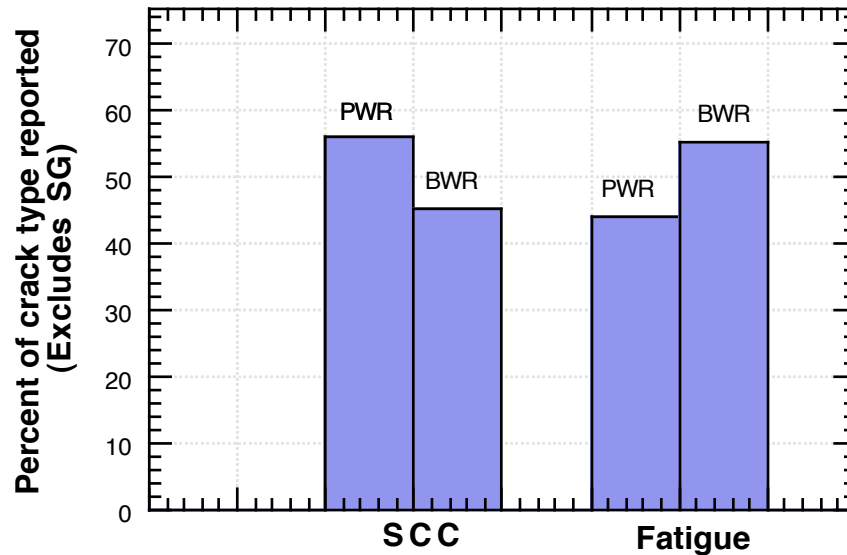


Figure 15a. The relative frequency of SCCs and fatigue cracks reported in the database for PWRs and BWRs. Many SCC involved a CRDM or pressurizer. The SCCs are tight and thus result in lower leak rates compared to fatigue cracks for a given crack length. For cracks with leak rates > 0.0063 kg/s (0.1 gpm) (excluding steam generators) fatigue cracks were noted to have about 50% more occurrences than SCCs.

For leak events in the current database, PWRs account for 70% of RCS leaks (PWRs account for about 66% of the nuclear power plants). In the 1988 report “Assessment of Leak Detection Systems for LWRs” [16], PWRs accounted for 73% of the leak events. The relative rate of occurrence of leak events for PWRs and BWRs has not changed much since 1988. However, the total number of reported leaks has declined steadily from 48 in 1985 to 14 in 2003, as shown in Figure 15b.

The RCS leaks in PWRs and BWRs are compared for both location and mechanism in Fig. 16 to show the ratio of leak events in PWRs and BWRs involving valves, seals, fatigue cracks, SCCs, and welds. The ratio of PWRs to BWRs in the U.S is two and is represented by the horizontal line. SCCs (excluding steam generator tubing) are found more often in PWRs than would be expected based on the relative number of PWRs and BWRs. The same is the case for valves and seals. Weld failures are more consistent with the number of occurrences in PWRs and BWRs.

In Fig. 17, the distribution of leak rates by magnitude is shown. The number of leaks in a given range of leak rates is given. Many leaks reported have very small leak rates (<0.001 kg/s). They are detected visually and are reported as drips, weeping, seepage, “very small,” etc. Large leaks have been detected primarily through increases in sump level, radiation alarms, inventory balance, or change in pressure. The trend in reported leak rates seen in Fig. 17 is comparable to that reported for PWRs [15].

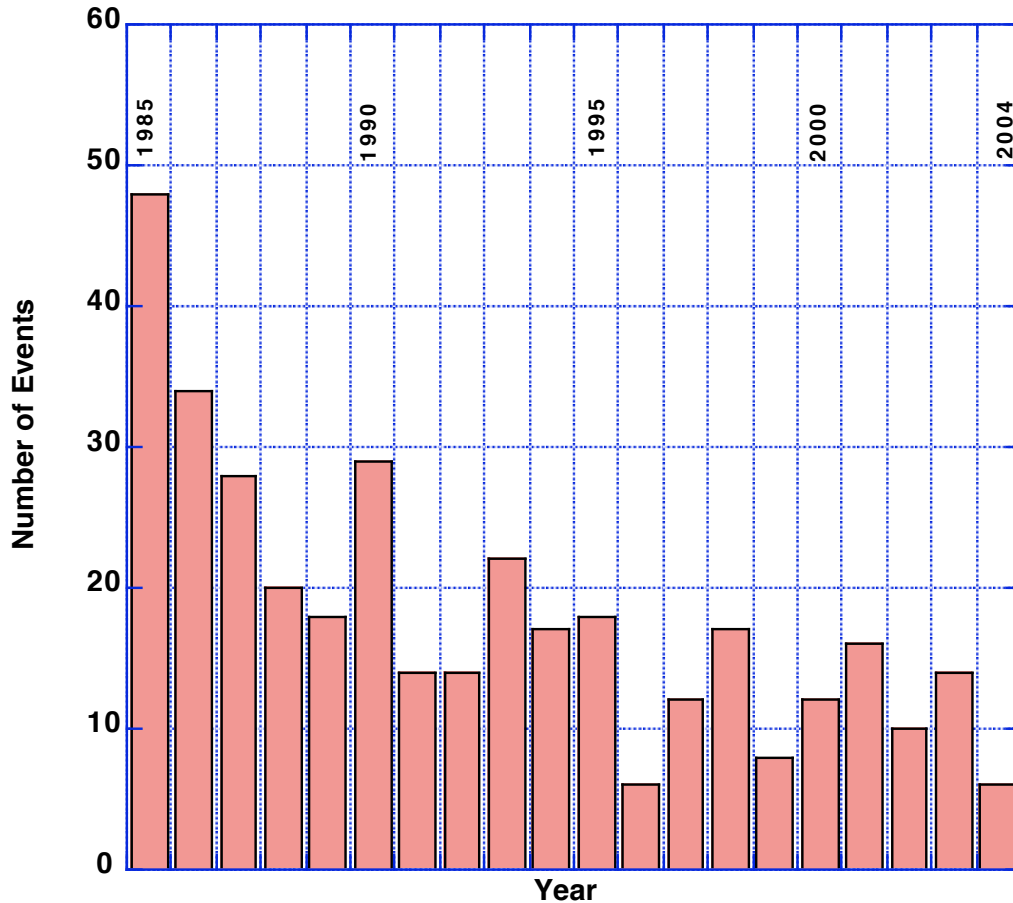


Figure 15b. Number of leakage events reported per year in database. A decrease in number of leakage events from 1985 is evident. Events for 2004 includes those recorded through June.

Consequences of Lowering Leak Rate Limits

Consequence of lowering leak rate limits have been considered. It appears that lowering the limit for a PWR would have no effect on safety system design or design basis other than requiring more-sensitive leak detection systems to minimize unnecessary shutdowns. Other consequences are (a) Lower limits would be supportive of leak-before-break analysis and evaluation (additional safety margin with respect to critical crack flow rate), (b) Limits may be exceeded more frequently, resulting in more shutdowns, inspections, and repairs and thus additional personnel exposure, (c) If PWR limits were cut in half, reactor operations would most likely not be affected excessively, (d) Current leak monitors could still be used, (e) Cutting the limit in half would not have resulted in detection of the leak that occurred at Davis-Besse (a localized system would have been needed), (f) The inability of current systems to locate a leak will lead to spurious shutdowns if leakage limits are reduced by more than a factor of two, (g) Because of the better fuel designs and better chemistry in current plants, neither the conventional airborne particulate or gaseous monitor is now capable of detecting a 0.063-kg/s (1 gpm) leak within an hour (response time could be on the order of 100 h) and (g) Lowering the leakage limits could make the air particulate monitor obsolete.

Correlation between Crack Size and Leak Rate

The results in Table 10 for SS and CS piping in PWRs show that a given leak can correspond to a wide range of crack sizes. For a 0.063 kg/s (1 gpm) leak, crack lengths can range from 26 to 460 mm (1.0 to 18.1 in.) for stainless steel piping and 51 to 310 mm (2.0–12.2 in.) for carbon steel piping, depending on pipe diameter and the loading during normal operation. Because the throughwall crack length corresponding to a given leak rate, Q , varies as $\approx Q^{0.24}$ for a given load level, decreasing the leak rate by a factor of 2, decreases the possible crack sizes by about only 20%.

The results in Table 10 underestimate the actual variability since they were computed for fixed crack parameters and only include the variability due to differences in pipe size and applied loading. The additional variability due to variations in path length, and crack roughness are fairly small compared to the variations due to the applied load. Deviations from the idealized rectangular shape (e.g., remaining ligaments) could have very significant effects.

These analytical predictions are consistent with field experience. Many of the leaking cracks in the database (mostly cracks in welds) have very low leak rates (<0.01 kg/s) despite significant through-wall crack lengths. Figure 18 shows the lack of correlation between crack length and leak rate for leak events in the database where both the through-wall crack length and the leak rate were reported. As expected, no correlation is evident and the crack lengths for leak rates 0.0063 kg/s (0.1 gpm) or less vary from 2.5 to 76.0 mm (0.1 to 3 in.) long.

Table 10. Variability of throughwall crack lengths for a given leak rate in SS (PS cases) and CS (PC cases) piping in PWR RCSs.

Case No.	Diameter, mm	Stress, psi/ % Service Level A - 1.5Sm	Leak Rate, kg/s	Through wall Crack length - mm	Percent of DPZP Crack Length
PSS-100-1C	114	100%	0.0063	11	9.7%
PSM-100-1C	356	100%	0.0063	14	5.3%
PSL-100-1C	813	100%	0.0063	18	5.0%
PSS-50-1C	114	50%	0.0063	33	21.4%
PSM-50-1C	356	50%	0.0063	44	10.1%
PSL-50-1C	813	50%	0.0063	52	6.2%
PSS-25-1C	114	25%	0.0063	76	40.7%
PSM-25-1C	356	25%	0.0063	159	29.2%
PSL-25-1C	813	25%	0.0063	314	27.6%
PSS-100-2C	114	100%	0.063	26	24.1%
PSM-100-2C	356	100%	0.063	38	14.1%
PSL-100-2C	813	100%	0.063	48	13.4%
PSS-50-2C	114	50%	0.063	65	42.1%
PSM-25-2C	114	25%	0.063	102	55.1%
PSM-50-2C	356	50%	0.063	107	24.6%
PSL-50-2C	813	50%	0.063	136	16.2%
PSM-25-2C	356	25%	0.063	243	44.6%
PSL-25-2C	813	25%	0.063	460	40.5%

Case No.	Diameter, mm	Stress, psi/ % Service Level A - 1.5Sm	Leak Rate, kg/s	Through wall Crack length - mm	Percent of DPZP Crack Length
PCS-100-1C	114	100%	0.0063	22	17.3%
PCM-100-1C	356	100%	0.0063	27	8.2%
PCL-100-1C	813	100%	0.0063	31	6.0%
PCS-50-1C	114	50%	0.0063	34	20.5%
PCM-50-1C	356	50%	0.0063	43	9.0%
PCL-50-1C	813	50%	0.0063	49	5.2%
PCS-25-1C	114	25%	0.0063	62	32.0%
PCM-25-1C	356	25%	0.0063	108	18.8%
PCL-25-1C	813	25%	0.0063	152	12.4%
PCS-100-2C	114	100%	0.063	51	40.7%
PCM-100-2C	356	100%	0.063	72	22.0%
PCS-50-2C	114	50%	0.063	72	43.1%
PCL-100-2C	813	100%	0.063	85	16.5%
PCS-25-2C	114	25%	0.063	98	50.3%
PCM-50-2C	356	50%	0.063	108	22.6%
PCL-50-2C	813	50%	0.063	134	14.2%
PCM-25-2C	356	25%	0.063	201	34.8%
PCL-25-2C	813	25%	0.063	310	25.3%

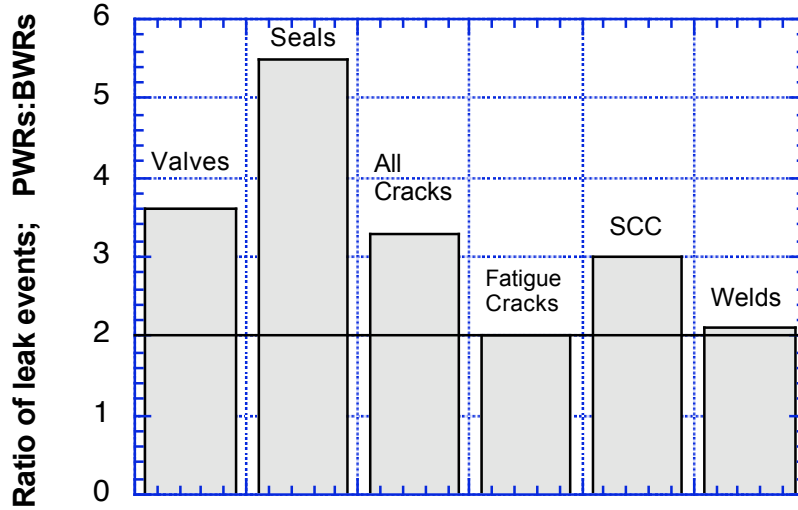


Figure 16. The PWR-to-BWR ratio of leak events involving valves, seals, fatigue cracks, SCCs, and welds. The ratio of PWRs to BWRs in the U.S. is 2 and is represented in the figure by the horizontal line.

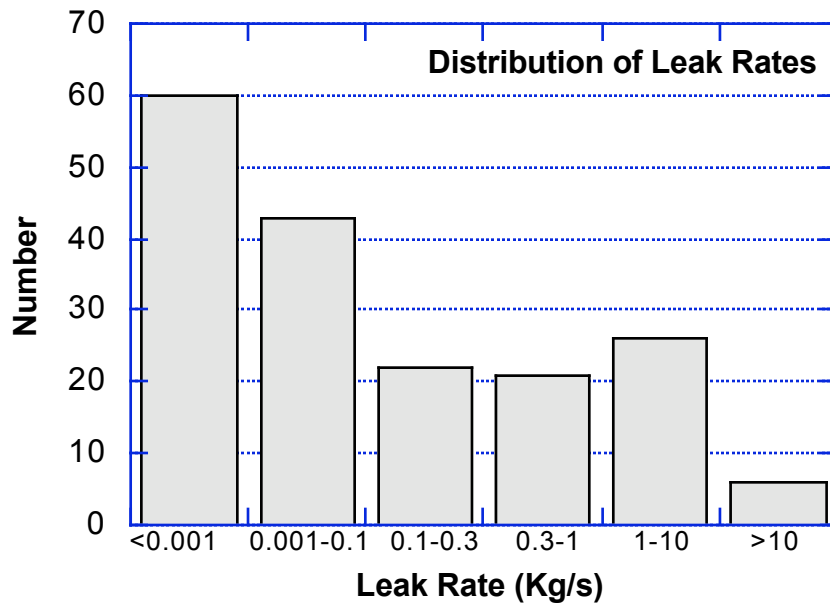


Figure 17. Distribution of leak rates by magnitude recorded in the database beginning with 1970. The number of leaks in a given leak rate range is indicated.

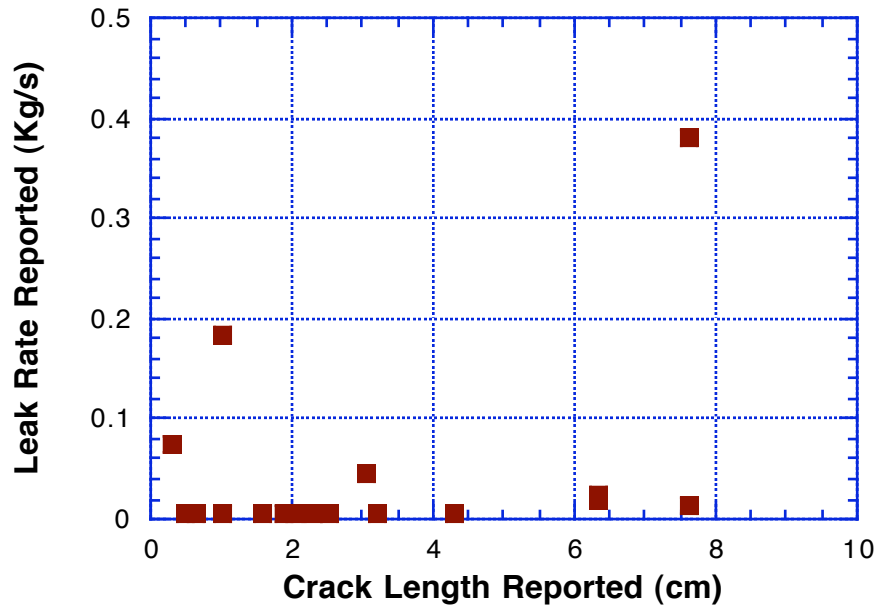


Figure 18. Through-wall crack length vs. leak rate for variety of leaks in database. Most of the leaks were cracks in welds.

5. Leak Monitoring Systems

The effectiveness of various conventional leak detection systems is summarized in Table 11. The sensitivity, accuracy, and location in Table 11 are based on the value reported in the Instrument Society of America Report, "Standard for Light Water Reactor Coolant Pressure Boundary Leak Detection" (ISA-S67.03-1982). The letter "G" implies the method can meet the intent of ISA-S67.03-1982, where "F" implies it may be acceptable or unacceptable depending on conditions, while "P" indicates the method is not recommended except possibly for monitoring specific locations. No single technique in this list is rated good in all categories, indicating that more than one monitoring system is needed to have an effective capability for leak detection.

Table 11. Effectiveness of leak monitoring systems

Type of Monitor	Sensitivity	Accuracy	Location
Sump monitor	G	G	P
Radiogas monitor (Xe-133, Iodine)	F*	F	F
Radioparticulate (Rb-88, Kr-88, spectrum)	F	F	F
Condensate flow	G	F	P
Coolant Inventory	G	G	P
Moisture sensors	G	P	G
Temperature	F	P	F
Pressure	F	P	P
Visual	F	P	G

*Sensitivity, accuracy, and location rated as good (G), fair (F), and poor (P). Note that the primary systems are becoming less contaminated and failed fuel is much less likely to occur now than in the 1980s, though the trend has reversed somewhat in the past two years (Fig. 19). As a result the gaseous radioactivity monitor is no longer equivalent to particulate monitors and the sensitivity of gaseous radioactivity could now be rated "P."

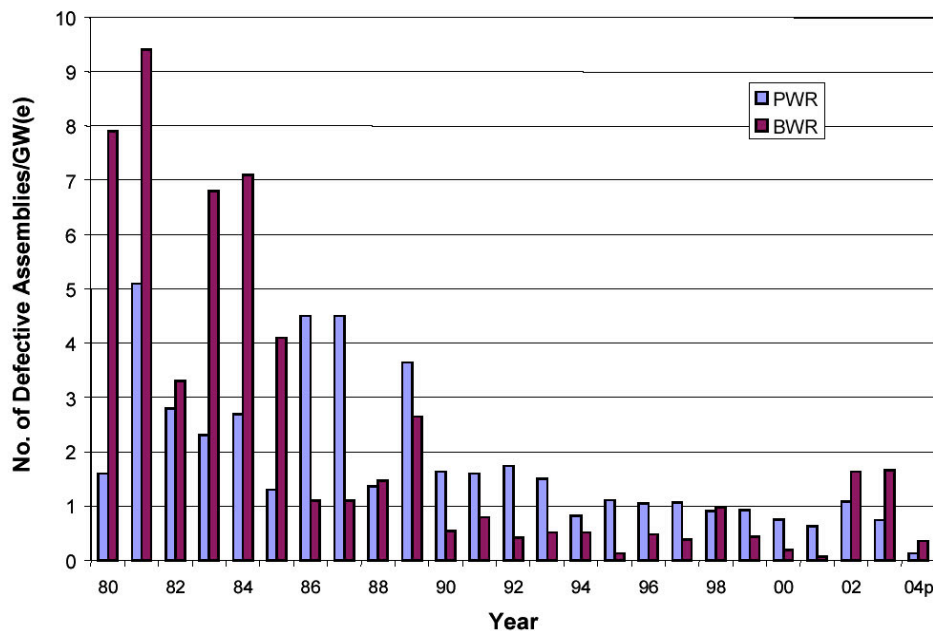


Figure 19. Trends in U.S. fuel failure rates (2004 results are incomplete).

The most flexible of the methods for detecting leaks is visual observation. However, the sensitivity and ability to quantify a leak by observation are poor. The adequacy depends on the frequency of inspection and the accessibility of areas of interest. The ASME Boiler and Pressure Vessel Code, Section XI (IWA-2211 VT-2 Examination), covers periodic mandatory inspection requirements of the RCPB. For example, IWA-5241(e) states that "Discoloration or residue on surfaces shall be examined for evidence of boric acid accumulations from borated reactor coolant leakage." Remote visual equipment, temperature-sensitive tapes, and paint can aid in locating leaks. While not a principal method for leak detection, the visual method is valuable in locating leaks. Over half of the leaks in the database had been detected visually and had very low leak rates.

The visual method, based on field experience, is capable of detecting leak rates as low as 0.0006 kg/s (0.01 gpm), but the reliability of the method depends on human factors. From Lange's *Handbook of Chemistry* (15th edition) we can estimate that an aspirin-size deposit of boric acid (approximately 400 mg) could deposit from about 0.95 L (0.25 gal) of water and would be detectable during a visual examination of reactor components. From a leak as small as 6.3×10^{-7} kg/s (10^{-5} gpm) that amount of boric acid could accumulate in about a week.

Humidity monitoring can detect an increase in vapor content of air resulting from a leak but suffers from a lack of quantitative information. The sensitivity could be on the order of gallons per minute when used in large volume containment areas [20]. Moisture sensitive tape is a continuous monitoring system in which the sensor is placed next to insulation. An electrical signal is activated when the tape becomes wet. Detection of an increase in leak rate of 0.063 kg/s (1 gpm) within an hour is possible. Such tapes monitor a small area and have been installed at a few plants. Field experience confirms that local humidity monitors, such as the FLUS system described later, can detect leakage less than 0.1 L (0.03 gal) [26].

The sensitivity of temperature monitoring to detect leaks depends on volume of space, distance between sensor and leak, heat losses, normal temperature fluctuations, and presence of abnormal heat sources. Temperature monitoring probably will not detect a 0.063-kg/s (1 gpm) leak within one hour. Nevertheless, temperature sensors were installed on the relief lines in French PWRs [15].

A leak from the RCPB will increase the containment pressure. The consequence of having a large volume containment structure is that a leak would have to be very large to be detected by an increase in pressure. Small leaks could result in pressure variations that are in the normal range of fluctuations. No source information is provided for the leak.

Reactor coolant inventory is monitored in PWR plants but not in BWRs. This method is not particularly useful for BWRs because of the poor accuracy in detecting small RCPB leakage. About 10% of all the leaks in the database were detected from inventory balance. Use of inventory balance for detecting a leak of 0.063 kg/s (1 gpm) within one hour is difficult. However, under steady-state conditions, detection of 0.044 kg/s (0.7 gpm) in 2 hours and 0.021 kg/s (0.33 gpm) in 4 hours has been demonstrated under field conditions [15]. Containment leakage, other than identified leakage which is delivered to the equipment drain sump, is drained to the containment sump as unidentified leakage.

The sump level is measured continuously by a level measuring device. One alarm monitors the increase in the rate of unidentified leakage and provides an alarm when the

increase in leak rate exceeds 0.032-0.063 kg/s (0.5–1.0 gpm). A sump level and flow rate monitor can detect a 0.063 kg/s (1 gpm) leak in less than 1 hour. In some plants a 0.063 kg/s (1 gpm) leak can be detected in 10 minutes [15]. Another alarm monitors the total of identified and unidentified leakage [20]. Open containment sumps collect unidentified containment leakage, including containment cooler condensate. Sump level and sump discharge flow can be monitored. Leak location is not provided. Sump pump monitors can detect a 0.063 kg/s (1 gpm) increase in leakage within one hour. Under field conditions, increases as low as a few tenths of a gpm have been detected (e.g., LER 354/1989-026-00). At Oconee, an increase in the volume of leakage on the order of 28.5 L (7.5 gal) can be detected by the sump pump [15], and thus a 0.063 kg/s (1 gpm) leak could, in principle, be detected in about 10 minutes. Historically, the reliability of the sump pump monitor has been good. About 10% of all the leaks in the database were reported as detected by the sump pump monitor.

Containment air cooler condensate flow runoff from the drain pans under each containment air cooler unit can be measured. A 0.063 kg/s (1 gpm) increase within one hour can be detected under normal operating conditions. This estimate is based on a calculation that shows condensate from 0.063 kg/s (1 gpm) leaks can reach steady state in about 30 minutes [15].

Assuming no fuel failure, for a containment-vessel free volume of 73,700 cubic meters and a particulate activity concentration in the reactor coolant of 1.5×10^3 Bq/cm³, airborne particulate monitors are capable of detecting, in principle, a 0.0063-kg/s (0.1 gpm) leak in 10 minutes [15]. However, this type of monitor is not capable of detecting a 0.063 kg/s (1 gpm) leak within one hour under all conditions. An event occurred at Oconee 3 [15] where it took about 100 minutes to detect a 0.063 kg/s (1 gpm) leak.

A clear understanding of the principles involved in detecting leaks from radiation monitors is necessary to avoid false alarms. For example, a decrease in reactor power level may cause an increase in the primary coolant radioactivity, and thus an apparent increase in leakage could be incorrectly surmised.

The airborne gaseous radioactivity monitor is inherently less sensitive than the particulate monitor. A leak rate of 0.13 kg/s (2 gpm) is estimated to be detectable in four hours with a gaseous monitor, assuming a coolant activity of 4×10^4 Bq/cm³ of Xe-133 [15]. With a detector sensitivity of 10^{-6} μ Ci/cm³ and reactor coolant gaseous activity of 0.5 μ Ci/cm³, corresponding to 0.1% fuel defects (per Southern California Edison, Ref. 12, p. 172), 0.063 kg/s (1 gpm) leak can be detected within one hour [15]. The difficulty with the use of a gaseous radioactivity monitor arises as failed fuel is much less likely to occur (see Fig. 19), and the primary systems become less contaminated. Thus, the gaseous radioactivity monitor may no longer be equivalent to a particulate monitor as it is in RG 1.45 and could be dropped from RG 1.45.

The fraction of leaks detected by the various methods is shown in Fig. 20. Most leaks recorded were detected visually and were quite small. They were reported as drips, weeping, seepage, "very small," boric acid deposits, etc. Large leaks have been detected primarily through inventory balance, change in containment pressure, rise in sump level, or radiation alarms. The median leak rate of the leaks detected by the sump pump is 0.095 kg/s (1.5 gpm) for a range of 0.006 to 2.2 kg/s (0.1 to 35 gpm). The median for radiation monitors (includes

particulate and gas monitors) is 0.032 kg/s (0.5 gpm) (Table 12). Based on the reported leak rates, detecting small leaks with either the radiation monitor or sump pump is possible. Leak rates detected for valves, pumps, and CDRM are summarized in Table 13. Leaks detected from valves, for example, are relatively large while those from CRDM are relatively small (on average, well below the allowed limit). Table 14 shows the median leak rate and range for all leak events that involve a crack, all leak events that do not involve a crack, leaks from cracks in welds, leaks from a crack not involving a welds, cracks when reported as an SCC, and cracks reported as a fatigue crack. Note that not all leaks have a leak rate reported. Also, some leaks from a crack are not associated with either fatigue or SCC, and thus the rate for all cracks differs from SCC. Leaks reported as seepage, weeping, or drips are excluded. A few leaks are reported as very large (or equivalent) but without a leak rate. For those cases the event is included in Table 14 using a leak rate of 6.3 kg/s (100 gpm). The table shows that the median leak rate reported for a crack is significantly less than that reported when not a crack. Note that the leak rates reported for SCC are very low, and while well below the 0.063-kg/s (1 gpm) limit, non-critical flaws can be expected to leak at below the limit.

In addition to the leak rate detected, the time to recognize that action is needed is important. The time to recognize that a leak requires action (that is, it must be identified or treated as unclassified) is shown for the sump pump and radiation monitor in Figs. 21 and 22. The range of time covers five orders of magnitude for leaks less than 0.063-kg/s (1 gpm), while for larger leaks, the time to recognize a problem is on the order of 100 min. Since the smaller leaks do not (at least initially) exceed the allowed limit for unidentified leakage, a considerable amount of time can be taken to monitor the leak and try to reduce the leak rate without shutting the plant down. Larger leaks, which exceed the allowed limit, require more rapid action. The events in Figs. 21 and 22, in which the time required to recognize that a leak requires action was greater than one day, all occurred before 1999. This is also the case for leaks in the database detected by means other than a radiation detector or sump pump monitor. Leaks that were detected by means other than radiation detectors or sump pump monitors and that required action and took longer than one day to recognize also all occurred before 1999. Sump pump and radiation monitors are required in RG 1.45, but their effectiveness in PWRs and BWRs differs. For PWRs, sump pump and radiation detectors were reported as the method of detection about equally often, whereas for BWRs the sump pump was the reported detection method about three times more often than a radiation monitor. A problem with radiation detectors is that high background levels could require alarm trip points to be set so high that the monitors are potentially insensitive to rises in radiation level due to leaks. In one case, a radiation alarm was not activated by a 1.6-kg/s (25 gpm) leak [16]. Conversely, if the set point is too low, the radiation monitor can raise false alarms [16].

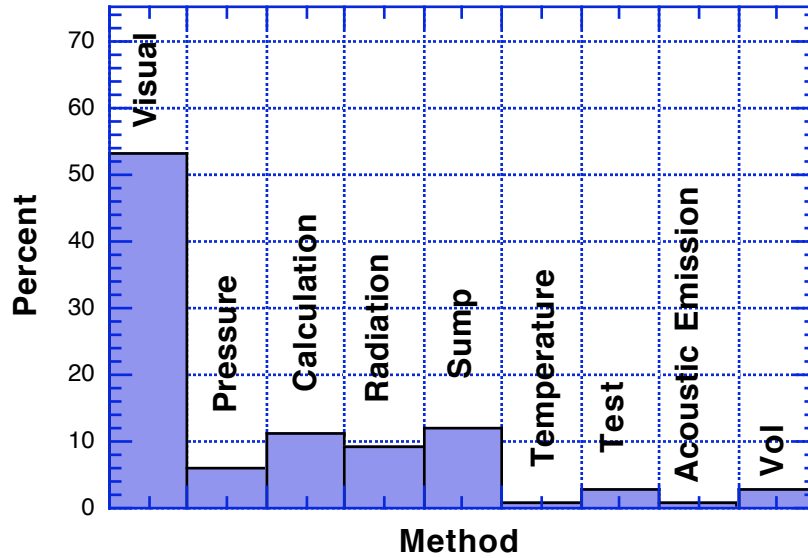


Figure 20. Comparison of leak detection methods reported in the leak event reports. Small leaks were detected visually. Test refers to hydrostatic pressure test. Vol refers to high makeup rate to volume control tank.

Table 12. Average reported median leak rate and range for sump pump, radiation monitors (includes particulate and gas monitors), and other leak detection methods (mainly visual and calculated).

Leak Detection System	Median Leak Rate Reported (kg/s)	Range (kg/s)
Sump pump	0.1	0.006 – 2.2
Radiation detector (particulate and gas)	0.03	0.006 – 0.44
Other (primarily visual and calculation)	0.1	0.006 – 5

Table 13. Reported leak rates for valves, pumps, and CRDM.

Component	Median Leak Rate Reported (kg/s)	Range (kg/s)
Valve	0.06	0.13 – 1.3
Pump	0.11	0.0006 – 0.4
CRDM	0.0006	0.0006 – 0.08

Table 14. Reported leak rates for cracks (SCC and fatigue) and valves and pump seals.

Information from leak events database	Median Leak Rate Reported (kg/s)	Range (kg/s)
All leak events with cracks involved	0.06	0.006 to > 6.3
Leaks not involving cracks (valves, pumps, etc.)	0.3	0.006 to > 6.3
Leaks from cracks in welds	0.06	0.006 to 5.5
Cracks not involving welds	0.02	0.006 to > 6.3
Cracks when reported as SCC	0.013	0.006 to 0.06
Cracks when reported as fatigue crack	0.06	0.02 to 5.5

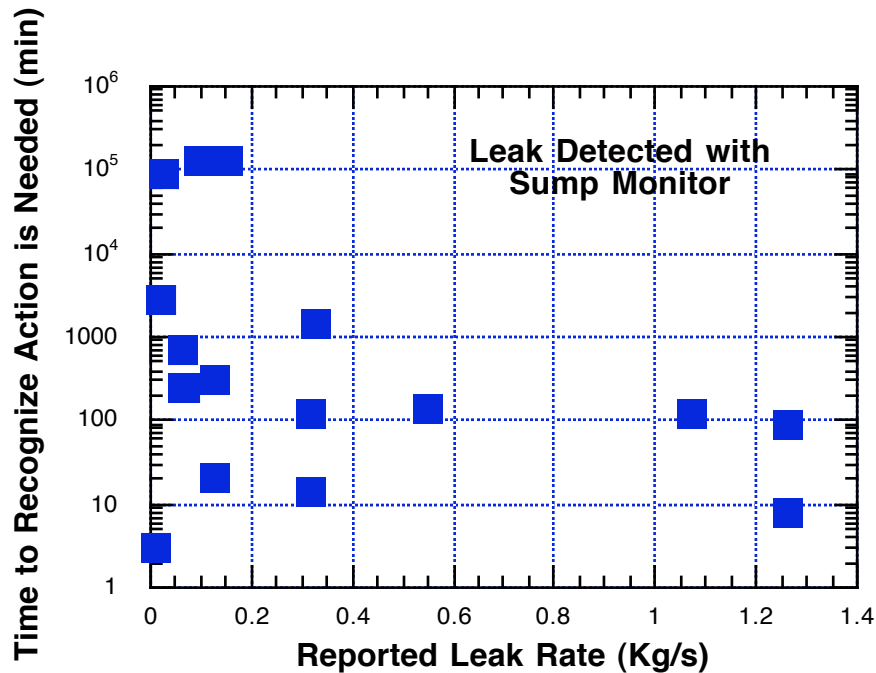


Figure 21. Time to recognize action is required after leak detected with sump monitor.

In the database, occasionally a leak was reported to be detected by more than one leak monitoring system. In those cases, in the tables and figures of this report, detection is assigned to the method that first detected the leak.

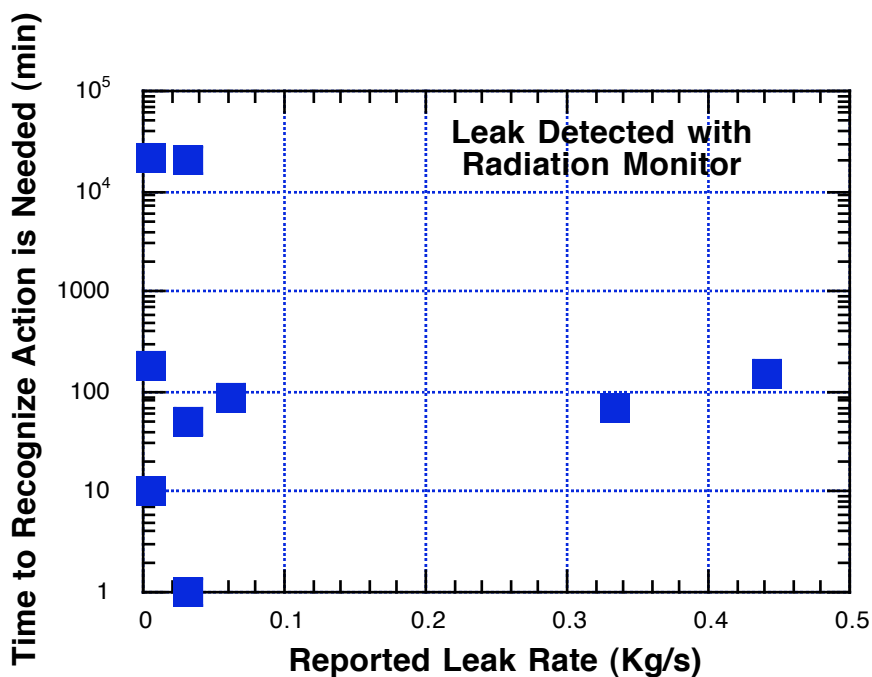


Figure 22. Time to recognize action is required after leak detected with radiation monitor.

Acoustic Emission Leak Monitoring

Acoustic emission (AE) technology has the potential to provide significant improvements in leak detection capability. AE systems can provide rapid response to even small leaks, locate leaks, and monitor an entire plant. A major advantage of AE is that crack growth can be detected before the crack is through-wall due to the release of elastic energy by the growing crack. No other technique can provide this information. Furthermore, AE can be used during heat-up and pressurization when airborne monitors would not be effective. Acoustic leak detection systems can be used to monitor the entire RCS or dedicated to the monitoring of components of particular interest, such as valves.

Currently, acoustic monitoring for leakage can be carried out with a commercially available system, the Framatome-ANP "ALUS" [21,26]. In-service monitoring involves an array of acoustic transducers attached to the reactor coolant system or pressurizer through waveguides. Signals in the 100 to 400 kHz range are processed and the root-mean-square (RMS) values of the signal amplitude are compared with individually adjustable fixed and sliding thresholds. Typically, leakage will be detectable if the total signal is 3 dB (41%) above the background noise [21]. For a near field sensor <3 m (10 ft) from the source, the detectable leak rate can be calculated. The estimated sensitivity varies from 0.0002 to 0.063 kg/s (0.003 to 1.0 gpm) depending on the background noise [21,26]. This range is similar to that reported in Ref. [16] (NUREG/CR-4813). The AE sensitivity in that report was estimated to be 0.0001 to 0.063 kg/s (0.002 to 1 gpm). A summary of that study is provided in Appendix B.

Table 15 provides detailed information on leakage sensitivity variations with background noise level (in a 100–400 kHz frequency window) [21, 26]. The lowest noise levels are in the

pressurizer where the leak rate sensitivity is estimated to be as low as 0.0002 kg/s (0.003 gpm). For coolant pumps, where the noise is highest, the best observed sensitivity according to the vendor is 0.0063 kg/s (0.1 gpm). The response time is determined by the data processing time, and thus can be very short. Signal processing and decision making can be automated and controlled by computers. To calibrate the system, ultrasonic transmitters attached to the plant structure can be automatically activated during plant outages. They produce a signal with a defined intensity that simulates a leak, and attenuation measurements can then be made. The ALUS system has been installed in several VVER reactors in Eastern Europe [26,27]. Ten years of field experience with operating reactors outside the U.S. has been accumulated with such systems monitoring reactor pressure vessels, reactor coolant lines, pressurizer systems, and safety valves [27]. Flange leaks were detected at the main flanges of the reactor pressure vessel and at the reactor coolant pumps in several VVER plants. These leaks occurred during start-up pressurization. A head penetration leak during hydrostatic testing was detected at leak rates consistent with the estimated sensitivity of 0.0002 kg/s (0.003 gpm). Training in mounting sensors to the reactor structure may be required. Figure 23 shows a flow chart for the ALUS system and a photograph of the waveguide. Note that since the more recent development of FLUS (humidity monitor described in the following section), ALUS systems are only installed along with a FLUS system.*

Some valves in the RCS are monitored with an acoustic sensor. Two valve leaks in the database were detected by acoustic sensors dedicated to the monitoring of the valves.

Monitoring with Humidity Sensors

The Framatome-ANP FLUS system measures local humidity [22] by using a temperature- and radiation-resistant sensor tube, fabricated from a flexible metal hose with porous sintered metal elements placed at intervals of around 0.5 m (Fig. 24). The contents of the sensor tube are pumped at fixed time intervals through a central moisture sensor that measures the absolute humidity level (the dew point) as a function of time. The location of the leak can be deduced from the time difference between the start of the pumping and the peak humidity vs. time history by using the known air velocity in the tube. The leak rate can be determined from the profile of the humidity vs. time history. The sensitivity for the FLUS system is reported to be 0.0003 kg/s (0.004 gpm) or less [26]. Up to eight monitoring loops, each up to 150-m long with a spacing of about 0.5 m between sensors, can be connected to a FLUS monitoring station, which implies that up to 1.2-km piping length can be monitored by the station. The FLUS systems have been installed at plants in Europe and Canada. The first FLUS system in the United States was installed at Davis-Besse by Framatome ANP in 2003. FLUS has been qualified to detect potential leaks from a RPV closure head for a German PWR at Obrigheim [26]. In this instance, two sensor tubes were used; one was placed inside the insulation and the other outside it. Calibration tests confirmed that a leakage rate of gpm 0.00001 kg/s (0.0002 gpm) could be reliably detected. Clear correlation between leakage rate and dew point was confirmed. The response time was as little as 15 min. The manufacturer's

* Personal communication from T. Richards/W Knoblach, Framatome ANP to D. Kupperman, Argonne National Laboratory, July 5, 2004.

specification gives a typical response time in one to two cycles; each cycle time is 15 min to 1 h. One 0.003 kg/s (0.05 gpm) leak in the flange of a control rod was detected during operation.

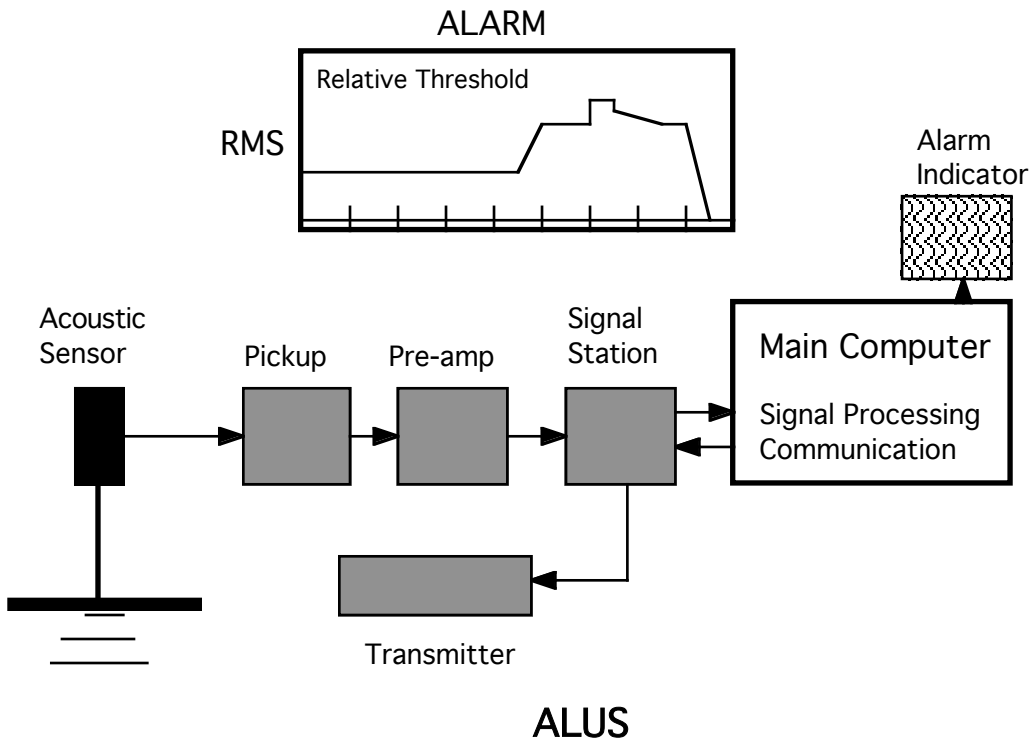


Figure 23. Schematic representation of the ALUS system [27].

Table 15. Estimated leakage sensitivity for the ALUS acoustic monitoring system as a function of background noise level (in 100–400 kHz frequency range) [21,27].

Component Position	Average Background Noise Level (dB)	Estimated Leakage Sensitivity Range with Lowest Limit (kg/s)
Main Isolation Valve (hot)	41.2	0.003 to 0.006
Reactor Coolant Pump	48.0	0.006–0.06
Reactor Pressure Vessel	41.7	0.03 to 0.006
Pressurizer	17.3	0.0002–0.006
Pressurizer Safety Valve	45.0	0.004 to 0.013

The calibration procedure involves injecting a fixed amount of vapor (test gas) into the sensor tube for each measuring cycle. The gas moves through the sensor tube to the monitoring system, which automatically records the arrival time of the gas. The amplitude and the time of arrival of the first peak are checked to be within proper ranges. Any deviation

triggers an alarm. The system will then perform a calibration procedure to correct the system functioning.

Field tests with FLUS have confirmed that leak rates less than 0.0003 kg/s (0.004 gpm) can be detected without false alarms [26]. No leaks have been missed in leak simulation tests, and one actual leak was detected [26]. Leaks can be located within distances less than 2% of the total length of the line monitored. In one example a 0.013-0.026 kg/s (0.02–0.04 gpm) flange leak at a VVER reactor was detected one month after installation of FLUS [26]. Since the development of FLUS, ALUS systems are installed along with a FLUS system.*

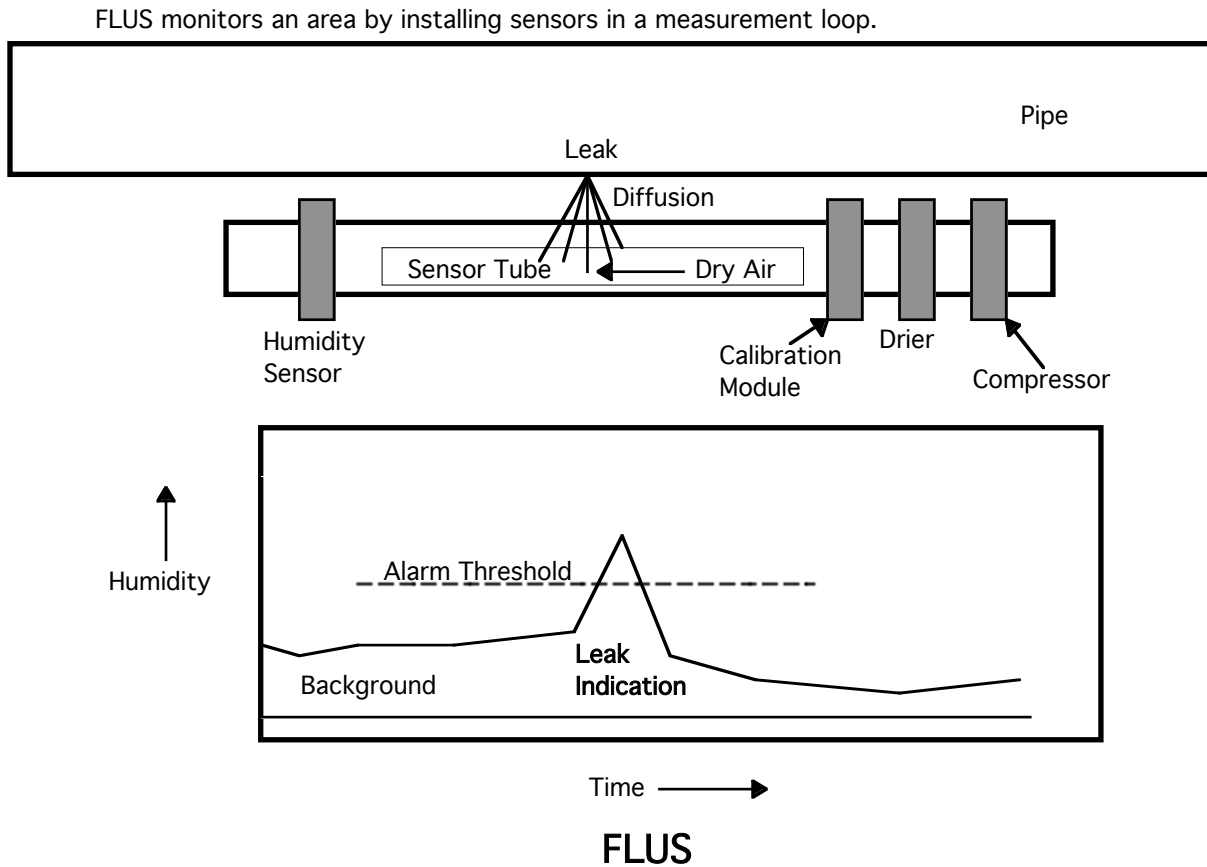


Figure 24. Schematic representation of the FLUS humidity sensor system. The sensitivity for the FLUS system is reported to be 0.0003 kg/s (0.004 gpm) [22].

Airborne Particulate Radiation Monitor

Westinghouse has developed an airborne particulate radioactivity monitoring system (ARMS). The first ARMS was installed and demonstrated at Turkey Point Unit 3 in 1988. In 1989 a similar system was installed at Turkey Point Unit 4, which operated for 10 years

* Personal communication from T. Richards/W Knoblach, Framatome ANP to D. Kupperman, Argonne National Laboratory, July 5, 2004.

without a false alarm. Another ARMS was installed with a site validation test at Electricite de France (EdF) Bugey Unit 2 Nuclear Power Plant in 1992 for detection of head penetration leakage [23]. False alarms at Bugey led to the removal of that unit.

The Westinghouse ARMS is used primarily to detect leaks in the head area of a PWR, such as CRDM canopy seals and nozzles and associated welds. Leakage in this head area releases radioactive particles, mainly Rb-88 and Cs-137, into the air volume surrounding the head. ARMS draws air from the volume through a filter to concentrate the particulates. Radiation from the collected particulates is detected by a detector consisting of a beta-sensitive plastic scintillator disk and a photomultiplier tube. The typical operation of ARMS involves collecting samples from two sources. One sample comes from the ambient atmosphere of the containment, while the other is from the reactor head. The difference of the radioactivity levels in the two samples provides a measure of leak rate. Each sampling time takes several hours. Therefore, the estimated response time is several hours to a day.

ARMS provides a measure of reactor vessel leakage, but it is difficult to accurately relate the amount of rubidium and cesium particulates collected by the sensor filter to the total mass of leakage, and thus the system may not be able to determine the leakage rate reliably. However the general location of a leak can be determined with ARMS. Westinghouse reports a sensitivity of 0.0001 kg/s (0.002 gpm).

Note that the ARMS, FLUS, and ALUS systems are not adequate for detection of very small leaks from the RPV head, such as those revealed by minor amount of boric acid crystals at Oconee and ANO-1. However, for larger leaks they may be more likely to detect a significant leak prior to rupture compared to other conventional existing systems for plant monitoring.

Improved Radioactive Gas Monitors

An N13-F18 gas monitor (Model SPLR201 1E) has been available through MGP Instruments, Inc., Atlanta, Georgia, and the VICNIS (Vessel Integrity Control using Nitrogen-13 Sensor) through Merlin Gein Provence, France [24]. The N13-F18 monitors from MGP were installed at two EdF sites (Paluel and Dampierre). Since 1992, more than 50 VICNIS units have been installed at EdF plants. The main areas of coverage are the reactor head and the bottom of the reactor vessel [15, 34].

Both the N13-F18 monitor and the VICNIS sensor detect leaks by monitoring the presence of nitrogen-13 and the evolution of its released volumetric activity. The N-13 arises in the reactor core from the reaction "Proton + O-16 → N-13 + He-4". The N-13 radioactivity (beta decay) is measured using a NaI (TI) scintillator coupled with a photomultiplier. The basic configuration of both monitors consists of two detection systems. One monitors the reactor head atmosphere, while the second measures the containment background.

A leak rate in the range of 0.0003 kg/s (0.004 gpm) is claimed to be detectable within one hour, provided the radiation background is reasonably low. Detection reliability and sensitivity depend on background levels and counting time. With the detection threshold criteria set to achieve a faulty alarm probability (FAP) not exceeding 1 error per year and a alarm ignored probability (AIP) not exceeding 0.01, a detection sensitivity of 0.0003 kg/s (0.004 gpm) within one hour is claimed. Nevertheless, high false alarm rates have led to discontinued use of

nitrogen gas sensors by EdF (to the best of the knowledge of the authors, such devices are not used worldwide).

Visual Observation of Leaks

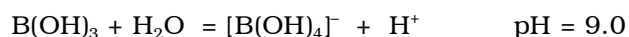
While not an on-line technique, a useful method for detecting and locating leaks is visual observation. However, the sensitivity and ability to quantify a leak by observation are poor except for boric acid leaks. The adequacy depends on the frequency of inspection and the accessibility of areas of interest. The ASME Boiler and Pressure Vessel Code, Section XI (IWA-2211 VT-2 Examination), covers periodic mandatory inspection requirements of the RCPB. For example, IWA-5241(e) states that "Discoloration or residue on surfaces shall be examined for evidence of boric acid accumulations from borated reactor coolant leakage." Remote visual equipment, temperature sensitive tapes, and paint can aid in locating leaks. While not a principal method for on-line leak detection (despite the numerous leaks in the database detected visually) visual detection of leaks is valuable in locating leaks.

Detection of Boric Acid from Leaks

Boric acid or orthoboric acid, $B(OH)_3$, is used as a neutron absorber in the coolant of pressurized water reactors. Lessons learned from the Davis-Besse incident call for re-evaluation of the boric acid corrosion control program, including the ability to detect boric acid from a leak. At present, the method of detecting boric acid leaks is basically visual inspection (tens of gallons of leakage would produce about a pound of crystals). Periodic walk-downs to detect boric acid leaks are recognized in Generic Letter 88-05 as an effective method to detect leakage of boric acid solutions. Visual detection of boric acid crystal deposits can reveal a leak well before any other method. However, in the case of very small leaks insulation must be removed to detect the deposits.

In this research effort we explored the technologies to detect the accumulation of boric acid from a leak without removing insulation.

Boric acid is white and needle-like, and is moderately soluble in water with a large negative heat of solution. The solubility increases markedly with temperature. The amount of boric acid that can be dissolved in 100 grams of water increases from 2.67 g at 0°C to 40.25 g at 100°C according to Lange's *Handbook of Chemistry* [33]. Boric acid is a very weak and exclusively monobasic acid which acts, not as a proton donor, but as a Lewis acid, accepting OH^- :



Boric acid melts at 171°C and decomposes at about 300°C. Its vapor pressure at room temperature is approximately 2.6 mm Hg. In general, orthoboric acid at room temperature is a crystalline solid with structure based on hydrogen-bonded planar units. When heated above 100 °C at atmospheric pressure, it converts into metaboric acid, HBO_2 . Evidence for the existence of a vapor-phase boric acid molecule is remarkably sparse. Ogden, Young, and Bowsher, in 1987, [25] applied mass spectrometry and matrix-isolated infrared (IR) spectroscopy to the characterization of the molecular boric acid. Their results showed that boric acid not only had a finite vapor pressure at room temperature but that its volatility was

greatly enhanced in the presence of steam. Their work suggests the possibility of detecting boric acid leakage by techniques, such as infrared (IR) spectroscopy, that can characterize the vapor phase. IR spectroscopy identifies substances by their rotational and vibrational spectra. When light of a particular frequency, and therefore a particular energy, strikes a molecule, the molecule can absorb the energy, and the rotations and vibrations that the molecule is experiencing at that time can change to a higher energy rotation or vibration state. The energies needed to change the rotational and vibrational states of the molecules lie in the IR region of the electromagnetic spectrum. Because these changes occur at discrete energy levels and depend on the structure and composition of the molecule, each molecule has a different response to IR energy. Other than the frequencies absorbed by the substance, all others are transmitted through [28].

A typical mass spectrum obtained by heating boric acid to about 40°C contains ion peaks at 44/45 and 61/62 amu (atomic mass units) corresponding to B(OH)_2^+ and B(OH)_3^+ , respectively. Typical absorption bands appear in the region of 513.8 to 3668.5 cm^{-1} , which confirmed some of the reported spectra for vapor phase boric acid, particularly the in-plane B–O stretch band at 1430 cm^{-1} .

The low vapor pressure of boric acid at room temperature makes it difficult to identify the vapor phase by IR spectroscopy. However, as noted previously, the volatility of boric acid is enhanced in the presence of steam. While the presence of steam increases the vapor pressure of boric acid, to detecting boric acid with IR spectroscopy requires a distinguishable absorbance peak that is different from the absorbance peak of water. In the vapor phase, boric acid has absorbance peaks at 1017 cm^{-1} , 1429 cm^{-1} , and 3706 cm^{-1} [25] ($1 \text{ cm}^{-1} = 10^4 / \lambda$, where λ is in μm). When examining the IR spectrum of water in the vapor phase, the peaks of boric acid at 1429 cm^{-1} and 3706 cm^{-1} must be ignored, because water absorbance peaks near or at the values for boric acid would overlap them [29].

Detection limits of trace element gases in a mixture are very low for IR spectroscopy. With a conventional dispersive IR spectrometer, detection limits are in the 1–20% range, with the limiting factor being the signal-to-noise (S/N) ratio. The detection limits can be further reduced by using a Fourier Transform IR (FT-IR) spectrometer. While using an FT-IR spectrometer, a longer cell can be used, increasing the absorption percentage, and a wide-band mercury-cadmium-telluride (MCT) detector lowers the limits even further. Together, these modifications can lower the detection limits to 10–100 ppb [30]. Stalard *et al.* have reported that a next generation FT-IR spectrometer can have detection limits for water in corrosive gases of 1 ppb [30], and Gurka *et al.* have detected environmental gases with gas chromatography/FT-IR (GC/FT-IR) in the 20–120 ng (nanogram) range [31]. Also using GC/FT-IR and deposition methods, detection limits have been lowered to below the nanogram level [32]. Detection limits can also be lowered by increasing the length of the gas cell or by raising the pressure inside the cell with a dry, non-IR-absorbing gas, like nitrogen [29].

For detection of boric acid, an FT-IR spectrometer with a liquid-nitrogen-cooled wide-band MCT detector could be used. An FT-IR spectrometer could be used over a double-beam spectrometer because it is faster, and multiple runs of the machine can be averaged to create better printouts. An MCT detector could be used over a deuterated triglycine sulfate (DTGS) detector because the MCT has a lower detection limit. By cooling the MCT detector with liquid nitrogen, the detection limits are lowered even further.

6. Crack Growth Monitoring Systems

Improvements in acoustic emission (AE) monitoring technology have led to test systems that provide a rapid response to crack initiation and growth. The release of elastic energy during crack growth can be detected before a crack grows through the wall. No other technique has the potential to provide this information during plant operation. Monitoring an entire plant is feasible.

The technology for AE crack monitoring is described in NUREG/CR-5645 [18]. High-temperature sensors and stainless steel waveguides are used. The AE from crack growth and leaks was separated from noise by monitoring at a high enough transducer frequency and applying pattern recognition techniques to the received acoustic signals (the signals from crack propagation have a distinct pattern easily distinguished from background noise [18]). Crack growth rates can be estimated. The same instrumentation and equipment are used for crack monitoring and leak detection. The technology has been validated in laboratory tests and field trials [18], and is now included in the ASME Boiler and Pressure Vessel Code Section V as a technique for leak detection and crack monitoring. Article 13 of the Code describes "Continuous Acoustic Emission Monitoring" for leaks and crack monitoring. Article 29 describes the "Standard Practice for Leak Detection and Location Using Surface Mounted AE Sensors." Acoustic emission monitoring also discussed in Section XI as substitution for ultrasonic monitoring of known non-throughwall cracks. Relevant sections of the ASME Code are presented in Appendix E.

Figure 25 shows the schematic of the sensor developed by Pacific Northwest National Laboratory (PNNL) for continuous monitoring of reactor components. The sensor consists of a transducer and built-in tunable pre-amplifier, and uses a 304SS waveguide with 3.18-mm diameter with a 1.3-mm-diameter tip. A minimum of three sensors is needed for the monitoring of a pressure vessel head.

Proper coupling of waveguides to structures has to be assured. Periodic testing to verify that the sensors are operating properly is necessary. Calibration can be carried out with an electronic pulser or breaking of standard pencil leads. Detectable crack growth rates in the laboratory range from 1×10^{-7} to 1.5×10^{-4} cm/s. Stress corrosion cracks have been detected successfully under laboratory conditions. A sensor exposed to gamma radiation in the 1 to 1.3 MeV range at 5×10^4 R/h with a cumulative dose of 14×10^7 R showed no degradation. Pattern recognition of the received acoustic signal in the time domain is used to correctly classify the origin of AE signals.

Field trials include monitoring of selected locations at Watts Bar and Limerick and the ZB-1 test vessel at the Materialpruefungsanstalt (MPA) laboratory in Germany. A fatigue crack was detected by AE in the ZB-1 test vessel. There were no false calls with the AE system during any of the trials. The AE could be detected at a distance of 3 m (10 ft) from the source of acoustic signal with coolant flow noise present using high-frequency tuned waveguide sensors [18].

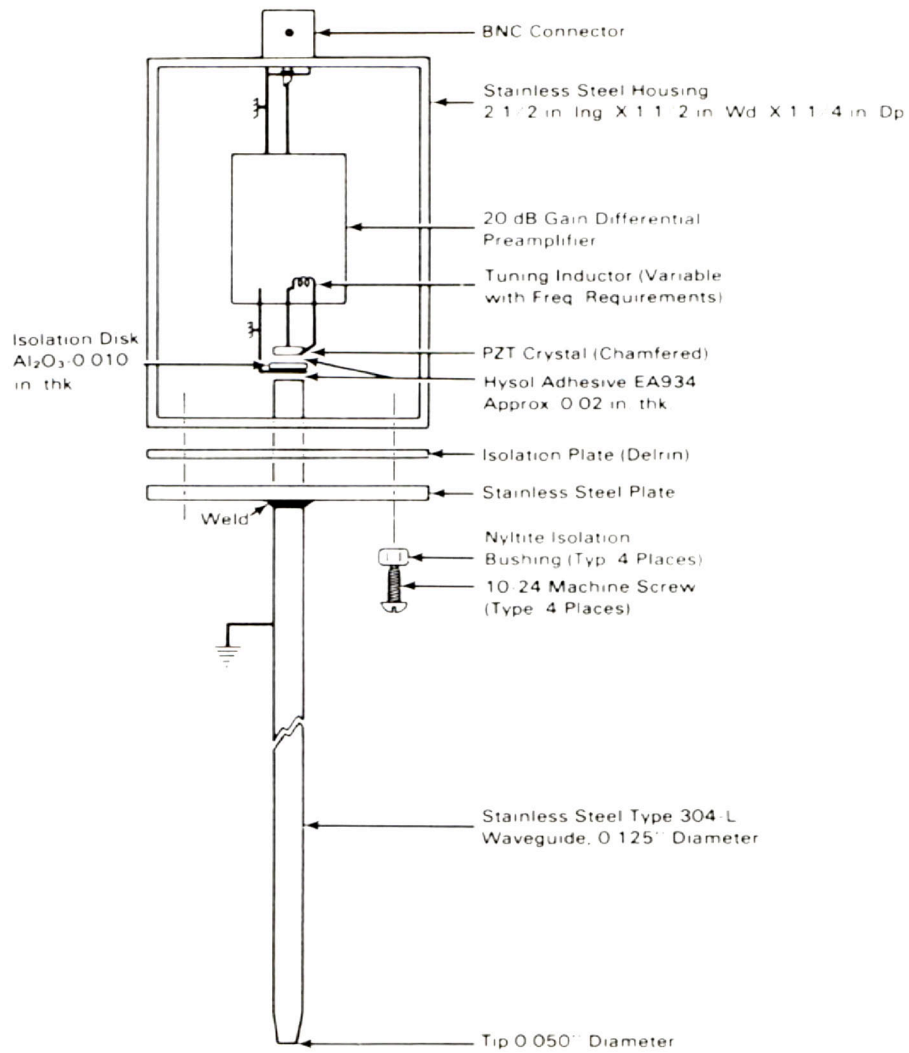


Figure 25. Schematic of AE sensor developed by PNNL for continuous monitoring of nuclear reactor components [18].

7. Conclusions

New leak detection technology can be used to provide greater detection sensitivity and more accurate determination of leakage locations. Even existing systems have sufficient sensitivity to detect unidentified leakage of 0.032 kg/s (0.5 gpm), which is below the current 0.063 kg/s (1 gpm) limit. The analyses presented in this report confirm that the current technical specification limits on unidentified leakage can be expected to provide significant margin against structural failure of piping systems. However, leak rates well below the current limits are sufficient to result in corrosion of carbon and low alloy steel components in systems containing boric acid. In some structural components like CRDM nozzles, current leak detection requirements do not appear to provide sufficient margin against gross structural failure. .

As part of a defense-in-depth philosophy for ensuring the integrity of the RCPB, improved leakage requirements (e.g., establishment of action requirements based on increases in unidentified leak rates, and more accurate identification, measurement, and collection of leakage from known sources to minimize interference with the detection of leakage from unknown sources) could better identify RCPB breaches and prevent additional degradation of the pressure boundary. However, existing systems may not be adequate to provide assurance that leakage is low enough to avoid boric-acid induced corrosion of carbon and low alloy steel components. The potential consequences to reducing leak rate limits include additional shutdowns, inspections, and personnel exposures. Global leakage monitoring and leakage limits by themselves may not always ensure that degradation of and leakage from the RCPB does not occur. As noted previously, there are portions of the RCPB for which global leakage monitoring may give very little assurance against potential loss of structural integrity. In such cases, localized leak detection systems could provide the needed margin. Localized leak detection can also be sensitive enough to provide a high degree of assurance that leak rates are low enough to avoid boric acid corrosion.

Current systems have advantages and disadvantages. The most flexible method for detecting leaks is visual observation. However, the sensitivity and ability to quantify a leak by observation are poor. The adequacy depends on the frequency of inspection and the accessibility of areas of interest. The visual method, based on field experience, is capable of detecting leak rates as low as 0.0006 kg/s (0.01 gpm), but the reliability of the method depends on human factors. Humidity monitoring can detect an increase in vapor content of air resulting from a leak but suffers from a lack of quantitative information. The sensitivity could be on the order of gallons per minute when used in large volume containment areas. A leak from the RCPB will result in an increase in containment pressure. The consequence of having a large volume containment structure is that a leak would have to be very large to be detected by an increase in pressure. Reactor coolant inventory is monitored in PWR plants but not in BWRs. This method is not particularly useful for BWRs because of the poor accuracy in detecting small RCPB leakage. Detection of a leak of 0.063 kg/s (1 gpm) within one hour is difficult using inventory balance. A sump level and flow rate monitor can detect a 0.063 kg/s (1 gpm) leak in less than 1 hour. A 0.063 kg/s (1 gpm) leak could, in principle, be detected in about 10 minutes by a sump pump. Historically, the reliability of the sump pump monitor has been good. However, leak location is not provided.

Significant improvements in leak requirements will require new systems that are not only sensitive and accurate but provide the location of leaks and thus help to minimize unnecessary shutdowns. Newer commercially available systems include (with vendor reported sensitivity) acoustic emission monitoring (ALUS; 0.0002 to 0.016 kg/s; 0.003 to 0.25 gpm), humidity sensors (FLUS; 0.0003 to 0.032 kg/s; 0.005 to 0.5 gpm), and air particulate detectors (ARMS; <0.006 kg/s; 0.1 gpm;). Instrumentation of the pressure vessel head with an AE system has the potential to detect leaks as small as 0.0003 kg/s (0.005 gpm). While additional technologies for leak detection, such as the use of IR spectroscopy to detect boric acid vapor in the vessel head region, may be possible, existing technologies (especially AE) already offer demonstrated capability and flexibility. Additional research is needed on fundamentally different approaches to leak detection technology at this time.

AE sensors can be used on components of special interest to detect crack initiation and growth during plant operation as well as for early detection and quantification of leak rates. For new plants, the entire plant could be instrumented with AE monitors.*

There may be significant advantages if the AE monitoring of crack growth during plant operation can be fully demonstrated and implemented. A performance demonstration would require intentional introduction of degradation in an operating reactor leading to leaks in the RCPB. This type of demonstration is not feasible. Nevertheless, documented testing indicated that cracks could be detected prior to leakage. On-line monitoring of cracks could replace periodic UT inspections, which could result in significant cost savings. Cracks could be detected at locations not normally inspected, or in materials where UT inspection has not been appropriately demonstrated (i.e., cast stainless steels). With greater assurance that no cracks of significant size exist, current leak-before-break requirements could perhaps be relaxed.

If RG 1.45 is revised, it could include the addition of acoustic emission monitoring as an acceptable method for leak detection. AE is a validated technique that is sensitive and can provide location information rapidly. AE is described in ASME Boiler and Pressure Vessel Code Sections V and XI.

Because of the reductions in coolant activity levels, the value of monitoring gaseous radioactivity has been greatly diminished. Thus, gaseous radioactivity monitoring could be dropped from RG-1.45, if it is revised, as it can no longer be considered an adequate substitute for particulate monitoring.

Since other methods besides leak monitoring can ensure integrity, the question arises whether localized highly sensitive leak detection systems alone would be needed to ensure against a significant loss-of-coolant accident. Whether such localized systems are needed is an assessment beyond the scope of this report.

* Personal communication from T. Richards/W Knoblach, Framatome ANP, to D. Kupperman, Argonne National Laboratory, July 5, 2004.

8. References

1. D. D. Paul, et al., "Evaluation and Refinement of Leak-Rate Estimation Models," NUREG/CR-5128, Rev. 1, June 1994.
2. R. P. Collier, F. B. Stulen, M. E. Mayfield, D. B. Pape, and P. M. Scott, "Two-Phase Flow Through Intergranular Stress Corrosion Cracks and Resulting Acoustic Emission," EPRI Report No. NP-3540-LD, 1984.
3. K. Matsumoto, S. Nakamura, N. Gotoh, T. Narabayashi, Y. Tanaka, and Y. Horimizu, "Study of Coolant Leak Rates Through Pipe Cracks," ASME PVP, Vol. 165, pp. 121-127, 1989.
4. J. M. Boag, et al., "Leak Rate Experiments for Through-Wall Artificial Cracks," In. J. Pres. Ves. and Piping, Vol. 43, pp. 413-424, 1990.
5. D. Norris, et al., "PICEP: Pipe Crack Evaluation Program," EPRI Report NP 3596-SR, 1984.
6. G. M. Wilkowski, R. J. Olson, and P. M. Scott, "State-of-the-Art Report on Piping Fracture Mechanics," NUREG/CR-6540, BMI-2196, February 1998.
7. P. Scott, et al., "Report for Subtask 1a for Technical Development of Loss of Coolant Accident Frequency Distribution Program, Finalize and QA SQUIRT Code," Battelle Letter Report to USNRC under Contract RES-02-074, 2003.
8. S. Rahman, N. Ghadiali, D. Paul, and G. Wilkowski, "Probabilistic Pipe Fracture Evaluations for Leak-Rate Detection Applications," NUREG/CR-6004, April 1995.
9. D. Rudland, R. Wolterman, and G. Wilkowski, "Impact of PWSCC and Current Leak Detection on Leak-Before-Break," Final Report by Engineering Mechanics Corporation of Columbus to USNRC, January 31, 2003.
10. D. Rudland, R. Wolterman, and G. Wilkowski, "Leakage through CRDM Nozzles with PWSCC Cracks," Letter report to USNRC (non-proprietary version), December 31, 2002.
11. F. W. Brust, P. Scott, S. Rahman, N. Ghadiali, T. Kilinski, B. Francini, C. W. Marschall, N. Miura, P. Krishnaswamy, and G. M. Wilkowski, "Assessment of Short Through-Wall Circumferential Cracks in Pipes-Experiments and Analysis," NUREG/CR-6235, BMI-2179, April 1995.
12. E. S. Hunt, "Boric Acid Corrosion Guidebook, Revision 1: Managing Boric Acid Corrosion Issues at PWR Power Stations," EPRI Final Report 1000975, November 2001.
13. Nuclear Regulatory Commission (U.S.) (NRC). ADAMS Accession Number ML033010208, "Degradation of RPV Boundary Components in Concentrated Boric Acid Solutions: Task 3: Corrosion of Reactor Steels in Concentrated Boric Acid Solutions." NRC: Washington, D. C. (24 October 2003)

14. Materials Reliability Program Reactor Vessel Closure Head Penetration Safety Assessment for U.S. PWR Plants (MRP-110NP), EPRI TR-1009807-NP, 2004.
15. V. N. Shah, M. B. Sattison, C. L. Atwood, A. G. Ware, G. M. Grant, and R. S. Hartley, "Assessment of Pressurized Water Reactor Primary System Leaks," NUREG/CR-6582, 1998.
16. D. S. Kupperman, "Assessment of Leak Detection Systems for LWRs," NUREG/CR-4813, October 1988.
17. D. S. Kupperman, D. Prine, and T. Mathieson, "Application of Acoustic Leak Detection Technology for the Detection and Location of Leaks in Light Water Reactors," NUREG/CR-5134, October 1988.
18. P. H. Hutton, R. J. Kurtz, M. A. Friesel, J. R. Skorpik, and J. F. Dawson, "Acoustic Emission/Flaw Relationships for Inservice Monitoring of LWRs," NUREG/CR-5645, 1991.
19. S. Bush, A. Chockie, W. Nicholson, and A. Slavich, "Nuclear Reactor Piping Failures at U.S. Commercial LWRs," Electric Power Research Institute (EPRI) TR-110102 and Swedish Nuclear Power Inspectorate (SKI) S-106 58, 1998.
20. Instrument Society of America, "Standard for Light Water Reactor Coolant Pressure Boundary Leak Detection," ISA-67.03, 1982.
21. U. Kunze and B. Bechtold, "New Generation of Monitoring Systems with On-line Diagnostics," Progress in Nuclear Energy, Vol. 29, No. 3/4, pp. 215-227, 1995.
22. P. Jax, "Detecting and Locating the Smallest Leaks Early," Nuclear Engineering International, (39) R22, 1994.
23. G. Champion and L. Chauvel, "EdF Installs N-13 Leak Monitoring," Nuclear Engineering International, pp. 44-45, October 1993.
24. G. Champion, A. Dubail and J. M. Houin, "Tracking Low SG Leak Rates with VAMCIS," Engineering International, pp. 39-40, February 1991.
25. J. S. Ogden, N. A. Young, and B. R. Bowsher, "The Characterization of Molecular Boric Acid by Mass Spectrometry and Matrix Isolation Infrared Spectroscopy," United Kingdom Atomic Energy Authority AEEW-R 2305, October 1987.
26. P. Jax, "Redefining the Large Break LOCA: Technical Basis and Its Implication," Joint Committee on the Safety of Nuclear Installations/Committee on Nuclear Regulatory Activities (CSNI/CNRA) Workshop, Zurich, Switzerland, June 23-24, 2003.
27. U. Kunse, "Acoustic Leak Monitoring Systems in VVER Plants: Ten Years of Experience," Nuclear Europe Worldscope, p. 114, 1999.
28. Trevor R. Gilson, "Characterization of Ortho- and Meta-boric Acids in the Vapour Phase," Journal of the Chemical Society: Dalton Transactions, pp. 2463-2466, 1991.

29. Takehiko Shimanouchi, "Tables of Molecular Vibrational Frequencies," NSRDS, 1968.
30. B. R. Stallard, R. K. Rowe, M. J. Garcia, D. M. Haaland, L.H. Espinoza, and T. M. Niemczyk, "Trace Water Vapor Determination in Corrosive Gases by Infrared Spectroscopy," SAND-93-4026, 1993.
31. D. F. Gurka, R. Titus, P. R. Griffiths, D. Henry, and A. Giorgetti, "Evaluation of an Improved Single-Beam Gas Chromatography/Fourier Transform Infrared Interface for Environmental Analysis," *Analytical Chemistry*, Vol. 59, pp. 2362-2369, 1987.
32. Patricia B. Coleman, *Practical Sampling Techniques for Infrared Analysis*, CRC Press, Boca Raton, pp. 19-21, 168-169, (1993).
33. J. A. Dean, *Lange's Handbook of Chemistry*, 14th Edition, McGraw Hill, New York, 1992.
34. G. Champion and L. Chavel, "EdF Installs N-13 Leak Monitoring," *Nuclear Engineering International*, 1993.

Appendix A

Failure Scenarios for Reactor Coolant Systems

Tables of failure scenarios for reactor coolant systems (RCS) from NRC's Elicitation on LB-LOCA redefinition in 2003 are given in this appendix.

Table A-1. BWR LOCA–Sensitive Piping Systems

System	Piping Materials	Piping Size (in.)	Safe End Materials	Welds	Significant Degradation Mechanisms	Significant Loads.	Mitigation/ Maint.
Recirc	304 SS, 316 SS, 347 SS	4, 10, 12, 20, 22, 28	304 SS, 316 SS, A600*	SS, NB	UA, FDR, SCC, LC, MA	RS, P, S, T, DW, SUP, SRV, O	ISI w TSL, REM
Feed Water	CS	10, 12 (typ), 12 – 24	304 SS, 316 SS*	CS, NB	UA, FDR, MF, TF, FS, LC, GC, MA	T, TFL, WH, P, S, SRV, RS, DW, O	ISI w TSL, REM
Steam Line	CS – SW	18, 24, 28	CS	CS	UA, FDR, FS, GC, LC, MA	WH, P, S, T, RS, DW, SRV, O	ISI w TSL, REM
HPCS, LPCI	CS (bulk), 304 SS, 316 SS	10, 12	304 SS, 316 SS, A600*	CS, SS, NB	UA, FDR, SCC, TF, LC, GC, MA	RS, T, P, S, DW, TS, WH, SUP, SRV, O	ISI w TSL, REM
RHR	CS, 304 SS, 316 SS	8 – 24	CS, 304 SS, 316 SS	CS, SS, NB	UA, FDR, SCC, TF, FS, LC, GC, MA	RS, T, P, S, DW, TS, O SUP, SRV	ISI w TSL, REM
RWCU	304 SS, 316 SS, CS	8 – 24	CS, 304 SS, 316 SS	CS, SS, NB	UA, FDR, SCC, TF, FS, LC, GC, MA	RS, TS, T, P, S, DW, SUP, SRV, O	ISI w TSL, REM
CRD piping	304 SS, 316 SS (low temp)	< 4	Stub tubes – A600 and SS*	Crevice A182 to head	UA, FDR, MF, SCC	RS, T, P, S, DW, V, O, SRV	ISI w TSL, REM
SLC	304 SS, 316 SS	< 4	304 SS, 316 SS	SS, NB	UA, FDR, MF, SCC	RS, T, P, S, DW, V, O, SRV	ISI w TSL, REM
INST	304 SS, 316 SS	< 4	304 SS, 316 SS	SS, NB	UA, FDR, MF, SCC, MA	RS, T, P, S, DW, V, O, SRV	ISI w TSL, REM
Drain lines	304 SS, 316 SS, CS	< 4	304 SS, 316 SS, CS	SS, NB	UA, FDR, MF, SCC, LC, GC	RS, T, P, S, DW, V, O, SRV	ISI w TSL, REM
Head spray	304 SS, 316 SS, CS	< 4	304 SS, 316 SS, CS	SS, NB	UA, FDR, SCC, TF, LC, GC	RS, P, S, T, DW, SRV, O	ISI w TSL, REM
SRV lines	CS	6, 8, 10, 28	CS	CS	UA, FDR, MF, FS, GC, LC, MA	RS, P, S, T, DW, SRV, O	ISI w TSL, REM
RCIC	304 SS, 316 SS, CS	6, 8	304 SS, 316 SS	SS NB	UA, FDR, SCC, LC, MA	RS, P, S, T, DW, SRV, O	ISI w TSL, REM

* See note in text.

304 SS = Type 304 stainless steel (Table 2)
 316 SS = Type 316 stainless steel (Table 2)
 A600 = Alloy 600
 HPCS = high pressure coolant spray
 LPCI = low pressure coolant injection
 RHR = residual heat removal
 RWCU = reactor water cleanup system
 CRD = control rod drive
 SLC = standby liquid control
 INST = instrument lines
 SRV = = safety relief valve
 RCIC = reactor core isolation cooling
 CS = carbon steel
 CS – SW = carbon steel seam welded
 DW = dead weight
 FDR = fabrication defect and repair
 FS = flow sensitive (inc. flow assisted corrosion and erosion/cavitation)
 GC = general corrosion

ISI w TSL = Current inservice inspection (ISI) procedures with technical specification leakage (TSL) detection requirements considered.
 LC = local corrosion
 MA = material aging
 MF = mechanical fatigue
 NB = nickel-based weld (Alloy 82/182)
 O = overload
 P = pressure
 REM = all remaining mitigation strategies possible (e.g., not unique to piping system)
 RS = residual stress
 S = seismic
 SCC = stress corrosion cracking
 SUP = support loading
 TF = thermal fatigue
 T = thermal
 TFL = thermal fatigue loading from striping
 TS = thermal stratification
 UA = unanticipated mechanisms
 V = vibration
 WH = water (and steam) hammer

Table A-2. PWR LOCA-Sensitive Piping Systems

System	Piping Materials	Piping Size (in.)	Safe End Materials	Welds	Sig. Degrad. Mechanisms	Significant Loads.	Mitigation/ Maint.
RCP: Hot Leg	304 SS, 316 SS, C-SS, SSC-CS, CS - SW	30 - 44	A600, 304 SS, 316 SS, CS	NB, SS, CS	TF, SCC, MA, FDR, UA	P, S, T, RS, DW, O, SUP	ISI w TSL, REM
RCP: Cold Leg/Crossover Leg	304 SS, 316 SS, C-SS, SSC-CS, CS - SW	27 - 34	A600, 304 SS, 316 SS, CS	NB, SS, CS	TF, SCC, MA, FDR, UA	P, S, T, RS, DW, O, SUP	ISI w TSL, REM
Surge line	304 SS, 316 SS, C-SS	10 - 14	A600, 304 SS, 316 SS,	NB, SS	TF, SCC, MA, FDR, UA	P, S, T, RS, DW, O, TFL, TS	TSMIT, ISI w TSL, REM
SIS: ACCUM	304 SS, 316 SS, C-SS	2 - 12	A600, 304 SS, 316 SS,	NB, SS	TF, SCC, MA, FS, FDR, UA	P, S, T, RS, DW, O	ISI w TSL, REM
SIS: DVI	304 SS, 316 SS	2 - 6	A600, 304 SS, 316 SS,	NB, SS	TF, SCC, MA, FS, FDR, UA	P, S, T, RS, DW, O	ISI w TSL, REM
Drain line	304 SS, 316 SS, CS	< 2"			MF, TF, GC, LC, FDR, UA	P, S, T, RS, DW, O, V, TFL	ISI w TSL, REM
CVCS	304 SS, 316 SS	2 - 8	A600 (B&W and CE)	NB	SCC, TF, MF, FDR, UA	P, S, T, RS, DW, O, V	ISI w TSL, REM
RHR	304 SS, 316 SS	6 - 12			SCC, TF, MA, FDR, UA	P, S, T, RS, DW, O, TFL, TS	ISI w TSL, REM
SRV lines	304 SS, 316 SS	1 - 6			TF, SCC, MF, FDR, UA	P, S, T, RS, DW, O, SRV	ISI w TSL, REM
PSL	304 SS, 316 SS	3 - 6		NB	TF, SCC, MA, FDR, UA	P, S, T, RS, DW, O, WH, TS	ISI w TSL, REM
RH	304 SS, 316 SS	< 2	A600		MF, SCC, TF, FDR, UA	P, S, T, RS, DW, O, V, TS	ISI w TSL, REM
INST	304 SS, 316 SS	< 2	A600		MF, SCC, TF, FDR, UA	P, S, T, RS, DW, O, V	ISI w TSL, REM

* See note in text.

RCP = reactor coolant pump
 SIS = safety injection system
 CVCS = chemical volume control system
 ACCUM = accumulators
 DVI = direct vessel injection
 RHR = residual heat removal
 SRV = safety relief valve
 PSL = pressurizer spray line
 RH = reactor head lines
 INST = instrument lines
 304 SS = Type 304 stainless steel (Table 2)
 316 SS = Type 316 stainless steel (Table 2)
 A600 = Alloy 600
 CS = carbon steel
 CS - SW = carbon steel seam welded
 C-SS = cast stainless steel
 DW = dead weight
 FDR = fabrication defect and repair
 FS = flow sensitive (inc. flow assisted corrosion and erosion/cavitation)
 FW = fretting wear
 GC = general corrosion
 HREPL = vessel head replacement

ISI w TSL = Current inservice inspection (ISI) procedures with technical specification leakage (TSL) detection requirements considered.

LC = local corrosion
 MA = material aging
 MF = mechanical fatigue
 NB = nickel-based weld (Alloy 82/182)
 O = overload
 UA = unanticipated mechanisms
 P = pressure
 REM = all remaining mitigation strategies possible (eg. not unique to piping system)
 RS = residual stress
 S = seismic
 SCC = stress corrosion cracking
 SSC-CS = stainless steel clad carbon steel
 SUP = support loading
 T = thermal
 TF = thermal fatigue
 TFL = thermal fatigue loading from striping
 TS = thermal stratification
 TSMIT = thermal stratification mitigation
 V = vibration
 WH = water (and steam) hammer

Table A-3. BWR Reference Case Conditions^a

System	Piping Material	Piping Sizes (in .)	Safe End	Welds	Degradation Mechanisms	Loading	Mitigation /Maint.
Recirc	304 SS	10, 12, 20, 22, 28	304 SS	SS	SCC, FDR	P, T, RS, DW, SRV	NWC, ISI w. TSL, 88-01 (AI), 182
Feed Water	CS	10, 12, 12 - 24	304 SS	CS	FAC, FDR	P, T, RS, DW, WH, TFL	NWC, ISI w. TSL, 88
Steam Line	CS - SW	18, 24, 28	CS	CS	FAC, FDR	P, T, RS, DW, SRV	NWC, ISI w. TSL, 88
HPCS, LPCS	CS	10, 12	304 SS	CS	TF, FDR	P, T, RS, DW, TS, SRV	NWC, ISI w. TSL, 88
RHR	304 SS	8 - 24	304 SS	SS	SCC, FDR	P, T, RS, DW, TS, SRV	NWC, ISI w. TSL, 88
RWCU	304 SS	8 - 12	304 SS	SS	SCC, FDR	P, T, RS, DW, TS, SRV	NWC, ISI w. TSL, 88
CRD piping	304 SS	< 4	A600 and SS	Crevice ed NB welds	SCC, FDR	P, T, RS, DW, O	NWC, ISI w. TSL, 88
SLC	304 SS	< 4	304 SS	SS	SCC, FDR	P, T, RS, DW, SRV	NWC, ISI w. TSL, 88
INST	304 SS,	< 4	304 SS	SS	MF, FDR	P, T, RS, DW, V, SRV	NWC, ISI w. TSL, 88
Drain lines	304 SS	< 4	304 SS	SS	SCC, FDR	P, T, RS, DW, SRV	NWC, ISI w. TSL, 88
Head spray	304 SS,	< 4	304 SS	SS	TF, FDR	P, T, RS, DW, SRV	NWC, ISI w. TSL, 88
SRV lines	CS	6, 8, 10, 28	CS		MF, FDR	P, T, RS, DW, SRV	NWC, ISI w. TSL, 88
RCIC	304 SS	6, 8	304 SS	SS	SCC, FDR	P, T, RS, DW, SRV	NWC, ISI w. TSL, 88

^aFor explanation of abbreviations, see note at bottom of Table A-2.

Table A-4. PWR Reference Case Conditions^a

System	Piping Material	Piping Sizes (in.)	Safe End	Welds	Degradation Mechanisms	Loading	Mitigation/Maint.
RCP: Hot Leg	304 SS	30 – 44	A600	NB	TF, SCC, FDR	P, T, RS, DW	ISI w TSL
RCP: Cold/Crossover Legs	304 SS	22 – 34	A600	NB	TF, FDR	P, T, RS, DW	ISI w TSL
Surge line	304 SS	10 – 14	A600	NB	TF, FDR	P, T, RS, DW, TFL, TS	ISI w TSL
SIS: ACCUM	304 SS	10 – 12	304 SS	SS	TF, FDR	P, T, RS, DW	ISI w TSL
SIS: DVI	304 SS	2 – 6	304 SS	SS	TF, FDR	P, T, RS, DW	ISI w TSL
Drain line	304 SS	< 2"		SS	MF, TF, FDR	P, T, RS, DW, V	ISI w TSL
CVCS	304 SS	2 – 8		SS	TF, MF, FDR	P, T, RS, DW, V	ISI w TSL
RHR	304 SS	6 – 12			TF, FDR	P, T, RS, DW, TS	ISI w TSL
SRV lines	304 SS	1 – 6			TF, FDR	P, T, RS, DW, SRV	ISI w TSL
PSL	304 SS	3 – 6		NB	TF, FDR	P, T, RS, DW, WH	ISI w TSL
RH	304 SS	< 2	A600		TF, FDR	P, T, RS, DW, TS	ISI w TSL
INST	304 SS	< 2			MF, TF, FDR	P, T, RS, DW, V	ISI w TSL

^aFor explanation of abbreviations, see note at bottom of Table A-2.

Table A-5. Pressurizer Failure Scenarios^a

Component	Geometry	Material	Degradation Mechanisms	Loading	Mitigation/ Maint.	Comments
Shell		A600C-LAS, SSC-LAS	GC, SCC, MF, FDR, UA			Boric acid wastage from OD
Manway		NB-LAS, SSC-LAS, LAS, HS- LAS (Bolts)	GC, SCC, MF, SR, FDR, UA			Bolt failures
Heater Sleeves	Small diam. (3/4 to 1 in.)	A600, SS	TF, MF, SCC, FDR, UA			Req. multiple failures
Bolted relief valves		C-SS	MA, FDR, UA			
Nozzles		SSC-LAS C-SS	CD, TF, SCC, MA, FDR, UA, GC			Same as surge line

^aNB-LAS = nickel-base clad low alloy steel and SR = stress relaxation and loss of preload. For explanation of other abbreviations, see note at bottom of Table A-2.

Table A-6. Reactor Pressure Vessel (RPV) Failure Scenarios^a

Component	Geometry	Material	Degradation Mechanisms	Loading	Mitigation / Maint.	Comments
Vessel Head Bolts		High-strength steel	GC, FDR, UA		Human error	Removal leading to human error (common-cause failure) during refueling
RPV wastage		SSC-LAS LAS	GC, FDR, UA, MA			LAS = some BWR upper head, Boric acid wastage (upper & lower head, shell)
CRDM connections		SS	FDR, UA			Welded, bolted, threaded + seal weld
CRDM	4-6	A600 base nozzle, SS, C-SS, and NB-LAS housing with NB weld	SCC, TF, MF, LC, GC, FDR, UA	P, S, T, RS, DW, O	HREPL, ISI w TSL, REM	Nozzles and piping up to connection
Nozzles		LAS, SSC-LAS,	TF, MF, LC, GC, SCC, FDR, UA			LAS = BWR only
ICI	< 2"	304 SS, 316 SS	MF, SCC, TF, FW, FDR, UA	P, S, T, RS, DW, O, V	ISI w TSL, REM	
RPV Corrosion Fatigue		SSC-LAS, LAS	LC, MF, MA FDR, UA			LAS = some BWR upper head; Initiate at cladding cracks (upper & lower head, shell)
BWR penetrations		SS	SCC, LC, FDR, UA			Stub tubes, drain line, SLC, instrumentation, etc.
PWR penetration		SS, A600	SCC, FDR, UA, LC, MF, TF			

^aNB-LAS = nickel-base clad low alloy steel; SR = stress relaxation and loss of preload. For explanation of other abbreviations, see note at bottom of Table A-2.

Table A-7. Valve Failure Scenarios^a

Component	Geometry	Material	Degradation Mechanisms	Loading	Mitigation/ Maint.	Comments
Valve Body		CS, SS C-SS	FAC, CAV, LC, TF, MA, GC, CD, SCC, FDR, UA			CS, SS = BWR only
Valve Bonnet		CS, SS C-SS	FAC, LC, GC, SCC, MA, CD, FDR, UA			CS, SS = BWR only
Bonnet Bolts		HS-LAS	GC, SCC, FDR, UA SR			
Hot Leg/Cold leg loop isolation valves			FDR, UA			
MSIV Body			CAV, TF, MA, CD			

^aHS-LAS = high-strength low-alloy steel (SA-540, Gr. B23, SA-193, Gr. B7), CAV = cavitation damage, and SR = stress relaxation and loss of preload. For explanation of other abbreviations, see note at bottom of Table A-2.

Table A-8. Pump Failure Scenarios^a

Component	Geometry	Material	Degradation Mechanisms	Loading	Mitigation/ Maintenance	Comment
Pump Body		C-SS, SSC-CS	CAV., TF, CD, MA, SCC, fatigue			
RECIRC Bonnet Bolts		HS-LAS	SCC, GC, SR			
RCP nozzle						
Flywheel failure						Initiating collateral damage – secondary pipe failure

^aHS-LAS = high-strength low-alloy steel (SA-540, Gr. B23, SA-193, Gr. B7); SR = stress relaxation and loss of preload. For explanation of other abbreviations, see note at bottom of Table A-2.

Appendix B

Review of NRC-Sponsored Argonne National Laboratory Study of Acoustic Leak Detection

Research at Argonne National Laboratory [16,17] has demonstrated that improvements in leak detection, location, and sizing are possible with advanced acoustic leak detection technology. Detection sensitivity has been established, and it has been demonstrated that cross-correlation analysis can be used to improve location capability, and spectral analysis can be employed to help identify the cause of a leak. Some results of the ANL program are discussed below.

Detection of a leak by AE requires that $S_e = S_1 - T - N + PG > 0$, where S_e = signal excess at detector output, S_1 = source level (affected by waveguide geometry, insulation, and circumferential position), T = transmission loss down pipe, N = background noise level, and PG = system gain (all in dB). The acquisition of acoustic leak data, background noise estimates, and attenuation data at ANL allows a rough estimation of the sensitivity of an AE system under field conditions. Figure A1 shows predicted signal-to-noise ratios (in dB) vs. distance along a 25-cm (10-in.) Schedule 80 pipe for three leak rates and three levels of estimated acoustic background noise. The highest level is estimated from the maximum acoustic level observed during the Watts Bar (PWR) hot functional test when the reactor was at operating temperature and pressure. The lowest level is obtained from an indirect estimate of background noise from Hatch (BWR), and the assumptions that the reactor acoustic background level will vary by a factor of 10 in the plant and that the measurement at Watts Bar was an upper-limit value. The striped area suggests possible enhancement of the acoustic signal for a 379-cm³/min (0.1 gal/min; 0.0063 kg/s) leak rate in a situation where the leak plume strikes the reflective insulation. Results of laboratory experiments suggest that for leak rates greater than 75.7 cm³/min (0.02 gal/min; 0.0013 kg/s) but less than 757 cm³/min (0.2 gal/min; 0.013 kg/s), signals could be enhanced significantly, given the correct circumstances.

Consider a BWR with 100 m of monitored piping (the approximate length of the primary pressure boundary), divided into low-, moderate-, and high-background-noise zones with lengths of 40, 40, and 20 m, respectively. For a detection sensitivity of 1 gal/min (0.063 kg/s), a signal in the 300–400 kHz range, and a 3-dB S/N ratio, the required sensor spacing are approximately 10, 2, and 1 m, respectively. Therefore, 4 sensor sites are required in the 40-m low-noise zone, 20 sites in the 40-m moderate-noise zone, and 20 sites in the 20-m high-noise zone. For location analysis, three sensors are required at each site to carry out the correlation averaging routine, so altogether, 132 sensors are needed to adequately cover the reactor primary pressure boundary under the conditions proposed. For a PWR, assume 150 m of piping, divided into low-, moderate-, and high-noise zones with lengths of 60, 60, and 30 m, respectively. With an increase of 6 dB in signal intensity for a PWR compared to a BWR, Fig. A1 indicates sensor spacing of 12, 4, and 2 m, respectively, for a 3-dB S/N ratio. Approximately 105 sensors will be required to completely monitor the plant under the scenario presented. Obviously, the number of sensors can be significantly reduced if only isolated sections of the plant are monitored.

The relationship of signal amplitude in the 300–400 kHz frequency range to flow rate for a variety of leak morphologies is shown in Fig. A2. The signal was acquired from a transducer on

a waveguide 1 m (3 ft) from the leak. Fluid temperature was 274°C (525°F) with pressure at 7.4 MPa (1070 psi). Flow rates varied from 0.0003 to 0.54 kg/s (0.004 to 8.5 gpm). Leaks were from SCC, fatigue cracks, valves, and flanges. The general size of a leak can be estimated from the signal amplitude if the distance to the leak is known.

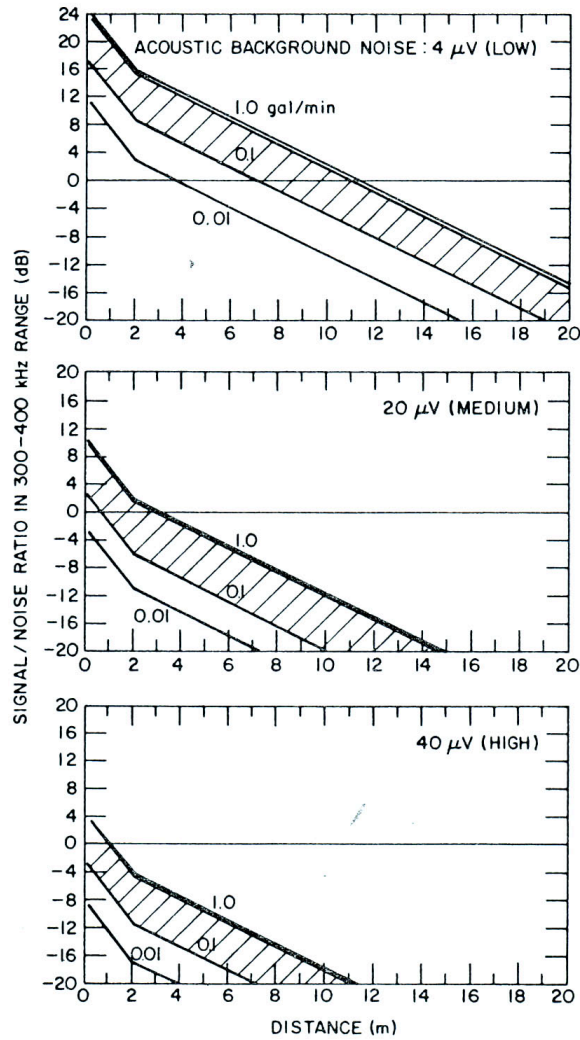


Figure B1. Predicted signal-to-noise ratios (in dB) vs. distance along a 254-mm Schedule 80 pipe for three leak rates and three levels of estimated acoustic background noise [17].

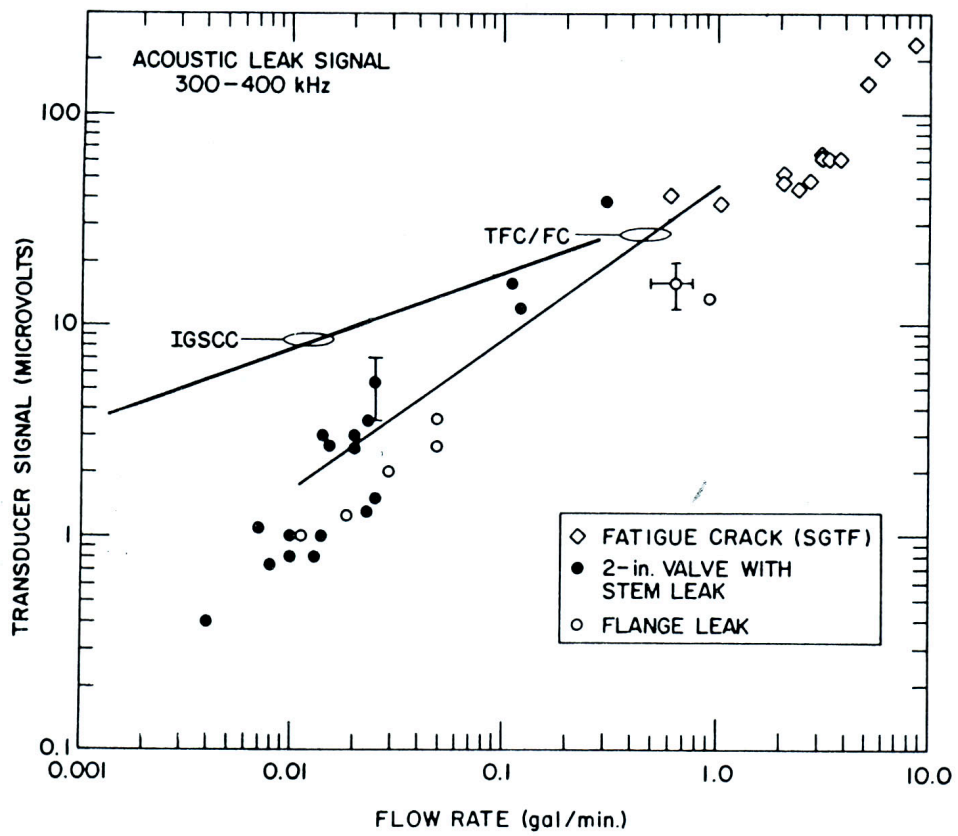


Figure B2. Leak rate vs. acoustic signal amplitude in the 300–400 kHz bandwidth for SCC, fatigue crack, valve, and flange leaks [17].

Computational Fluid Dynamics (CFD) Analysis of 2-Dimensional Duct Flow with Turns

1 Background

This document summarizes the computational-fluid-dynamics (CFD) analyses conducted under the Barrier Integrity Research Program.

One of the fundamental aspects of the thermal-hydraulics model for two-phase critical flow inside a crack is to estimate the pressure losses due to various factors. In SQUIRT, the factors considered include crack surface friction, path turns, phase-change acceleration, change in crack cross-section area, and entrance effect. For typical crack geometries, it has been found that, by running SQUIRT, the first two factors, i.e., the pressure losses due to friction and path turns, are often dominant. Unfortunately, as shown in NUREG/CR-5128¹, these two also introduce significant uncertainties in the analyses. The uncertainties stem from the complicated morphologies for different types of cracks on roughness, path length, and path turns.

Emc² (Engineering Mechanics Corporation of Columbus) has conducted detailed measurements and analyses to determine the morphologies of these different types of cracks. One methodology was established for the evaluation of effective roughness of the crack surface, the effective length, and number of turns of the crack, as these three parameters are needed for the thermal-hydraulic model to evaluate the pressure losses due to friction and flow path turns². In the evaluation of effective roughness on the crack surface, it was assumed that for very tight crack, the effective roughness is equal to the local roughness of the crack surface, while for a very wide crack, the effective roughness is equal to the global roughness of the crack. There is a transition region between these two extreme situations, and the effective roughness is then interpolated between the global roughness and the local roughness. The question for this approximation is then, what are the lower and upper bounds to define tight and wide cracks for the interpolation? In other words, under what conditions does the effective roughness switch among the local roughness, the global roughness, and the transition region. The present work will try to answer the question by conducting a set of CFD numerical experiments.

The problem considered here is 2D duct with multiple turns, as shown in Fig. C1.

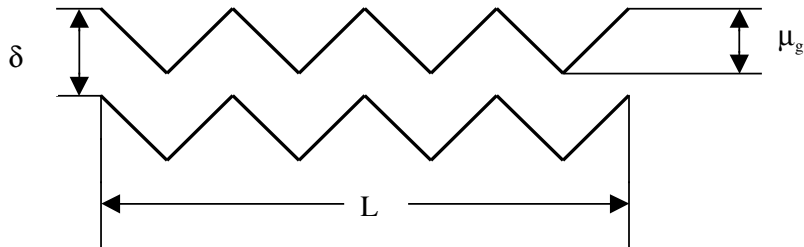


Figure C1. Sketch of a 2D duct with turns.

where δ is the duct opening (also called crack opening displacement or COD), μ_g is the height of the path waving, or global roughness of the crack. In addition, the crack surface can have a local roughness, μ_L .

For a fluid that flows through the duct shown in the above figure with a density of ρ and an averaged velocity of u , the friction coefficient λ is defined by the following relation,

$$\frac{\Delta P}{L} = \frac{\lambda}{\delta} \frac{1}{2} \rho u^2$$

where ΔP is the pressure drop over the duct length L . In theory, λ is related to the Reynolds number of the flow, $Re = (u\delta)/\nu$, with ν being the fluid kinematic viscosity, and two ratios of the geometry's characteristic sizes: δ/μ_g and μ_L/μ_g (here we assume the turning angle is always 90°), or $\lambda = \lambda(Re, \delta/\mu_g, \mu_L/\mu_g)$. To the authors' knowledge, there is no publication dedicated to this type of flow's resistance correlation as contrast to the straight duct or pipe flow, where ample experimental data are available in the public domain. So we start our investigation by examining the friction correlation for a straight duct flow.

1.1 Correlation for Straight Duct Flow

For a straight, smooth (no roughness) pipe or duct flow, a universal law of friction has been proposed by Prandtl and has been proved to be quite accurate:

$$\frac{1}{\sqrt{\lambda}} = 2 \log(Re \sqrt{\lambda}) - 0.8$$

For pipe or duct with roughness, the above relation is modified as

$$\frac{1}{\sqrt{\lambda}} = 1.74 - 2 \log\left(\frac{\mu_L}{\delta} + \frac{18.7}{Re \sqrt{\lambda}}\right)$$

This new relation will recover the correlation for smooth duct flow as μ_L approaches to zero, and it will also approach the so-called completely rough limit:

$$\lambda = \frac{1}{\left(2 \log \frac{\delta}{\mu_L} + 1.74\right)^2}$$

as Reynolds number approaches infinity.

Figure C2 shows the plot of the above correlation and experimental data.

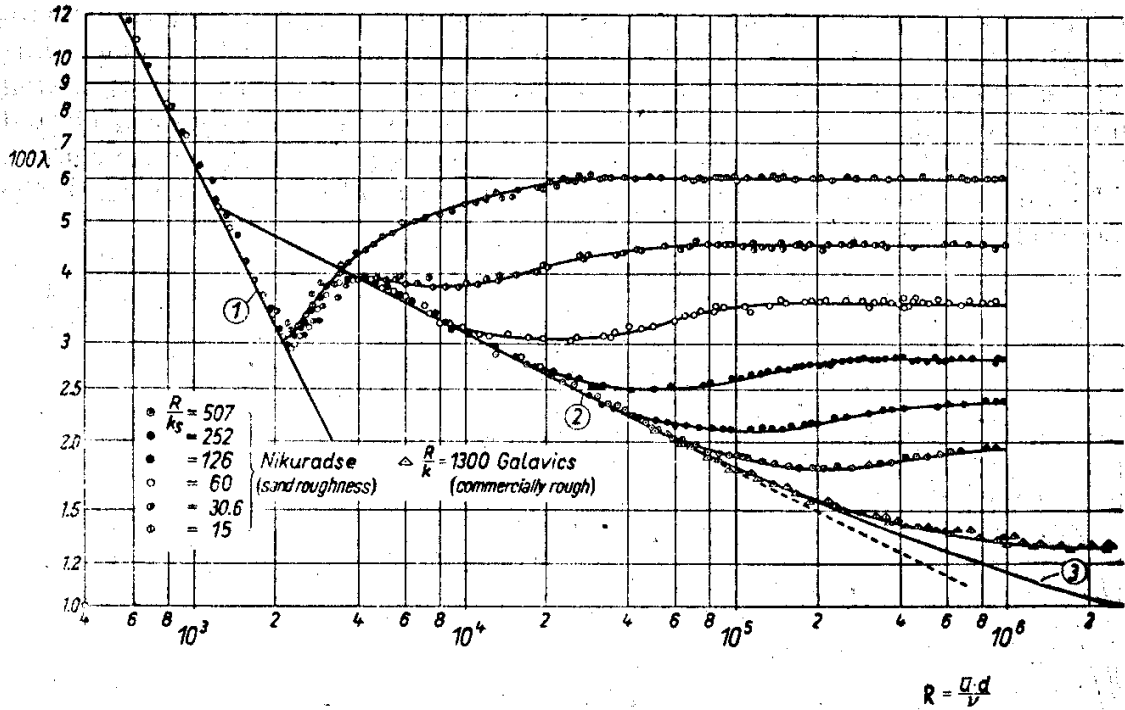


Figure C2. Rough pipe friction correlation and experiment data. Curve 1 for laminar flow; curve 2 for turbulent flow; curve 3 is the plot for the universal law of friction. K_s is equivalent to the local roughness μ_L , and R to δ , the duct opening.

An interesting observation of this plot is that for a given roughness, there are three regimes of flow: the hydraulic smooth regime, the transition regime, and the completely rough regime. The division into three regimes are predicated on the relative protrusion height with respect to the thickness of the so-called laminar sub-layer near the wall, i.e., the thin layer outside the turbulent core in which flow is still laminar due to the zero velocity at the wall. The hydraulic smooth regime occurs when the height of the roughness is lower than the laminar sub-layer, so the effect of the roughness is totally buried under the laminar layer; the completely rough regime is the opposite of the hydraulic smooth regime, i.e., the roughness protrusion reaches outside the laminar sub-layer, and the largest part of resistance to the flow is due to the form drag which acts on them; between the hydraulic smooth regime and the completely rough regime is the transition regime where protrusion extends partly outside the laminar sub-layer. All these correlation equations and experimental data can be found in Schlichting³. John et al.⁴ proposed a different correlation for tight crack:

$$\lambda = \frac{1}{(3.39 \log \frac{\delta}{\mu_L} - 0.866)^2}$$

1.2 Correlation for Duct Flow with Multiple Turns

All the above correlations are for straight pipe or duct flows with or without roughness. For a duct flow with many turns such as the flows in cracks, these correlations are obviously not applicable. If we examine two limit situations of the duct flow we consider here, however,

these correlations for straight pipe/duct flows can be utilized to formulate the correlations we need. The first limit situation is when the crack is very tight, i.e., very small δ/μ_g . In this case, the waving duct can be divided into many straight segments. Each of these segment's friction coefficients follows the above correlation with its local roughness. The pressure losses associated with each of these segments are combined with the pressure losses by the bends or turns between two straight segments. The other limit situation is when the value of δ/μ_g is high, i.e., wide crack opening. In this case, the waving duct can be treated as a straight duct as the global roughness acts as local roughness since the original local roughness is buried under the height of the global roughness.

The issues we need to address here for duct flow with multiple turns are:

1. Under what condition, in particular for the value of δ/μ_g , the crack can be considered tight, so local roughness can be used directly. Under this situation, how do we formulate the pressure losses caused by the multiple turns?
2. Under what conditions can we treat a wavering crack as a wide crack (i.e., it is a straight duct with its global roughness acts as local roughness)?

2 Numerical Results

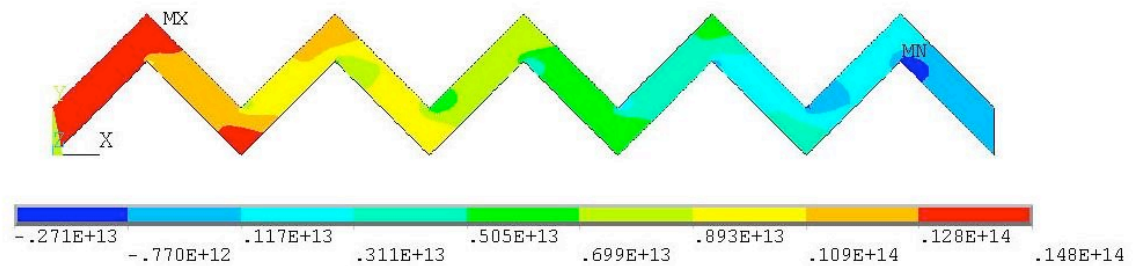
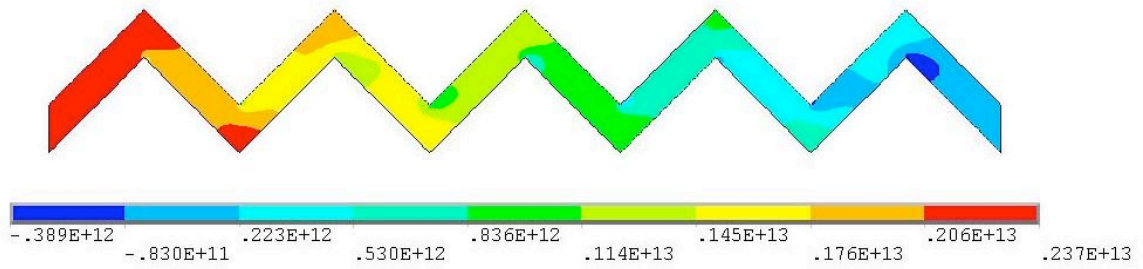
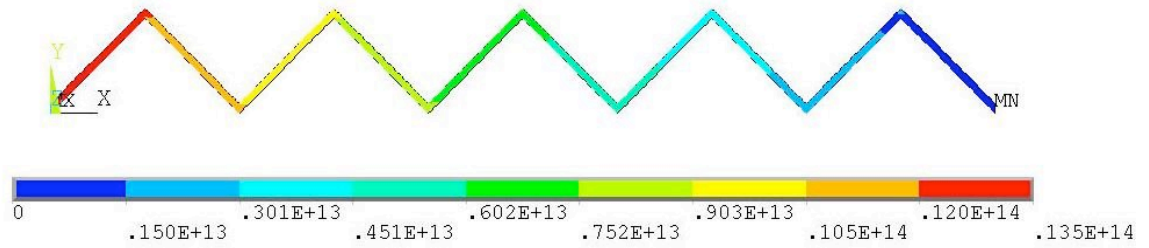
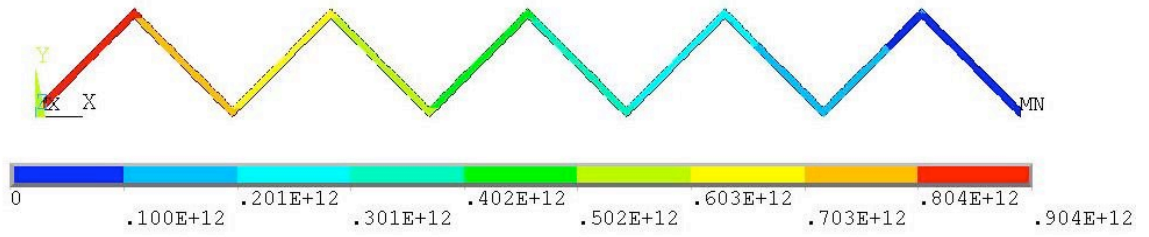
Standard CFD analyses were conducted on the geometries shown above for different Reynolds numbers and different values of δ/μ_g . The flow fields were calculated, and pressure drop is retrieved for the calculation of friction coefficients.

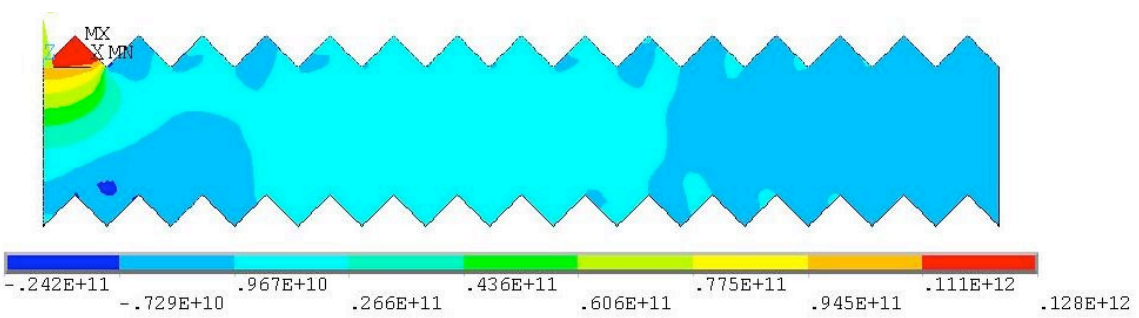
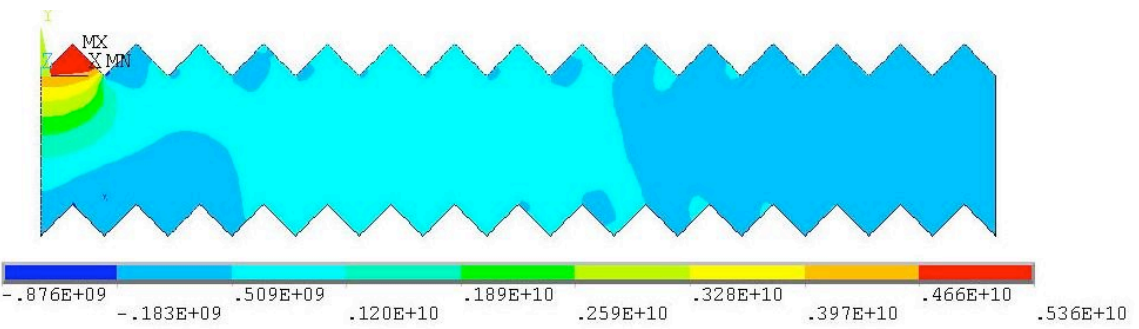
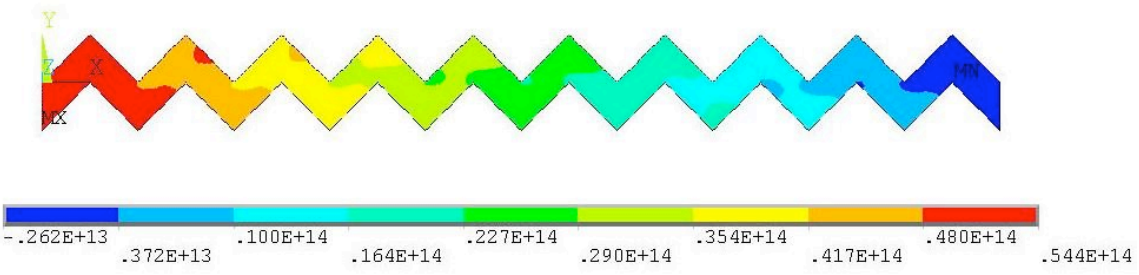
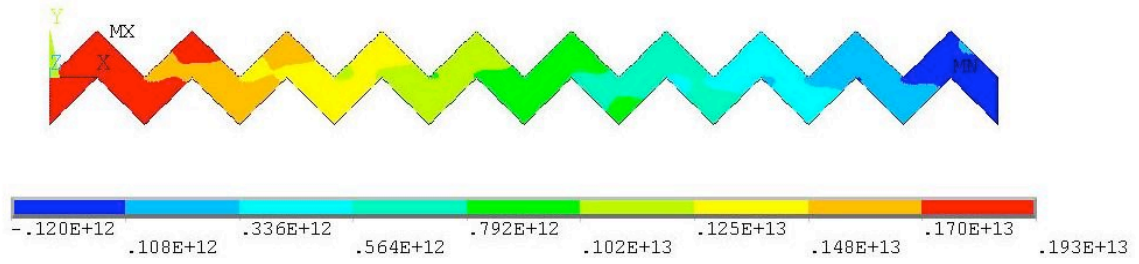
The Reynolds numbers considered are 1, 100, 1000, 3000, 10000, and 50000. The three lower values are for laminar flows, and the three high values are for turbulent flows. For each Reynolds number, six values of δ/μ_g are considered: 0.1, 0.5, 1, 3, 5, and 10. Additionally, three roughness levels are considered for each combination of Reynolds number and δ/μ_g value. The first roughness level is smooth (i.e., no roughness on the duct wall); the second is 0.01, and the third one is 0.02. These roughness values are chosen with respect to the global roughness μ_g so that their ratio is close to the ones typical of the real application (the ratio of local roughness to global roughness for cracks ranges from 0 to 0.2).

Those cases for laminar flows are of little significance in real application since almost all crack flows are in the turbulent mode, unless it is an extremely tight crack. Since a laminar flow calculation requires minimum computational time, we conduct the analyses anyway for comparison reason.

2.1 Velocity, Pressure, and Turbulence Contours

Here we plot the velocity, pressure, and turbulent kinetic energy contours for the two turbulent conditions: $Re= 10,000$ and $50,000$, and $\delta/\mu_g=0.1, 0.5, 1, 5, \text{ and } 10$.





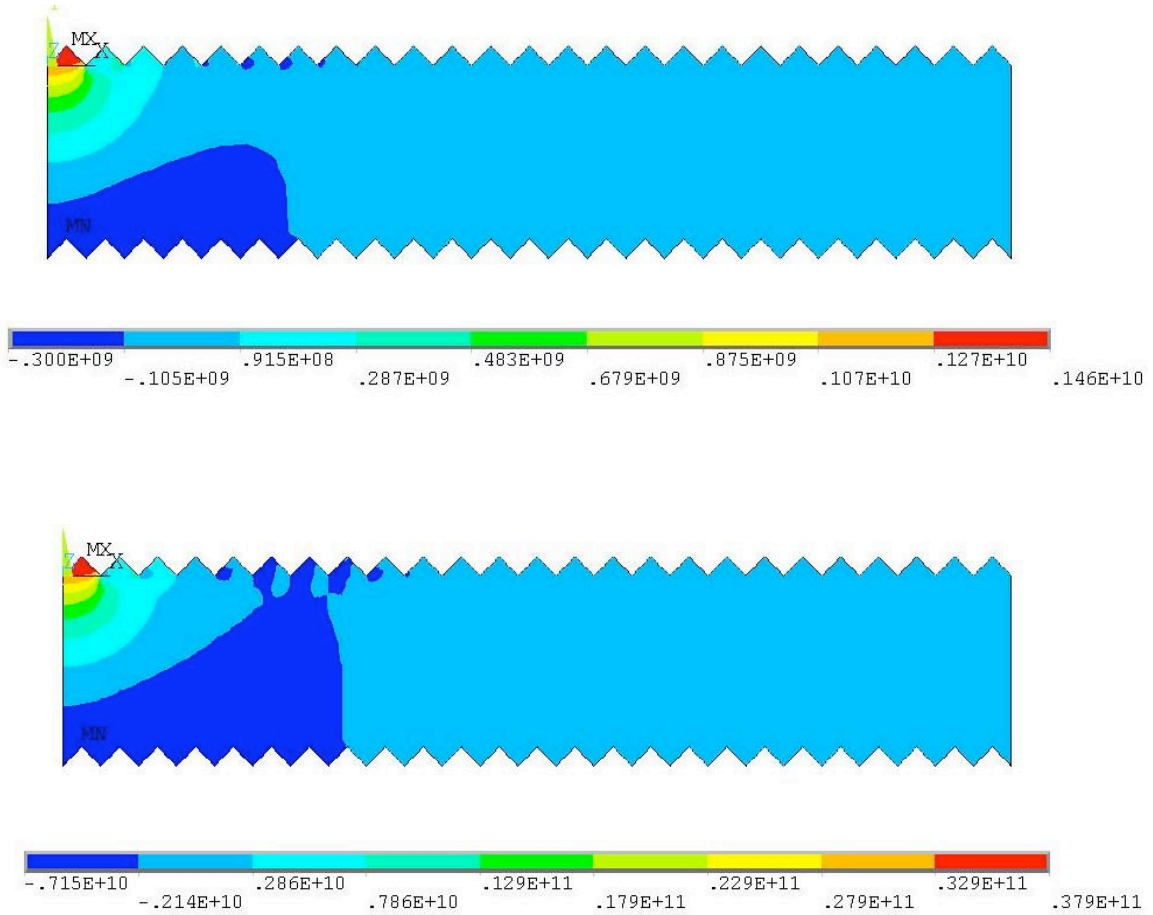
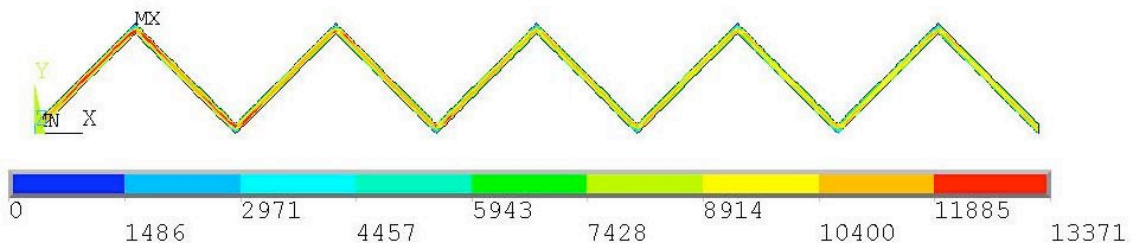
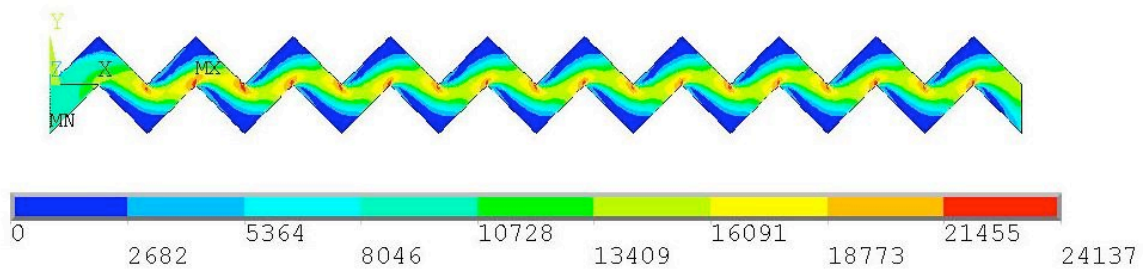
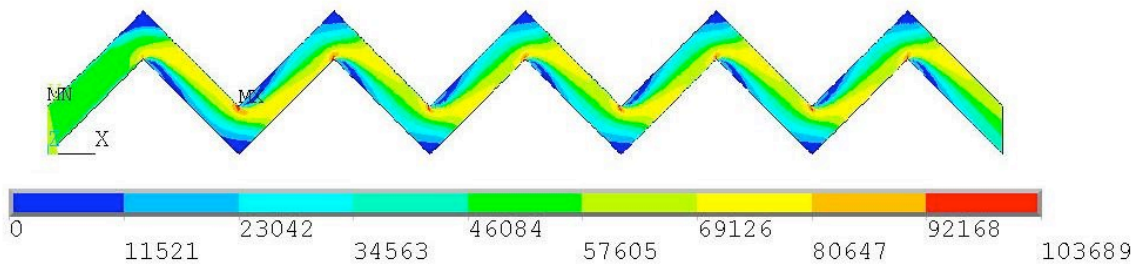
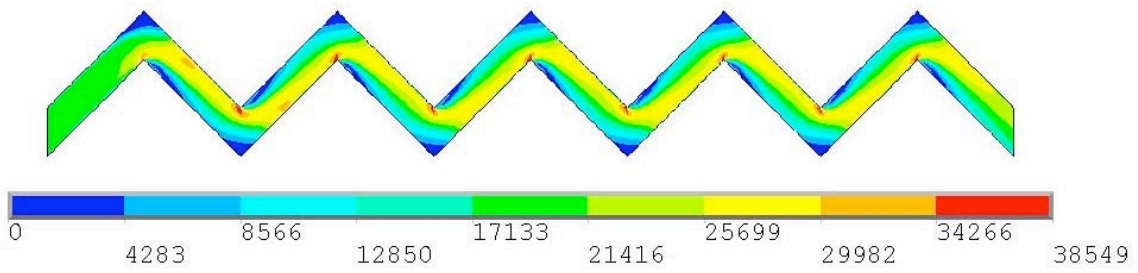
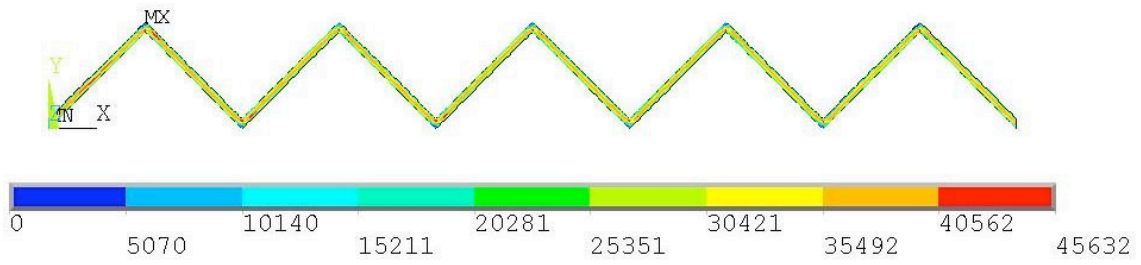
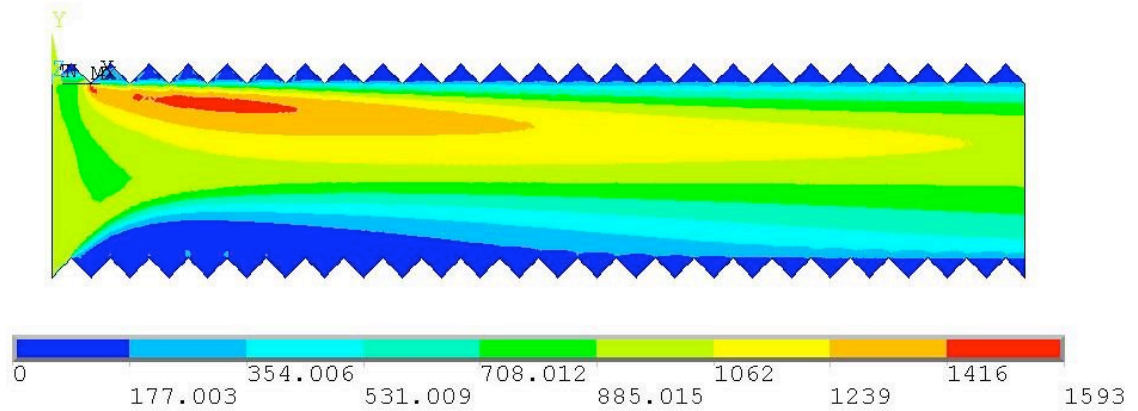
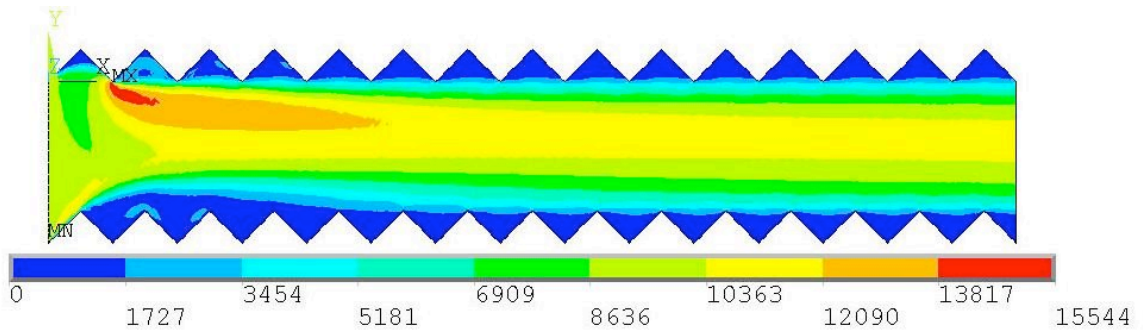
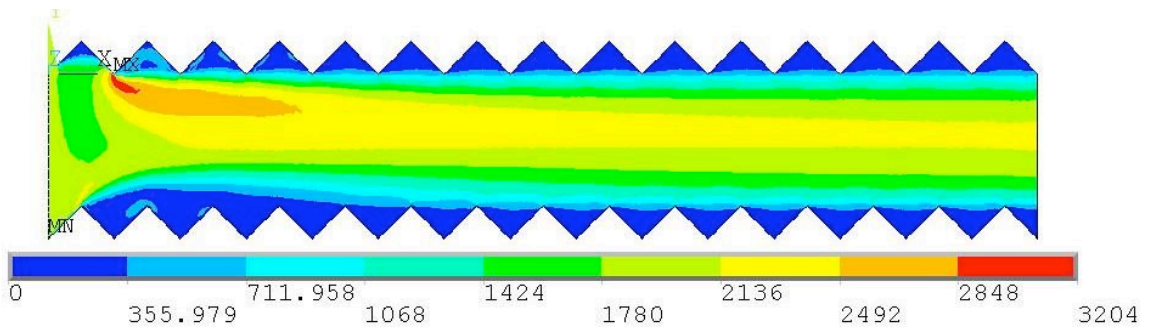
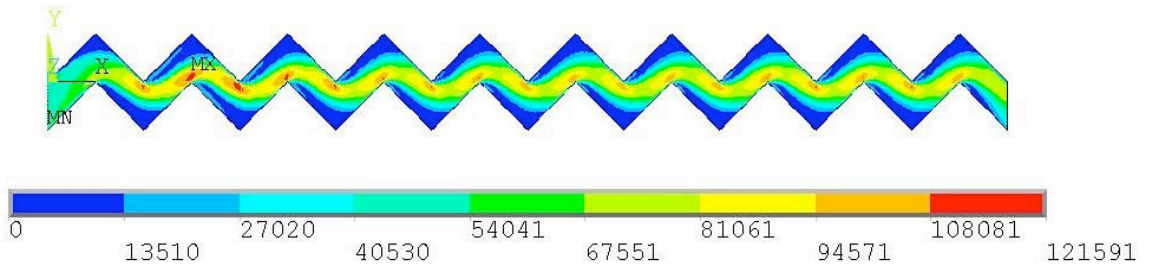


Figure C3. Pressure contours for $Re=10,000$ and $50,000$ for COD-to-global-roughness ratio = 0.1, 0.5, 1, 5, and 10. For each case there are two pictures showing results for $Re=10,000$ and $50,000$, respectively.

For the pressure distribution in the duct, it is found that for a tight or narrow duct flow, the pressure distributes itself in a one-dimensional way along the duct path. For wide duct, a large portion of the pressure drop takes place at the inlet, and thereafter, the pressure drop follows the same pattern for a straight duct.







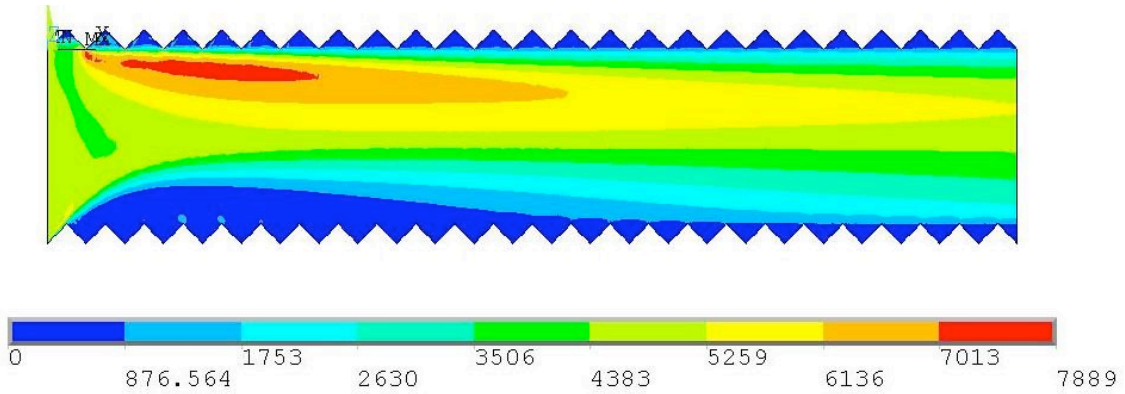
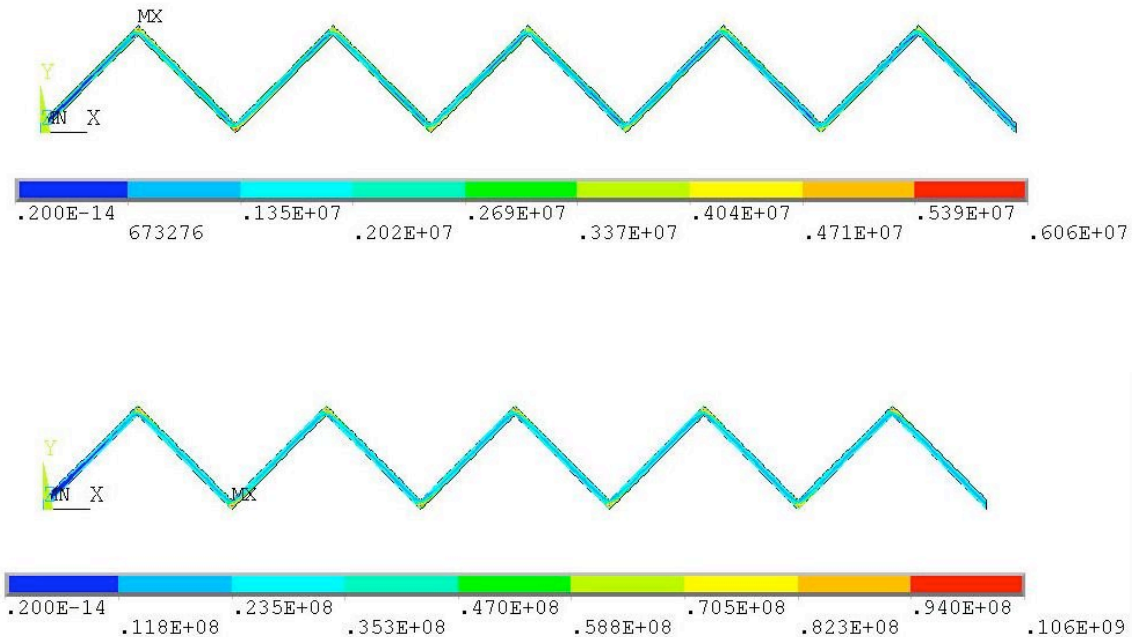
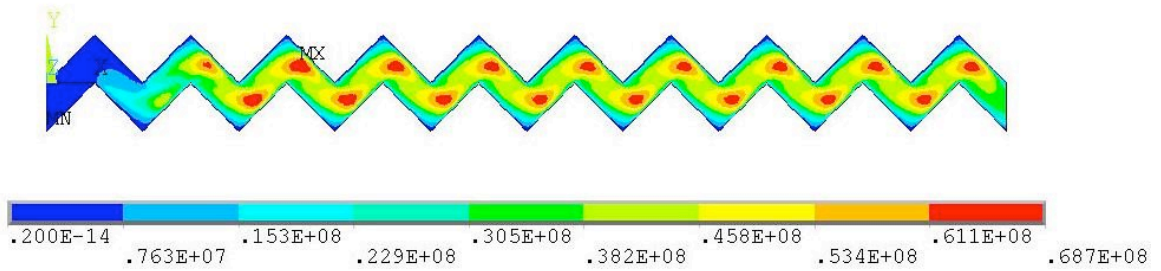
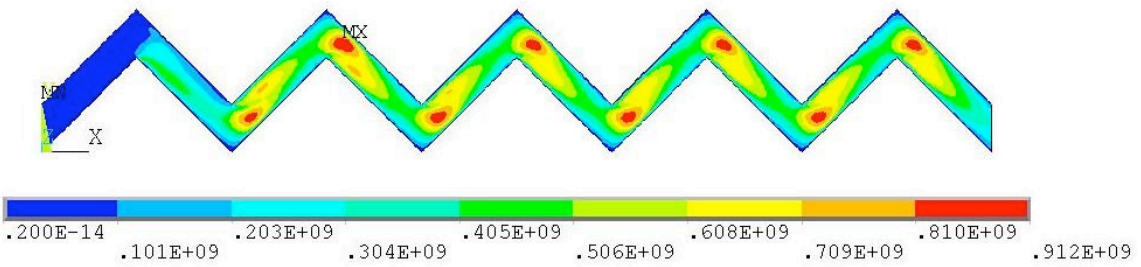
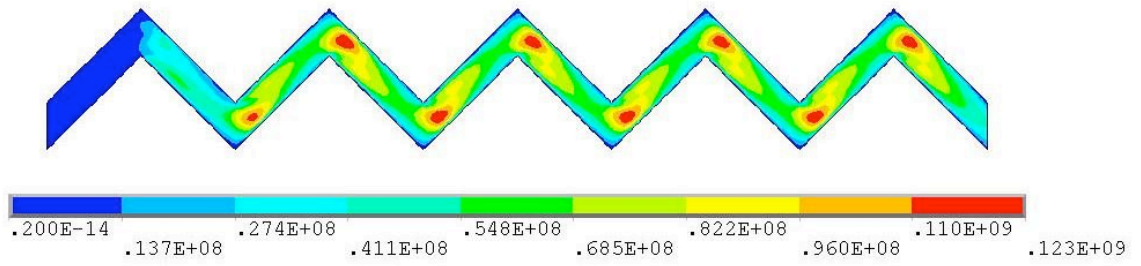
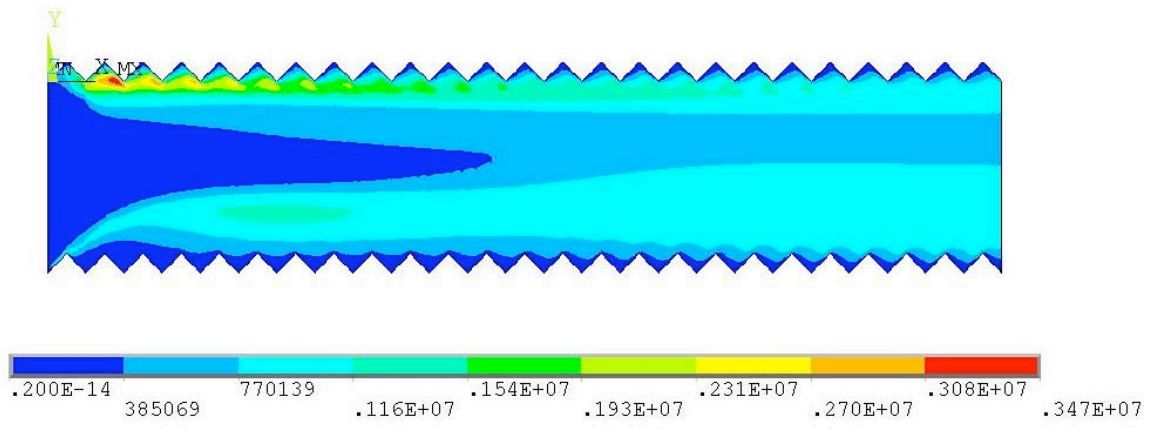
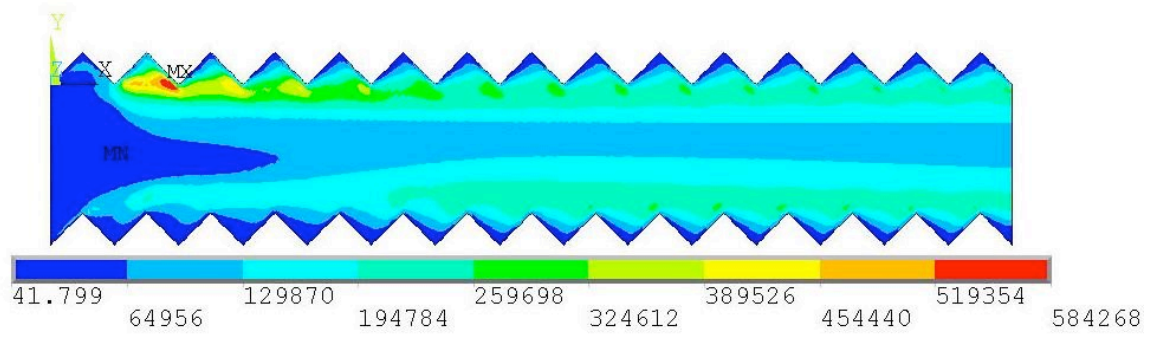
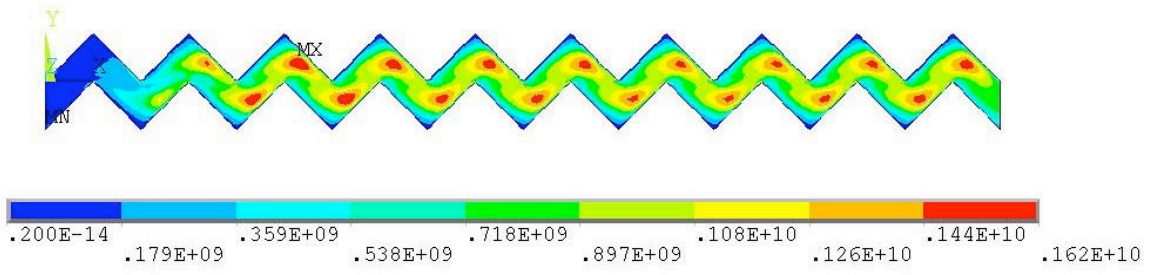


Figure C4. Velocity fields for flows of $Re=10,000$ and $50,000$ with COD-to-global-roughness ratio = 0.1, 0.5, 1, 5, and 10.

In Figure C4, the velocity distributions for the moderate COD-to-global-roughness ratio present a rather interesting picture. Though they show a cyclic behavior along the path, there is never appearance of a fully developed profile as in a straight duct; rather, there are flow separations at the turns or corners. For a wide duct, velocity fields clearly show it is approaching the fully developed profiles. Figure C5 gives the turbulence intensity contours for the flow conditions in Figure C4. Figure C6, a closer look at the velocity field at a turn in a very tight duct, shows that before and after the turn, the flow is at the fully-developed state.







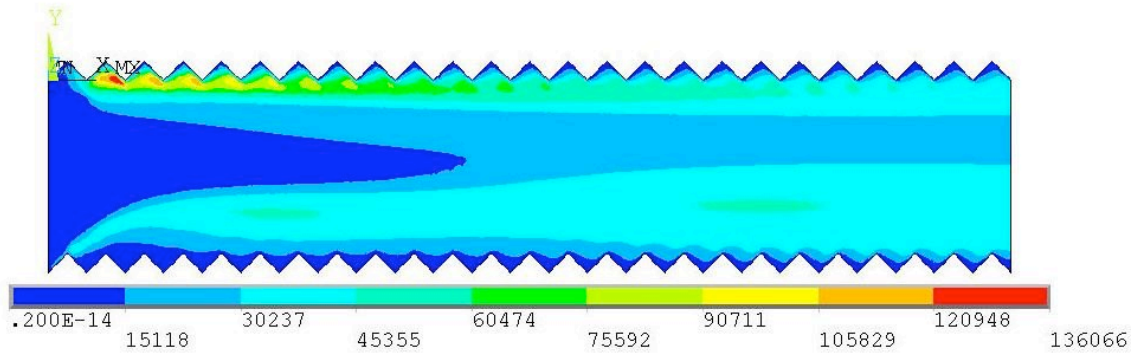


Figure C5. Turbulence intensity contours for flows of $Re=10,000$ and $50,000$ with COD-to-global-roughness ratio = 0.1, 0.5, 1, 5, and 10.

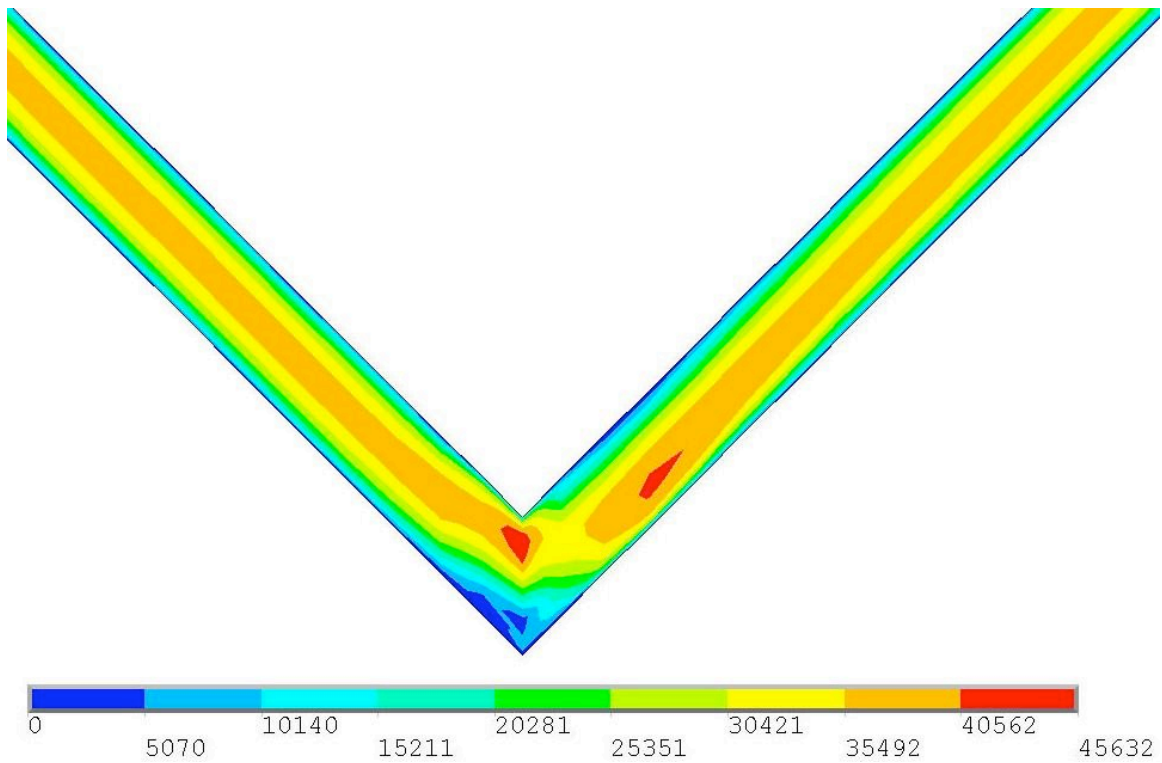


Figure C6. Detailed velocity profiles for a tight duct at $Re=50,000$. Fully developed velocity profiles are observed before and after the turn.

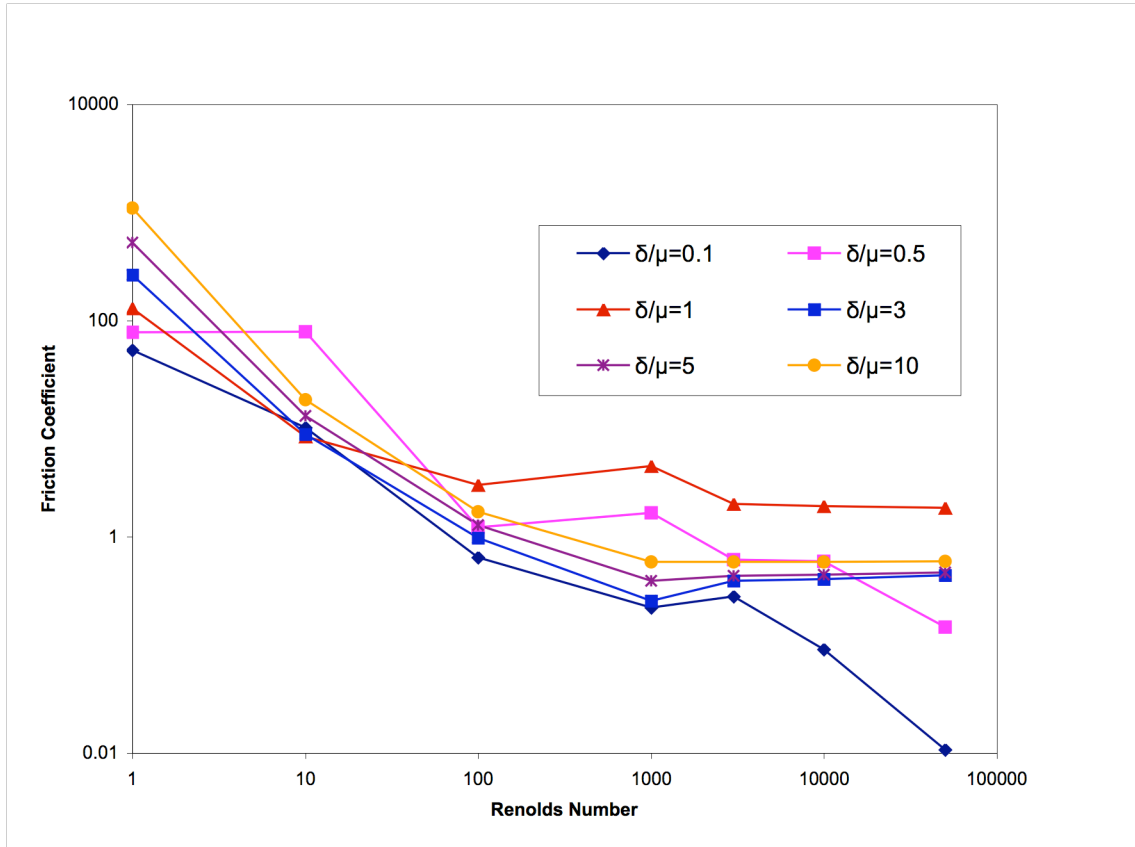


Figure C7. Friction coefficient vs. Reynolds number for different δ/μ_g values.

Figure C7 is a plot of friction coefficient as a function of Reynolds number under different δ/μ_g values. For tight crack flow, such as $\delta/\mu_g=0.1$ or below, the curve shows a steady decrease as the Reynolds number increases, with the exception when transition from laminar flow to turbulent flow at $Re=3000$ occurs. Still the curve's shape is very different from that in Figure C2. The reason is that in addition to the friction contributed from those straight segments of the duct, a significant portion of the friction is also introduced by the turns along the duct. Since the duct is narrow and long between two successive turns, the friction caused by the straight segments is larger than that caused by the turns. In this region, the overall friction can be separated into two independent portions: one by the turns, and the other by the straight duct segments. We make this division of the friction so both can be evaluated independently.

At $0.1 < \delta/\mu_g < 5$, the curves show ups and downs as the Reynolds number increases. This region is where the friction caused by the turns and those by the straight segments of the duct are comparable. Because the size of the turns and the length of the straight duct between two successive turns are close, the flow never reaches a fully developed pattern in a straight segment of the duct, in contrast to the situation for a tight crack. Consequently, the friction can't be separated and evaluated easily.

When $\delta/\mu_g > 5$, the curves return to a smooth shape. If we compare the curves of $\delta/\mu_g = 5$ and $\delta/\mu_g = 10$ to Figure C2, these two curves demonstrate the same pattern as those in Figure

C2 with large roughness. This is a clear indication that when the crack is wide, and the turns act as wall roughness. As shown later, in this region, the local roughness is totally eclipsed by the global roughness. Therefore, for $\delta/\mu_g > 5$, the friction caused by the turns can be ignored; instead, the turns can be treated as roughness in the evaluation of friction coefficient.

Going back to the transition region for $0.1 < \delta/\mu_g < 5$, the friction can be interpolated between the tight-crack situation and the wide-crack situation.

To further verify the above inference, Figure C8 plots the friction coefficient as a function of the COD-to-global roughness ratio for different Re numbers under turbulent flows. This plot shows that friction coefficient remains the same for different Re values except at relatively tight cracks. This is another indication that for wide cracks $\delta/\mu_g > 5$, the flow friction behaves like a straight duct with global roughness acting as roughness. When the crack becomes very narrow, the local roughness of the duct wall emerges from the shadow of the global roughness.

The above conclusion is further supported by Figure C9, where friction coefficient is plotted against the ratio of COD to global roughness under different local roughness levels and a high Reynolds number (50,000). Beyond $\delta/\mu_g = 5$, the friction coefficient hardly shows any difference for different local roughness. Only at the very tight limit of crack COD, does the friction coefficient differ as the local roughness changes. This is correct because as the crack becomes narrow and slender under high Reynolds number, the laminar sub-layer is so thin that the local roughness protrusions reach outside of this sub-layer and, consequently, cause additional resistance to the flow, whereas for a wide crack, the laminar sub-layer is so thick that only the global roughness can reach outside.

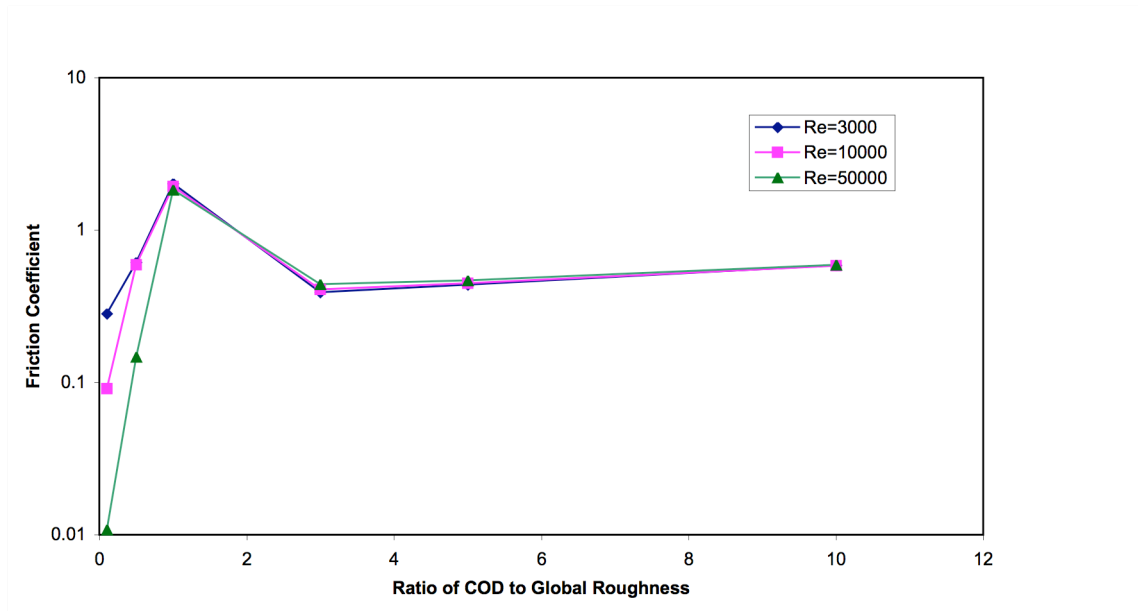


Figure C8. Friction coefficient as a function of the ratio of COD to global roughness.

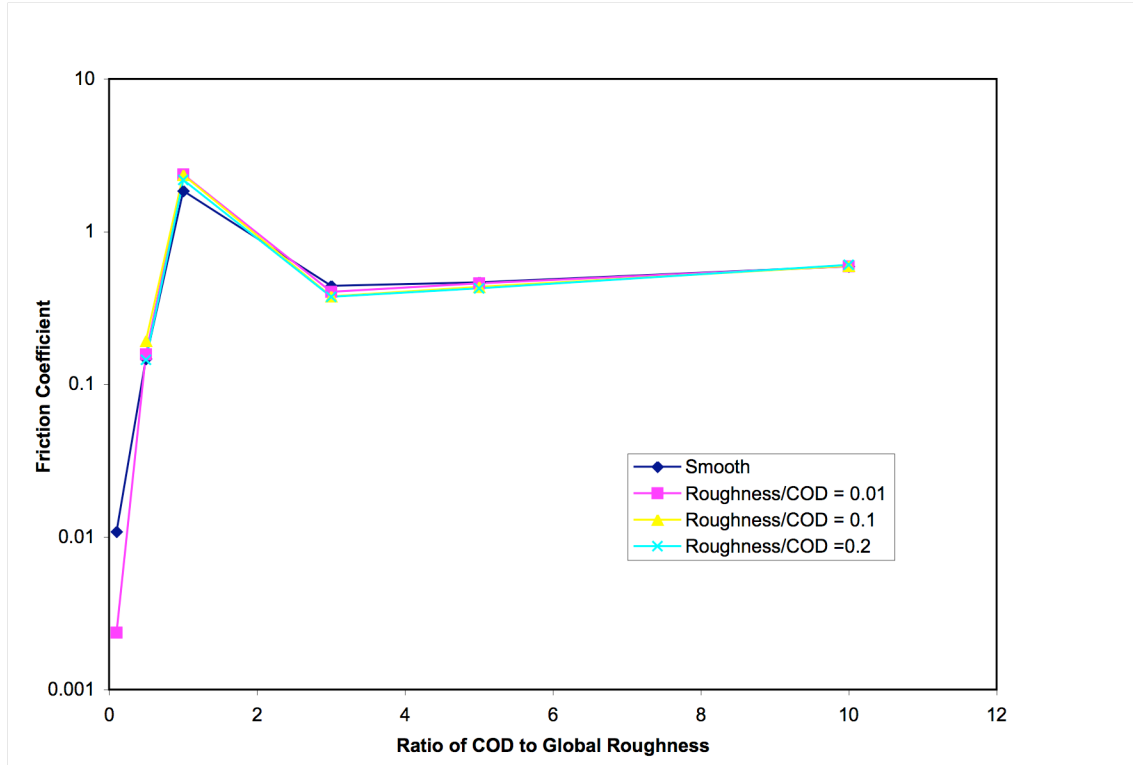


Figure C9. Friction coefficient as a function of ratio of COD to global roughness for different local roughnesses.

2.2 Conclusions from Numerical Results

We will limit our conclusions to the high Reynolds number situations.

1. When the crack is tight, i.e., $\delta/\mu_g < 0.1$, the friction to the flow inside the duct can be separated into two parts: the first being the friction caused by the local roughness on the straight portions of the duct, the second being the friction caused by the turns of the flow.
2. When the crack is wide, i.e., $\delta/\mu_g > 5$, the duct with turns behaves like a straight duct with the global roughness (the turns) acting as wall roughness. In this case, the friction caused by the turns is ignored. Instead, the friction should be calculated by using a correlation for straight duct with the global roughness as wall roughness.
3. In the transition region where $0.1 < \delta/\mu_g < 5$, the friction coefficient should be interpolated between the above two extreme situations.
4. Notice that our numerical analyses are for incompressible flow, which is quite different from the two-phase, choked flow in cracks. But as stated in fluid mechanics books, friction correlations are often carried out on incompressible flow and then extended to compressible flow with some or, frequently, with little modification. In fact, all the correlations used in the SQUIRT or other early models for the same application were obtained from experiment on incompressible flow

(water). Here we follow the same practice by assuming our results from incompressible analyses can be applied to the two-phase flow.

3. Formulation for Pressure Losses due to Wall Friction and Turns

In the thermal-hydraulic model of crack flow, several pressure losses need to be evaluated along the flow path. Two of them, the pressure drop due to wall friction, and that due to the turns (termed as path loss in SQUIRT), are the sources of high uncertainties. These uncertainties can cause significant errors in the flow-rate calculation, especially for a tight crack.

To apply the above conclusions to the thermal-hydraulic model for the two-phase choked flow in cracks, we need to evaluate the effective length, the effective wall roughness, and the effective number of turns of the crack. These three parameters are used in the model to evaluate the pressure losses due to wall friction and path turns.

We follow the proposed formulation in Ref. 2, as further supported by this study, the three parameters are set according to the ratio of crack COD to its global roughness.

Overall pressure drop due to wall friction and turns consisted of two independent parts:

$$P = P_{\text{wall}} + P_{\text{turn}}$$

where P_{wall} represents the pressure drop due to the wall friction, and P_{turn} represents the pressure drop due to the turns of the flow path. In the case of $\delta/\mu_g < 0.1$, these two parts can be evaluated separately because the flow path is relatively narrow and slim, so a fully developed velocity profile exists for the segments of the straight duct. When $\delta/\mu_g > 5.0$, p_{turn} approaches zero as the global roughness behaves like wall roughness.

3.1 Calculation of Pressure Drop due to Wall Friction

To calculate the pressure drop due to wall friction, the friction coefficient f_{wall} is evaluated according to the duct's local roughness and the flow Reynolds number (i.e., second correlation equation in Section 1.1 of this Appendix). Notice that the effective roughness is needed here, and it is evaluated according to the following:

$$\mu = \begin{cases} \mu_1, & \text{when } \frac{\delta}{\mu_1} < 0.1 \\ \mu_1 + (\mu_g - \mu_1) \left(\frac{\delta}{\mu_1} - 0.1 \right) / 4.9, & \text{when } 0.1 < \frac{\delta}{\mu_1} < 5.0 \\ \mu_g, & \text{when } \frac{\delta}{\mu_1} > 5.0 \end{cases}$$

Then P_{wall} is evaluated according to the effective length of the crack. This approach is well documented in the development of SQUIRT. At this point, we need the effective length of the crack, and it is evaluated according to the following:

$$L = \begin{cases} L_c, & \text{when } \frac{\delta}{\mu_1} < 0.1 \\ L_c + (L_d - L_c) \left(\frac{\delta}{\mu_1} - 0.1 \right) / 4.9, & \text{when } 0.1 < \frac{\delta}{\mu_1} < 5.0 \\ L_d, & \text{when } \frac{\delta}{\mu_1} > 5.0 \end{cases}$$

where L_c is the actual length of the curved crack along its turns, and L_d is the measured length from crack inlet to its exit along a straight line.

Another measurement of the crack path's morphology is the number of turns per unit length. We employ the same interpolation scheme as the above for effective roughness and effective length of the crack. This parameter is used to evaluate the pressure loss due to the path turns along a crack length:

$$n = \begin{cases} n_1, & \text{when } \frac{\delta}{\mu_1} < 0.1 \\ L_c - L_c \left(\frac{\delta}{\mu_1} - 0.1 \right) / 4.9, & \text{when } 0.1 < \frac{\delta}{\mu_1} < 5.0 \\ 0, & \text{when } \frac{\delta}{\mu_1} > 5.0 \end{cases}$$

Notice, as the crack becomes wide $\frac{\delta}{\mu_1} > 5.0$, the number of turns becomes zero, as the turns actually are counted as roughness, and the pressure drop due to turn is ignored.

3.2 Calculation of Pressure Drop due to Path Turns

With the effective number of turns available described in the above formulation, for each turn, we can evaluate the corresponding pressure loss.

At present, few experimental works have been completed on pressure loss with turn. The correlation by Ito⁵ was done on pipes with a single bend and water inside. While this is far from the situation of the compressible flow inside a tight crack, this is also the only related work in publication that the authors are aware of.

Ito's work concluded that for Reynolds number $2 \times 10^4 < Re < 4 \times 10^5$,

$$\lambda = \begin{cases} 0.000873\alpha\theta \frac{R}{r}, & R(r/R)^2 < 91 \\ 0.00241\alpha\theta R^{-0.17} \left(\frac{R}{r}\right)^{0.84}, & R(r/R)^2 > 91 \end{cases}$$

where θ is the turning angle, Re is the Reynolds number, and α is a numerical coefficient. Approximate expressions for α are the following:

for $\theta=45^\circ$,

$$\alpha = 1 + 14.2(R / r)^{-1.47},$$

for $\theta=90^\circ$,

$$\alpha = \begin{cases} 0.95 + 17.2(R / r)^{-1.96}, & R / r < 19.7 \\ 1, & R / r > 19.7 \end{cases}.$$

With the above equations, we can evaluate the pressure loss by each turn if we can determine the value of R/r . Because no characteristic dimension is available for the approximation of the bend radius, we simply assume $R/r=1$ here. For virtually all the cases in practice for crack flows, $R/r=1$, and $R(r/R)^2 > 91$, $\alpha=15.2$ for $\theta=45^\circ$, and $\alpha=18.15$ for $\theta=90^\circ$, and the friction coefficient is,

$$\lambda = 0.00241\alpha\theta\text{Re}^{-0.17}$$

with α being interpolated between $\theta=45^\circ$ and $\theta=90^\circ$.

Finally, the total pressure loss by the turns will be $nL\lambda_t$, where n is the effective number of turns per unit length, L is the effective length of the crack, and λ_t is the friction coefficient by turns.

So far, we have presented numerical results for 2D duct flow with multiple turns and proposed ways to evaluate the pressure losses due to wall friction and path turns. We also determined the upper and lower bounds of μ_g/δ , so proper effective surface roughness, effective crack length, and effective number of turns can be determined. In addition, we also presented correlation equations for the calculation of pressure loss due to duct turns.

4. Thermal-hydraulic Model

To verify the above formulations proposed for the calculation of pressure losses due to wall friction and flow path turns, we developed a thermal-hydraulic model for the two-phase choke flow in cracks. The model follows closely the approach adopted by the SQUIRT code, and incorporates the ideas proposed above in the calculations of pressure losses by wall friction and turns. The fundamental components of such a model are documented in the details on the SQUIRT code.

For the first step validation of the present model, we compare our results to the experimental data by Sozzi and Sutherland⁶, Amos and Shrock⁷, and Collier⁸ for two-phase flows in rectangular slits. Then, we compare calculations with our model to the experimental results by Collier for corrosion fatigue cracks.

Some of the model's features are:

1. The condition inside the pipe (stagnation condition) can be either sub-cooled water or saturated water. The thermal properties of the fluid are modeled through a software package for Steam Table 1967.
2. The crack shape can be elliptic, rectangular, or diamond.
3. The crack can have different areas at its inlet and exit.
4. There are built-in approaches to evaluate the crack morphology for corrosion fatigue, IGCCS, or PWCCS types of cracks.

4.1 Two-Phase Critical Flow in Straight Channels

To benchmark the thermal-hydraulic model, we compare the predictions by the model to the experimental data by Sozzi on smooth pipe flow, and the results are shown in Figure C10.

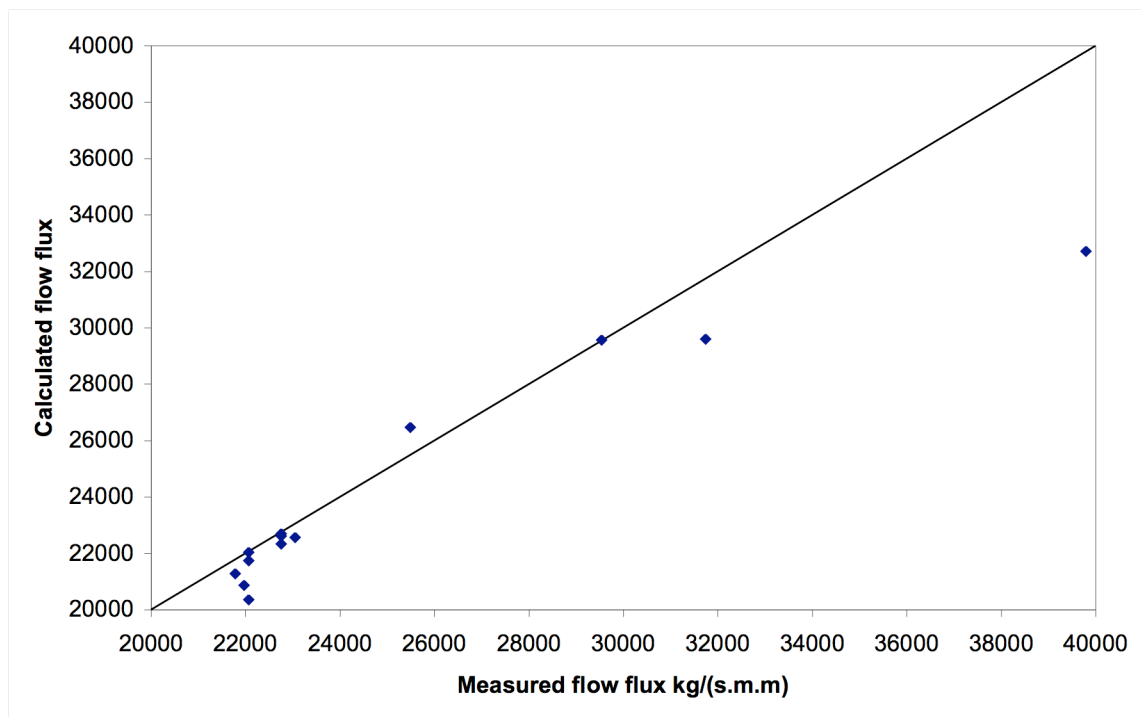


Figure C10. Comparison of calculated flow flux vs. measured data by Sozzi and Sutherland⁶.

Figure C11 plots the calculated and measured flow flux by Amos and Shrock for two-phase critical flow in slits. These comparisons demonstrate that the thermal-hydraulic model gives reasonable prediction for critical two-phase flows in regularly shaped channels. It can be seen that the predictions given by the software agree reasonably well with the measurements.

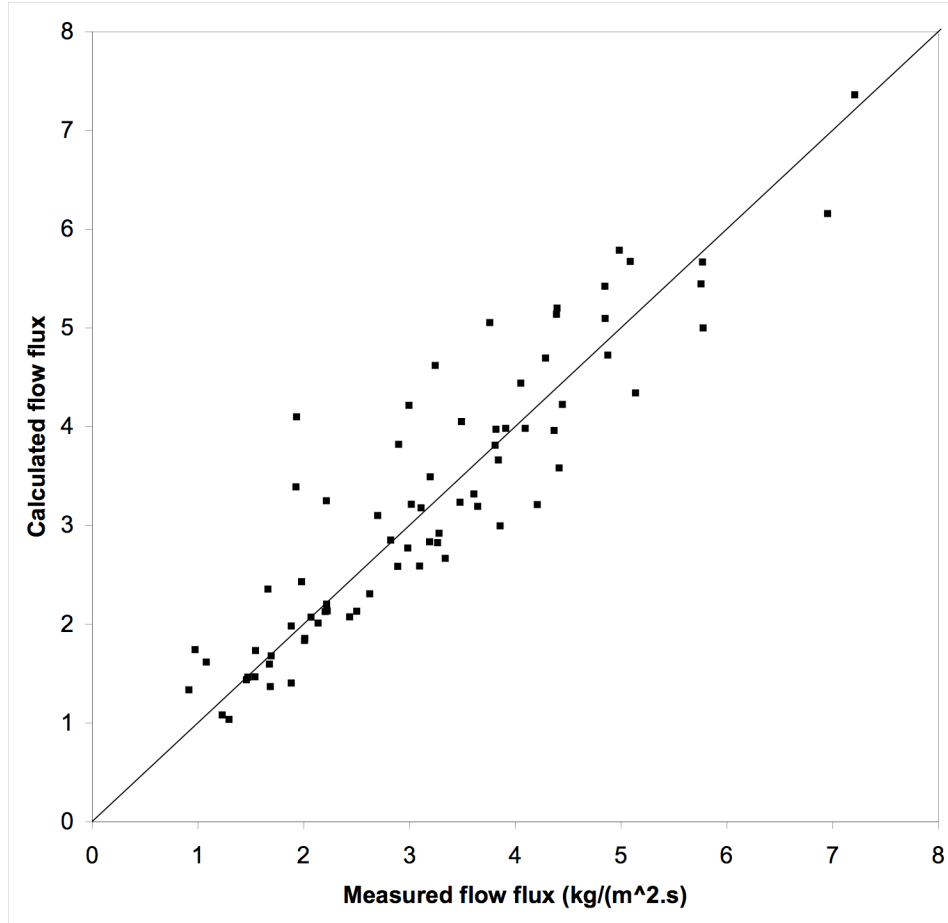


Figure C11. Comparison of calculated flow flux and the measurements by Amos and Shrock⁷.

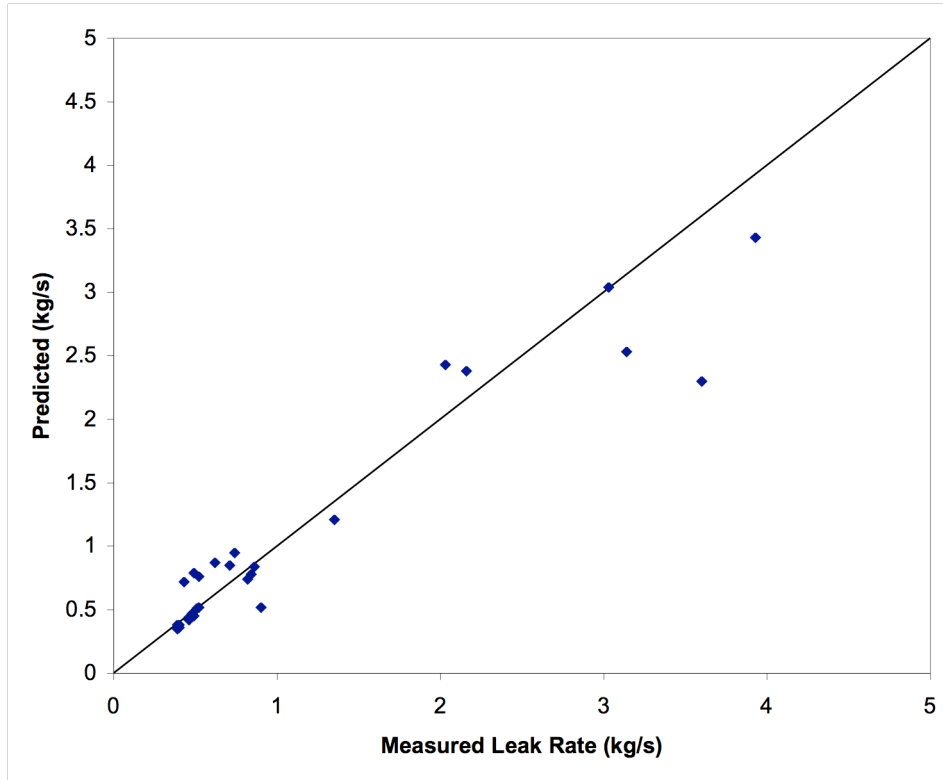


Figure C12. Comparison of calculated leak rate and the measurements by Collier et al.⁸

4.2 Critical Flows in Intergranular Stress Corrosion Cracks

To calculate the flow rate in intergranular stress corrosion cracks (IGSCC), we implemented the formulation outlined in the above sections for the evaluation of pressure drops due to surface friction and path turns. For the particular IGSCC cracks, we use the morphology parameters proposed in reference 2. Notice that these parameters were given in a statistical format of means and standard deviation:

- Local roughness, mean: $\mu_L=4.7 \mu\text{m}$, standard deviation: 3.937
- Global roughness, mean: $\mu_G=80.0 \mu\text{m}$, standard deviation: 39.01
- Number of turns, mean: $n_L=28.2 \text{ mm}^{-1}$, standard deviation: 18.9
- Global path deviation, mean: 1.07, standard deviation: 0.1

Instead of using a statistical approach for these parameters, we simply take the mean values of the three morphology parameters and run the analysis. It was found that the measured and predicted leak rates are far off each other. This finding might be due to the fact that the morphology of the crack(s) used was totally different from the one we used in the

model. Consequently, we simply ran the analysis by assuming a local roughness of 0.00178 mm without any global roughness. The following plots (Fig. C13-C17) present the comparisons between the measured leak rates and those predicted by the present thermal-hydraulic model. For the tightest crack COD = 0.02mm, the agreement between the measurements and predictions is fairly good. For a crack that has a COD of 0.108 mm, the agreement is even better. But for other cracks, significant differences are observed. Again, the uncertainties in the crack's morphology are a primary reason for the disagreement. Other uncertainties were discussed in detail in reference 1.

The current thermal-hydraulic model needs to be further tuned or refined in the implementation of the effective roughness/crack length/number of turns and that of the pressure loss due to path turns. To validate the current model, more experiment data are needed along with detailed crack morphology information.

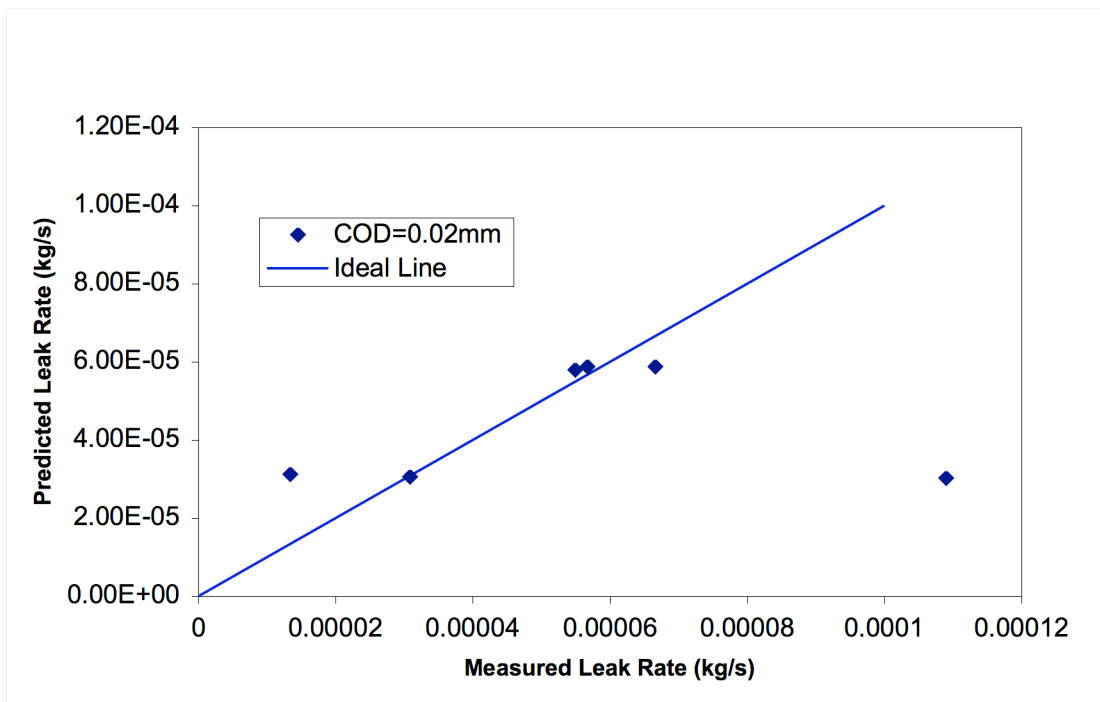


Figure C13. Measured versus predicted leak rate for COD = 0.02 mm.

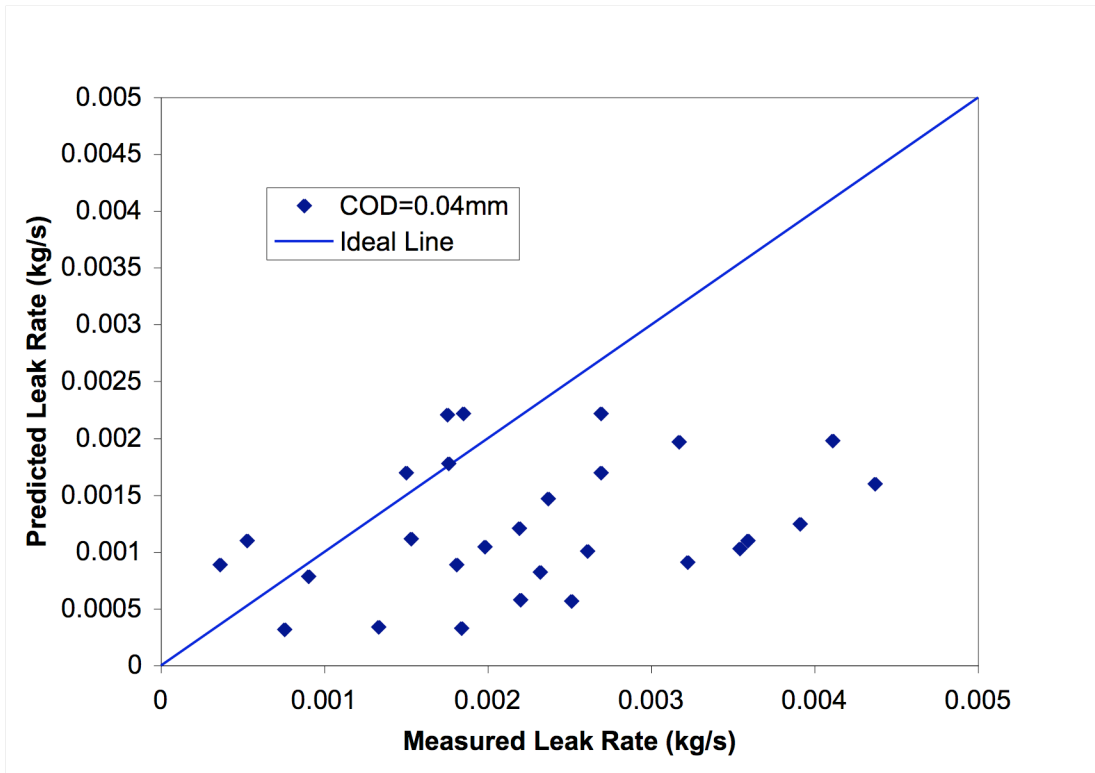


Figure C14. Measured versus predicted leak rate for COD = 0.04 mm.

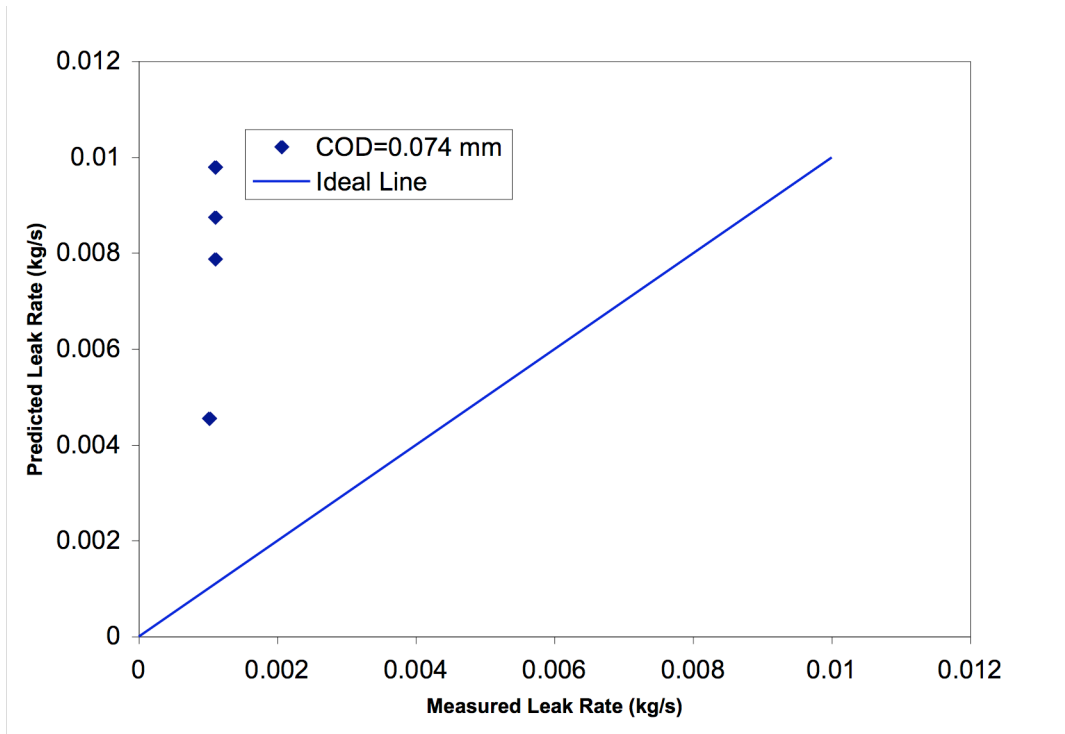


Figure C15. Measured versus predicted leak rate for COD = 0.074 mm.

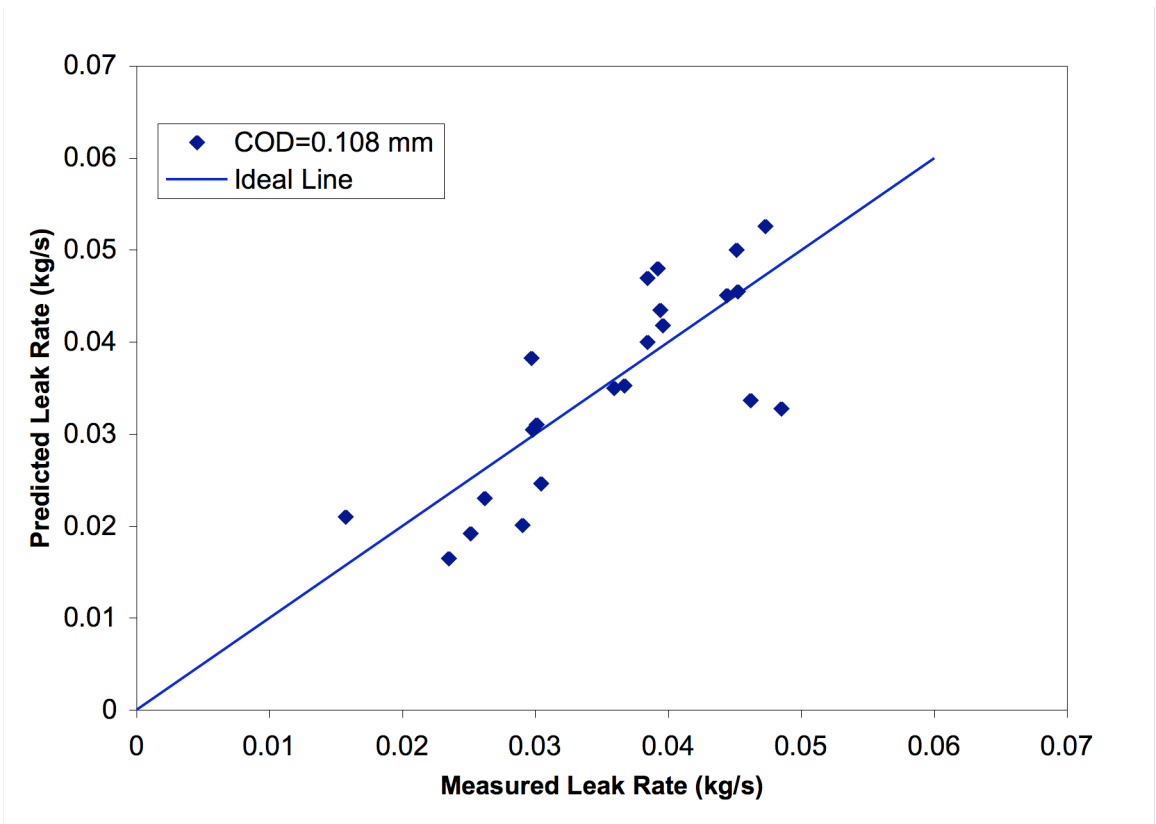


Figure C16. Measured versus predicted leak rate for COD = 0.108 mm.

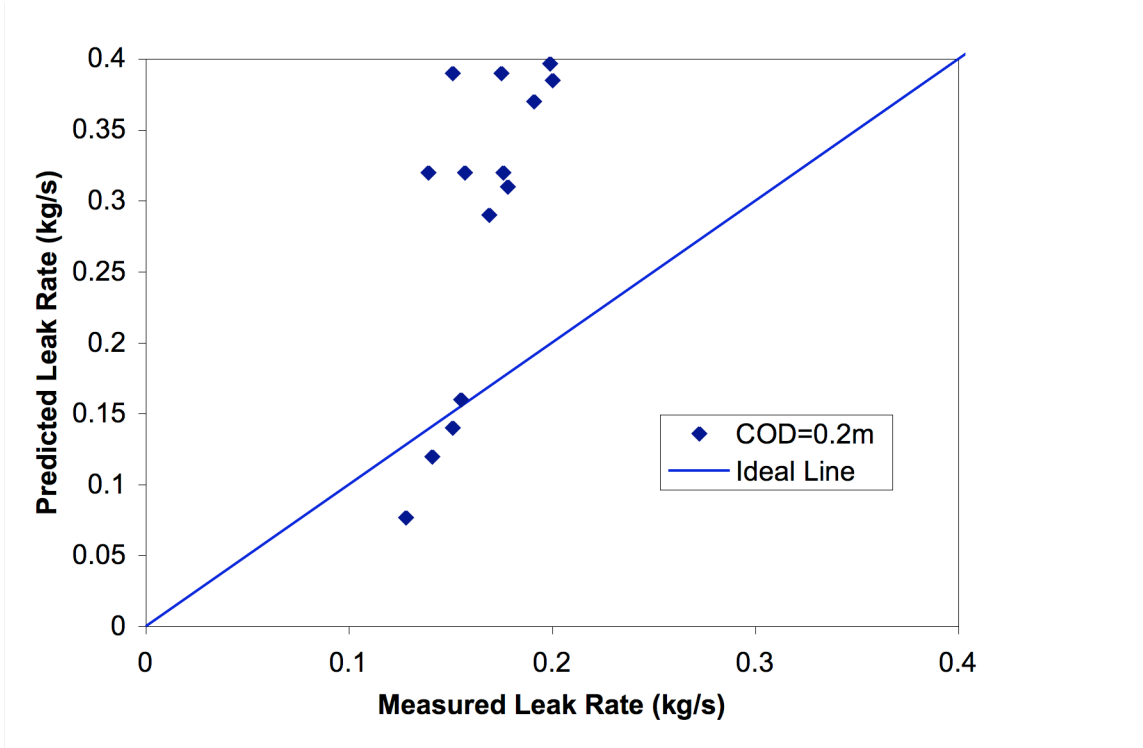


Figure C17. Measured versus predicted leak rate for COD = 0.2 mm.

-
- ¹D. D. Paul, J. Ahmad, P. M. Scott, L. F. Flanigan, and G. M. Wilkowski, "Evaluation and Refinement of Leak-Rate Estimation Models," NUREG/CR-5128, June 1994.
- ² D. Rudland, R. Wolterman, and G. Wilkowski, "Leakage through CRMD Nozzles with PWSCC Cracks," Final report to U.S. NRC, Office of Regulatory Research, December 2002.
- ³ Hermann Schlichting, *Boundary-Layer Theory*, McGraw-Hill, New York, 1979.
- ⁴ H. John, J. Reimann, F. Westphal, and L. Friedel, "Critical Two-Phase Flow through Rough Slits," *International Journal of Multiphase Flow*, Vol. 14, No. 2, pp. 155-174, 1988.
- ⁵ H. Ito, "Pressure Losses in Smooth Pipe Bends," *Journal of Basic Engineering*, ASME Transactions, pp.131-143, March 1960.
- ⁶ G. L. Sozzi and W. A. Sutherland, "Critical Flow of Saturated and Sub-cooled Water at High Pressure," NEDO-13418, 1975.
- ⁷ C. Amos and V. Shrock, "Critical Discharge of Initially Sub-cooled Water through Slits," NUREG/CR-3475, 1983.
- ⁸ R. P. Collier, F. B. Stulen, M. E. Mayfield, D. B. Pape, and P. M. Scott, "Two-Phase Flow through Intergranular Stress Corrosion Cracks and Resulting Acoustic Emission," EPRI Report No. NP-3540-LD, 1984.

Appendix D

Sensitivity Analysis Results for Leak Rate versus Crack Length

Leak Rate versus Crack Length

The results of the predicted leak rates as a function of circumferential crack length are presented next in order to estimate the range of crack sizes that could result in a given value of leak rate. Figure D1a shows the leak rate as a function of crack length for the case of large-diameter PWR piping (32 inches). Figure D1b shows the same results on a log-log scale. The almost linear correlation indicates that the relation between leak rates and crack length can be described by a power-law function.

The more important observation from Figures D1a and D1b is that for any given leak rate the range of crack sizes varies significantly. For example, for a leak rate of 1 gpm, the crack length predicted would vary from 1.8 inches to 18 inches, depending on the normal operating stress or the type of degradation mechanism. This further confirms the fact that measuring the leak rate alone is not an indicator of the circumferential crack length and hence the integrity of the piping system. Figures D2 and D3 show similar results for intermediate- and small-diameter PWR piping. Again, depending on the range of crack length, the effect on leak rate can be significant. Alternatively, for a given leak rate the crack length may have considerable variations. For large-, intermediate-, and small-diameter BWR piping, the results are shown in Figures D4 through D6. Due to convergence problems associated with the SQUIRT code, the complete curves for the leak rate versus crack length for small-diameter BWR could not be obtained (Figure D6).

Effect of Complex Cracks (Duane-Arnold Type Cracks)

The next set of results presented includes the effect of complex cracks on the critical crack lengths, similar to those presented in Figures 11 and 12 for the PWR and BWR cases studied. A complex-crack involves a 360-degree surface flaw, where a part of the length of the surface flaw has broken through to create a circumferential through-wall flaw. The first step in the analysis of complex cracks was to verify the predictions of the dimensional plastic zone parameter (DPZP) methodology in predicting the maximum load-carrying capacity of the pipe. Experimental data on the maximum load capacity for complex-cracked piping are available from the NRC's Degraded Piping Program conducted at Battelle (NUREG 4687). The values for the moment ratio (complex crack to through-wall crack) predicted by DPZP for these experiments were 0.79 and 0.48 for a 28% and 61% surface flaw, respectively. The experimental values were 0.75 and 0.49, respectively, for the two cases, indicating very good agreement.

Once the DPZP methodology was verified with experimental predictions, the next step involved predicting the percent of the critical crack length for failure for 25% and 50% deep surface flaws assuming a 50% Service Level A loading. While the presence of the surface flaw does not affect the leak rate detected, the maximum load-carrying capacity of the pipe would be reduced. Alternatively, the percent of critical through-wall-crack length for failure would be

higher for the cases of complex cracks. Figure D7 shows the effect of 25% and 50% deep 360-degree surface flaws on the percent of critical crack length. As can be seen, for a leak rate of 1 gpm the percent of critical crack length increases from 42% to 61% for the smallest diameter case for PWR stainless (SS) piping. Figure D8 shows similar results for PWR carbon (CS) piping. The results from the BWR SS and CS piping are shown in Figures D9 and D10. The only anomaly observed was in the 50% deep flaw for a BWR SS pipe at a leak rate of 1 gpm (see Figure D9). The calculations for all three diameters were checked to confirm that the predicted values were not as a result of any obvious errors in input data.

Effect of Residual Stresses

The next variable investigated was the effect of residual stresses in welds on the predicted crack length for a given leak rate. SQUIRT does have the option of either including or not including the effect of residual stresses in circumferential welds. Figures D11 through D14 show the results for PWR SS, PWR CS, BWR SS, and BWR CS. Again, the calculations assumed a normal operating stress equal to 50% Service Level A loading.

In every case shown in the four figures, the presence of residual stresses increases the percent of critical crack length. As seen in Figures D11 and D12 for the PWR cases, the effect of residual stresses seems to be more pronounced at the smaller diameter and more specifically at the lower leak rates (<0.1 gpm). The residual stress effect on the leak rate for smaller diameters pipes is not as pronounced for the BWR SS piping. The limitation of the current version of SQUIRT was encountered again for the case of BWR CS piping (see Figure D14).

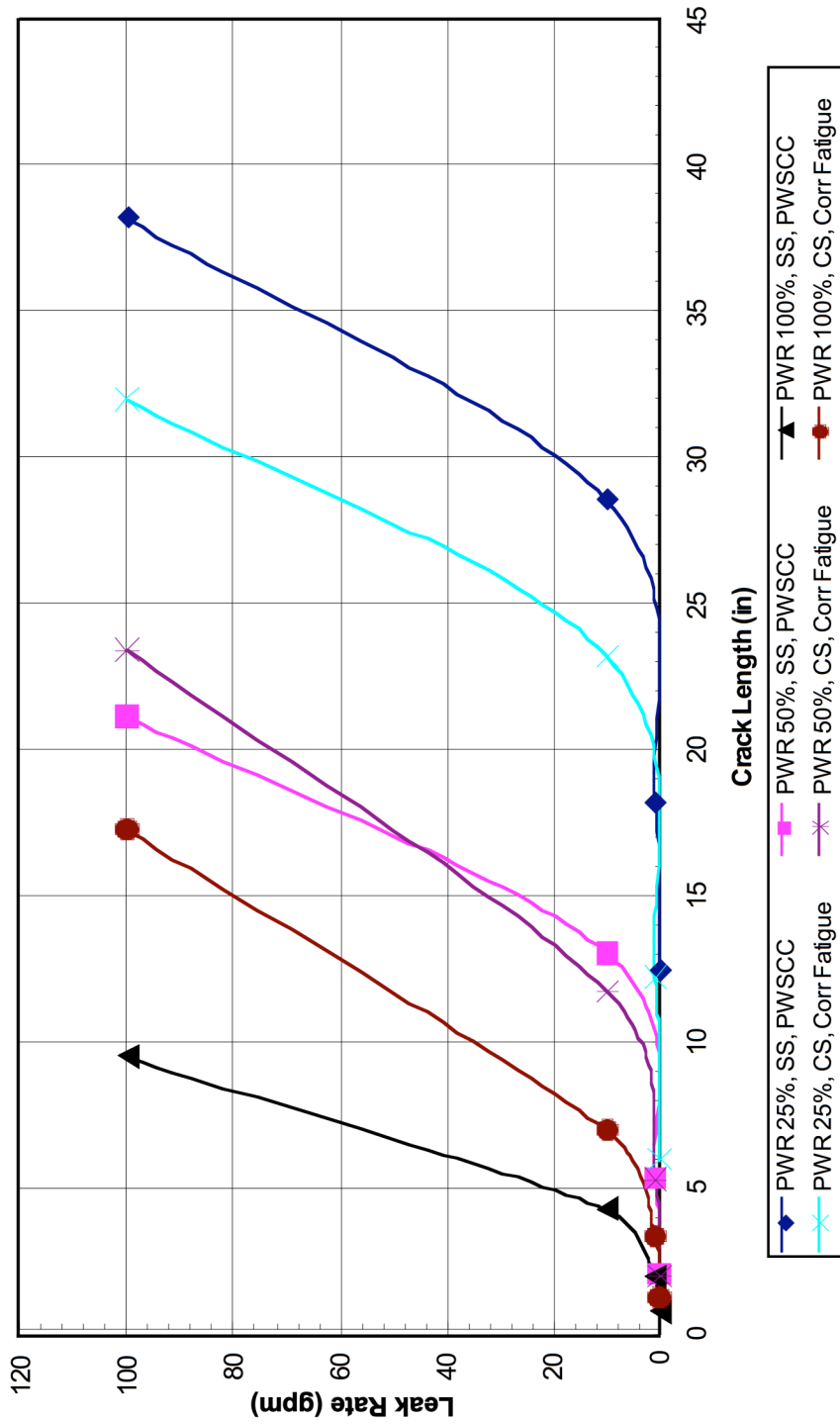


Figure D1a. Predicted leak rate versus crack length for large-diameter PWR piping.

Leak Rate v Crack Length for Large Diameter (32" OD x3" Wall) PWR Pipe

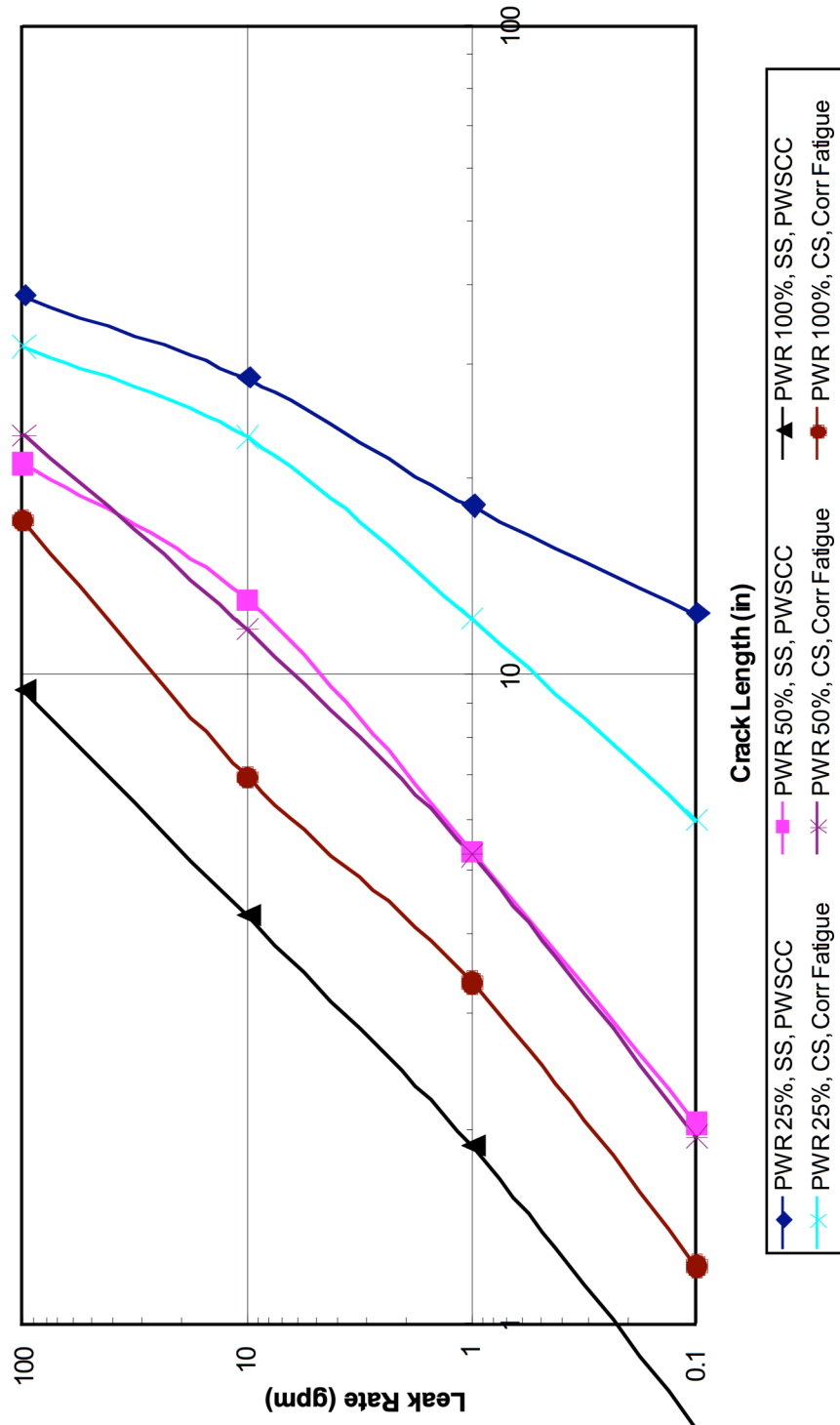


Figure D1b. Predicted leak rate versus crack length for large-diameter PWR piping (log-log scale showing power law correlation).

Leak Rate v Crack Length for Intermediate Diameter (12.75" OD x 3" Wall) PWR Pipe

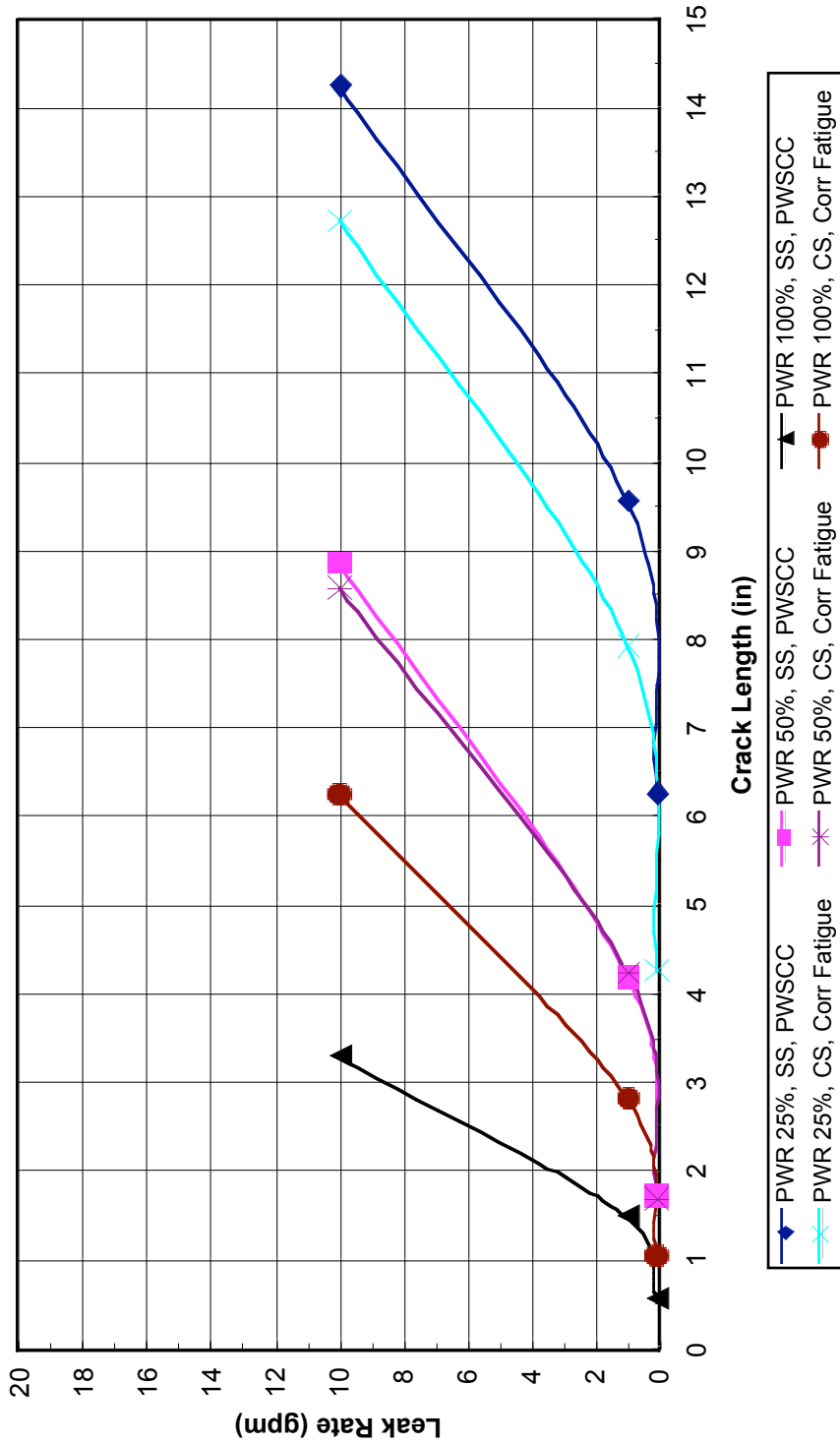


Figure D2. Predicted leak rate versus crack length for intermediate-diameter PWR piping.

Leak Rate v Crack Length for Small Diameter (4.5" OD x 0.53" Wall) PWR Pipe

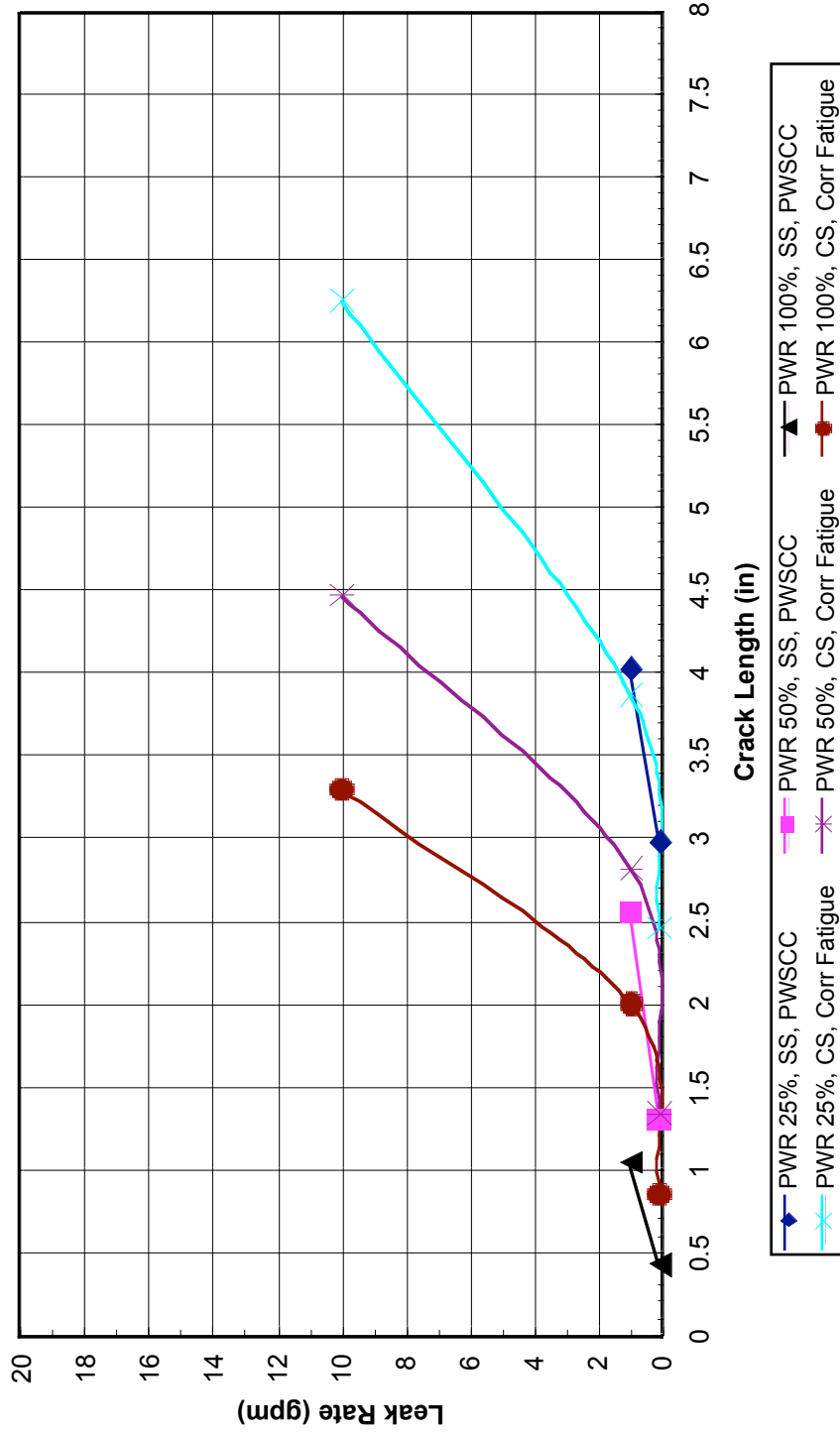


Figure D3. Predicted leak rate versus crack length for small-diameter PWR piping.

Leak Rate v Crack Length for Large Diameter (28" OD x 1.41" Wall) BWR Pipe

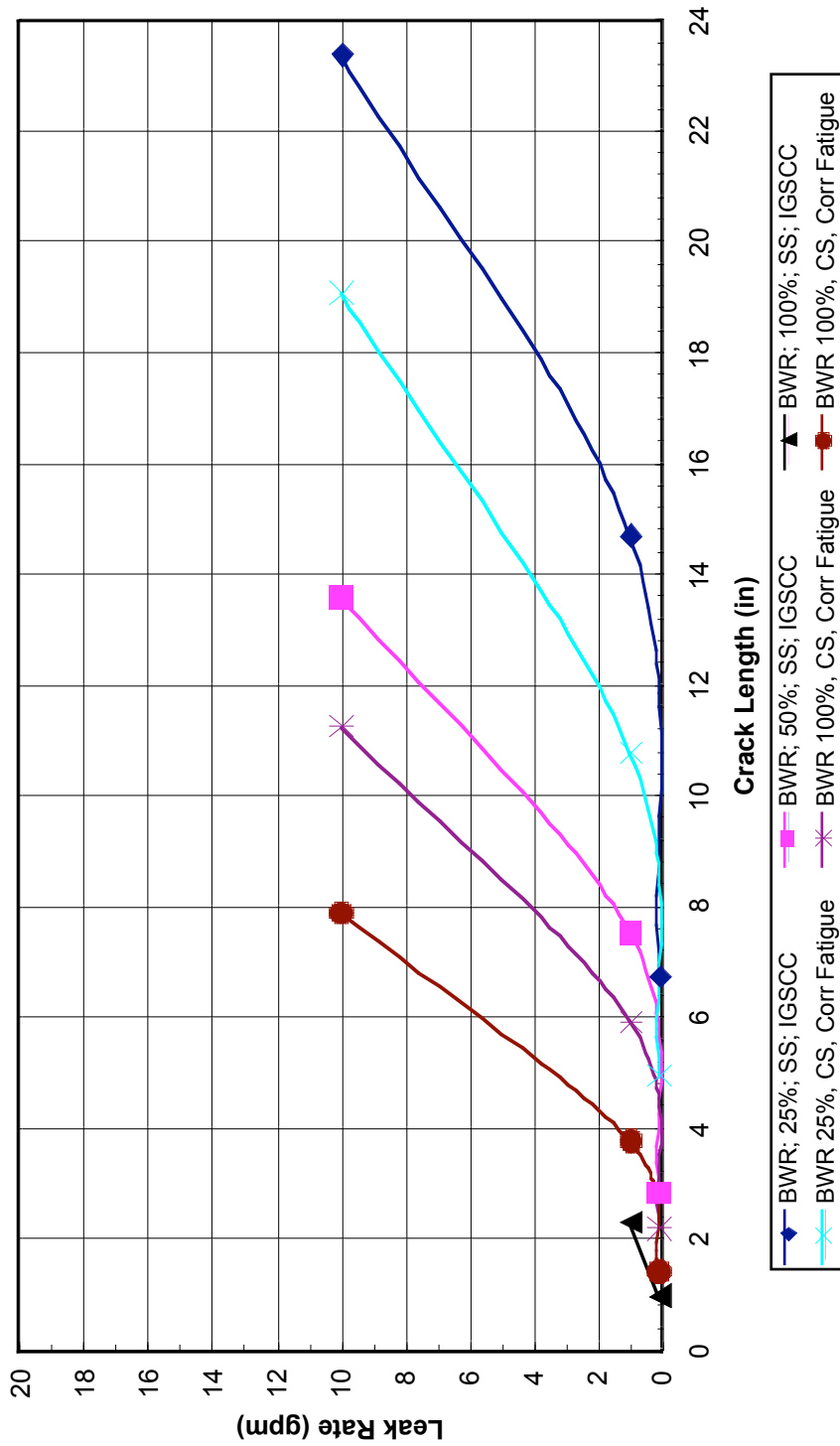


Figure D4. Predicted leak rate versus crack length for large-diameter BWR piping.

Leak Rate v Crack Length for Intermediate Diameter (12.75" OD x 0.687" Wall) BWR Pipe

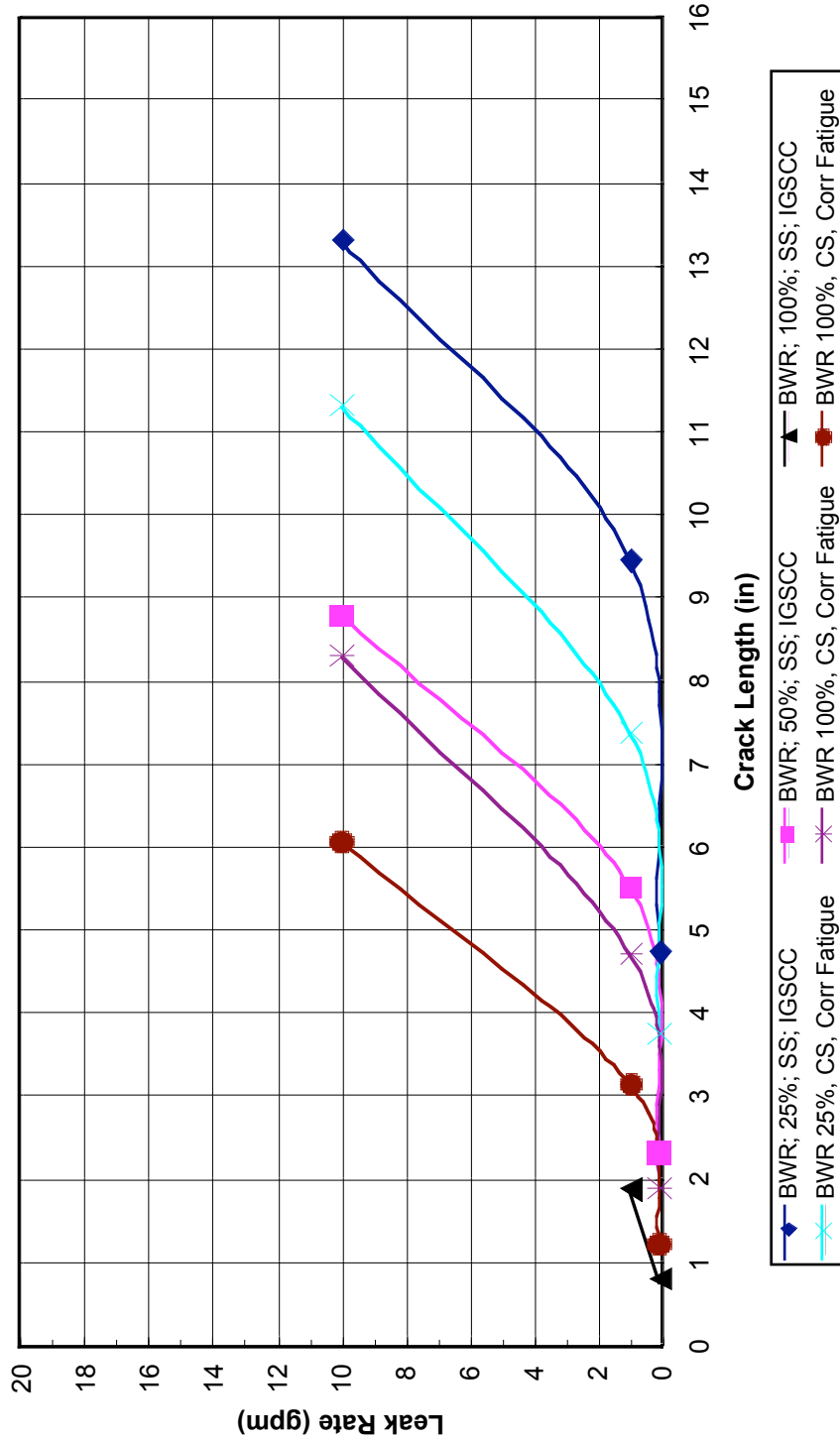


Figure D5. Predicted leak rate versus crack length for intermediate-diameter BWR piping.

Leak Rate v Crack Length for Small Diameter (4.5" OD x 0.337" Wall) BWR Pipe

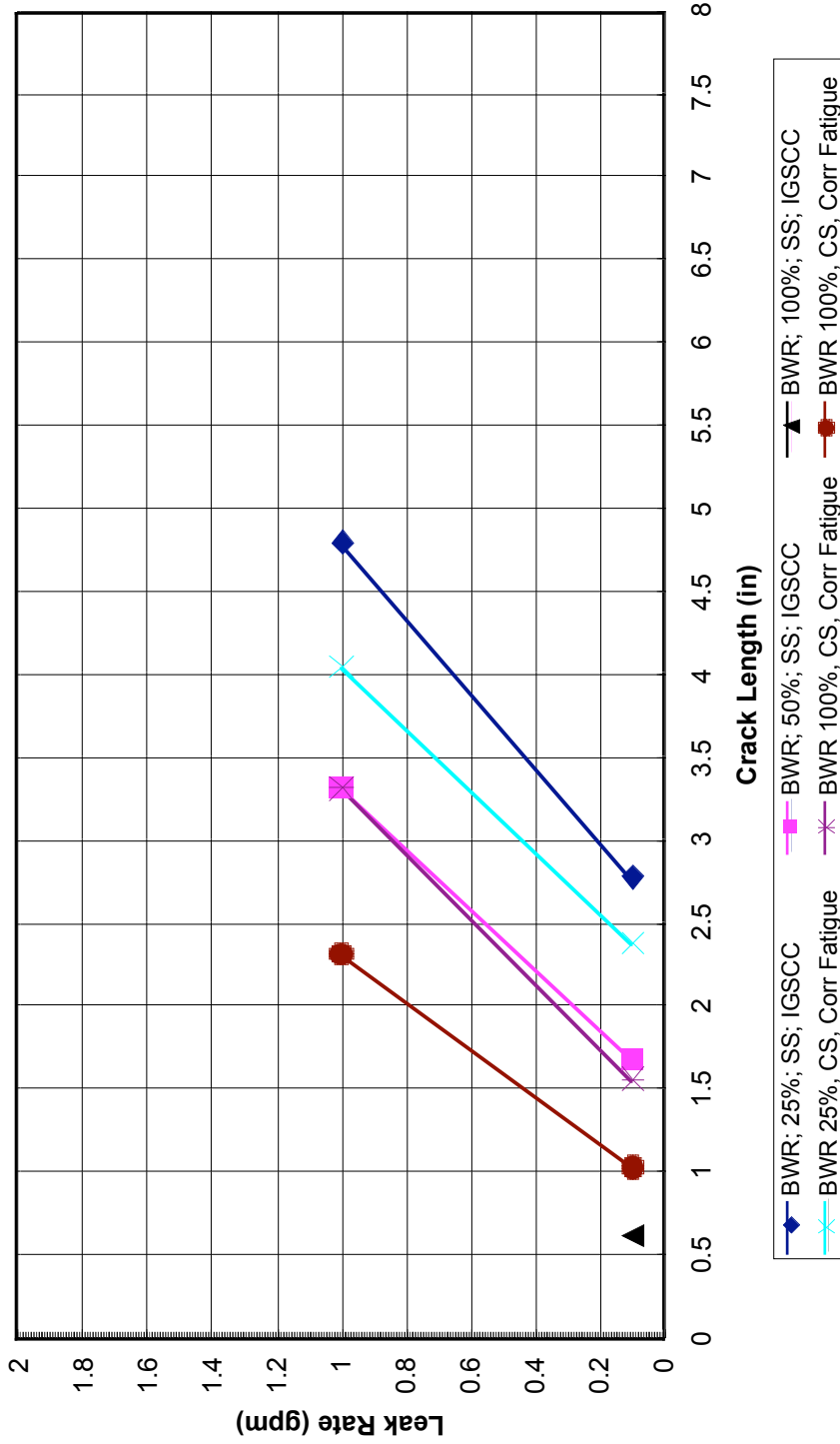


Figure D6. Predicted leak rate versus crack length for small-diameter BWR piping.

PWR - PWSCC Cases at 50% Service Level A - Complex Crack (CC) Analysis Results

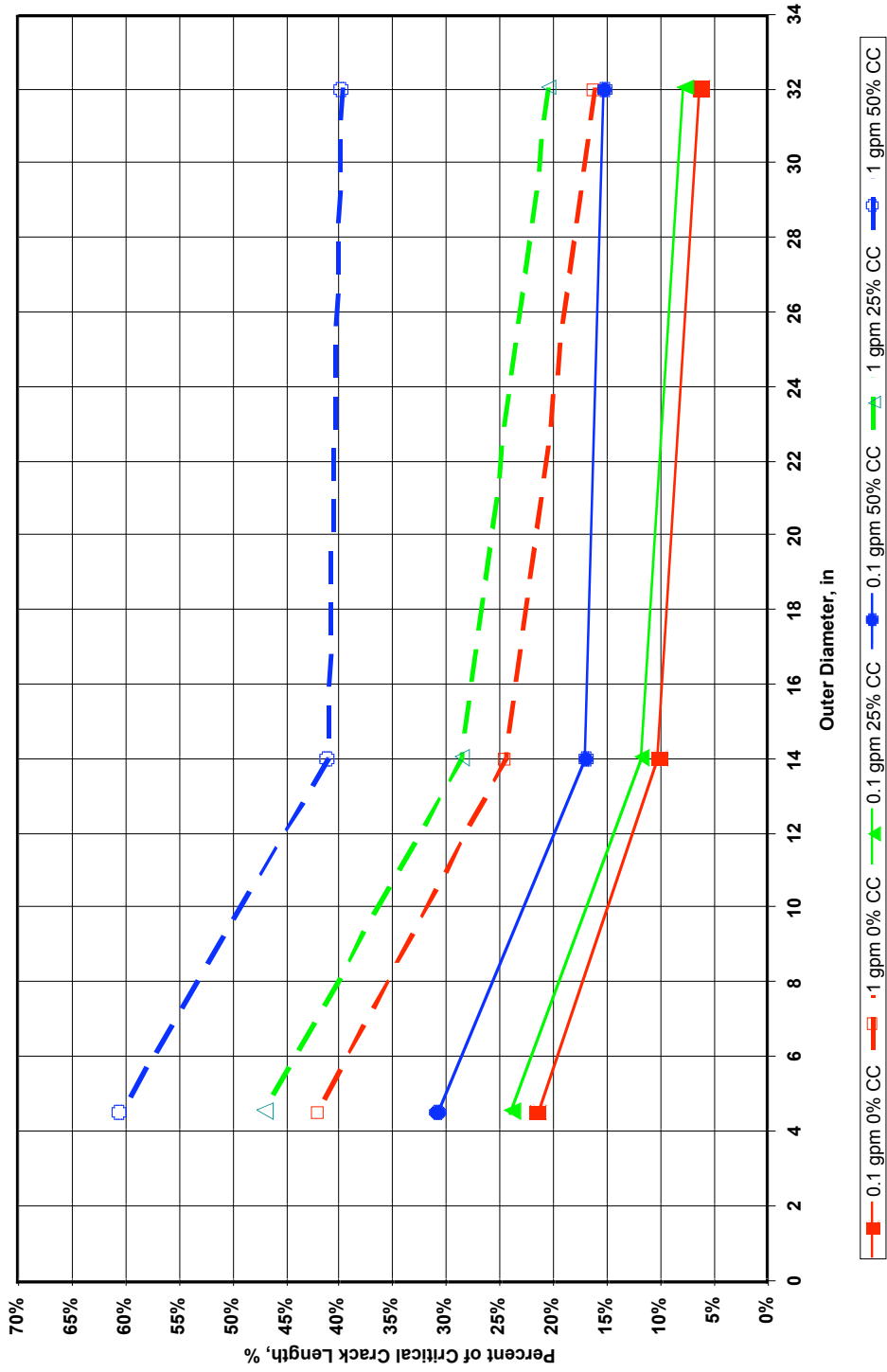


Figure D7. Effect of surface crack depth on critical crack length as a function of diameter (PWR SS piping).

PWR - Corrosion Fatigue Cases at 50% Service Level A - Complex Crack (CC) Analysis Results

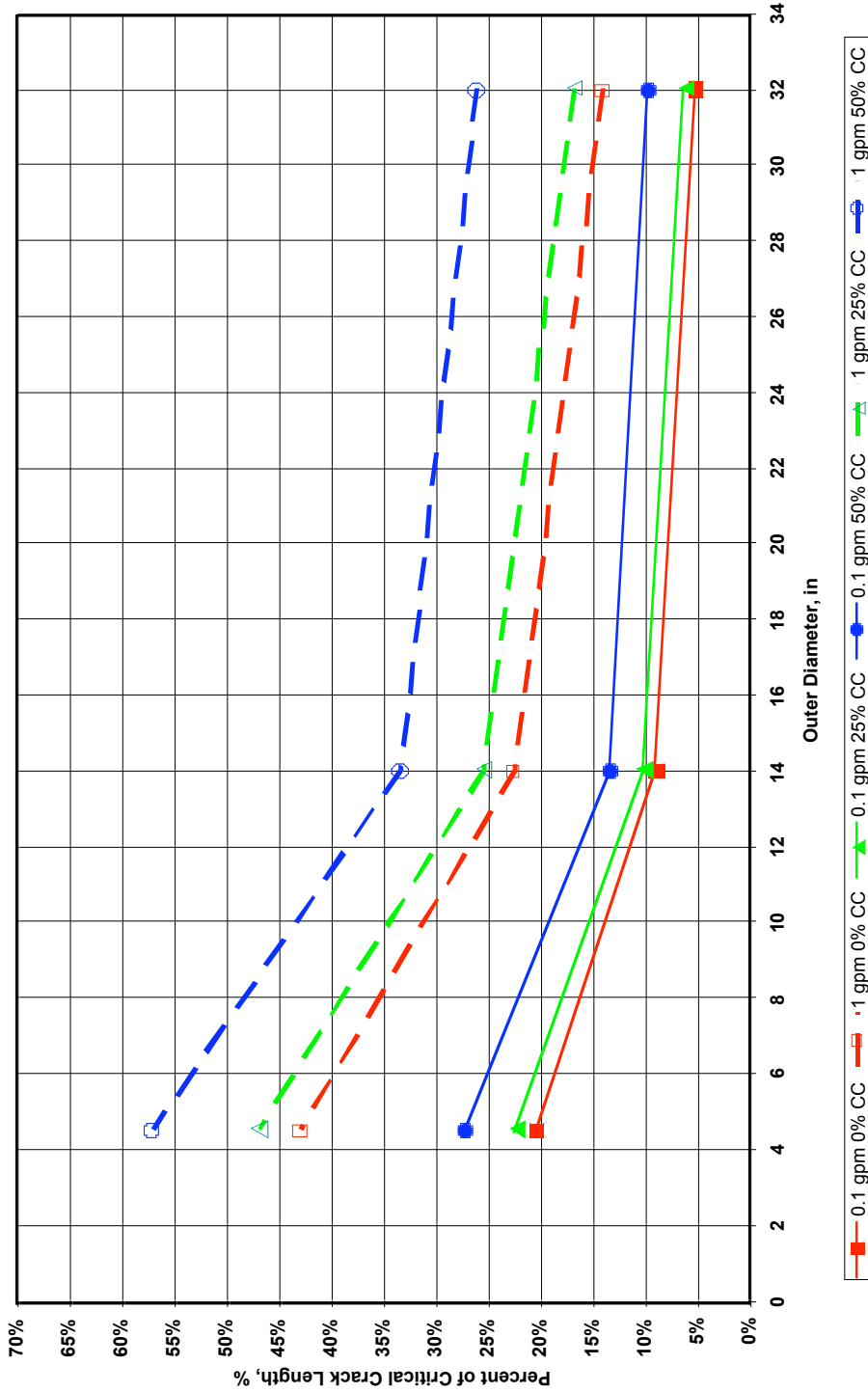


Figure D8. Effect of surface crack depth on critical crack length as a function of diameter (PWR CS piping).

BWR - IGSCC Cases at 50% Service Level A - Complex Crack (CC) Analysis Results

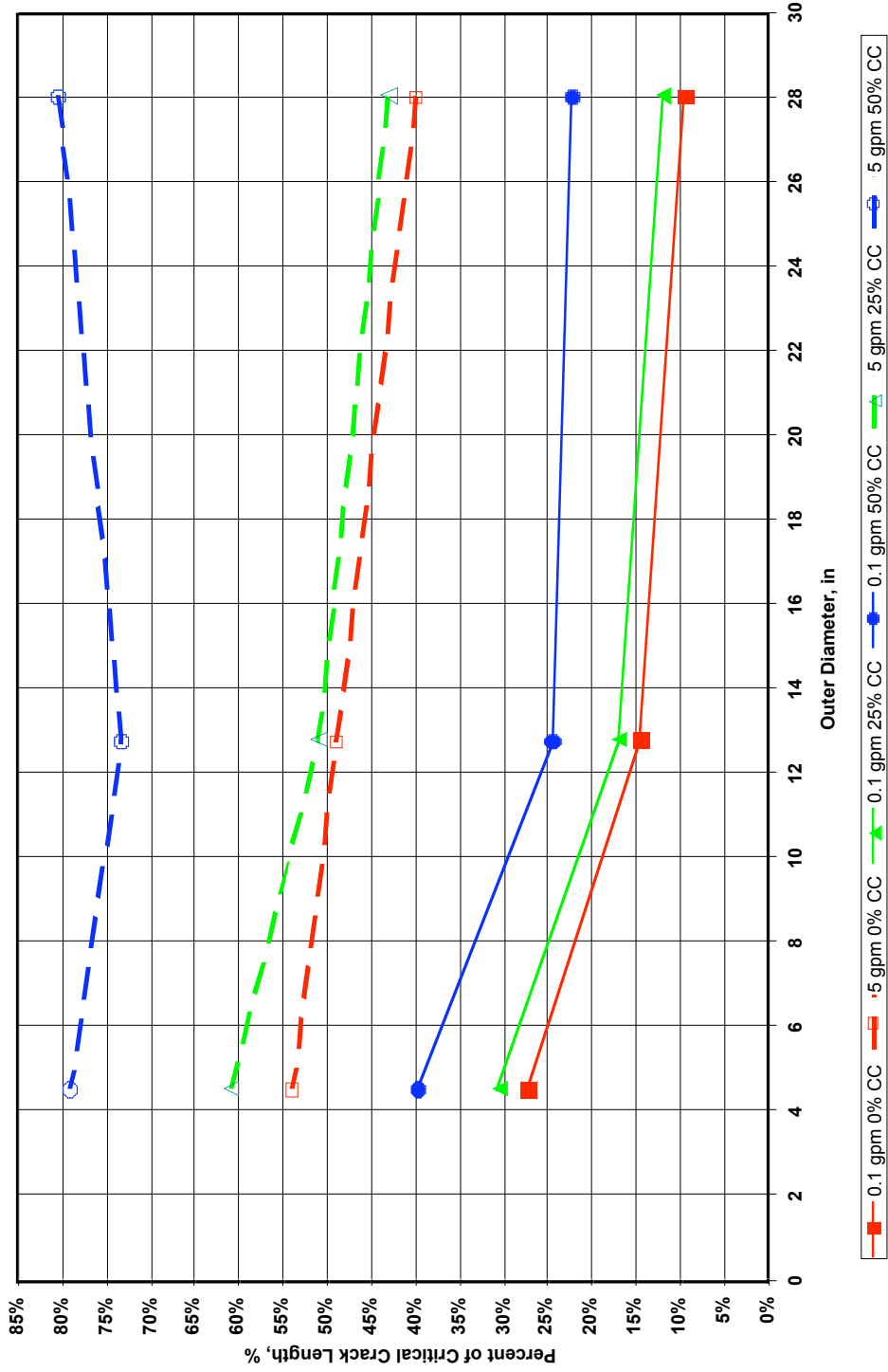


Figure D9. Effect of surface crack depth on critical crack length as a function of diameter (BWR SS piping).

BWR - Corrosion Fatigue Cases at 50% Service Level A - Complex Crack (CC) Analysis Results

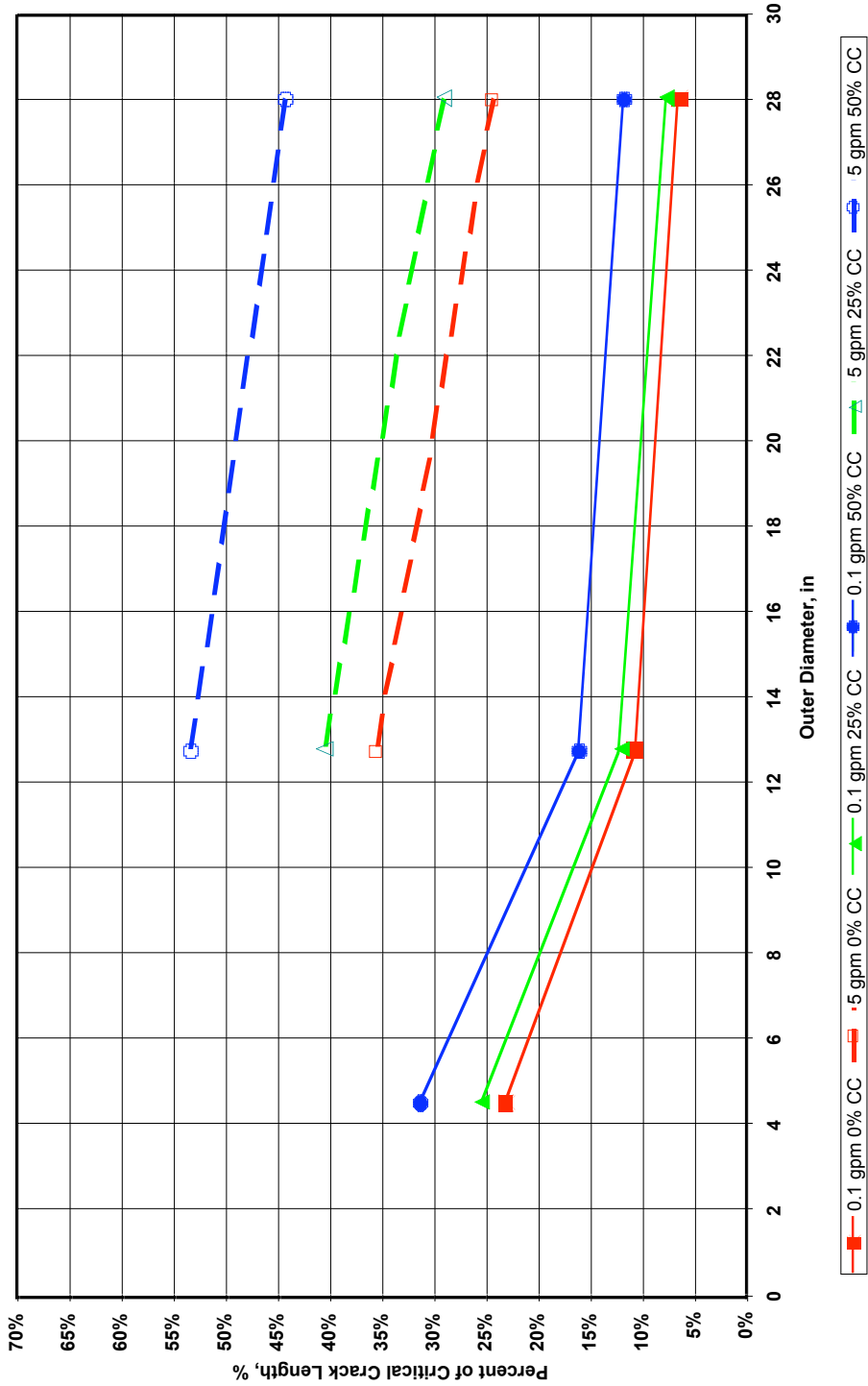


Figure D10. Effect of surface crack depth on critical crack length as a function of diameter (BWR CS piping).

PWR - PWSCC Cases at 50% Service Level A - Residual Stress Analysis Results

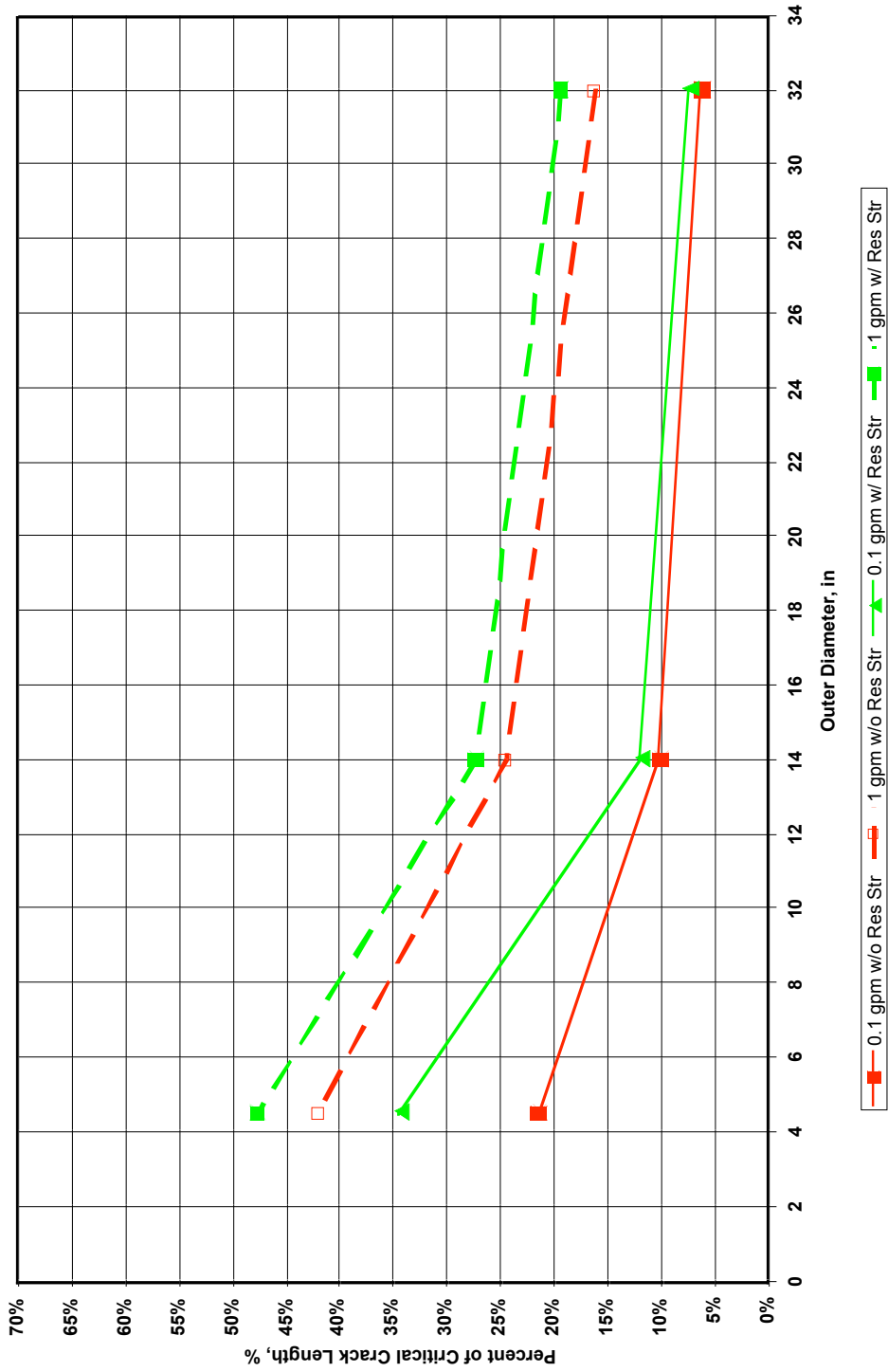


Figure D11. Effect of residual stresses on critical crack length as a function of diameter (PWR SS piping).

PWR - Corrosion Fatigue Cases at 50% Service Level A - Residual Stress Analysis Results

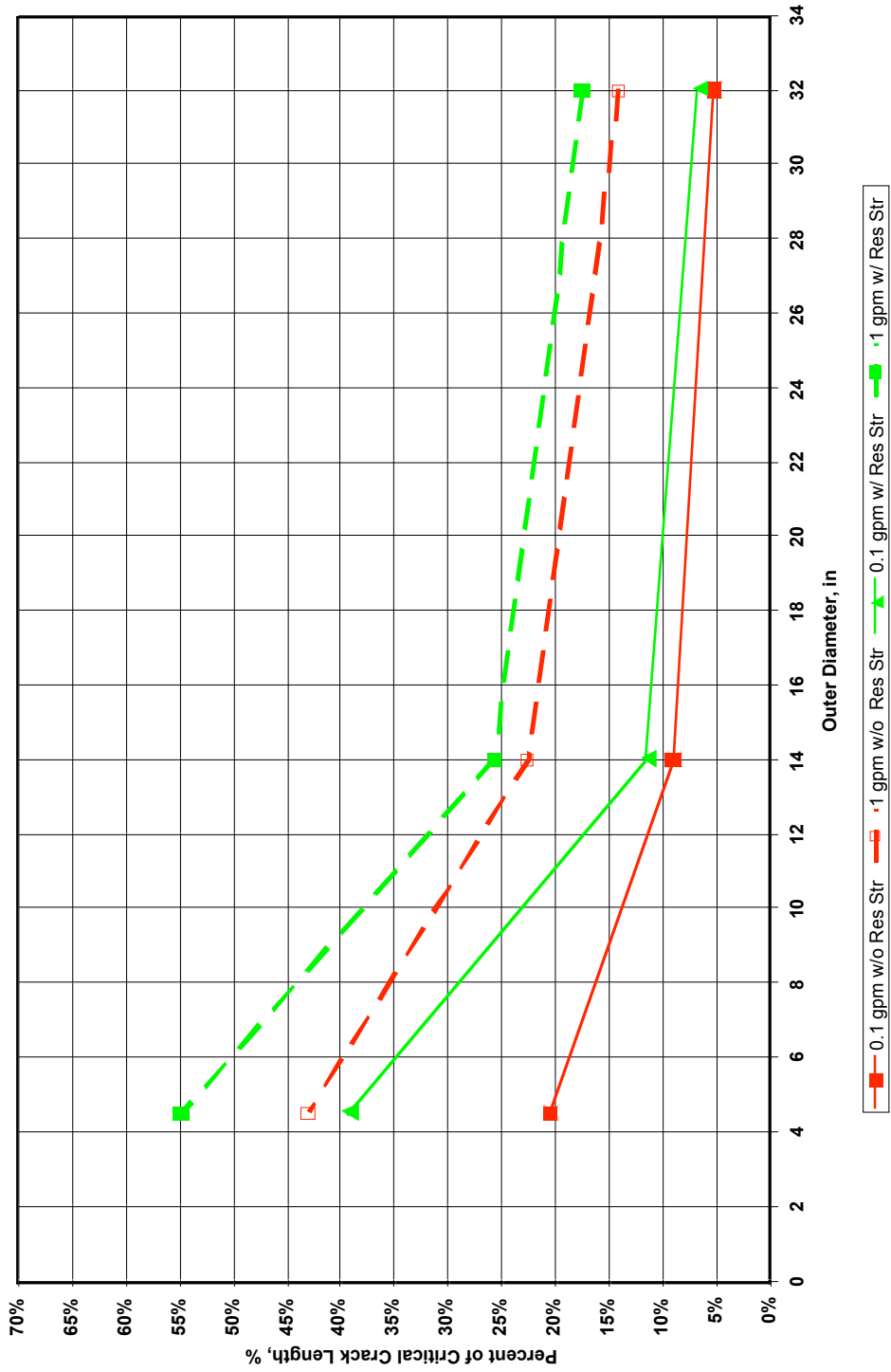


Figure D12. Effect of residual stresses on critical crack length as a function of diameter (PWR CS piping).

BWR - IGSCC Cases at 50% Service Level A - Residual Stress Analysis Results

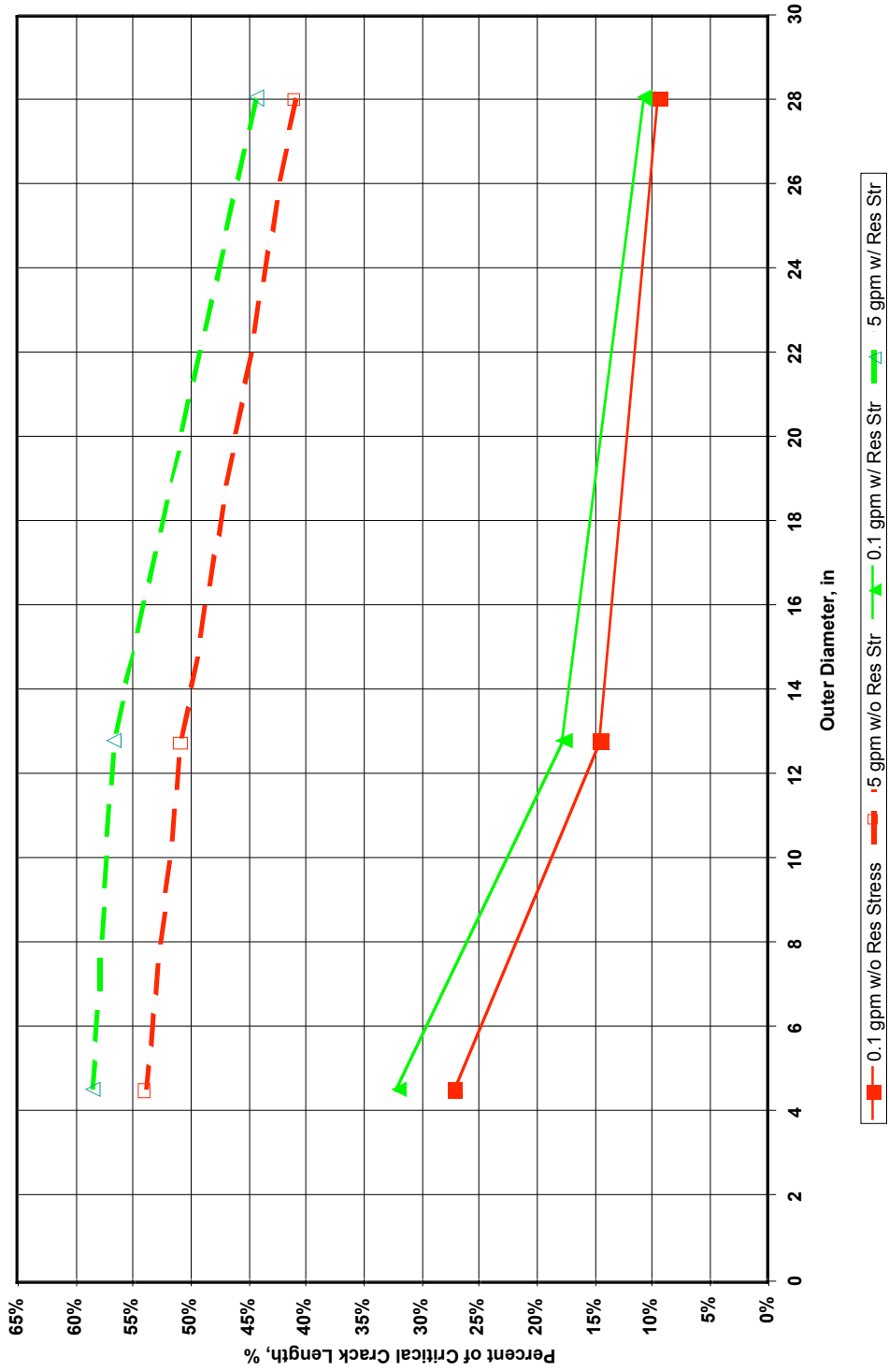


Figure D13. Effect of residual stresses on critical crack length as a function of diameter (BWR SS piping).

BWR - Corrosion Fatigue Cases at 50% Service Level A - Residual Stress Analysis Results

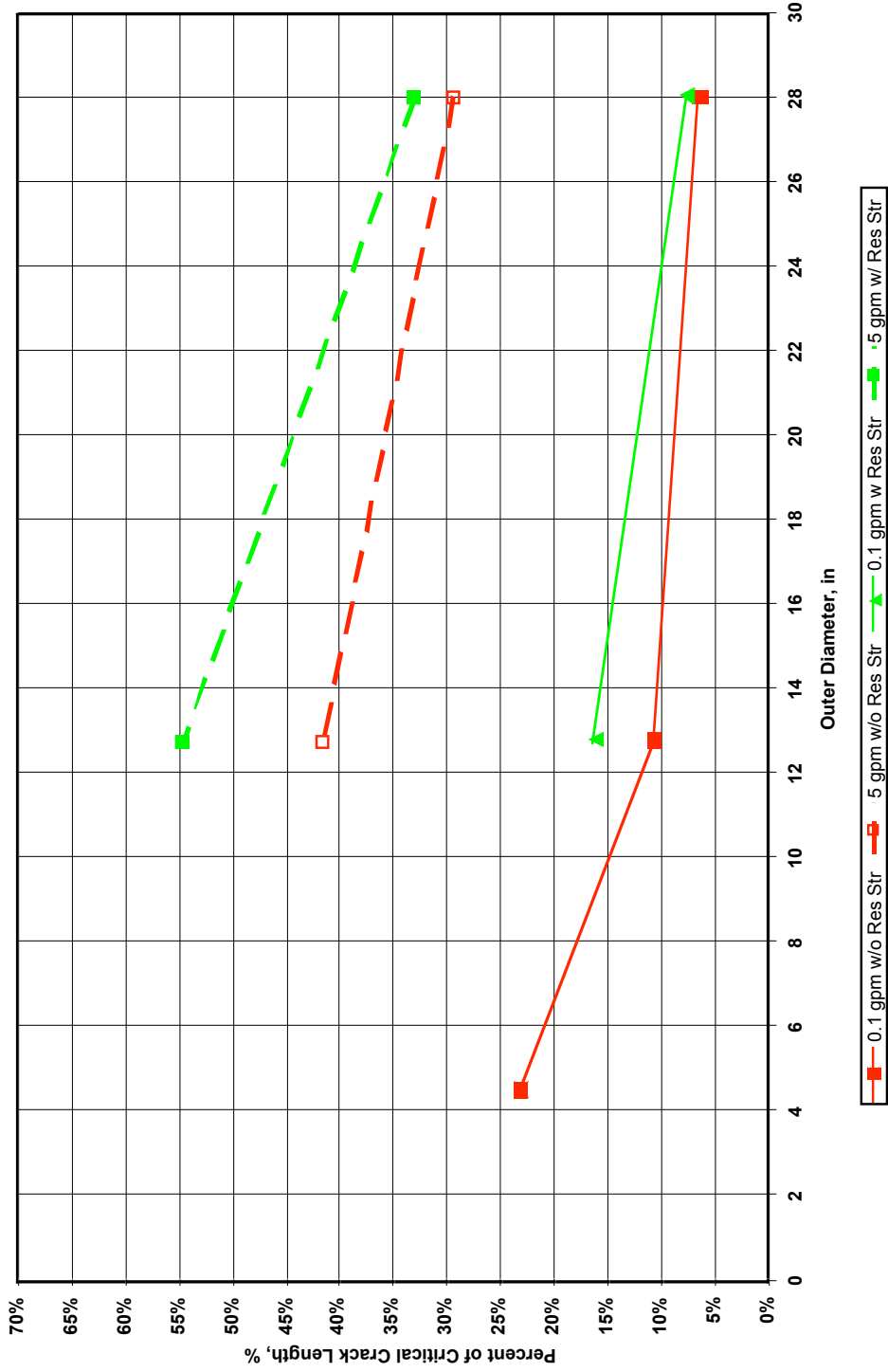


Figure D14. Effect of residual stresses on critical crack length as a function of diameter (BWR CS piping).

Appendix E

ASME Codes on Continuous Acoustic Emission (Article 13)

Reprinted from ASME 2001 BPVC, Section V, by permission of the American Society of Mechanical Engineers. All rights reserved.

ARTICLE 13

CONTINUOUS ACOUSTIC EMISSION MONITORING

T-1310 SCOPE

This Article describes requirements to be used during continuous acoustic emission (AE) monitoring of metal or non-metal pressure boundary components used for either nuclear or non-nuclear service. Monitoring may be performed as a function of load, pressure, temperature, and/or time.

When AE monitoring in accordance with this Article is required, the referencing Code Section should specify the following:

- (a) personnel qualification/certification requirements
- (b) extent of examination and/or area(s)/volume(s) to be monitored
- (c) duration of monitoring period
- (d) acceptance/evaluation criteria
- (e) reports and records requirements

When this Article is specified by a referencing Code section, the technical requirements described herein shall be used together with Article I, General Requirements. Definitions of terms used in this Article are in Mandatory Appendix VII of this Article.

Generic requirements for continuous acoustic emission monitoring of pressure boundary components during operation are addressed within this Article. Supplemental requirements for specific applications such as nuclear components, non-metallic components, monitoring at elevated temperatures, limited zone monitoring, lead detection, etc., are provided in the Mandatory Appendices to this Article.

T-1311 References

- SE-650, Standard Guide for Mounting Piezoelectric Acoustic Emission Sensors
- SE-976, Standard Guide for Determining the Reproducibility of Acoustic Emission Sensor Response
- SE-1211, Standard Practice for Leak Detection and Location using Surface-Mounted Acoustic Emission Sensors
- SE-1316, Standard Terminology for Nondestructive Examinations

SE-1419, Standard Test Method for Examination of Seamless, Gas-Filled Pressure Vessels Using Acoustic Emission

ASTM E 750-88 (1993), Standard Practice for Characterizing Acoustic Emission Instrumentation

ASTM E 1067-89 (1991), Standard Practice for Acoustic Emission Examination of Fiberglass Reinforced Plastic Resin (FRP) Tanks/Vessels

ASTM E 1118-89, Standard Practice for Acoustic Emission Examination of Reinforced Thermosetting Resin Pipe (RTRP)

ASTM E 1139-92, Standard Practice for Continuous Monitoring of Acoustic Emission from Metal Pressure Boundaries

T-1320 GENERAL

T-1321 Monitoring Objectives

The objectives of AE examination are to detect, locate, and characterize AE sources, and interpret the AE response signals to evaluate significance relative to pressure boundary integrity. These AE sources are limited to those activated during normal plant system operation, i.e., no special stimulus is applied exclusively to produce AE. In the context of this Article, normal system operation may include routine pressure tests performed during plant system shutdown.

T-1322 Relevant Indications

All relevant indications detected during AE monitoring should be evaluated by other methods of nondestructive examination.

T-1323 Personnel Qualification

T-1323.1 Procedures and Equipment Installation. All procedures used for qualifying, calibrating, installing, and operating the AE equipment, and for data analysis activities, shall be approved by a certified AE Level III.

VII-1310	Scope	260
VII-1320	General Requirements	260
VII-1330	Requirements	260
 Figures		
V-1322	Metal Waveguide AE Sensor Construction	258
V-1323	Mounting Fixture for Steel Waveguide AE Sensor	259
 Tables		
II-1351	An Example of Evaluation Criteria for Zone Location	254
II-1352	An Example of Evaluation Criteria for Multisource Location	256

Installation, calibration, and checkout of the AE equipment shall be performed under the direction of a certified AE Level III.

T-1323.2 AE System Operation. Routing operation of the AE system for collection and interpretation of data may be performed by competent personnel that are not necessarily AE specialists. However, AE system operation and data interpretation shall be verified by a certified AE Level III on approximately monthly intervals or more often if the system appears to be malfunctioning, relevant signals are detected, or an abrupt change in the rate of AE signals is observed.

T-1324 Component Stressing

Several means of stressing are applicable to AE examination including startup, continuous and cyclic operation, and shut-down of operating plant systems and components, as well as pressure tests of non-operating plant systems. Stress may be induced by either pressure or thermal gradients or a combination of both. It is the intent of this Article to describe examination techniques that are applicable during normal operation of pressurized plant system or component. During startup, the pressurizing rate should be sufficient to facilitate the examination with minimum extraneous noise. If appropriate, provisions should be made for maintaining the pressure at designated hold points. Advice on the use of compressed gas as a pressurizing medium is contained in SE-1419.

T-1325 Noise Interference

Noise sources that interfere with AE signal detection should be controlled to the extent possible. For continuous monitoring, it may be necessary to accommodate background noise by monitoring at high frequencies, shielding open AE system leads, using differential sensors, and using special data filtering techniques to reduce noise interference.

T-1326 Coordination With Plant System Owner/Operator

Due to operational considerations unique to the AE method, close coordination between the AE monitor operator and the owner/operator of the plant should be established and maintained. Provisions for this coordination function should be described in the written procedures submitted for approval prior to initiation of AE monitoring activities.

T-1327 Source Location and Sensor Mounting

Sources shall be located with the specified accuracy by multichannel sensor array, zone location, or both. As required by the referencing Code section, requirements for sensor mounting, placement, and spacing are further defined in the applicable Appendix.

T-1330 EQUIPMENT

T-1331 General

The AE system will consist of sensors, preamplifiers, amplifiers, filters, signal processors, and a data storage device together with interconnecting cables. Simulated AE source(s) and auxiliary equipment such as pressure and temperature inputs are also required. The AE monitoring system shall provide the functional capabilities shown in Fig. T-1331.

T-1332 Sensors

Sensors shall be one of two general types — those mounted directly on the surface of the component being monitored and those that are separated from the surface of the component by a connecting waveguide. Sensors shall be acoustically coupled to the surface of the component being monitored and be arranged in arrays capable of providing AE signal detection and source location to the required accuracy. Selection of sensor type shall be based on the application; i.e., low or high temperature, nuclear or non-nuclear, etc. The sensor selected for a specific application shall be identified in the procedure prepared for that application. The sensor system (i.e., sensors, preamplifiers, and connecting cables) used to detect AE shall limit electromagnetic interference to a level not exceeding 0.7 V peak after 90 dB amplification.

T-1332.1 Sensor Response Frequency. For each application, selection of the sensor response frequency shall be based on a characterization of background noise in terms of amplitude vs. frequency. The lowest frequency compatible with avoiding interference from background noise should be used to maximize sensitivity of AE signals and minimize signal attenuation.

T-1332.2 Differential and Tuned Sensors. Two sensor designs have been effective in overcoming noise interference problems. One is a differential sensor that operates to cancel out electrical transients entering the system through the sensor. The other is an inductively tuned sensor that operates to shape the sensor response around a selected frequency; i.e., inductive tuning allows

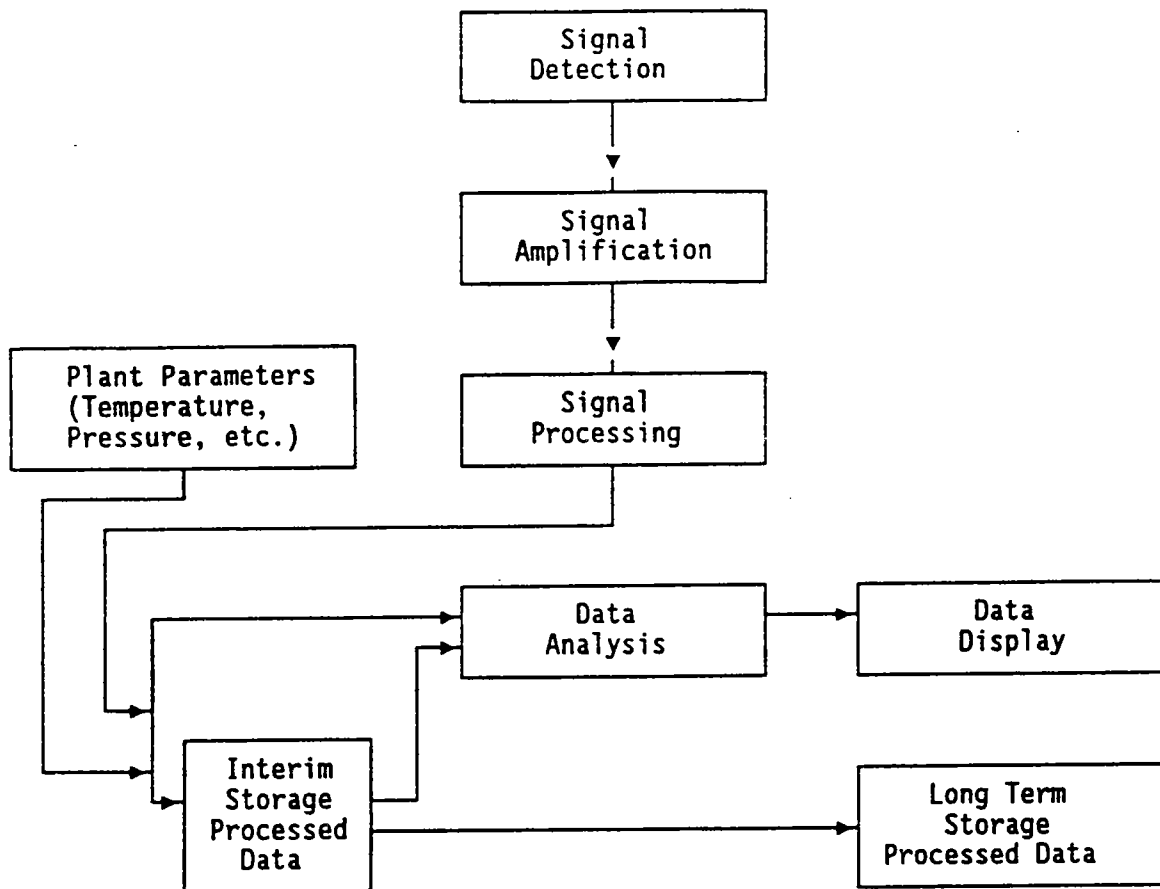


FIG. T-1331 FUNCTIONAL FLOW DIAGRAM — CONTINUOUS AE MONITORING SYSTEM

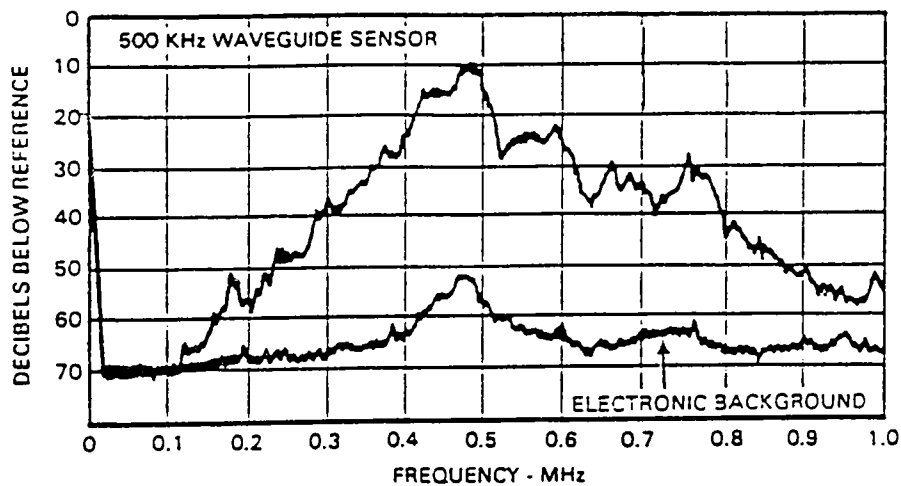


FIG. T-1332.2 RESPONSE OF A WAVEGUIDE AE SENSOR INDUCTIVELY TUNED TO 500 kHz

discrimination against frequencies on either side of a selected response frequency as shown in Fig. T-1332.2. These sensor designs may be used separately or together.

T-1332.3 Sensor Mounting. Sensors shall be mounted to the component surface using two basic methods. One is to bond the sensor directly to the surface with an adhesive. Temperature and vibration can adversely affect the bond between the sensor and the surface being monitored. Also, the chemical content of the adhesive shall be checked to assure that it is not deleterious to the surface of the component.

The second method for mounting a sensor employs pressure coupling using either a strap or a magnetic mount. A thin, soft metal interface layer between the sensor and the surface is often effective for achieving acoustic coupling with minimal pressure. In the case of waveguide sensors, the tip of the waveguide may be shaped to reduce the required force to maintain acoustic coupling.

T-1333 Signal Cables

Coaxial cables shall be used to conduct the AE signals from the sensors to the monitoring instrument (monitor). Whenever a protective barrier or containment structure must be penetrated using a bulkhead fitting or penetration plug to transmit signals from the sensor to the monitor, extreme care must be taken to avoid incurring excessive signal loss or noise. When the coaxial (signal) cables are used to supply DC power to the preamplifiers/line drivers, they should be terminated with the appropriate characteristic impedance.

T-1334 Amplifiers

At least one preamplifier shall be used with each sensor to amplify the AE signals for transmission to the monitor. Where long signal cables are required, a preamplifier and line driver between the sensor and the monitor may be needed.

With the high signal amplification required to detect AE signals, the internal noise of the preamplifiers must be minimized to avoid interference with AE signal detection. The frequency response band of the amplifiers shall be matched to the response profile determined for the AE sensors.

T-1335 AE Monitor

The AE monitor shall include a post amplifier, a signal identification function, and a signal processing module for each signal channel. The monitor shall also

include a video display function that can be used at the operator's discretion to display AE data as well as a data storage capability suitable for long term, nonvolatile data storage. A data analysis function may be integral with the AE monitor or be a separate function that draws from the stored AE data.

The post amplifier shall meet the requirements of T-1334. The AE monitor shall be capable of processing and recording incoming data at a rate of at least 50 hits/sec for all channels simultaneously for an indefinite time period and at a rate of at least 100 hits/sec for all channels simultaneously for any 15 sec period.

T-1335.1 AE Signal Identification. A real-time signal discrimination function to process incoming signals and identify relevant AE signals shall be included. The discrimination function may either exclude all signals not identified as AE from crack growth, or flag those signals identified as crack growth AE while accepting all signals above the voltage threshold.

T-1335.2 Signal Processing. The dynamic range of the signal processor shall be at least 36 dB for each parameter being measured. The signal processor shall be controlled by voltage threshold circuits that limit accepted data to signals that exceed the voltage amplitude threshold. The voltage threshold shall be determined on the basis of the background noise.

Signal parameters to be measured shall include AE hit count, total number of signal hits at each sensor, signal peak amplitude, time for threshold crossing to signal peak, measured area under the rectified signal envelope (MARSE) in V-secs, and difference in time of signal arrival (δt) at all sensors in a sensor array used for AE source location. In addition to the AE signal features above, clock time, date, and the value of plant parameters (internal pressure, temperature, etc., that can be identified as significant to crack growth) associated with the time of signal detection shall be recorded for each signal. The signal processor section shall also measure the overall RMS background signal level for each sensing channel for leak detection purposes.

T-1335.3 Data Storage. Data storage shall be nonvolatile and capable of storing the data described in T-1335.2 continuously over time periods of several weeks to several months depending on the application. One recording method that has proven satisfactory for continuous monitoring is a digital tape recorder using $\frac{1}{4}$ in. (6 mm), 16 track digital tape cartridges.

T-1335.4 Data Analysis and Display. The data analysis function of the AE monitor shall determine the location of AE sources as specified in the procedure

(T-1350). Location accuracies within one wall thickness of the pressure boundary or 5% of the minimum sensor spacing, whichever is greater, are typical for metal components.

The data analysis function shall be capable of providing a display and plot of selected AE information (e.g., AE events, crack growth AE from a given source area, AE energy) vs. plant system parameters and vs. time for correlation evaluations. Data analysis shall also provide continuous assessment of RMS signal level information derived from the signal measurement section.

The AE monitor system shall provide a means of presenting analyzed data; either a computer printout or a printout in conjunction with a video display. When the AE rate from an array exceeds the rate specified in the written procedure, the system shall activate an operator alert and identify the sensor array producing the high AE rate.

T-1340 REQUIREMENTS

T-1341 Equipment Qualification

Acceptable performance, including dynamic range, of the complete AE monitor (without sensors) shall be verified using an electronic waveform generator prior to installation. Sinusoidal burst signals from the waveform generator shall be input of each preamplifier to verify that the signal amplification, data processing functions, data processing rate, and data analysis, display, and storage meet the requirements of this Article. (NOTE: AE signal source location performance is tested under T-1362.1.) With the AE monitor gain set at operating level, the system shall be evaluated using input signals that will test both the low and high ends of the dynamic range of the AE monitor system. Signal frequencies shall include samples within the range of intended use.

T-1342 Sensor Qualification

T-1342.1 Sensor Sensitivity and Frequency Response. Each sensor shall produce a minimum signal of $0.1 \text{ mV}_{\text{peak}}$ referred to the sensor output at the selected monitoring frequency when mounted on a calibration block and excited with a helium gas jet as described in SE-976. Appropriate calibration blocks are identified in the Appendices as a function of specific applications. Helium gas excitation shall be performed using a 30 psi (207 KPa) helium source directed onto the surface of the calibration block through a #18 hypodermic needle held perpendicular to the calibration block surface. The needle tip shall be $\frac{1}{8}$ in. (3.2 mm)

above the surface of the block and $1\frac{1}{2}$ in. (38 mm) from the mounted sensor. The process may also be used to verify the sensor response profile in terms of frequency to assure that the response roll-off on either side of the selected monitoring frequency is acceptable.

An optional technique for determining the reproducibility of AE sensor response is referred to as the "Pencil Lead Break" technique, which is described in SE-976.

T-1342.2 Uniformity of Sensor Sensitivity. The sensitivity of each sensor shall be evaluated by mounting it on a calibration block as it will be mounted on the plant component and measuring its response to the energy produced by fracturing a 0.3-mm, 2H pencil lead against the surface of the block in accordance with SE-976 at a point 4 in. (102 mm) from the center of the sensor. When performing this evaluation, it is useful to use a 40 dB preamplifier with the sensor to produce an adequate output signal for accurate measurement. The peak response of each sensor to the simulated AE signal shall not vary more than 3 dB from the average for all sensors at the selected monitoring frequency.

T-1343 Signal Pattern Recognition

If AE signal pattern recognition is used, this function shall be demonstrated and qualified as follows:

(a) Assemble the AE monitor including two representative sensors mounted on a calibration block with the same acoustic coupling process to be used for monitoring. The sensors shall be excited ten times by each of the following three methods:

(1) Fracture a 0.3 mm, 2H pencil lead against the surface of the block in accordance with SE-976.

(2) Strike the surface of the block with 0.25 in. (6 mm) diameter steel ball dropped from a uniform height sufficient to produce a response from the sensors that does not saturate the AE monitor.

(3) Inject a multi-cycle (five cycles minimum) burst signal into the block with a transducer and waveform generator.

(b) The pattern recognition function shall identify at least 8 out of 10 lead fracture signals as AE crack growth signals and at least 8 out of 10 of each other type signals as signals not associated with crack growth.

T-1344 Material Attenuation/Characterization

Prior to installation of AE system for monitoring plant components, the acoustic signal attenuation in the material shall be characterized. This is necessary for

determining the sensor spacing for effective AE detection. Attenuation measurements shall be made at the frequency selected for AE monitoring and shall include both surface and bulk wave propagation. The attenuation measurements should be performed with the material temperature within $\pm 200^\circ\text{F}$ ($\pm 111^\circ\text{C}$) of the expected temperature during actual component monitoring.

T-1345 Background Noise

The AE system response to background noise shall be characterized. With 90 dB amplification, the AE system signal level response to continuous process background noise shall not exceed $1.5 V_{\text{peak}}$ output. This shall be achieved by restricting the frequency response of the sensor system. Reducing sensitivity is not acceptable.

T-1346 Qualification Records

Documentation of the equipment qualification process shall include the following:

- (a) a copy of the equipment qualification procedure
- (b) personnel certificate records
- (c) description of the AE equipment and qualification equipment used
- (d) quantitative results of the qualification
- (e) signature of the AE Level III responsible for the qualification
- (f) date of the qualification

Equipment qualification records shall be retained as part of the monitoring application records.

T-1347 Sensor Installation

T-1347.1 Coupling. Adequate acoustic coupling between the sensor and the component surface shall be verified as the sensors are mounted. This can be done by lightly tapping the surface or by breaking a pencil lead against the component surface while observing the sensor output. Guidance for sensor mounting is provided in SE-650 and in T-1332.3. The use of drilled and tapped holes in the component is generally not acceptable.

T-1347.2 Array Spacing. A sufficient number of sensors shall be located on the component in a multi-source array(s) to provide for AE signal detection and source location. Each sensor shall produce an output of at least $0.3 \text{ mV}_{\text{peak}}$ when a 0.3 mm, 2H pencil lead is broken against the bare surface of the component at the most remote location that the sensor is expected to monitor. When a location algorithm is used, the

location of each lead break shall be surrounded with a material (mastic or putty) to absorb surface waves. A 0.1 in. (2.5 mm) lead extension shall be broken at an angle of approximately 30 deg. to the component surface.

T-1347.3 Functional Verification. One or more acoustic signal sources, with an output frequency range of 100 to 700 kHz shall be installed within the monitoring zone of each sensor array for the purpose of periodically testing the functional integrity of the sensors during monitoring. This is not intended to provide a precise sensor calibration but rather a qualitative sensitivity check. It shall be possible to activate the acoustic signal source(s) from the AE monitor location.

T-1348 Signal Lead Installation

The coaxial cable and other leads used to connect the sensors to the AE monitor shall be demonstrated to be capable of withstanding extended exposure to hostile environments as required to perform the monitoring activities.

T-1349 AE Monitor Installation

The AE monitor shall be located in a clean, controlled environment suitable for long-term operation of a computer system. The electronic instrumentation (preamplifiers and AE monitor components) shall be located in an area that is maintained at temperatures not exceeding 125°F .

T-1350 PROCEDURE REQUIREMENTS

01

AE monitoring activities shall be performed in accordance with a written procedure. Each procedure shall include at least the following information, as applicable:

- (a) Components to be monitored include dimension, materials of construction, operating environment, and duration of monitoring
- (b) a description of the AE system to be used and its capabilities in terms of the functional requirements for the intended application
- (c) AE system calibration and qualification requirements
- (d) number, location, and mounting requirements for AE sensors
- (e) interval and acceptable performance during the AE system functional check (T-1373.2)
- (f) data recording processes and data to be recorded

(g) data analysis, interpretation, and evaluation criteria

(h) supplemental NDE requirements

(i) personnel qualification/certification requirements

(j) reporting and record retention requirements

The procedure described below need not be large documents, and preprinted blank forms (technique sheets) may be utilized provided they contain the required information.

T-1351 AE System Operation

A written procedure describing operation of the AE system shall be prepared, approved by the cognizant AE Level III, and made available to the personnel responsible for operating the AE system. Each procedure shall be tailored to recognize and accommodate unique requirements associated with the plant system or component being monitored.

T-1352 Data Processing, Interpretation, and Evaluation

A written procedure for processing, interpreting, and evaluating the AE data shall be prepared and approved by the cognizant AE Level III. This procedure shall be made available to the personnel responsible for operating the AE system, the personnel responsible for AE data interpretation and evaluation, and a representative of the owner of the plant system being monitored. This procedure shall be tailored to recognize and accommodate unique requirements associated with the plant system or component being monitored.

T-1353 Data Recording and Storage

Specific requirements for recording, retention, and storage of the AE and other pertinent data shall be prepared for approval by representatives of the plant system owner or operator. These requirements shall be made available to the personnel responsible for data recording and storage.

T-1360 CALIBRATION

T-1361 Sensors

The frequency response for each AE channel shall be measured with the sensors installed on a plant pressure boundary component. Sensor response shall be measured at the output of the preamplifier using a spectrum analyzer. The excitation source shall be a

helium gas jet directed onto the component surface from a nominal 30 psi (207 kPa) source through a #18 hypodermic needle held perpendicular to the component surface at a stand-off distance of $\frac{1}{8}$ in. (3.2 mm) located $1\frac{1}{2}$ in. (38 mm) from the mounted sensor. The gas shall not impinge on the sensor or the waveguide. AE sensor peak response to the gas jet excitation at the monitoring frequency shall be at least 0.1 mV_{peak} referred to the output of the sensor. Any AE sensor showing less than 0.1 mV_{peak} output shall be reinstalled or replaced, as necessary, to achieve the required sensitivity.

An optional technique for determining the reproducibility of AE sensor response is referred to as the "Pencil Lead Break" technique which is described in SE-976.

T-1362 Complete AE Monitor System

T-1362.1 Detection and Source Location. The signal detection and source location accuracy for each sensor array shall be measured using simulated AE signals injected on the component surface at not less than 10 preselected points within the array monitoring field. These simulated AE signals shall be generated by breaking 2H pencil leads (0.3 or 0.5 mm diameter) against the component surface at the prescribed points. The pencil leads shall be broken at an angle of approximately 30 deg. to the surface using a 0.1 in. (2.5 mm) pencil lead extension (see SE-976). The location of each pencil lead break shall be surrounded with a material (mastic or putty) to absorb surface waves. Location accuracies within one wall thickness at the AE source location or 5% of the minimum sensor array spacing distance, whichever is greater, are typical.

T-1362.2 Function Verification. Response of the AE system to the acoustic signal source described in T-1347.3 shall be measured and recorded for reference during later checks of the AE system.

T-1363 Calibration Intervals

The installed AE monitor system shall be recalibrated in accordance with T-1360 at the end of each plant operating cycle. This is defined more explicitly in the Appendices describing requirements for each AE monitoring application.

T-1364 Calibration Records

Documentation of the installed system calibration shall include the following:

- (a) a copy of the calibration procedure(s)
- (b) personnel certification records
- (c) description of the AE equipment and the calibration equipment used
- (d) quantitative results of the calibration
- (e) signature of the individual responsible for the calibration
- (f) date(s) of the calibration(s).

Retention of the calibration records shall be in accordance with T-1393.

T-1370 EXAMINATION

The AE monitor system shall comply with the requirements of approved procedures (T-1350) that have been accepted by the plant owner/operator.

T-1371 Personnel

Operation of the AE system for routine collection and interpretation of data may be performed by a competent individual not necessarily specialized in AE who has received training and has at least limited AE Level II certification. However, AE system operation and data interpretation shall be verified by a certified AE Level III on a monthly interval or sooner if the system appears to be malfunctioning or there is an abrupt change in the rate of AE data accumulation.

T-1372 Plant Startup

During plant startup, AE rate and source location information shall be evaluated at least once per shift for indications of flaw growth. The RMS signal level shall also be evaluated for indications of pressure boundary leaks.

T-1373 Plant Steady-State Operation

T-1373.1 Data Evaluation Interval

AE data shall be evaluated at least weekly during normal plant operation. When a sustained AE activity rate from one or more sensors occurs or when a consistent clustering of AE signals accepted by the signal identification analyzer and which cluster in one source location of AE signals is concentrated within a diameter of three times the wall thickness of the component or 10% of the minimum sensor spacing distance in the array, whichever is greater. Also refer to Appendices II and III.

T-1373.2 AE System Functional Check. AE system response to the installed acoustic signal source shall be evaluated periodically as specified in the procedure. Deterioration of sensitivity exceeding 4 dB for any channel shall be recorded and the affected component shall be replaced at the earliest opportunity.

T-1374 Nuclear Components

Specific and supplemental examination requirements for nuclear components are specified in Appendix I.

T-1375 Non-Nuclear Metal Components

Specific and supplemental examination requirements for non-nuclear metal components are specified in Appendix II.

T-1376 Non-Metallic Components

Specific and supplemental examination for non-metallic components are specified in Appendix III.

T-1377 Limited Zone Monitoring

Specific and supplemental examination requirements for limited zone monitoring are specified in Appendix IV.

T-1378 Hostile Environment Applications

Specific and supplemental examination requirements for hostile environment applications are specified in Appendix V.

T-1379 Leak Detection Applications

Specific and supplemental examination requirements for leak detection applications are specified in Appendix VI.

T-1380 EVALUATION/RESULTS

T-1381 Data Processing, Interpretation, and Evaluation

Data processing, interpretation, and evaluation shall be in accordance with the written procedure (T-1350) for that specific application and the applicable Mandatory Appendices. The methodology and criteria will vary substantially with different applications.

T-1382 Data Requirements

The following data shall be acquired and recorded:

(a) AE event count versus time for each monitoring array.

(b) AE source and/or zone location for all acoustic signals accepted.

(c) AE hit rate for each AE source location cluster.

(d) Relevant AE signal parameter(s) versus time for each data channel.

(e) Location monitored, date, and time period of monitoring.

(f) Identification of personnel performing the analysis.

In addition, the data records shall include any other information required in the applicable procedure (T-1350).

T-1390 REPORTS/RECORDS**T-1391 Reports to Plant System Owner/Operator**

T-1391.1 A summary of AE monitoring results shall be prepared monthly. This should be a brief, concise report for management use.

T-1391.2 Reporting requirements in the event of unusual AE indications shall be specified by the plant system owner/operator and identified in the procedure (T-1350).

T-1391.3 A summary report on the correlation of monitoring data with the evaluation criteria shall be provided to the plant system owner/operator.

T-1391.4 Upon completion of each major phase of the monitoring effort, a comprehensive report shall be prepared. This report shall include the following:

(a) complete identification of the plant system/component being monitored including material type(s), method(s) of fabrication, manufacturer's name(s), and certificate number(s)

(b) sketch or manufacturer's drawing with component dimensions and sensor locations

(c) plant system operating conditions including pressurizing fluid, temperature, pressure level, etc.

(d) AE monitoring environment including temperature, radiation and corrosive fumes if appropriate, sensor accessibility, background noise level, and protective barrier penetrations utilized, if any

(e) a sketch or manufacturer's drawing showing the location of any zone in which the AE response exceeded the evaluation criteria

(f) any unusual events or observations during monitoring

(g) monitoring schedule including identification of any AE system downtime during this time period

(h) names and qualifications of the AE equipment operators

(i) complete description of the AE instrumentation including manufacturer's name, model number, sensor types, instrument settings, calibration data, etc.

T-1392 Records

T-1392.1 Administrative Records. The administrative records for each AE monitoring application shall include the applicable test plan(s), procedure(s), operating instructions, evaluation criteria, and other relevant information, as applicable.

T-1392.2 Equipment Qualification and Calibration Data. The pre-installation and post-installation AE system qualification and calibration records including signal attenuation data and AE system performance verification checks shall be retained. Disposition of these records following AE system recalibration shall be specified by the plant system owner/operator.

T-1392.3 Raw and Processed AE Data. The raw data records shall be retained at least until the AE indications have been independently verified. The retention period for the processed data records shall be as specified in the procedure (T-1350).

T-1393 Record Retention Requirements

All AE records shall be maintained as required by the referencing Code section and the procedure (T-1350).

ARTICLE 13

MANDATORY APPENDICES

APPENDIX I — NUCLEAR COMPONENTS

I-1310 SCOPE

This Appendix specifies supplemental requirements for continuous AE monitoring of metallic components in nuclear plant systems. The requirements of Appendix V — Hostile Environment Applications shall also apply to continuous AE monitoring of nuclear plant systems.

I-1320 TERMS SPECIFIC TO THIS APPENDIX

See Appendix VII for definitions of terms specific to this Appendix.

I-1330 EQUIPMENT QUALIFICATION

I-1331 Preamplifiers

The internal electronic noise of the preamplifiers shall not exceed 7 microvolts rms referred to the input with a 50-ohm input termination. The frequency response band of the amplitude shall be matched to the response profile determined for the AE sensors.

I-1332 Monitor System

Acceptable performance, including dynamic range, of the complete AE monitor (without sensors) shall be verified using an electronic waveform generator prior to installation. Sinusoidal burst signals from the waveform generator shall be input to each preamplifier to verify that the signal amplification; data processing functions; data processing rate; and data analysis, display, and storage meet the requirements of this Article. (NOTE: AE signal source location performance is tested under T-1362.1.) The system shall be evaluated using input signals of 0.5 and 10.0 mV peak-to-peak amplitude; 0.5 and 3.0 millisecond duration; and 100 kHz, and 1.0 MHz frequency from the waveform generator.

I-1340 SENSORS

I-1341 Sensor Type

The AE sensors shall be capable of withstanding the ambient service environment (i.e., temperature, moisture, vibration, and nuclear radiation) for a period of two years. Refer to T-1332 and Appendix V, para. V-1320, for additional sensor requirements. In monitoring nuclear components, in addition to high temperature [$\approx 600^{\circ}\text{F}$ (316°C) in most locations], the environment at the surface of the component may also include gamma and neutron radiation. In view of the neutron radiation, a waveguide high temperature AE sensor such as the type described in Appendix V should be used to isolate the critical elements of the sensor (piezoelectric crystal and associated preamplifier) from the neutron radiation field.

I-1342 Frequency Response

The frequency response band of the sensor/amplifier combination shall be limited to avoid interference from background noise such as is caused by coolant flow. Background noise at the locations to be monitored shall be characterized in terms of intensity versus frequency prior to selection of the AE sensors to be used. This information shall be used to select the appropriate frequency bandwidth for AE monitoring. The sensor response roll off below the selected monitoring frequency shall be at a minimum rate of 15 dB per 100 kHz, and may be achieved by inductive tuning of the sensor/preamplifier combination. The high end of the frequency response band should roll off above 1 MHz at a minimum rate of 15 dB per octave to help reduce amplifier noise. These measurements shall be made using the helium gas jet technique described in T-1342.1 and T-1361.

I-1343 Signal Processing

The threshold for all sensor channels shall be set at 0.5 to 1.0 V_{peak} above the sensor channel background noise level and all channels shall be set the same.

I-1350 CALIBRATION**I-1351 Calibration Block**

The calibration block used to qualify AE sensors shall be a steel block with minimum dimensions of 4 × 12 × 12 in. (101.6 × 304.8 × 304.8 mm) with the sensor mounted in the center of a major face using the acoustic coupling technique to be applied during in-service monitoring.

I-1352 Calibration Interval

The installed AE monitor system shall be recalibrated in accordance with T-1360 during each refueling or maintenance outage, but no oftener than once every 24 months.

I-1360 EVALUATION/RESULTS

(a) The monitoring procedure (T-1350) shall specify the acceptance criteria for crack growth rate.

(b) The AE data shall be evaluated based on AE rate derived from signals accepted by the signal identification function and identified with a specific area of the pressure boundary.

(c) The data shall be analyzed to identify an increasing AE rate that is indicative of accelerating crack growth.

(d) The quantitative crack growth rate shall be estimated using the relationship:

$$\frac{da}{dt} = 290 \left(\frac{dN}{dt} \right)^{0.53}$$

where

da/dt = crack growth rate in microinches/second
 dN/dt = the AE rate [AE as defined in (b) above] in events/second

(e) If the estimated crack growth rate exceeds the acceptance criteria, the flaw area shall be examined with other NDE methods at the earliest opportunity.

APPENDIX II — NON-NUCLEAR METAL COMPONENTS

II-1310 SCOPE

This Appendix specifies supplemental requirements for continuous AE monitoring of non-nuclear metal components. The principal objective is to monitor/detect acoustic emission (AE) sources caused by surface and

internal discontinuities in a vessel wall, welds, and fabricated parts and components.

II-1320 EQUIPMENT/QUALIFICATIONS**II-1321 Sensor Response**

Acoustic emission sensors shall have a resonant response between 100 kHz to 400 kHz. Minimum sensitivity shall be -85 dB referred to 1 volt/microbar determined by a face-to-face ultrasonic test. Sensors shall have a frequency response with variations not exceeding 4 dB from the peak response. Acoustic emission sensors in a face-to-face ultrasonic test (or equivalent) shall not vary in peak sensitivity by more than 3 dB from when they were new.

II-1322 Couplant

Couplant shall provide consistent coupling efficiency for the duration of the test.

II-1323 Preamplifier

The preamplifier shall be located within 6 ft (1.8 m) from the sensor, and differential preamplifiers shall have 40 dB of common-mode noise rejection. Frequency response shall not vary more than 3 dB over the operating frequency range of the sensors when attached. Filters shall be of the band pass or high pass type and shall provide a minimum of 24 dB of common-mode rejection.

II-1324 Signal Cable

Power signal cable shall be shielded against electromagnetic noise. Signal loss shall be less than 1 dB per foot of cable length. Recommended maximum cable length is 500 ft (152 m).

II-1325 Power Supply

A stable, grounded electrical power supply should be used.

II-1326 Main Amplifier

The main amplifier gain shall be within 3 dB over the range of 40°F to 125°F (4°C to 52°C).

II-1327 Main Processor

The main processor(s) shall have circuits for processing sensor data. The main processor circuits shall be capable of processing hits, counts, peak amplitudes, and MARSE on each channel, and measure the following:

(a) *Threshold.* The AE instrument shall have a threshold control accurate to within ± 1 dB over its useful range.

(b) *Counts.* The AE counter circuit shall detect counts over a set threshold with an accuracy of $\pm 5\%$.

(c) *Hits.* The AE instrument shall be capable of measuring, recording, and displaying a minimum of 20 hits/sec total for all channels.

(d) *Peak Amplitude.* The AE circuit shall measure peak amplitude with an accuracy of ± 2 dB. Useable dynamic range shall be a minimum of 60 dB with 1 dB resolution over the frequency bandwidth used. Not more than 2 dB variation in peak detection accuracy shall be allowed over the stated temperature range. Amplitude values shall be specified in dB and must be referenced to a fixed gain output of the system (sensor or preamplifier).

(e) *Energy.* The AE circuit shall measure MARSE with an accuracy of $\pm 5\%$. The useable dynamic range for energy shall be a minimum of 40 dB.

(f) *Parametric Voltage.* If parametric voltage is measured, it shall be measured to an accuracy of $\pm 2\%$ of full scale.

II-1330 SENSORS**II-1331 Sensor Mounting/Spacing**

Sensor location and spacing shall be based on attenuation characterization, with the test fluid in the vessel, and a simulated source of AE. Section V, Article 12, Nonmandatory Appendices should be referenced for vessel sensor placement. Consideration should be given to the possible attenuation effects of welds.

II-1332 Sensor Spacing for Multichannel Source Location

Sensors shall be located such that a lead break at any location within the examination area is detectable by at least the minimum number of sensors required for the multichannel source location algorithm, with the measured amplitude specified by the referencing Code Section. Location accuracy shall be within a maximum of 2 wall thicknesses or 5% of the sensor spacing distance, whichever is greater.

II-1333 Sensor Spacing for Zone Location

When zone location is used, sensors shall be located such that a lead break at any location within the examination area is detectable by at least one sensor with a measured amplitude not less than specified by the referencing Code Section. The maximum sensor spacing shall be no greater than one-half the threshold distance. The threshold distance is defined as the distance from a sensor at which a pencil-lead break on the vessel produces a measured amplitude equal to the evaluation threshold.

II-1340 CALIBRATION**II-1341 Manufacturer's Calibration**

Purchased AE system components shall be accompanied by manufacturer's certification of performance specifications and tolerances.

II-1342 Annual Calibration

The instrumentation shall have an annual, comprehensive calibration following the guideline provided by the manufacturer using calibration instrumentation meeting the requirements of a recognized national standard.

II-1343 System Performance Check

Prior to beginning the monitoring period, the AE instrument shall be checked by inserting a simulated AE signal at each main amplifier input. The device generating the simulated signal shall input a sinusoidal burst-type signal of measurable amplitude, duration, and carrier frequency. On-site system calibration shall verify system operation for threshold, counts, MARSE, and peak amplitude. Calibration values shall be within the range of values specified in II-1327.

II-1344 System Performance Check Verification

Verification of sensor coupling and circuit continuity shall be performed following sensor mounting and system hookup and again following the test. The peak amplitude response of each sensor to a repeatable simulated AE source at a specific distance from the sensor should be taken prior to and following the monitoring period. The measured peak amplitude should not vary more than ± 4 dB from the average of all the sensors. Any channel failing this check should be

TABLE II-1351
AN EXAMPLE OF EVALUATION CRITERIA FOR ZONE
LOCATION

	Pressure Vessels (Other Than First Hydrostatic Test) Using Zone Location
Emissions during hold	Not more than E hits beyond time T
Count rate	Less than N counts per sensor for a specified load increase
Number of hits	Not more than E hits above a specified amplitude
Large amplitude	Not more than E hits above a specified amplitude
MARSE or amplitude	MARSE or amplitudes do not increase with increasing load
Activity	Activity does not increase with increasing load
Evaluation threshold, dB	50 dB

repaired or replaced, as necessary. The procedure will indicate the frequency of system performance checks.

II-1350 EVALUATION

II-1351 Evaluation Criteria — Zone Location

All data from all sensors shall be used for evaluating indications. The AE criteria shown in Table II-1351 provide one basis for assessing the significance of AE indications. These criteria are based on a specific set of AE monitoring conditions. The criteria used for each application shall be as specified in the referencing Code Section and the AE procedure (see T-1350).

II-1352 Evaluation Criteria — Multisource Location

All data from all sensors shall be used for evaluating indications. The AE criteria shown in Table II-1352 provide one basis for assessing the significance of AE indications. These criteria are based on a specific set of AE monitoring conditions. The criteria used for each application shall be as specified in the referencing Code Section and the AE procedure (see T-1350).

APPENDIX III — NON-METALLIC COMPONENTS

III-1310 SCOPE

This Appendix specifies supplemental requirements for continuous monitoring of non-metallic (fiber reinforced plastic) components.

III-1320 BACKGROUND

Non-metallic (FRP) components such as pressure vessels, storage tanks, and piping, are typically used at relatively low temperature. Due to high attenuation and anisotropy of the material, AE methodology has proven to be more effective than other NDE methods.

III-1321 References

- (a) *Pressure Vessels*. Section V, Article 11 — Acoustic Emission Examination of Fiberglass Tanks/Vessels
- (b) *Atmospheric Tanks*. Section V, Article 11 — Acoustic Emission Examination of Fiberglass Vessels, ASNT/CARP Recommended Practice ASTM E 1067: Acoustic Emission Examination of Fiberglass Reinforced Plastic Resin Tanks/Vessels
- (c) *Piping*. ASTM E 1118 — Standard Practice for Acoustic Emission Examination of Reinforced Thermo-setting Resin Pipe (RTRP)

III-1330 MATERIAL CONSIDERATIONS

High attenuation and anisotropy of the material are controlling factors in sensor frequency, source location accuracy, and sensor spacing.

III-1331 Sensor Frequency

Sensors used for monitoring FRP equipment shall be resonant in the 20–200 kHz frequency range.

III-1332 Source Location Accuracy

III-1332.1 Exact solution source location techniques shall be used in monitoring FRP where high accuracy is required. For these applications special precautions will be taken to account for unpredictable acoustic velocity variations in the material. Sensor spacing shall be no greater than 20 in. (508 mm).

III-1332.2 Zone location techniques require the AE signal to hit only one sensor to provide useful location

data. Sensor spacing of 5 ft–20 ft (1.5 m–6.0 m) may be used to cover large areas or the entire vessel.

III-1340 CALIBRATION

III-1341

A manufacturer's calibration of the instrumentation should be conducted on an annual basis. Instrumentation used for calibration shall be referenced to NIST.

III-1342

Periodic field calibration shall be performed with an AE waveform generator to verify performance of the signal processor.

III-1343

Hsu-Nielsen lead break and/or gas jet performance verification techniques (T-1362.2) shall be performed periodically to check all components including couplant, sensor, signal processor, and display.

III-1344

Low amplitude threshold (LAT) shall be determined using the 4 ft by 6 ft by $\frac{1}{2}$ in. (1.2 m \times 1.8 m \times 13 mm) 99% pure lead sheet. The sheet shall be suspended clear of the floor. The LAT threshold is defined as the average measured amplitude of ten events generated by a 0.3 mm pencil (2H) lead break at a distance of 4 ft, 3 in. (1.3 m) from the sensor. All lead breaks shall be done at an angle of approximately 30 deg. to the surface with a 0.1 in. (2.5 mm) lead extension. The sensor shall be mounted 6 in. (152 mm) from the 4 ft (1.2 m) side and mid-distance between 6 ft (1.8 m) sides.

III-1345

High amplitude threshold (HAT) shall be determined using a 10 ft by 2 in. by 12 in. (3.0 m \times 51 mm \times 305 mm) clean, mild steel bar. The bar shall be supported at each end on elastomeric or similar isolating pads. The HAT threshold is defined as the average measured amplitude of ten events generated by a 0.3 mm pencil (2H) lead break at a distance of 7 ft (2.1 m) from the sensor. All lead breaks shall be done at an angle of approximately 30 deg. to the surface with a 0.1 in. (2.5 mm) extension. The sensor shall be mounted 12 in. (305 mm) from the end of the bar on the 2 in. (51 mm) wide surface.

III-1350 EVALUATION/RESULTS

III-1351 Evaluation Criteria

The monitoring procedure (T-1350) shall specify the acceptance criteria.

III-1351.1 AE activity above defined levels indicates that damage is occurring.

III-1351.2 Felicity ratio from subsequent loadings to a defined level can indicate the amount of previous damage.

III-1351.3 Emission activity during periods of contact load indicates that damage is occurring at an accelerating rate.

III-1352 Source Mechanism

III-1352.1 Matrix cracking, fiber debonding, and matrix crazing are characterized by numerous low amplitude acoustic emission signals. Matrix cracking and fiber debonding are generally the first indications of failure. Matrix crazing is normally an indication of corrosion or excessive thermal stress.

III-1352.2 Delamination is characterized by high signal strength, medium amplitude AE activity. This type of failure is typically found at joints with secondary bonds.

III-1352.4 High amplitude AE activity (over High Amplitude Threshold) is associated with fiber breakage and is an indication of significant structural damage.

APPENDIX IV — LIMITED ZONE MONITORING

IV-1310 SCOPE

This Appendix specifies supplemental requirements for applications involving limited zone monitoring, where one of the objectives is to consciously limit the area or volume of the component or pressure boundary that is monitored by AE. Typical reasons for limiting the monitored area include: (a) observe the behavior of a known flaw at a specific location; (b) restrict the AE response to signals emanating from specific areas or volumes of the pressure boundary (e.g., restrict the area monitored by AE to one or more nozzle-to-vessel welds, monitor specific structural welds, etc.); (c) restrict the AE examination to areas of known susceptibility to failure due to fatigue, corrosion, etc.; or (d) improve the signal-to-noise ratio.

TABLE II-1352
AN EXAMPLE OF EVALUATION CRITERIA FOR
MULTISOURCE LOCATION

	Pressure Vessels (Other Than First Hydrostatic Test) Using Multisource Location
Emissions during hold	Not more than E hits from a cluster beyond time T
Count rate	Less than N counts from a cluster for a specified load increase
Number of hits	Not more than E hits from a cluster above a specified amplitude
Large amplitude	Not more than E hits from a cluster above a specified amplitude
Marse or aplitude	MARSE or amplitudes from a cluster do not increase with increasing load
Activity	Activity from a cluster does not increase with increasing load
Evaluation threshold, dB	50 dB or specified in procedure

IV-1320 TERMS SPECIFIC TO THIS APPENDIX

See Appendix VII for definitions of terms specific to this Appendix.

IV-1330 GENERAL

IV-1331 Techniques

Limited zone monitoring is accomplished by installing sensors in or around the area of interest. Signals originating from outside the area of interest are excluded from the analysis using techniques such as triangulation, amplitude discrimination, coincidence detection, or signal arrival sequence.

IV-1332 Guard Sensor Technique

One common signal arrival sequence technique uses guard sensors to limit the area of interest. The guard sensor technique involves placing additional sensors further outside the area of interest than the detection sensors. Signals arriving at a guard sensor before any of the detection sensors are rejected. Signals originating from within the area of interest arrive at a detection sensor before any of the guard sensors and are accepted by the data acquisition and analysis process.

IV-1333 Other Techniques

The preceding descriptions of typical limited zone monitoring techniques shall not preclude the use of other techniques to provide this function.

IV-1340 REQUIREMENTS

IV-1341 Procedure

When limited zone monitoring is intended, the technique used to accomplish this function shall be described in the procedure (T-1350). Any technique, or combination of techniques, may be utilized to accomplish limited zone monitoring provided the technique(s) is described in the applicable procedure.

IV-1342 Redundant Sensors

Where appropriate, redundant sensors should be used to provide additional assurance that the failure of a single sensor will not preclude continued operation of the AE system throughout the specified monitoring period.

IV-1343 System Calibration

During the system calibration performed in accordance with T-1362, the effectiveness of the limited zone monitoring technique(s) shall be demonstrated by introducing artificial AE signals both inside and outside the area of interest. The AE system shall accept at least 90% of the signals that originate inside the area of interest, and reject at least 90% of the signals that originate outside the area of interest. Such signal discrimination may be accomplished using any of the techniques listed above as specified in the procedure (T-1350).

IV-1350 EVALUATION/RESULTS

Data processing and interpretation shall be performed consistent with the objectives of limited zone monitoring. Precautions shall be taken to confirm that signals originating from inside the area of interest are not confused with signals originating from outside the area of interest. Care shall also be taken to check that the system's ability to monitor the area of interest was not compromised by excessive noise from outside the area of interest.

IV-1360 REPORTS/RECORDS

All reports of data acquired using the limited zone monitoring approach shall clearly and accurately identify the effective area of interest.

APPENDIX V — HOSTILE ENVIRONMENT APPLICATIONS

V-1310 SCOPE

This Appendix specifies supplemental requirements for continuous AE monitoring of pressure containing components during operation at high temperatures and in other hostile environments. As used herein, high temperature means as any application where the surface to be monitored will exceed 300°F (149°C), which is the nominal upper temperature limit for most general purpose AE sensors. Other hostile environments include corrosive environments, high vapor atmospheres, nuclear radiation, etc.

V-1320 SENSORS

For high temperature applications, special high temperature sensors shall be used. There are two basic types of sensors for such applications. Surface mounted sensors constructed to withstand high temperatures and waveguide sensors which remove the sensor's piezoelectric sensor from the high temperature environment through the use of a connecting waveguide. A thin, soft metal, interface layer between the sensor and the component surface has proven effective for reducing the interface pressure required to achieve adequate acoustic coupling.

V-1321 Surface Mounted Sensors

Sensors to be mounted directly on the surface shall be evaluated for their capability to withstand the environment for the duration of the planned monitoring period. Some sensors rated for high temperature service are limited in the time for which they can survive continuous exposure at their rated temperature.

V-1322 Waveguide Sensors

The waveguide sensors described below are suitable for hostile environment applications where the sensor unit (piezoelectric crystal and 20 dB preamplifier) can be placed in a less hostile environment [e.g., lower temperature of about 200°F (93°C)] through the use

of a waveguide no more than 20 ft (6.1 m) long. The length of the waveguide is not an absolute; however, as the waveguide length increases, the signal attenuation in the waveguide also increases.

Waveguide sensors are a special type of sensor used for hostile environments. A type of waveguide sensor that has been used effectively to monitor components with surface temperatures to 1800°F (982°C) is shown in Fig. V-1322. A waveguide 20 ft (6.1 m) long was used to move the sensor unit (piezoelectric crystal and 20 dB preamplifier) away from the high temperature to an environment of about 200°F (93°C). The sensor was still exposed to a nuclear radiation environment of about 45,000 Rad/hr gross gamma. When monitoring was completed after 120 days, the sensors were still operating with no evidence of deterioration. These sensor types have been used in various applications with waveguide lengths ranging from 2 to 20 ft (0.6 m to 6.1 m) for periods up to 2½ years, and the attenuation in a 0.130 in. (3.30 mm) diameter Type 308 stainless steel waveguide has been measured to be 0.45 dB/ft.

V-1323 Sensor Monitoring

Refer to T-1332.3 for a discussion of sensor mounting. Most extreme temperature applications require mechanical mounting with pressure coupling of the sensors due to the temperature limitations of glues or epoxies. A sensor mounting fixture held in place by stainless steel bands or magnets has proven to be effective; however, if magnets are used, the ability of the magnet to retain its magnetic properties in the temperature environment must be evaluated. The fixture shown in Fig. V-1323 has been successfully used in a variety of waveguide sensor applications.

This fixture design provides a constant load on the waveguide tip against the component surface through the use of a spring. It has been found through practice that an interface pressure of about 16,000 psi (110 MPa) is required for good acoustic coupling. For the waveguide sensor shown in Fig. V-1322 with a waveguide tip diameter of 0.05 in. (1.27 mm), 30 pounds (0.13 kN) force for the mounting fixture provides the required interface pressure.

V-1324 Signal Cables

Special coaxial cables rated for the expected temperature shall be used to conduct AE signal information from the AE sensor to a location outside of the environment. Refer also to T-1333 and T-1348.

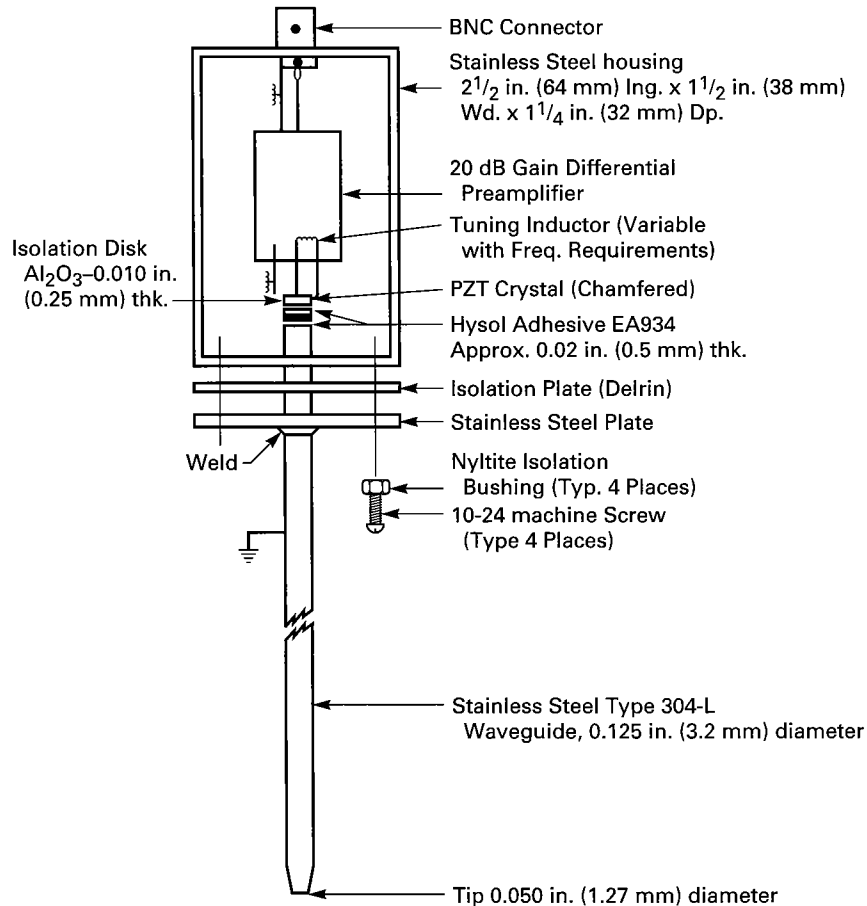


FIG. V-1322 METAL WAVEGUIDE AE SENSOR CONSTRUCTION

APPENDIX VI — LEAK DETECTION APPLICATIONS

VI-1310 SCOPE

This Appendix specifies supplemental requirements for continuous AE monitoring of metallic and non-metallic components to detect leaks from the pressure boundary. The objective in examining the pressure boundary of systems and components is to assess the leak integrity and identify the leakage area. The requirements of Appendix I — Nuclear Components and Appendix V — Hostile Environment Applications may also be applicable. SE-1211 should be consulted as a general reference.

VI-1320 GENERAL

The desire to enhance leak detection capabilities has led to research to improve acoustic leak detection

technology including technology that is applicable to the pressure boundary of nuclear reactors. Several methods are available for detecting leaks in pressure boundary components including monitoring acoustic noise due to fluid flow at a leakage site. The advantages of acoustic monitoring are rapid response to the presence of a leak and the capability to acquire quantitative information about a leak. Acoustic leak detection methods may be used to detect gas, steam, water, and chemical leaks for both nuclear and non-nuclear applications.

VI-1330 EQUIPMENT

VI-1331 Sensor Type

AE sensors with known sensitivity in the frequency range 200 kHz to 500 kHz shall be used in the presence of high background noise. For components in the

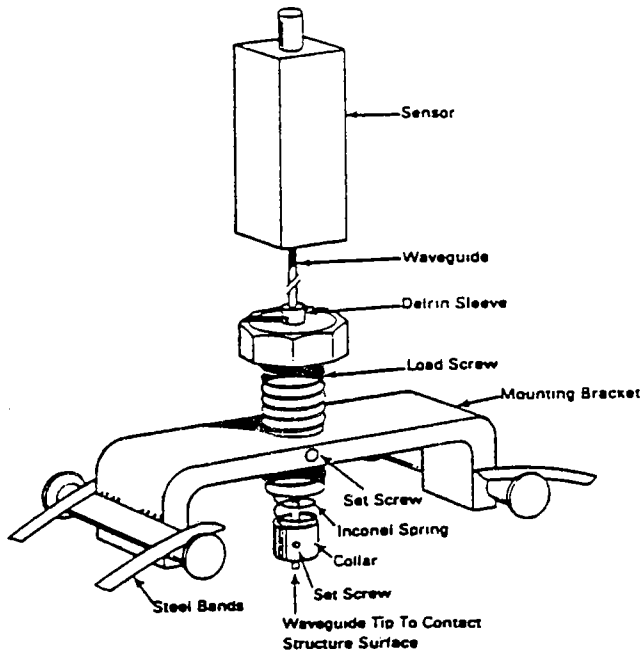


FIG. V-1323 MOUNTING FIXTURE FOR STEEL WAVEGUIDE AE SENSOR

presence of low background noise, monitoring shall be carried out at lower frequencies. Leak detection at frequencies below 100 kHz and as low as 1 kHz may be necessary for leak detection with non-metallic components.

VI-1331.1 Sensor selection shall be based on consideration of the following:

- (a) center frequency
- (b) bandwidth
- (c) ruggedness
- (d) response to temperature
- (e) humidity
- (f) ability of cables and preamplifiers to withstand the specific environment.

Using a simulation, sensor response characteristics and curves of leak rate vs. acoustic signal intensity shall be determined before installation to maximize the utility of the information in the acoustic signal.

VI-1331.2 Sensors not specified in this Appendix may be used if they have been shown to be appropriate for the application and meet the requirements of this Article. Alternate sensors, such as accelerometers, microphones, and hydrophones shall be included.

VI-1332 Waveguide

Waveguides may be used to isolate the sensor from hostile environments such as high temperatures or nuclear radiation for nuclear reactor applications.

VI-1332.1 Waveguide installations shall consider the following waveguide parameters:

- (a) length
- (b) diameter
- (c) surface finish
- (d) material of construction (i.e., ferritic steel, stainless steel, aluminum, and ceramic materials)

Waveguides having 3 mm to 13 mm in diameter and up to 250 mm in length have been shown to be effective and shall be used.

VI-1332.2 Coupling. Appendix V, para. V-1323 describes one method for mounting the waveguide. Others that have been shown effective are:

- (a) weld the waveguide to the pressure boundary
- (b) screw the waveguide into a plate attached to the order to mechanically press the waveguide against the metal component
- (c) screw the waveguide directly into the pressure boundary component
- (d) attach the sensor directly to the component.

Either gold foil or rounded waveguide tips have been shown to be effective when mechanically coupling the waveguide to the pressure boundary component. Occasionally, sensors are mounted and passed through the pressure boundary of a component in order to have the sensor in the process fluid. The sensor(s) shall then be capable of withstanding the ambient service environment of the process fluid. In addition, a safety analysis for installation and monitoring of the system shall be performed.

VI-1333 Electronic Filters

The response of the electronic filter(s) shall be adjustable to achieve the selected monitoring frequency range of operation as needed (see Appendix I). Frequency bandwidths in the range of 200–250 kHz should be available for high background noise environments and 1–200 kHz for low background noise environments.

VI-1340 CALIBRATION

VI-1341 Procedure

A calibration procedure shall be established and shall incorporate either the pencil-lead break and/or gas jet techniques described in T-1360 and Appendix I.

VI-1342 Calibration Checks

Sensor calibration checks may be conducted by electronically pulsing one of the sensors while detecting the associated acoustic wave with the other sensors.

VI-1350 EXAMINATION**VI-1351 Implementation of System Requirements**

In order to implement an acoustic leak detection and location system, the following preliminary steps shall be accomplished.

(a) identify the acoustic receiver sites

(b) determine the spacing between waveguides or sensors

(c) meet the sensitivity needs for the system requirements

(d) establish the level of background noise

(e) estimate signal-to-noise ratios as a function of distance and level of background noise for acoustic signals in the frequency range selected.

VI-1352 Calibration Procedure

A calibration procedure shall be established. During the monitoring period, a self-checking system shall be performed to assure the system is functioning properly.

VI-1353 Equipment Qualification and Calibration Data

The acoustic equipment qualification and calibration data requirements shall be in accordance with T-1392.

VI-1360 EVALUATION/RESULTS**VI-1361 Leak Indications**

Detection of a leak or leakage indication near or at a sensor site will be indicated by an increase in the RMS signal over background noise. The signal increase shall be at least 3 dB or greater above background for a period of at least 30 min.

VI-1362 Leak Location

The general location of a leak can be established by the analysis of the relative amplitude of the RMS signals received by the sensor(s). Leak location may

also be determined by cross-correlation analysis of signals received at sensors, to either side of the leak site. When leakage location accuracy is desired, it may be necessary to spatially average the correlograms of the acoustic signals at each sensor site by installing an array of sensors. A minimum of three waveguides, separated by a minimum of 10 cm, is required for averaging of correlograms. This allows nine correlograms to be generated and averaged for each pair of sensor locations. Self-checking and calibration for the system shall be in accordance with VI-1340. If acoustic background levels are relatively constant, they may also be used to determine whether a probe is failing.

APPENDIX VII — GLOSSARY OF TERMS FOR ACOUSTIC EMISSION EXAMINATION

VII-1310 SCOPE

This Mandatory Appendix is used for the purpose of establishing standard terms and definitions of terms that appear in Article 13, Continuous Acoustic Emission Monitoring.

VII-1320 GENERAL REQUIREMENTS

(a) The Standard Terminology for Nondestructive Examinations (ASTM E 1316) has been adopted by the Committee as SE-1316.

(b) SE-1316 provides the definitions of terms listed in VII-1330(a).

(c) For general terms, such as *Interpretation*, *Flaw*, *Discontinuity*, *Evaluation*, etc., refer to Article 1, Mandatory Appendix I.

(d) Paragraph VII-1330(b) provides a list of terms and definitions that are in addition to SE-1316 and are Code specific.

VII-1330 REQUIREMENTS

(a) All of the terms listed in SE-1316 are used in conjunction with this Article.

(b) The following Code terms are used in conjunction with this Article:

AE Monitor — all of the electronic instrumentation and equipment (except sensors and cables) used to detect, analyze, display, and record AE signals

Continuous Monitoring — the process of monitoring a pressure boundary continuously to detect acoustic emission during plant startup, operation, and shutdown

dB_{AE} — the peak voltage amplitude of the acoustic emission signal waveform expressed by the equation $dB_{AE} = 20 \log V/V_{Ref}$, where V_{Ref} is $1 \mu V$ out of the AE sensor crystal

Limited Zone Monitoring — the process of monitoring only a specifically defined portion of the pressure boundary by using either the sensor array configuration, controllable instrumentation parameters, or both to limit the area being monitored

Penetrations — In nuclear applications, the term penetrations refers to step-plugs containing electronic instrumentation cable sections installed through

shielding or containment walls to permit passing instrumentation power and information signals through these protective walls without compromising the protective integrity of the wall

Plant/Plant System — the complete pressure boundary system including appurtenances, accessories, and controls that constitute an operational entity

Plant Operation — normal operation including plant warmup, startup, shutdown, and any pressure or other stimuli induced to test the pressure boundary for purposes other than the stimulation of AE sources

Sensor Array — multiple AE sensors arranged in a geometrical configuration that is designed to provide AE source detection/location for a given plant component or pressure boundary area to be monitored

NRC FORM 335 (9-2004) NRCMD 3.7	U. S. NUCLEAR REGULATORY COMMISSION	1. REPORT NUMBER (Assigned by NRC. Add Vol., Supp., Rev., and Addendum Numbers, if any.) NUREG/CR- ANL-04/26			
BIBLIOGRAPHIC DATA SHEET <i>(See instructions on the reverse)</i>		2. TITLE AND SUBTITLE Barrier Integrity Research Program: Final Report			
5. AUTHOR(S) D. S. Kupperman, S. H. Sheen, W. J. Shack, and D. R. Diercks; Argonne National Laboratory, Argonne, IL 60439 P. Krishnaswamy, D. Rudland, and G. M. Wilkowski; Engineering Mechanics Corporation of Columbus, Columbus, OH 43221	3. DATE REPORT PUBLISHED <table border="1" style="width: 100%;"> <tr> <td style="text-align: center;">MONTH</td> <td style="text-align: center;">YEAR</td> </tr> <tr> <td></td> <td style="text-align: center;">2004</td> </tr> </table>	MONTH	YEAR		2004
	MONTH	YEAR			
	2004				
4. FIN OR GRANT NUMBER Y6869					
8. PERFORMING ORGANIZATION – NAME AND ADDRESS <i>(If NRC, provide Division, Office or Region, U.S. Nuclear Regulatory Commission, and mailing address; if contractor, provide name and mailing address.)</i> Argonne National Laboratory 9700 South Cass Avenue Argonne, IL 60439	6. TYPE OF REPORT Technical; Semiannual, etc.				
9. SPONSORING ORGANIZATION – NAME AND ADDRESS <i>(If NRC, type "Same as above"; if contractor, provide NRC Division, Office or Region, U.S. Nuclear Regulatory Commission, and mailing address.)</i> Division of Engineering Technology Office of Nuclear Regulatory Research U.S. Nuclear Regulatory Commission Washington, DC 20555-0001	7. PERIOD COVERED (Inclusive Dates)				
10. SUPPLEMENTARY NOTES M. Srinivasan, NRC Project Manager					
11. ABSTRACT (200 words or less) <p>In response to the vessel head event at the Davis-Besse reactor, the NRC formed a Lessons Learned Task Force (LLTF). Four action plans were formulated to respond to the recommendations of the LLTF. The action plans involve barrier integrity, stress corrosion cracking (SCC), operating experience, and inspection and program management. One part of the action plan on barrier integrity is an assessment to identify potential safety benefits from changes in requirements pertaining to leakage in the reactor coolant system (RCS). In this report, experiments and models were reviewed to identify correlations between crack size, crack-tip-opening displacement (CTOD), and leak rate in the RCS. Sensitivity studies using SQUIRT (Seepage Quantification of Upsets In Reactor Tubes) were carried out to correlate crack parameters, such as crack size and CTOD, with leak rate for various types of crack configurations in RCS components. A database that identifies the leak source, leak rate, and resulting actions from RCS leaks discovered in U.S. light water reactors was developed. For each leak event, the database provides information on what equipment detected the leakage, how it was determined that the leakage was through the pressure boundary, and what caused the leakage. The sensitivity, reliability, response time and accuracy of each type of leakage detection system were evaluated. Acoustic emission crack monitoring systems for the detection of crack initiation and growth before a leak occurs were also considered. New approaches to the detection of a leak in the reactor head region by monitoring boric-acid aerosols were also considered. Infrared spectroscopy could be used for this purpose. The focus of the report is on the available technologies.</p>					
12. KEY WORDS/DESCRIPTORS <i>(List words or phrases that will assist researchers in locating this report.)</i> barrier integrity, reactor coolant system, leak rate models, leakage database, leak monitors	13. AVAILABILITY STATEMENT unlimited				
	14. SECURITY CLASSIFICATION <i>(This Page)</i> unclassified <i>(This Report)</i> unclassified				
	15. NUMBER OF PAGES				
	16. PRICE				